A STUDY OF MODELLING AND MONITORING TIME-BETWEEN-EVENTS WITH CONTROL CHARTS

LIU JIYING

NATIONAL UNIVERSITY OF SINGAPORE

2006

A STUDY OF MODELLING AND MONITORING TIME-BETWEEN-EVENTS WITH CONTROL CHARTS

LIU JIYING

(*M.Eng, Northwestern Polytechnic University, China*)

A THESIS SUBMITTED

FOR THE DEGREE OF DOCTOR OF PHILOSOPHY

DEPARTMENT OF INDUSTRIAL & SYSTEMS ENGINEERING

NATIONAL UNIVERSITY OF SINGAPORE

2006

ACKNOWLEDGEMENTS

Over the past four years I have had the privilege to work with a number of people who have generously offered their help, encouragement and support to me, without which this thesis would not be possible.

First and foremost, I owe a particular gratitude to my "coaches", Professor Goh Thong Ngee and Professor Xie Min, for their invaluable guidance and warmly concern throughout the whole period. Their penetrating ideas, clear thought, and great enthusiasm in research made working with them an exceptional experience for me, and I believe such experience will definitely benefit me for the whole life.

Besides, I would like to thank the National University of Singapore for offering me the Research Scholarship as well as President's Graduate Fellowship. I am indebted to the faculty members of Department of Industrial and Systems Engineering, from whom I have learnt not only knowledge but also skills in research as well as teaching. I am very grateful to my colleagues in ISE Department for their kindly help, and the co-authors of the papers for their cooperation. Especially, I would like to thank Lai Chun and my friends Aldy, Caiwen, Chaolan, Hendry, Henry, Jiang Hong, Josephine, Lifang, Liu Qihao, Long Quan, Pan Jie, Philippe, Priya, Qingpei, Tang Yong, Tingting, Xin Yan, Yanping, Yongbin, Zhang Jun, Zhecheng, among others who have helped me in one way or the other and made my life in NUS enjoyable and fruitful.

Special appreciation goes to the staffs in Advanced Micro Devices (Singapore) Pte. Ltd. for their support and collaboration in the project of Time-between-events (TBE) charts implementation, which enriches this research from practical point of view.

Last, but not the least, my wholehearted thankfulness goes to my parents and brother for their endless love, support and encouragement. I feel deeply indebted to my husband Xiaoxun who always provides the best he could to help me continue and concentrate on my study. This thesis contains much of their effort not in terms of paragraphs, tables or figures, rather, their understanding and support all the way.

Liu Jiying

December 2006

TABLE OF CONTENTS

SUMMARY

With the development of automation and high-quality manufacturing techniques, effective process monitoring schemes have become essential for enterprises to ensure product quality and reduce cost. However, when dealing with high-quality processes, the existing control charting schemes may face some difficulties. The Time-between-events (TBE) chart is one of the approaches proposed to solve these problems. The purpose of this study was to overcome the disadvantages of Shewhart attributes chart as well as existing TBE charts, improve the performance of the control charts and thus make the monitoring of high-quality processes more effective and economical.

In Chapter 1, some basic concepts of statistical process control and TBE chart are introduced, and the objective of the study is stated. Chapter 2 presents a literature review on the TBE control charts. Recent advancements in the area of TBE monitoring are also substantially reviewed.

Chapter 3 discusses the comparative performance of exponential TBE charts, from which some insights of the comparative preference are found among all those TBE charts under different circumstances.

In Chapters 4 and 5, the CUSUM and EWMA chart with transformed exponential data are proposed, in which the TBE data are transformed to approximately normal with double square-root transformation, and CUSUM (or EWMA) method is applied

subsequently. The proposed control charts provide alternatives for TBE monitoring with good performance and relatively simple design procedures.

Chapter 6 applies the variable sampling interval scheme to the CCC chart. The results showed that with a proper set of design parameters, it can detect the shifts in a shorter period of time without increasing the average number of samples inspected. Subsequently, Chapter 7 develops the CCC chart with sampling plan based on random-shift model, followed by a case study which stresses some implementation issues of CCC chart. Improvement strategies are proposed with consideration of customers' requirements.

In Chapter 8, a Weibull EWMA is proposed and its performance in terms of Average Run Length (ARL) as well as Average Time to Signal (ATS) is evaluated. Weibull TBE chart is a more general chart which considers the variable events occurrence rate and is very useful especially for reliability monitoring when aging factor exists.

This study focused on not only theoretical analysis, but also practical applications. These control charting methods present some effective approaches to the quality control of high-quality processes for both on-line monitoring and off-line analysis. Economic considerations were also involved in the design process to minimize the cost without losing efficiency of the monitoring system. Moreover, the methods proposed can also be applied to other areas for monitoring process stability from the aspect of events occurrence rate.

LIST OF TABLES

LIST OF FIGURES

NOMENCLATURE

ANI	Average Number of items Inspected
ANN	Artificial Neural Network
ARL	Average Run Length
ATE	Automatic Test Equipment
ATS	Average Time to Signal
CCC	Cumulative Count of Conforming
CDF	Cumulative Distribution Function
CL	Central Line
CQC	Cumulative Quantity Control
CUSUM	Cumulative Sum
DOE	Design of Experiment
EWMA	Exponentially Weighted Moving Average
FAR	False Alarm Rate
FIR	Fast Initial Response
FNC	Fraction of NonConforming
FSI	Fixed Sampling Intervals
LCL	Lower Control Limit
ppb	parts per billion
ppm	parts per million
SPC	Statistical Process Control
SQC	Statistical Quality Control
TBE	Time Between Events

UCL	Upper Control Limit
VSI	Variable Sampling Intervals
ZD	Zero Defects

Chapter 1 Introduction

The rapid development of modern technology has brought lots of opportunities together with challenges for companies all over the world. Most of them devote a great deal of efforts to enhancing the quality of products, as well as the quality of service, in order to survive in the competitive market. Quality, thus, becomes one of the keys to success, and has attracted a lot of interest among researchers and engineers.

The history of quality can be traced back to the beginning of the 20^{th} century when Taylor introduced the ideas of scientific management to industry. Throughout the years of its development, many quality analysis and control tools have been developed, among which Statistical Process Control (SPC) is one of the most effective techniques that have been widely adopted in practice.

In recent years, the rapid development of modern technology and the growing emphasis on customers' satisfaction have promoted the quality of products to higher and higher levels. As a result, Zero-defects (ZD) or high-quality processes become more and more popular, and their Fraction of Nonconforming (FNC) can be very low up to parts per million (ppm) or even parts per billion (ppb) levels. Most of those processes are highly-automated, and a delay in detection of a process shift in a production line may result in many defective items produced, which in turn results in a big cost and loss of profit. Therefore, effective monitoring and control techniques become a great need. On the other hand, the low FNC also brings many practical challenges to the traditional control charts. As a result, a new type of control chart,

namely, time-between-events (TBE) chart, was proposed in order to solve the problems with traditional control charts.

Time-between-events data are available in industries such as manufacturing, maintenance, and even in service. The TBE chart is an effective approach for process analysis, control, and improvement especially when the events occurrence rate is very low. This thesis discusses different statistical control techniques for modelling and monitoring TBE. The rest of this chapter will focus on the basic ideas and methods of SPC, the general methods and principles of SPC, the problems with current methods, and the motivation of this study.

1.1 Statistical Process Control (SPC)

Statistical Process Control (SPC) originated in the 1920's when Dr. Shewhart developed control charts as a statistical approach to the monitoring and control of manufacturing process variation (Shewhart, 1926, 1931). SPC involves using statistical techniques to monitor and control a process through the analysis of process variation. It is an important branch of Statistical Quality Control (SQC), which also includes other statistical techniques, e.g. Design of Experiment (DOE), acceptance sampling, process capability analysis, and process improvement plans. Most often SPC is used for manufacturing processes; however, nowadays it is also applied in other areas such as health care (Tsacle and Aly, 1996; Benneyan *et al.*, 2003; Guthrie *et al.*, 2005; Woodall, 2006), financial analysis (Schipper & Schmid, 2001; Wong *et al*. 2004), and service management (Herbert *et al.* 2003; Pettersson 2004).

Generally speaking, the purpose of implementing SPC is to monitor the process, eliminate variances induced by assignable causes, and at the end improve the process to its best target value. One of the primary tools to achieve these aims is the control chart, which is a graphical representation of certain descriptive statistics for specific quantitative measurements of the process. These descriptive statistics are displayed in a run chart together with their in-control sampling distributions so as to isolate the assignable causes of variation with the natural variability. Any statistics beyond the natural variance levels could indicate an assignable cause with the process. The assignable causes may be caused by defective raw materials, faulty setup, untrained operators, and the cumulative effects of heat, vibration, shock, etc. Besides, control charts can also be used with product information to analyze process capability and for continuous process improvement efforts.

Shewhart control charts are the most basic control charts to fulfill those tasks. Basically, two types of Shewhart control charts were developed to monitor the process variation, i.e. control charts for variables (e.g. the *X*-bar *R* chart, *X*-bar *S* chart), and control charts for attributes such as the *p* chart, *np* chart, *c* chart and *u* chart. Control charts for variables are used to monitor quality characteristics that are measured on a numerical scale, while control charts for attributes are designed for those quality characteristics that conform to specifications or do not conform to specifications. All these control charts, namely Shewhart charts, are set up based on the 3-sigma limits and normal approximation. General formulas for the Upper Control Limits (UCL), Central Line (CL) and Lower Control Limits (LCL) of Shewhart control charts are:

$$\begin{aligned} UCL &= \mu_x + k\sigma_x \\ CL &= \mu_x \\ LCL &= \mu_x - k\sigma_x \end{aligned} \tag{1.1}$$

where μ_x and σ_x is the mean and variance of the sample statistic that is of concern. k is a constant that determines the distance of the UCL and LCL from the CL. By convention k is set to be 3 because 3-sigma limits are a good balance point between two types of errors:

- Type I errors occur when a point falls outside the control limits even though no assignable cause is operating and process is in-control. The probability that type I error occurs is referred to as False Alarm Rate (FAR, α) or producer's risk. A control chart with large FAR may lead to a high producer's risk and may even distort a stable process as well as waste time and energy.

- Type II errors occur when an assignable cause is missed out because the control chart is not sensitive enough to detect it. A control chart with high probability of type II error will not be able to detect the process shifts in a short time. The probability of type II error (β) is sometimes called the consumer's risk because it represents the probability of operating a control chart without raising any out-of-control signal while the process is actually in an unsatisfactory status due to assignable causes.

All control charts are vulnerable to the risk of these two types of errors. Shewhart control charts with 3-sigma control limits are set up based on independent and normal assumption, i.e., the sample statistic X in formula (1.1) is assumed to be independent

and normally distributed. Under these assumptions, data points will fall inside 3-sigma limits 99.73% of the time when a process is in control. This makes the type I error infrequent but still makes it likely that assignable causes of variation will be detected within an acceptable time period.

The statistical performance of control charts is usually measured by Average Run Length (ARL). ARL is defined as the average number of points that must be plotted before a point indicated an out-of-control condition, and it can be calculated by

$$ARL = \frac{1}{p} \tag{1.2}$$

where p is the probability that any point exceeds the control limits. Therefore, the in-control ARL can be presented with

$$ARL_0 = \frac{1}{\alpha} \tag{1.3}$$

and the out-of-control ARL can be obtained by

$$ARL_1 = \frac{1}{1-\beta} \tag{1.4}$$

where α and β stand for the probability of type I error and type II error, respectively. A good design scheme of control chart should have longer in-control ARL to restrict the risk of type I error and shorter out-of-control ARL to detect the assignable causes of the process quickly.

Although Shewhart control charts are widely applied in practice due to the simplicity for understanding and implementation, they are not very sensitive to detect small process shifts because the decision made only depends on a single point. To enhance the sensitivities of the Shewhart control charts, some researchers proposed adding run rules to the control charts, such as Western Electric (1956), Nelson (1984,1985), Champ (1992), Davis and Woodall (2002), and Zhang and Wu (2005). Modern techniques, e.g. pattern recognition, neural network, artificial intelligence, and expert system, can be used to help in this rule for on-line SPC monitoring (Zorriassatine and Tannock, 1998; Guh, 2003; Pacella and Semeraro, 2005; Yang and Yang, 2005).

Besides, some advanced control charts were also proposed to enhance the sensitivity of Shewhart control charts, such as the Exponentially Weighted Moving Average (EWMA) chart, and the CUmulative SUM (CUSUM) chart. Instead of using only the information in the last plotted point, EWMA and CUSUM incorporate information from the entire sequence of points and thus are more effective in detecting small process shifts.

The EWMA chart was introduced by Roberts (1959), and the general statistics of EWMA is expressed by

$$z_i = \lambda x_i + (1-\lambda) z_{i-1} \tag{1.5}$$

where $0<\lambda\leq 1$ is a constant that determines how older data points affect the moving average compared to more recent ones, and it will reduce to Shewhart chart when $\lambda=1$. The starting value is usually set to be the target value of X_i. The control limits for the EWMA chart are

$$\begin{aligned} UCL &= \mu_0 + L\sigma\sqrt{\frac{\lambda}{2-\lambda}\left[1-(1-\lambda)^{2i}\right]} \\ CL &= \mu_0 \\ LCL &= \mu_0 - L\sigma\sqrt{\frac{\lambda}{2-\lambda}\left[1-(1-\lambda)^{2i}\right]} \end{aligned} \tag{1.6}$$

where L is the factor that determines the width of the control limits. An optimal design can be achieved by selecting the value of λ and L properly (Crowder 1989; Lucas and Saccucci, 1990). EWMA chart can be used to monitor not only process mean, but also process variation (Crowder and Hamilton, 1992; MacGregor and Harris, 1993; Knoth, 2005), and it is not limited to normal variables. The main strengths of EWMA include the robustness to non-normality, and the ability of forecasting the control statistics value for the next time period.

The CUSUM chart, first proposed by Page (1954), plots the cumulative sums of the deviations of the sample values from a target value. Upper and lower CUSUMs can be used to accumulate deviations from the target value that are above and below target, respectively. Let μ_0 denote the process mean (target value). The tabular CUSUMs are computed as,

$$\begin{aligned} C_i^+ &= \max\left\{0, x_i - (\mu_0 + K) + C_{i-1}^+\right\} \\ C_i^- &= \max\left\{0, (\mu_0 - K) - x_i + C_{i-1}^-\right\} \end{aligned} \tag{1.7}$$

where K is the reference value (or slack value, or allowance). The process is considered to be out-of-control if either C_i^+ or C_i^- exceeds the decision interval H. Similar to the EWMA chart, CUSUM can also be applied to monitor the process variance (Acosta-Mejia and Pignatiello, 2000), or data following other distributions

(Lucas, 1985; Gan, 1994). Basically, both EWMA and CUSUM charts are more effective alternatives to the Shewhart control charts when small shifts are of great concern. Comparative studies show that the performances of EWMA and CUSUM are similar, and they only have slight differences in detecting different shifts (Gan, 1998; de Vargas *et al.* 2004).

All these SPC tools have been widely adopted in industries to help monitor, control, and improve the process or product quality. However, the rapid developments of technology and increasing effort on process improvement have led to so called high-quality processes, where traditional control charts showed some practical problems. Therefore, it is necessary to look for solutions and alternatives to overcome these problems.

1.2 Control Charts for High-quality Processes

High-quality processes refer to those processes with very low FNC up to ppm or ppb levels. In such situations, many Shewhart control charts would face practical difficulties, and those difficulties are more serious with attribute control charts (Xie *et al.*, 2002). On the other hand, attribute control charts attract increasing interests from engineers because they are much easier and cheaper to obtain attribute data quickly from high-quality processes, and thus enable the process to be monitored continuously at a lower cost. Therefore, the solution of the problems with attribute control charts becomes a great concern.

The primary reason that induces these problems is the normal assumption. Shewhart control charts are set up based on normal assumption, i.e., it assumes that the sample

statistics can be approximately modeled by a normal distribution. Unfortunately, this assumption is difficult to meet for high-quality process with very low nonconforming rate and a large sample size is required. The deviation from the normal approximation will lead to the following problems for attribute control charts in practice:

- **High false alarm**

When process FNC p is very small and the sample size n is not large enough, the normal approximation will be invalid. As a result, the exact false alarm rate (FAR) could be much higher than 0.0027, which corresponds to the 3-sigma limits under normal assumption. For example, Table 1.1 shows the exact FAR for *np*-chart with 3-sigma limits assuming that the number of nonconforming X in a sample with size n follows binomial distribution with parameters n and p.

Table 1.1 Exact FAR for *np*-chart with 3-sigma limits

p	n=5	n=10	n=20	n=50	n=100	n=200
0.01	0.0490	0.0043	0.0169	0.0138	0.0184	0.0043
0.02	0.0038	0.0162	0.0071	0.0178	0.0041	0.0075
0.03	0.0085	0.0345	0.0210	0.0037	0.0032	0.0031
0.04	0.0148	0.0062	0.0074	0.0036	0.0068	0.0030
0.05	0.0226	0.0115	0.0159	0.0032	0.0043	0.0027
0.06	0.0319	0.0188	0.0056	0.0027	0.0026	0.0023
0.07	0.0031	0.0036	0.0107	0.0073	0.0041	0.0040
0.08	0.0045	0.0058	0.0038	0.0056	0.0024	0.0030
0.09	0.0063	0.0088	0.0068	0.0043	0.0035	0.0023
0.10	0.0086	0.0128	0.0024	0.0032	0.0023	0.0034

The control limits of *np*-chart are calculated by

$$\begin{aligned} UCL &= np + 3\sqrt{np(1-p)} \\ CL &= np \\ LCL &= np - 3\sqrt{np(1-p)} \end{aligned} \tag{1.8}$$

and the false alarm rate α is obtained by

$$\alpha = 1 - P(LCL < X < UCL) \tag{1.9}$$

It can be found from Table 1.1 that the exact FAR of the *np*-chart could be much higher than 0.0027 with sample size *n* less than 50 if the process FNC *p* is within the range of (0.01, 0.10).

- **Meaningless control limits**

If the FNC *p* is very low, the probability that at least one nonconforming item could be found in a sample will be very small. As a result, the *UCL* can be smaller than one so that even only one nonconforming item in a sample would raise an out-of-control signal. Meanwhile, the *LCL* will usually be less than zero, and thus the control chart will not be able to detect process improvement unless some run rules are applied.

Sufficiently large sample size is needed to avoid the meaningless control limits. For example, the sample size can be chosen so that the probability of one or more nonconforming item in a sample is at least a certain level, say 0.95. Also, Duncan (1986) suggested a criterion that the sample size should be large enough so that the probability of detecting a specified process deterioration shift is approximately 0.5. Based on his criterion, the sample size *n* should satisfy

$$n \geq \left(\frac{k}{p_1 - p_0} \right)^2 p_0 (1 - p_0) \tag{1.10}$$

where p_1 is the specified out-of-control process FNC level, p_0 is the in-control FNC ($p_1 > p_0$), and k is the control limits factor which is usually set to be 3.

Besides, another criterion of choosing sample size n is to make the LCL positive. To meet this criterion, the sample size n has to satisfy

$$n > \left(\frac{1 - p_0}{p_0} \right) k^2 \tag{1.11}$$

A proper sample size n can be determined by considering all the above criteria as well as the practical factors.

- **Difficulty in forming rational subgroup**

Most control charts rely on Rational Subgroups to estimate the short term variation in the process. This short-term variation is then used to predict the longer-term variation defined by the control limits. A Rational Subgroup is simply "a sample in which all of the items are produced under conditions in which only random effects are responsible for the observed variation" (Nelson, 1988). A general rule of forming a rational subgroup is to maximize the variation among different subgroup and meanwhile minimize the variation within a subgroup. Since the process FNC is low, and sample size has to be very large, it may take a long time to form a rational subgroup, which in turn leads to a long setting-up time of the control charts and a delay in raising an out-of-control signal upon process shifts. Meanwhile, the

process shift may have larger probability to occur within a subgroup instead of just at the start of a new sample that is assumed by most of the models.

A possible method to solve these problems caused by deviation from independent normal assumption is to use transformations. The performance of control charts can be improved by transforming the data to normal, and then plotting the charts (Nelson, 1994; Sun and Zhang, 2000; Chen *et al.* 2005; Wang, 2005). Another effective approach is to employ TBE charts which will be reviewed in the next section.

1.3 Time Between Events (TBE) Charts

Unlike traditional attribute control charts which monitor the number or the proportion of events occurring in a certain sampling interval, time-between-events (TBE) charts, from another angle, monitor the time between successive occurrences of events. The word *events* may have different meanings under different circumstances. For example, *events* usually refer to the occurrence of nonconforming items in manufacturing process monitoring, failures in reliability analysis, accidents in a traffic system, diseases in healthcare, etc. Besides, the word *time* is used to represent not only time but also other variable that measures the quantity observed between occurrences of the events and it can be either discrete or continuous. TBE charts can overcome the difficulties with traditional attributes control chart, and they are particularly suitable when the events rarely occur and therefore it is quite difficult to form rational subgroups as the traditional attributes control chart requires.

There are several kinds of TBE charts that can be used for monitoring processes with low events occurrence rate. Some researchers suggested employing a control chart

based on run length like the Cumulative Count of Conforming (CCC) chart (Calvin,1983) and the Cumulative Quantity Control (CQC) chart (Chan *et al.* ,2000). Others proposed applying the CUSUM and the EWMA charts for TBE data directly, as shown by Gan (1998) and Lucas (1985). Moreover, Shewhart control charts can also be used to monitor TBE data after a proper transformation (Radaelli, 1998; Jones & Champ, 2002). A detailed discussion of these methods will be presented in Chapter 2.

1.4 Objective of the Study

The overall objective of this study was to solve the problems with Shewhart attributes chart as well as existing TBE charts, and thus make the monitoring of high-quality processes with low events occurrence rate more effective and efficient. Specifically this thesis focuses on several topics regarding TBE charts in order to fulfill the following targets.

- To compare the performance of different TBE charts and provide guidelines on the choice of TBE chart in various situations.

Previous studies proposed several types of TBE chart and explored their performance respectively. A comparative study was conducted among several commonly used TBE charts in order to provide guidelines to the users on how to choose a most suitable TBE chart under a specific circumstance.

- To develop advanced CUSUM/EWMA TBE charts with transformation.

Transformation is a useful approach to deal with the nonnormality. Most of the current studies on the TBE chart focus on monitoring TBE data directly. Some researchers also looked at transformed data and found that Shewhart control charts perform well

with transformed data. In this study, the CUSUM and EWMA charts with transformed data were considered, the ARL properties were investigated and comparisons with other TBE charts were also conducted.

- To improve the cost effectiveness of the CCC chart.

Instead of using 100% inspection as usual, the variable sampling scheme was employed when implementing the CCC chart. Samples are taken from the process, and the sampling interval varies according to the status of the process. As a result, the CCC chart will take a shorter time to detect the process shifts without increasing the average number of items inspected. Some application issues of CCC chart were also discussed through a case study.

- To explore TBE charts for Weibull-distributed TBE data.

The cases where the TBE data do not follow exponential distribution were also investigated. The extended CQC and CQC-*r* charts for Weibull data were described, and the EWMA and CUSUM methods were also applied to the Weibull distributed TBE data in order to improve the sensitivity of the chart for small process shifts.

The TBE charting methods presented in this thesis can improve the effectiveness of both on-line processes monitoring and off-line analysis of high-quality processes. The variable sampling schemes can also enhance the economic performance of the CCC chart with respect to cost. The CUSUM and EWMA charts with transformed data provides effective alternatives for TBE monitoring, and make the traditional control charts applicable to TBE data with only a simple transformation of the data, which is very easy to implement based on the current system. Moreover, the underlying

distribution of TBE data was extended to Weibull so that these TBE charts become appropriate to other general situations, e.g. reliability processes where the failure rate can be variable rather than constant.

This study focused on the control charting methods for TBE data, which can be modeled as exponential or Weibull distribution. Although the study was motivated by quality issues and focused on the control charting techniques with quality concern, the proposed methods are applicable to various areas in practical applications for events-driven processes. The events occurrence rate is not necessarily constant, and it can be increasing, or decreasing as well. In practical applications, engineers may need to perform goodness-of-fit tests for distributions before choosing a proper TBE chart for process control and improvement. If the TBE data do not follow either of the distributions assumed, the users may not be able to apply the control charting methods proposed in this thesis directly. Additional data analysis and processing may be needed to identify the reasons, and regroup the data so that they can follow the underlying distributions. Other control charting methods can also be employed according to the specific situations.

1.5 Organization of the Thesis

This thesis consists of nine chapters. The rest of the thesis will be organized as follows:

Chapter 2 presents a thorough literature review of the recent research on TBE charts. The problems of existing methods will also be raised in order to specify the motivation and the emphasis of this study. Chapter 3 compares the properties of several exponential TBE charts and provides guidelines on the choice of different TBE charts

under different situations. On-line monitoring methods with TBE charts are also discussed.

In Chapter 4, a CUSUM scheme for transformed exponential TBE data is proposed, different transformation methods are examined and the calculation of ARL with Markov chain approach is presented. The performance of CUSUM chart with transformed exponential data is compared with that of the X-MR (Moving Range) chart, the CQC chart, and the exponential CUSUM chart. Chapter 5, with similar motivation, presents a EWMA scheme with transformed exponential TBE data. The properties of the proposed chart are investigated based on which the optimal design methods are developed.

In Chapter 6, the CCC chart with variable sampling intervals is proposed, and its performance is compared with the CCC chart with fixed sampling intervals. Chapter 7 discusses some implementation issues of the CCC chart based on a project with a semiconductor manufacturing company. Chapter 8 extends the TBE charting methods to Weibull-distributed data, which represents more general situations where events occurrence rate can be increasing, decreasing or constant.

At the end, some conclusions, major contributions of the study, as well as suggestions for future research are presented in Chapter 9.

Chapter 2 Literature Review

It can be seen from Chapter 1 that high-quality processes become more and more popular nowadays; hence the statistical control techniques for the monitoring of those processes are in great need in order to keep the pace of the development. TBE charts have attracted increasing interests recently, due to its ability of avoiding the problems indicated in Section 1.2, and the effectiveness of monitoring high-quality processes. The existing control charts for monitoring time between events can be categorized into three types based on their methodology: TBE charts with probability limits; TBE charts based on EWMA and CUSUM methods; and TBE chart based on Shewhart charts. Under each category, there are several control charts applicable for various time-between-events distributions. In this chapter, the most recent published research and development will be reviewed to provide an initial mapping for the modeling and monitoring of TBE with control charts. The weaknesses as well as strengths of existing studies are also incorporated which stress the motivation of this study.

2.1 Control Charts for Monitoring Time between Events

2.1.1 TBE Charts with Probability Limits

Control chart with probability limits is usually employed when the control statistic does not follow normal distribution and the traditional 3-sigma limits are not appropriate. The probability limits can be achieved by fixing the probability of false alarms (α) at a certain acceptable level. For example, it can be 0.0027 so as to be consistent with 3-sigma limits. Let F(X) denote the cumulative distribution function

(CDF) of the control statistic *X*, then the probability limits can be obtained by solving the following equations,

$$F(UCL) = 1 - \frac{\alpha}{2};\ F(CL) = \frac{1}{2};\ F(LCL) = \frac{\alpha}{2} \tag{2.1}$$

The Cumulative Count of Conforming (CCC) chart, first proposed by Calvin (1983) and further developed by Goh (1987) and Bourke (1991), monitors the cumulative number of conforming items to obtain a nonconforming item with probability limits. Let *X* denotes the cumulative counts of items inspected until a nonconforming item is observed, and the fraction of nonconforming of the process is *p*. *X* can be modeled using the geometric distribution with parameter *p*, and the mass probability function of *X* is:

$$P(X = x) = (1 - p)^{x-1} p, x = 1,2,\cdots \tag{2.2}$$

Fixing the false alarm probability α at an acceptable level, the probability limits *UCL*, *CL*, and *LCL* of CCC charts can be derived from the CDF of geometric distribution as follows:

$$UCL = \frac{\ln(\alpha/2)}{\ln(1-p)},\ CL = \frac{\ln(0.5)}{\ln(1-p)},\ LCL = \frac{\ln(1-\alpha/2)}{\ln(1-p)} \tag{2.3}$$

Because the geometric distribution is discrete, the control limits can be rounded to integers and the points that fall on the *UCL* or *LCL* are regarded as out-of-control signals, i.e., $P\{X \geq UCL\} = P\{X \leq LCL\} = \alpha/2$. In this case, the *UCL* and *LCL* of CCC chart can be calculated as follows:

$$UCL = \left[\frac{\ln(\alpha/2)}{\ln(1-p)} + 1 \right]; \; LCL = \left[\frac{\ln(1-\alpha/2)}{\ln(1-p)} \right] \tag{2.4}$$

where [Y] stands for the largest integer not greater than Y.

Note that in order to get a meaningful LCL, $p < \alpha/2$ should be satisfied. Since the value of α is usually very small, then the value of p should be small too. It implies that the CCC chart is particularly suitable for high-quality processes.

The continuous counterpart of the CCC chart is the Cumulative Quantity Control (CQC) chart (Chan *et al.*, 2000). It plots the quantity produced before observing one event, which is not necessarily an integer. CQC can be employed for monitoring continuous TBE data. Assuming that the event occurrence rate is constant and the occurrence of events can be modeled by a homogeneous Poisson process. Therefore, the cumulative quantity before observing one event follows exponential distribution. The control limits of CQC chart can be calculated as:

$$UCL = -\frac{1}{\lambda}\ln(\alpha/2), \; CL = \frac{1}{\lambda}\ln(2), \; LCL = -\frac{1}{\lambda}\ln(1-\alpha/2) \tag{2.5}$$

where λ is the events occurrence rate of the exponential distribution. When the actual parameter is unknown, an estimation parameter should be used instead of the true value. Some authors compared different estimators for the parameter λ and discussed their properties; see Bischak & Sliver (2001). The performance of CQC charts will no doubt be affected by the accuracy of estimation. This will be discussed in the later part of this chapter.

Motivated by the idea of the CCC chart and the CQC chart, Chan *et al.* (2002) proposed another type of chart, namely cumulative probability control (CPC) chart based on geometric and exponential distributions. In a CPC chart, the cumulative probability of the geometric or exponential random variable is plotted against the sample number, and hence the actual cumulative probability is indicated on the chart. The CPC chart has all the favorable features of CCC and CQC charts, and can resolve the technical plotting inconvenience of CCC and CQC charts. Moreover, since its vertical axis is standardized to be [0,1], this makes it possible to compare several characteristics simultaneously by plotting their corresponding CPC-chart at the same time.

2.1.2 TBE CUSUM Chart

Page (1954) first proposed the CUmulative SUM (CUSUM) control scheme based on normal distribution, and was proved to be effective for detecting small shift of process. The Exponential CUSUM was first studied by Vardeman & Ray (1985) and Lucas (1985) based on the inter-arrival times for monitoring the Poisson rate. A simple procedure for designing an optimal exponential CUSUM chart was given by Gan (1994). An algorithm for computing the average run length (ARL) of an exponential CUSUM chart can be found in Gan and Choi (1994).

Lucas (1985) described design and implementation procedures for both Poisson CUSUM and exponential CUSUM, and for detecting either an increase or a decrease in event occurrence rate. He suggested that an exponential CUSUM should be used if it is convenient to update the CUSUM with each new event and it is possible to record the time since the last event occurs.

In the design of exponential CUSUM, the first step is to determine the reference value *k*. The mean time between events is the reciprocal of the number of events per sampling interval. The reference value *k* for the exponential CUSUM depends on the acceptable event occurrence rate (μ_0) (event occurrence rate is the number of events occurring per sampling interval) and the event occurrence rate that is to be detected quickly (μ_1). The reference value *k* for the exponential CUSUM chart can be achieved by

$$k = \frac{\ln(\mu_1) - \ln(\mu_0)}{\mu_1 - \mu_0} \tag{2.6}$$

Once the reference value *k* has been calculated, a suitable value of *h* can be found out to give an acceptable in-control average run length. The average run length of the CUSUM scheme can be approximately calculated by the Markov Chain approach, see Brook and Evans (1972) and Lucas (1985). There's also an accurate method of evaluating ARL for exponential CUSUM charts by solving a set of differential equations, see Vardeman and Ray (1985). The value of *h* should give an appropriately large ARL when the event occurrence rate is at the acceptable level. It should also be chosen to give an appropriately small ARL value when the process is running at the event occurrence rate that should be detected quickly.

Then the exponential CUSUM can be implemented using the formulas

$$\begin{aligned} S_i^+ &= \max\{0, S_{i-1}^+ + (X_i - k)\} \\ S_i^- &= \min\{0, S_{i-1}^- + (X_i - k)\} \end{aligned} \tag{2.7}$$

The decision on the statistical control of the process is taken depending on whether $S_t^- \leq -h$ or $S_t^+ \geq h$.

Borror *et al.* (2003) investigated the robustness of TBE CUSUM, which refers to the sensitivity of the TBE CUSUM to make proper decisions regarding a shift in the mean defect rate when the TBE is not exponentially distributed. They examined the Average Run Length (ARL) properties under both Weibull and lognormal distributions, and the results indicated that the TBE CUSUM is extremely robust for a wide variety of parameter values for both Weibull and lognormal distributions.

The discrete counterpart of exponential CUSUM is the geometric CUSUM chart, which monitors the cumulative count of conforming items until a nonconforming item is found. Bourke (2001) studied the geometric CUSUM chart with both 100% inspection and sampling inspection for monitoring discrete TBE data. In the study, Bourke considered two cases where the shift occurs at a defective item or the shift occurs at any item in the process. The zero-state and steady-state performance of the geometric CUSUM were evaluated in terms of ARL, ANI (Average Number of items Inspected), and ANDO (Average Number of Defectives Observed) by Markov chain approach. The comparisons with the *np* chart showed that the geometric CUSUM is efficient in detecting upward shifts in fraction of nonconforming with sampling inspection. A more interesting finding is that the geometric CUSUM is better for detecting both small and large shifts compared with *p* chart and *np* chart; besides, a geometric CUSUM designed for detecting a specified shift can work quite well for a moderate range of neighboring shift-sizes.

2.1.3 TBE EWMA Chart

Gan (1998) introduced an exponential EWMA method based on the inter-arrival times of events, which are independent and identically distributed exponential random variables. A decrease in the mean of inter-arrival times indicates that more events occur, and an increase in the mean indicates that fewer events occur on the average. Gan discussed the design of one-sided and two-sided EWMA chart, and provided a simple design procedure for determining the chart parameters of an optimal exponential EWMA chart. With examples, he also compared the performance of EWMA, CUSUM and Shewhart charts for monitoring the time-between-events (TBE).

Let $X_1, X_2, \ldots$ be a sequence of TBE data with the exponential probability density function

$$f(x) = \begin{cases} \theta^{-1} e^{-\frac{x}{\theta}}, if \ \ x \geq 0 \\ 0, \quad otherwise \end{cases} \tag{2.8}$$

The upper-sided EWMA chart is intended for detecting an increase in the exponential mean θ and is obtained by plotting

$$Q_t = \max\{A, (1-\lambda_Q)Q_{t-1} + \lambda_Q X_t\} \tag{2.9}$$

against t, for t =1, 2, …, where λ_Q is a smoothing constant such that $0 < \lambda_Q \leq 1$, A is a nonnegative boundary and $Q_0 = u, A \leq u < h_Q$. h_Q is the upper control limit, and an out-of-control signal is issued at the first t for which $Q_t \geq h_Q$.

Similarly, the lower-sided EWMA chart is intended for detecting a decrease in the mean and is obtained by plotting

$$q_t = \min\{B, (1-\lambda_q)q_{t-1} + \lambda_q X_t\} \tag{2.10}$$

against t, for t =1, 2, …, where λ_q is a smoothing constant such that $0 < \lambda_q \leq 1$, B is a positive boundary and $q_0 = v, h_q < v \leq B$. h_{q} is the lower control limit, and an out-of-control signal is issued at the first t for which $q_t \leq h_q$.

Two-sided EWMA chart is obtained by plotting

$$Z_t = (1-\lambda_Z)Z_{t-1} + \lambda_Z X_t \tag{2.11}$$

against t, for t =1, 2, …, where λ_Z is a smoothing constant such that $0 < \lambda_Z \leq 1$, and $Z_0 = w, h_l < w < h_u$ are the lower and upper control limits, respectively. A signal is issued at the first t for which $Z_t \leq h_l$ or $Z_t \geq h_u$.

The exact method of computing ARL of exponential EWMA charts by solving a set of differential equations is discussed in Gan (1998). Subsequently, Gan and Chang (2000) provided a FORTRAN program for computing both the in-control and out-of-control ARL.

The discrete TBE EWMA was described by Sun and Zhang (2000). They introduced the method of using CUSUM and EWMA charts based on the number of consecutive conforming items which can be modeled by geometric distribution. Tables and figures were also provided to facilitate the choice of control parameters for the design of

CUSUM and EWMA charts. Comparisons of the geometric CUSUM, the geometric EWMA and the two-stage CCC chart (Chan *et al.* 1997) were conducted, and the results show that CUSUM and EWMA charts are more efficient than the two-stage CCC chart in terms of Average Number of Nonconforming (ANNC).

2.1.4 Shewhart Control Charts for TBE Monitoring

Standard Shewhart charts for attributes like the *c, u, p* and *np* charts that are generally used for the monitoring of the number of defects/defectives in a sample can also be used to monitor the TBE data. This can be accomplished by grouping the TBE data into sub-intervals with a proper subgroup size and then plotting the defects/defectives observed in that sub-interval. Radaelli(1998) presented a unified methodology for planning one-sided and two-sided TBE Shewhart charts which can be applied to any underlying distribution of the events. The methods of selecting control limits and evaluating the sensitivity of the chart were also described.

However, as explained in Section 1.2, this approach requires a large number of defects/defectives (events) per interval and it is not appropriate especially for application in a high quality environment. When there are an excessive number of events, the chart will signal an out-of-control situation. In such cases, the actual false alarm probability will be much higher than the anticipated probability of 0.0027, corresponding to the 3σ limits, due to the poor approximation. Moreover, as pointed out before, the lower control limit is usually set at zero, thus making the chart unsuitable for identifying any improvement in the process.

Another approach to use Shewhart control chart for TBE monitoring is to transform the TBE data to Normal distribution first, and then use the traditional Shewhart chart for monitoring the process. Nelson (1994) proposed a method by raising exponential data to the 1/3.6 power so that the transformed data become approximately normal. Subsequently, McCool and Joyner-Motley (1998) compared the Nelson's transformation and logarithmic transformation for setting up control charts with 3-sigma control limits, probability control limits, and the EWMA chart. Their results indicate that either power or log transformation can improve the control chart performance effectively when an EWMA scheme is applied. Besides, the power transformation is recommended over the log transformation for setting up an EWMA chart. Kittlitz (1999) further demonstrated why the double square root (SQRT) transformation is recommended for transforming exponentially-distributed data to normal for SPC application like I chart, EWMA and CUSUM chart. Moreover, some advanced techniques for Shewhart control chart can be applied, such as using synthetic control chart which combines Shewhart with EWMA scheme. These will be presented in the next section.

2.2 Some Advanced Design Schemes for TBE Charts

2.2.1 Extensions of the CCC & CQC Chart

Studies found that the conventional CCC charting technique, in which a point is plotted whenever a nonconforming item is observed, is not sensitive enough to detect small changes in the process fraction non-conforming. Therefore, the idea of CCC chart was extended to monitoring the cumulative count of conforming items until obtaining a fixed number of non-conforming items. This extended chart is referred to as a CCC-*r* chart, which is based on negative binomial distribution, where *r* is the

number of non-conforming items observed before a point is plotted, see Xie *et al.* (1999) and Ohta *et al.* (2001).

For an acceptable probability of false alarm α, let *p* be the probability that an item is nonconforming, the control limits of CCC-*r* chart can be obtained by solving the following equations,

$$\begin{aligned} F(UCL, r, p) &= \sum_{i=r}^{UCL} \binom{i-1}{r-1} p^r (1-p)^{i-r} = 1 - \frac{\alpha}{2} \\ F(CL, r, p) &= \sum_{i=r}^{CL} \binom{i-1}{r-1} p^r (1-p)^{i-r} = \frac{1}{2} \\ F(LCL, r, p) &= \sum_{i=r}^{LCL} \binom{i-1}{r-1} p^r (1-p)^{i-r} = \frac{\alpha}{2} \end{aligned} \tag{2.12}$$

Similar to the idea of CCC-*r* chart, CQC-*r* chart was proposed to monitor the time between *r* defects/events based on Gamma distribution. This approach gives more credibility to the decision regarding the statistical control of the process as the decision is made on the basis of *r* points rather than a single point.

Given acceptable probability false alarm α, the control limits UCL_r, CL_r, LCL_r of CQC-*r* chart can be calculated using the following equations,

$$\begin{aligned} F(UCL_r, r, \lambda) &= 1 - \sum_{k=0}^{r-1} e^{-\lambda \cdot UCL_r} \frac{(\lambda \cdot UCL_r)^k}{k!} = 1 - \frac{\alpha}{2} \\ F(CL_r, r, \lambda) &= 1 - \sum_{k=0}^{r-1} e^{-\lambda \cdot CL_r} \frac{(\lambda \cdot CL_r)^k}{k!} = \frac{1}{2} \\ F(LCL_r, r, \lambda) &= 1 - \sum_{k=0}^{r-1} e^{-\lambda \cdot LCL_r} \frac{(\lambda \cdot LCL_r)^k}{k!} = \frac{\alpha}{2} \end{aligned} \tag{2.13}$$

where λ and *r* are the parameters of Gamma distribution.

A disadvantage of the CQC-*r* chart compared with the CQC chart is that the average time taken to plot a point increases with *r*. Another problem is that the Average Time to Signal (ATS) increases as the process improves beyond a certain level. This problem also exists for the CQC chart. However, it is more significant in the case of CQC-*r* chart due to the effect of *r*.

2.2.2 ARL-unbiased Design

An undesirable feature of the CCC chart is that the average time to give an alarm may initially increase when the process deteriorates, i.e., the ARL achieves its maximum value at process FNC level which is a bit lower than the in-control FNC. In order to solve this problem, Xie *et al.* (2000) proposed a modified CCC chart with adjusted control limits either to minimize the undesirable increasing ARL area or to maximize the ARL at the desired process average. The new control limits can be derived by multiplying the probability limits with a constant adjustment factor γ_α, where

$$\gamma_\alpha = \ln\left[\frac{\ln(1-\alpha/2)}{\ln(\alpha/2)}\right] \Big/ \ln\left[\frac{(\alpha/2)}{(1-\alpha/2)}\right] \tag{2.14}$$

With similar motivation, Zhang *et al*. (2004) proposed another improvement design of CCC chart, which results in a nearly ARL-unbiased design. In their design, possible design parameters (LCL, UCL) are first found so that the probability

$$P\{X < LCL\} + P\{X > UCL\} = 1 - \left[(1-p)^{LCL} - (1-p)^{UCL-1}\right] \tag{2.15}$$

is most nearly equal to α.

Let (LCL, UCL) $\in C$ and set

$$\rho^* = \left[1 - \left(\frac{LCL}{1+UCL}\right)^{\frac{1}{UCL-LCL+1}}\right] \Big/ p \tag{2.16}$$

where ρ is the ratio of out-of-control FNC and in-control FNC ($\rho = p'/p$). Then ARL (ρ) attains the maximum value at ρ^*. If a certain pair of control limits (LCL, UCL) $\in C$, and ρ^* equals 1, then the pair of (LCL, UCL) is the ARL-unbiased design. This method is much more tedious compared with the method proposed by Xie *et al.* (2000). On the other hand, they proposed another optimal design method called two points criterion (TPC) design in which the CCC chart can be designed to be optimal at certain out-of-control levels. Let ARL (ρ; LCL, UCL) denotes the ARL of the CCC chart with parameters ρ, LCL, and UCL. The optimal design is that minimizing

$$ARL(1-\varepsilon_1; LCL, UCL) + ARL(1+\varepsilon_2; LCL, UCL) \tag{2.17}$$

among all possible pairs of (LCL, UCL) $\in C$, where the parameters ε_1 and ε_2 are the percentage decrease and increase, respectively, from the in-control FNC level p.

The ARL-unbiased design method proposed by Zhang *et al.* (2004) is much more complicated compared with the scheme discussed in Xie *et al.* (2000). On the other hand, it provides another design method for the CCC chart so that the optimal design can be achieved according to the specified out-of-control FNC p level and this makes the CCC chart more flexible and efficient especially when the out-of-control FNC can be well estimated.

2.2.3 Conditional Decision Procedures

For the CCC chart, since the decision is only based on a single point, it is relatively insensitive to process shifts. In order to solve this problem, Kuralmani *et al.* (2002) proposed a conditional decision procedure which adds some supplementary run rules to the decision procedure. The conditional procedure is used when the process is outside of the control limits whereas the supplementary run rules focus on the in-control situation. Besides, optimal limits are defined so that the ARL becomes the maximum when the process average is at the nominal level. The performance analysis showed that the conditional procedure can improve the sensitivity of the CCC chart without sacrificing its original in-control probability.

With the similar motivation, Chan *et al.* (1997) developed a two-stage decision procedure based on the CCC chart. The idea of this two-stage CCC chart is analogous to that of double sampling plan in acceptance sampling. The occurrence of a defective within n_1 items inspected in the first stage indicates that the process is out-of-control. If no defective occurs within n_1 items inspected, the occurrence of two defectives within the next (n_2 - n_1) items in the second stage also indicates that the process is out-of-control. The probabilities of making a false alarm at the first and second stages are equal to α_1 and α_2, respectively. This procedure combines the advantages of the CCC chart and the CCC-r chart, and also overcomes their weakness, i.e. it improves the sensitivity of the control chart while keeping the Average Number of Items Inspected (ANI) to obtain a signal short.

Lai *et al.* (2001) investigated the distributions of runs in a two-stage CCC chart. Chan *et al.* (2003) continued studying on the two-stage CCC chart, namely $CCC_{1+\gamma}$ chart,

with the same decision rules. However, the FAR of a $CCC_{1+\gamma}$ chart is set to be $(1-\gamma)\alpha$ at the first stage and $\gamma\alpha$ at the second stage. Let q=1- p. The analytic expression for the ANI of the $CCC_{1+\gamma}$ chart can be expressed by

$$ANI(p) = \frac{(1-a_1)\mu_1 + a_2\mu_2 + a_3\mu_0}{1-a_3} \tag{2.18}$$

where a_1, a_2, a_3 , μ_0, μ_1, and μ_2 can be calculated by

$$\begin{aligned} a_1 &= q^{n_1}; \\ a_2 &= q^{n_1}\left(1-q^{n_2-n_1-1}\right) - pq^{n_2-1}(n_2-n_1-1); \\ a_3 &= a_1 - a_2. \end{aligned} \tag{2.19}$$

and

$$\begin{aligned} \mu_0 &= p^{-1}q^{n_2-1}\frac{p(n_2p+1)(n_2-n_1)+q(n_2p+2)}{a_3}; \\ \mu_1 &= p^{-1}\frac{1-q^{n_1}(n_1+1-n_1q)}{1-a_1}; \\ \mu_2 &= p^{-1}q^{n_1}\frac{p((n_1+1)p+1)+q((n_1+1)p+2)}{a_2} - p^{-1}q^{n_2-1}\frac{p(n_2p+1)(n_2-n_1)+q(n_2p+2)}{a_2}. \end{aligned} \tag{2.20}$$

Furthermore, an economic model was proposed to calculate the optimal values of probabilities of false alarm set at the first and second stages of the two-stage CCC chart so that an expected total cost can be minimized.

Another conditional decision procedure is the synthetic control chart proposed by Scariano and Calzada (2003) for the monitoring of exponentially-distributed TBE. The study was motivated by Wu and Spedding (2000)'s paper on a synthetic control chart for detecting changes in the mean of a normally distributed process.

Wu and Spedding's synthetic chart integrates a Shewhart $\overline{X}$ chart with a conforming run length chart (i.e. the CCC chart) in order to detect the shift in normal process mean. The synthetic chart consists of an $\overline{X}$ /S sub-chart and a CRL/S (CRL: Conforming Run Length) sub-chart. The sample mean $\overline{X}$ is plotted in the $\overline{X}$ /S sub-chart first, and the chart continues until a point outside the UCL or LCL is found. The number of samples until the last out-of-control point is taken as CRL, and is then plotted in the CRL/S sub-chart with only LCL, and the process is still considered as in-control if the CRL is above the LCL; otherwise, an out-of-control signal will arise. The performance tests show that this synthetic chart is more effective in detecting shifts in the process mean than the Shewhart $\overline{X}$ chart, and it is even better than Shewhart $\overline{X}$ chart with run rules, the EWMA chart, and the synthetic EWMA-$\overline{X}$ chart especially when the shift is between 0.5σ and 1.5σ.

Following their procedures, Scariano and Calzada (2003) extended the synthetic chart for exponentially-distributed TBE data. The synthetic chart consists of a lower-sided Shewhart individual sub-chart and a CCC chart for tracking the number of samples observed between nonconforming observations. Hence, this synthetic chart will be useful when the increase of the events occurrence rate (i.e. the decrease of the exponential mean) is the only concern. Comparisons of the ARL for the synthetic control chart were conducted to that of the lower-sided Shewhart, lower-sided exponential EWMA and CUSUM. Results indicate that the synthetic chart outperforms the Shewhart chart for individuals, but the worst case exponential EWMA and CUSUM (Gan, 1998) are still superior for detecting the decreases in the exponential mean.

The conditional decision procedures can improve the performance as well as cost effectiveness of the charts at the expense of increasing the complexity of the implementation. Therefore, they should be used if the efficiency gain overrides the operational inconvenience caused by the conditional decision procedures.

2.2.4 Estimation Error, Inspection Error and Correlation

Woodall (1997) and Woodall & Montgomery (1999) pointed the research issue that estimation error of distribution parameters, as well as the inspection error, would affect the performance of control charts. Chen (1997) discussed the mean and standard deviation of the run length distribution of $\overline{X}$ charts when control limits are estimated. Later, Chen (1998) also studied the run length distribution of R, s, and s^2 control charts when σ is estimated. Besides, Braun (1999) investigated the effect of estimation error on the run length distributions for attribute charts. Jones (2002) looked into the estimation problem in EWMA chart and developed the design procedures for EWMA control charts that do not require the assumption of known parameters to achieve a specified ARL.

As for the TBE control chart, Yang *et al.* (2002) investigated the performance of CCC charts with estimated control limits. The error in estimated control limits is caused by the estimation error of FNC p, which in turn is attributed to the limited sample size used to estimate FNC p. The traditional estimator used is:

$$\hat{p}_0 = \frac{r}{n} \tag{2.21}$$

where r is the number of nonconforming items and n is the total number of items sampled. The effect of value of n was examined and results indicate that the true false alarm rate can deviate significantly from its desired value when the above estimator is used, especially when p_0 is small and the sample size n is not large enough. In their study, explicit equations for the false alarm probability and run length distribution were derived with estimated limits. The alternative measures of run length that show much faster detection of process deterioration are also introduced.

Another factor that may influence the performance of control chart is the inspection error. Collins & Case (1978) studied the performance of p chart under inspection error, and Suich (1988) investigated the case of c chart with consideration of inspection error. The similar studies also go for TBE charts. Ranjan *et al.* (2003) investigated the effect of inspection errors for the CCC chart and discussed the method of setting optimal control limits for CCC charts so as to maximize the average run length when the process is at the normal level. Let p_t denote the probability of non-conforming, and it can be represented as

$$p_t = (p_0 - \theta)/(1 - \theta - \psi) \tag{2.22}$$

Where p_0 is the estimated nonconforming fraction, θ is the probability of classifying a conforming item as non-conforming, and ψ is the probability of classifying a non-conforming item as conforming. The adjusted UCL and LCL can be shown as

$$UCL_p = \left\{ \ln\left(\frac{0.5\alpha p_t}{(1-\psi)p_t + (1-p_t)\theta} \right) \ln\left[\frac{\ln\{(1-\alpha p_t/2p_0)/(1-p_0)\}}{\ln(\alpha p_t/2p_0)} \right] \right\} \times \left\{ \ln\left[1-(1-\psi)p_t-(1-p_t)\theta\right] \ln\left[\frac{(\alpha p_t/2p_0)(1-p_0)}{(1-\alpha p_t/2p_0)} \right] \right\}^{-1} \tag{2.23}$$

and

$$LCL_p = \left\{ \ln\left(1 - \frac{0.5\alpha p_t}{(1-\psi)p_t + (1-p_t)\theta}\right) \ln\left[\frac{\ln\{(1-\alpha p_t/2p_0)/(1-p_0)\}}{\ln(\alpha p_t/2p_0)}\right]\right\} \times \left\{ \ln[1-(1-\psi)p_t - (1-p_t)\theta] \ln\left[\frac{(\alpha p_t/2p_0)(1-p_0)}{(1-\alpha p_t/2p_0)}\right]\right\}^{-1} \quad (2.24)$$

The new control limits that take into account the presence of inspection errors is actually the old control limits multiplied by an adjustment factor A_f, which can be shown as

$$A_f = \left\{ \ln\left[\frac{\ln\{(1-\alpha p_t/2p_0)/(1-p_0)\}}{\ln(\alpha p_t/2p_0)}\right]\right\} \cdot \left\{ \ln\left[\frac{(\alpha p_t/2p_0)(1-p_0)}{(1-\alpha p_t/2p_0)}\right]\right\}^{-1} \quad (2.25)$$

On the other hand, Tang and Cheong (2006) investigated the design of CCC chart when the inspections are taken in groups and the output characteristic within a group is correlated. The performance of the proposed scheme in terms of ARL and ATS is derived with a Markov model, and the effects of correlation and sample size are also discussed.

2.2.5 Monitoring TBE Data Following Weibull Distribution

Most of the studies on TBE monitoring, as discussed above, are based on the assumption that the TBE data follow exponential distribution. However, this is not always true. For example, in reliability monitoring, inter-failure time is usually modeled by Weibull distribution. Actually, Weibull distribution is a more general case compared with exponential distribution as it can take into consideration the increasing or decreasing as well as constant events occurrence rate.

Nelson (1979) designed a set of control charts for Weibull processes with standards given. The median chart, range chart, location chart, and scale chart were used at the same time to monitor Weibull processes. Bai & Choi (1995) described the design method of $\overline{X}$ and R chart for skewed population like exponential or Weibull distribution. Ramalhoto & Morais (1999) proposed the Shewhart control chart for monitoring scale parameter of a Weibull control variable with fixed and variable sampling intervals.

Xie *et al.* (2002b) developed a charting method, named *t*-chart, for monitoring Weibull distributed time between failures based on probability limits. Let X_1, X_2, …denote a sequence of time between events data, which are independent Weibull random variables with probability density function:

$$f(x) = \frac{\eta}{\theta}\left(\frac{x}{\theta}\right)^{\eta-1} e^{-\left(\frac{x}{\theta}\right)^{\eta}}, x > 0, \theta > 0, \delta > 0 \tag{2.26}$$

where θ and η are the scale parameter and shape parameter, respectively. The cumulative density function is

$$F(x) = 1 - \exp\left[-\left(\frac{x}{\theta}\right)^{\eta}\right], x > 0 \tag{2.27}$$

Given acceptable probability of false alarm α, the probability control limits UCL, CL, and LCL can be calculated as,

$$UCL = \theta\left[\ln\left(\frac{2}{\alpha}\right)\right]^{1/\eta}, CL = \theta[\ln(2)]^{1/\eta}, LCL = \theta\left[\ln\left(\frac{2}{2-\alpha}\right)\right]^{1/\eta} \tag{2.28}$$

Furthermore, a new procedure based on the monitoring of time between r failures, named t_r-chart, was also proposed in order to improve the sensitivity to process shift. Here the Erlang distribution was used to model the time until the occurrence of r failures in a Poisson process. Note that Erlang distribution is a special case of the Gamma distribution, and the probability control limits of t_r-chart is the same as that of the CQC-r chart mentioned above. This new procedure has the advantage of being able to detect process improvement as well as deterioration compared to traditional Shewhart attribute charts.

Xie *et al.* (2002b) also investigated the ARL properties when only shape or scale parameter changes, and both of them change at the same time. The results showed that when shape parameter is not very small, the t-chart is able to detect the increase or decrease of scale parameter. However, when the shape parameter shifts from the original value, this chart can only detect the decrease of shape parameter, and the increasing shift cannot be detected effectively. On the other hand, Kanji and Arif (2001) proposed a control chart, referred to as Median rankit control chart, to monitor Weibull data by using quantile approach.

The Cumulative Sum (CUSUM) and Exponentially Weighted Moving Average (EWMA) charts can also be applied for monitoring Weibull-distributed data. Johnson (1966) developed a V-mask CUSUM method for controlling the scale change of a Weibull distribution. Chang and Bai (2001) proposed a heuristic method of constructing $\overline{X}$, CUSUM, and EWMA charts for skewed populations with weighted standard deviations obtained by decomposing the standard deviation into upper and

lower deviations adjusted in accordance with the direction and degree of skewness. This method can be used for TBE data that follow exponential, Weibull, or Gamma distribution. Hawkins and Olwell (1998) provided the optimal design of CUSUM for Weibull data with fixed shape parameter based on Wald's sequential probability ratio test (SPRT) theory. Borror *et al.* (2003) investigated the robustness of TBE CUSUM for Weibull-distributed and Lognormal-distributed TBE data. However, they use the same design approach as well as ARL calculation method as shown in Lucas (1985). Another limitation of their study is that they fixed the scale parameter and only let the shape parameter changes when evaluating the ARL performances of TBE CUSUM for Weibull distributed data. However, the scale parameter is more likely to change when the process shifts from the target level. Few methods have been proposed using EWMA chart. Zhang and Chen (2004) developed a lower-sided and upper-sided EWMA chart for detecting mean changes of censored Weibull lifetimes with fixed censoring rate and shape parameter.

Since the monitoring techniques based on exponential-distributed TBE data is relatively well developed, another way to monitor Weibull distributed TBE data is to transform Weibull to exponential and then do the monitoring and analysis. Xie *et al.* (2000b) discussed the Weibull-to-exponential transformation when the mean time to failure or reliability is to be estimated, and investigated the effect of mis-specification of shape parameter. Transforming Weibull to normal is another possible approach to the monitoring of Weibull-distributed TBE with the help of well-designed control charts for normal.

2.2.6 Artificial Neural Network-based Procedure

Recently, Artificial Neural Networks (ANN) techniques have been introduced to the quality control area for the purpose of improving the efficiency and intelligence of process control (Guh, 2003; Guh, 2005; Guh and Shiue, 2005). The advantages of applying ANN to control charts analysis consist of the following: first, neural networks have the ability to learn the relationships through the data themselves rather than assuming probability distributions. Meanwhile, neural networks can handle multiple related or non-related inputs and outputs simultaneously. Besides, the performance of neural networks can be improved by performing incremental training, as more data become available.

The application of ANN approach to the TBE chart was explored by Cheng & Cheng (2001). They proposed a three-layer fully connected feed-forward network with a back-propagation training rule which can be used in combination with exponential CUSUM for the monitoring of exponential TBE mean. The performance of the neutral network is evaluated on the basis of ARL, and the sensitivity analysis for neural network was also performed for different in-control ARL values, and different exponential events occurrence rate. The results obtained with simulated data suggest that using exponential CUSUM chart and neural network together is feasible and significantly more sensitive to process shifts than the exponential CUSUM chart.

2.2.7 Economic Design of TBE Charts

Economic design of control charts attracts great interests from researchers with the growing concern on the production cost. Much research regarding the economic design was initiated from the time-between-events point of view. A common assumption is

that the sample average X-bar and the process in-control time follow normal and exponential distributions, respectively (see, for example, Duncan, 1956). Recent research on economic design of control charts extends the scope to adaptive control charts (Stoumbos and Reynolds, 2005; Yu and Chen, 2005), control chart for correlated or non-normal data (Chou *et al.*, 2001; Chen, 2004), multivariate control charts (Chen, 2006), control charts with multiple assignable causes or Weibull in-control time (Yang and Rahim, 2005; Chen and Cheng , 2006), etc.

The economic design of geometric TBE chart as first studied by Xie *et al.* (1997), was further developed by Tang *et al.* (2000), Xie *et al*.(2001). The economic design of geometric TBE chart was based on the Lorenzen and Vance (1986) model which involves cost considerations and can be applied to all control charts regardless of the monitoring statistic. In their study, the selection of design parameters is investigated from an economic point of view, and the sampling interval and the control limit for CCC charts were studied. A simplified procedure is used to derive the optimum setting of sampling and control parameters. Moreover, Tang *et al.* (2000) also proposed an economic-statistical model for CCC chart. The idea of economic-statistical design is to minimize the cost of control charts while keeping reasonable Type I and II error probabilities (in-control ARL and out-of-control ARL).

Ohta *et al.* (2001) also discussed the economic design of CCC-*r* chart, and proposed a simplified optimal method for the design of a CCC-*r* chart by applying Collani and Drager's economic design method for control charts that monitor discrete quality characteristics.

The economic design of exponential TBE charts was studied by Zhang *et al.* (2005). The economic model was described and the performance of the chart was evaluated in terms of ATS. An economic-statistical design approach was interpreted from a multi-objective optimization viewpoint. The performance of exponential TBE chart based on economic design was compared to those based on statistical design, and economic-statistical design. Results show that the economic-statistical design of exponential charts is virtually a multi-objective approach and has reasonably good statistical performance especially when the cost of false alarm and assignable causes is difficult to estimate.

2.3 Summary

In this chapter, the basic TBE charts and some advanced design schemes are substantially reviewed. The initial study on the TBE monitoring started with the CCC chart based on discrete TBE data, and then extended to the monitoring of continuous TBE with CQC chart, CUSUM or EWMA chart. The advanced design schemes considered the biased ARL problem, the estimation error, the inspection error, the correlation within the sample, etc., and made the TBE chart more applicable and efficient for practical situations. However, there are still some problems unsolved which motivate the study involved in this dissertation.

As can be seen from the previous sections, each TBE chart has its advantages, weaknesses and applicable conditions. Therefore, the choice and application of these control charts need to be carefully examined according to the particular conditions of the process where the control charts need to be applied. The first and most important step is to test the distribution of the TBE chart. As indicated from the review, most of

the TBE charts are set up based on either discrete TBE distributions like geometric or negative binomial, or continuous TBE, e.g. exponential, Gamma, Weibull or lognormal. Table 2.1 summarizes the possible charts that can be used for different TBE distributions. On the other hand, if the TBE data do not follow any of the distributions mentioned above, transformations can be employed to transform it to a proper distribution and then apply the TBE charts.

Table 2.1 Summary of TBE charts

Data type	Distributions	Probability limits	CUSUM	EWMA	Shewhart charts
Discrete	Geometric	CCC (Calvin,1983;Goh,1987; Bourke,1991) CPC (Chan *et al.*,2002)	Geometric CUSUM (Bourke,2001)	Geometric EWMA (Sun & Zhang,2000)	p, np, c or u chart (Radaelli, 1998; Kittlitz , 1999; Nelson, 1994; McCool & Joyner-Motley, 1998)
	Negative binomial	CCC-r (Xie *et al.* ,1999; Ohta *et al.* , 2001).			
Continuous	Exponential	CQC (Chan *et al.*,2000) CPC (Chan *et al.*,2002)	Exponential CUSUM (Vardeman & Ray, 1985; Lucas, 1985; Gan,1994)	Exponential EWMA (Gan,1998)	
	Gamma	CQC-r (Xie *et al.*,2002b)			
	Weibull	CQC (Xie *et al.*,2002b)	TBE CUSUM (Borror *et al.* 2003) Weibull CUSUM (Hawkins & Olwell, 1998)		
	Lognormal	CQC (Xie *et al.*,2002b)	TBE CUSUM (Borror *et al.* 2003)		

Another important consideration when choosing a suitable chart is the performance. It is hard if not impossible to design a control chart so that it has the best performance for all situations. The users may choose a TBE chart which performs best under the condition which is most compatible to the practical situation. Chapter 3 is motivated by this problem, and several most typical TBE charts are compared in order to provide some insights and guidelines for the users on how to find out the most suitable TBE charts for different situations.

Chapter 3 A Comparative Study of Exponential Time Between Events Charts

3.1 Introduction

As discussed in Chapter 1, control charts for attributes have been popularly adopted for monitoring the fraction nonconforming (*p*-chart) or nonconformities (*c*-chart or *u*-chart) in a process. However, they may face some practical problems when the process fraction of nonconforming is very low, say, at ppm or even ppb levels. A good solution to those problems is to employ TBE charts.

A common assumption for TBE charts is that the occurrence of events can be modeled by a homogeneous Poisson process, and thus the time between two successive events follows exponential distribution. Based on this assumption some TBE charts, referred to as Conforming Run Length (CRL) charts, are designed for discrete TBE data based on geometric or negative binomial distribution. Other TBE charts are designed for monitoring continuous TBE data based on exponential distribution.

All these TBE charts show some advantages in one way or another. Some comparing studies have been carried out for discrete TBE charts. Xie *et al.* (1998) did a comparative study between the CCC and CUSUM charts. Borror *et al.* (1998) compared the ARL of the Poisson EWMA with that of the Shewhart c-chart. Wu *et al.* (2000) compared the design and performance of the *np* chart, CRL-CUSUM and SCRL (Sum of CRLs) chart for discrete TBE data. Sun & Zhang (2000) conducted a

comparative study using discrete TBE data on the CUSUM, the EWMA chart, and the two-stage CCC chart proposed in Chan *et al.* (1997). On the other hand, even though the continuous TBE charts represent more general cases compared to the discrete TBE charts, little literature is available on their relative performance. Gan (1998) compared the ARL performance of exponential EWMA with that of the exponential CUSUM and Shewhart charts. The results indicated that the Shewhart chart is highly insensitive compared to the exponential EWMA or CUSUM chart. Ranjan *et al.* (2003) looked into the CQC chart, CQC-*r* chart and exponential CUSUM chart and compared their performance based on Average Time to Signal (ATS).

This chapter extends the comparisons to a wider range, and compares the performance of continuous TBE charts among the CQC chart, CQC-*r* chart, exponential EWMA and exponential CUSUM chart based on ATS performance. These TBE charts are referred to as exponential TBE charts since all of them are set up based on exponential distribution. The purpose of this study was to investigate the comparative performance of different exponential TBE charts and provide some insights of their strengths as well as shortcomings. The results will be useful for the quality engineers on the implementation of TBE charts under different situations.

A uniform model of the exponential TBE charts involved in this study is that the occurrence of events is modeled by a Poisson process, and the time between events X_i (i= 1, 2,…) are independent and identically distributed exponential random variables with probability density function:

$$f(x) = \begin{cases} \theta^{-1} e^{-\frac{x}{\theta}}, if \;\; x \geq 0 \\ 0, \quad otherwise \end{cases} \tag{3.1}$$

where θ is the reciprocal of the events occurrence rate, i.e. the mean of the time between events data.

3.2 ATS Properties of TBE Charts

The ARL is one of the most frequently used criteria to measure the performance of control charts. However, it is not a good measurement for TBE charts because the time spent on plotting each point is different, and the ARL does not consider the time factor. A better alternative is the ATS, which is defined as the expected value of total length of time to observe an out-of-control point.

Let S be the total amount of time before an out-of-control signal occurs. Then it is obvious that $S = \sum_{i=1}^{R} X_i$, where R is the number of points plotted on the chart until an out-of-control signal occurs. Using Wald's identity, the ATS of the CQC-r chart can be calculated as:

$$ATS_{CQC-r} = E(S) = E\left(\sum_{i=1}^{R} X_i\right) = E(R)E(X) = ARL \cdot \frac{r}{\lambda} = \frac{r}{\lambda(1-\beta)} = \frac{r\theta}{1-\beta} \qquad (3.2)$$

where β denotes the type II error of the CQC-r chart, λ is the event occurrence rate of the Poisson process, and θ is the reciprocal of λ, i.e. the mean of time between events data.

Since the time between r events follows Gamma distribution, the type II error β can be calculated as:

$$\beta = \sum_{k=0}^{r-1} e^{-\frac{LCL_r}{\theta}} \frac{(LCL_r)^k}{\theta^k k!} - \sum_{k=0}^{r-1} e^{-\frac{UCL_r}{\theta}} \frac{(UCL_r)^k}{\theta^k k!} \tag{3.3}$$

Substituting the values of β into equation (3.2), ATS of CQC-*r* chart is obtained as:

$$ATS_{CQC-r} = \frac{r \cdot \theta}{1 - \sum_{k=0}^{r-1} e^{-\frac{LCL_r}{\theta}} \frac{(LCL_r)^k}{\theta^k k!} + \sum_{k=0}^{r-1} e^{-\frac{UCL_r}{\theta}} \frac{(UCL_r)^k}{\theta^k k!}} \tag{3.4}$$

Using similar deduction method, the expression of ATS for exponential EWMA and exponential CUSUM can be derived as

$$\begin{aligned} ATS_{EWMA} &= E(S) = E(\sum_{i=1}^{R} X_i) = E(R)E(X) = ARL_{EWMA} \times \frac{1}{\lambda} = ARL_{EWMA} \cdot \theta \\ ATS_{CUSUM} &= E(S) = E(\sum_{i=1}^{R} X_i) = E(R)E(X) = ARL_{CUSUM} \times \frac{1}{\lambda} = ARL_{CUSUM} \cdot \theta \end{aligned} \tag{3.5}$$

Here in this study the exact methods of computing ARL are used following the methods shown in Gan (1998) for exponential EWMA and Vardeman and Ray (1985) for exponential CUSUM.

When detecting the process improvement or deterioration separately, the one-sided CQC and CQC-*r* chart are used instead of two-sided charts. The control limits of the lower-sided and the upper-sided CQC-*r* chart can be calculated by solving the following equations:

$$\begin{aligned} F(LCL_r', r, \theta) &= 1 - \sum_{k=0}^{r-1} e^{-\frac{LCL_r'}{\theta}} \frac{(LCL_r')^k}{\theta^k k!} = \alpha, \\ F(UCL_r', r, \theta) &= 1 - \sum_{k=0}^{r-1} e^{-\frac{UCL_r'}{\theta}} \frac{(UCL_r')^k}{\theta^k k!} = 1 - \alpha. \end{aligned} \tag{3.6}$$

Accordingly, the ATS for lower-sided CQC-*r* chart can be expressed as:

$$ATS_{CQC-r}^{L} = \frac{r}{\lambda F(LCL_r', r, \theta)} = \frac{r \cdot \theta}{1 - \sum_{k=0}^{r-1} e^{-\frac{LCL_r'}{\theta}} \frac{(LCL_r')^k}{\theta^k k!}} \tag{3.7}$$

and the ATS for upper-sided CQC-*r* chart can be expressed as:

$$ATS_{CQC-r}^{U} = \frac{r}{\lambda[1 - F(UCL_r', r, \theta)]} = \frac{r\theta}{\sum_{k=0}^{r-1} e^{-\frac{UCL_r'}{\theta}} \frac{(UCL_r')^k}{\theta^k k!}} \tag{3.8}$$

The control limits and the *ATS* formulae for CQC chart can be computed from (3.6), (3.7) and (3.8) for $r = 1$.

3.3 Comparisons of Performance

A series of comparative study have been done on the performance of these continuous exponential TBE charts, i.e. CQC chart, CQC-*r* chart, exponential CUSUM chart and exponential EWMA chart, with different design parameters combinations. Some representative results from the study is shown in this section, which reveal some insights of relative performance of these control charts.

3.3.1 Upper-sided TBE Charts

The upper-sided TBE chart is designed for monitoring process improvements. In order to assess the relative performance of upper-sided CQC-*r* chart (r =1, 2, 3, and 4), exponential EWMA and exponential CUSUM charts, the ATS performances of these exponential TBE charts are compared. In this comparison the in-control ATS value (ATS_0) is set to be the same (ATS_0=500), and the out-of-control ATS (ATS_1) values for

different shifts are then calculated. The in-control mean of TBE data is assumed to be 1 (θ_0=1.00), and the exponential EWMA chart and CUSUM chart are designed to be optimal in detecting the out-of-control TBE mean θ_1 of 2.00 and 5.00, respectively. The ATS values of the CQC-*r* chart, exponential EWMA and exponential CUSUM charts are listed in Table 3.1. The ATS curves of the CQC, CQC-*r* (r =4), exponential EWMA, and CUSUM charts are displayed in Figure 3.1.

It can be seen from Table 3.1 and Figure 3.1 that the exponential EWMA and CUSUM charts outperform the CQC-*r* charts at all shifts levels listed in Table 3.1. When detecting the shifts at designed optimal level, exponential EWMA and CUSUM show similar performance. On the other hand, when the shift is relatively small and moderate, the exponential EWMA chart shows better performance than the exponential CUSUM chart; and when the shift is large (up to 5 times of the in-control value and above), the exponential CUSUM chart is slightly better than the exponential EWMA chart .

For the CQC-*r* charts, when the shift is small, the larger the value of *r*, the better the performance of the chart is. When the shift becomes large, the CQC chart with a smaller *r* value will be better than the CQC chart with a larger *r* value. It also shows that when the mean of TBE θ increases, the ATS of the CQC chart decreases faster than that of the CQC-*r* charts, and thus make the CQC chart more sensitive to large process improvement.

To investigate the effect of different in-control ATS levels, which also represent different false alarm rate α, the above exponential TBE charts with in-control ATS of

370.37 are compared again and the corresponding ATS values are listed in Table 3.2. The in-control TBE mean is assumed to be 1 (θ_0=1.00), and the exponential EWMA chart and CUSUM chart are designed to be optimal in detecting the out-of-control TBE mean θ_1 of 3.00 and 4.00, respectively. Note that the exponential EWMA and CUSUM charts are designed such that the ATS may not be exactly equal to, however the values are very close to 370.37. The results are shown in Table 3.2 and Figure 3.2.

Table 3.1 ATS values of upper-sided CQC-*r* (*r* =1, 2, 3, 4) chart, exponential EWMA and exponential CUSUM charts (ATS_0 = 500)

θ	CQC α=0.002 UCL=6.21	CQC-2 α=0.004 UCL=7.68	CQC-3 α=0.006 UCL=9.05	CQC-4 α=0.008 UCL=10.35	EWMA1 λ_Q=0.10 h_Q=1.71 Q_0=1.00 θ_1=2.00	CUSUM1 k_S=1.39 h_S=7.42 S_0=1.00 θ_1=2.00	EWMA2 λ_Q=0.27 h_Q=2.60 Q_0=1.01 θ_1=5.00	CUSUM2 k_S=2.01 h_S=4.86 S_0=0.25 θ_1=5.00
1.00	500.00	500.00	500.00	500.00	500.00	500.00	500.00	500.00
1.02	451.46	446.43	442.45	439.08	411.16	419.93	433.09	440.13
1.04	409.42	400.61	393.73	388.02	342.68	356.10	377.73	389.58
1.10	312.59	297.48	286.13	277.02	212.96	228.80	260.59	278.41
1.20	212.96	195.59	183.19	173.66	116.64	127.32	156.60	173.40
1.30	154.90	138.72	127.64	119.43	75.92	82.55	104.65	117.91
1.50	94.49	82.16	74.29	68.81	43.80	46.20	58.65	66.15
2.00	**44.72**	**38.49**	**35.10**	**33.13**	**24.20**	**24.20**	28.00	30.20
5.00	**17.33**	**18.33**	**20.60**	**23.69**	16.00	15.50	**15.00**	**15.00**
10.00	18.62	24.39	32.04	40.87	19.00	19.00	18.00	18.00

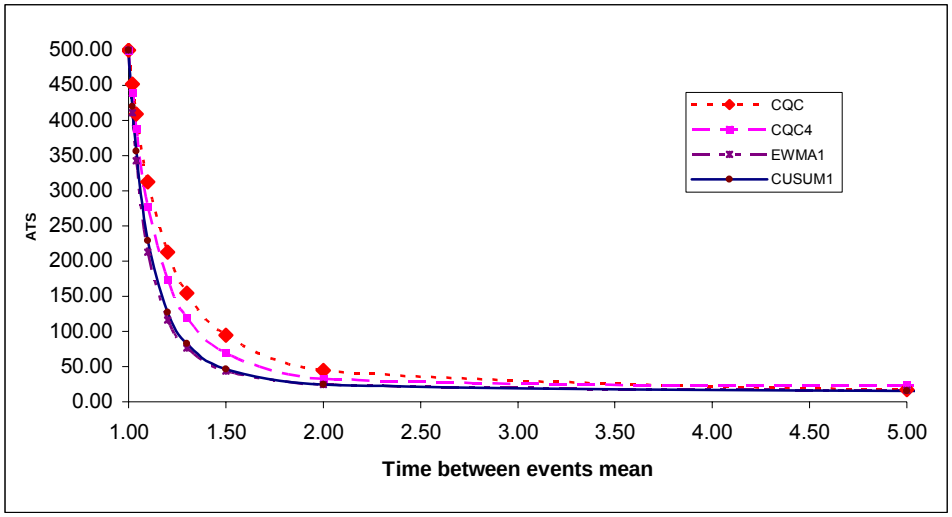

Figure 3.1 ATS curves for upper-sided CQC, CQC-*4*, exponential CUSUM and EWMA charts ($ATS_0 = 500$)

Comparing the results in Table 3.1 and Table 3.2, we notice that the superiority of exponential EWMA and CUSUM charts in ATS will be less obvious when the in-control ATS decreases from 500 to 370.37. Exponential EWMA and exponential CUSUM charts outperform and CQC-*r* charts when the upper shifts are small, while the superiority in ATS become less significant when the TBE mean increases up to 3 or 4 times of the in-control mean. Another interesting finding is that when the shift is up to 3.50 and above, the CQC chart shows better ATS performance compared to the CQC-*r* chart with r =2, 3, or 4. Therefore, the CQC chart is desirable when the shift is relatively large, and CQC-*r* charts can be employed when the shift is small.

Table 3.2 ATS values of upper-sided CQC-*r* (*r* =1, 2, 3, 4) chart, exponential EWMA and CUSUM charts (ATS_0 = 370.37)

θ	CQC α=0.0027 UCL=5.9145	CQC-2 α=0.0054 UCL=7.3428	CQC-3 α=0.0081 UCL=8.6718	CQC-4 α=0.0108 UCL=9.94	EWMA1 λ_Q=0.167 h_Q=2.00 Q_0=0.50 θ_1=3.00	EWMA2 λ_Q=0.229 h_Q=2.30 Q_0=0.50 θ_1=4.00	CUSUM1 k_S=1.648 h_S=5.473 S_0=0.00 θ_1=3.00	CUSUM2 k_S=1.848 h_S=4.86 S_0=0.00 θ_1=4.00
1.00	370.37	370.37	370.37	370.37	370.22	370.22	370.49	370.01
1.10	237.96	227.17	219.10	212.68	186.33	196.053	200.62	209.528
1.20	165.85	153.19	144.20	137.33	112.4	120.732	123.79	132.924
1.30	122.97	110.99	102.83	96.82	77.194	83.135	84.539	92.131
1.40	95.69	85.00	78.00	73.01	58.142	62.188	62.454	68.446
1.60	64.49	56.35	51.36	48.04	39.504	41.264	40.352	44.032
1.80	48.12	41.89	38.33	36.15	31.014	31.626	30.276	32.598
2.00	38.49	33.66	31.10	29.71	26.42	26.4	24.88	26.4
2.50	26.63	23.95	22.96	22.82	21.15	20.45	18.875	19.425
3.00	**21.54**	**20.12**	**20.08**	**20.78**	**19.05**	18.12	**16.59**	16.77
3.50	18.97	18.41	19.11	20.50	18.095	17.08	15.575	15.54
4.00	**17.55**	**17.69**	**19.01**	**21.03**	17.68	**10.28**	15.12	**15.00**

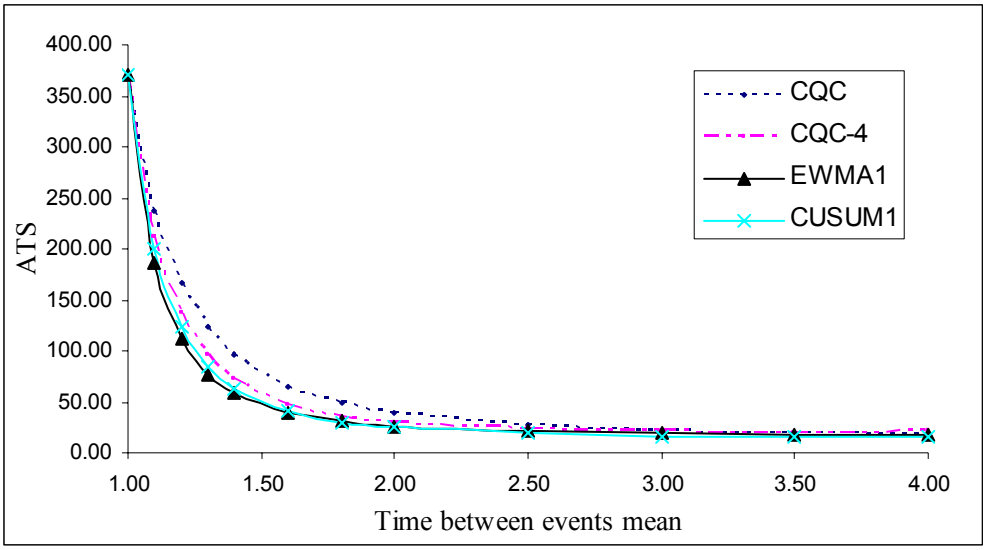

Figure 3.2 ATS curves for upper-sided CQC, CQC-4, exponential CUSUM and EWMA charts (ATS_0 = 370.37)

3.3.2 Lower-sided TBE Charts

Lower-sided TBE charts are employed to detect process deteriorations. Using the similar analysis method as the above, the in-control ATS value is assumed to be 500, and the out-of-control ATS values of the CQC-*r* chart (*r* =1, 2, 3, 4), exponential EWMA and exponential CUSUM charts for different shifts are compared. Again, the in-control mean of TBE data is assumed to be 1 (θ_0= 1.00), and the exponential EWMA chart and exponential CUSUM chart are designed to detect the out-of-control TBE mean of 0.50 and 0.20, respectively. Table 3.3 shows the ATS values of the CQC-*r*, exponential EWMA and exponential CUSUM charts.

Table 3.3 shows that for the intended design shifts, the exponential CUSUM charts outperform the exponential EWMA charts, and the exponential EWMA charts show better ATS performance than the CQC-*r* charts. However, when the process shift is relatively small, exponential EWMA charts show better performance than the CUSUM charts, and CUSUM charts outperform the CQC-*r* charts (including the CQC chart). When detecting large shifts, say, one tenth of the in-control mean, all these exponential TBE charts have similar ATS performance except for the CQC chart. For the CQC-*r* chart, the larger the value of *r*, the better the performance of the chart is at the expense of larger probability of false alarms. Therefore, we suggest using exponential EWMA or exponential CUSUM chart when the shift is relatively small and choosing CQC-*r* chart when the shift is large.

Table 3.3 ATS values of lower-sided CQC-*r* (*r* =1, 2, 3, 4) chart, exponential EWMA and exponential CUSUM charts (ATS_0 = 500)

θ	CQC α=0.002 LCL=0.002	CQC-2 α=0.004 LCL=0.092	CQC-3 α=0.006 LCL=0.361	CQC-4 α=0.008 LCL=0.771	EWMA λ_q=0.10 h_q=0.55 q_0=1.00 θ_1=0.50	CUSUM k_T=0.69 h_T=4.16 T_0=-0.78 θ_1=0.50	EWMA λ_q=0.33 h_q=0.25 q_0=0.98 θ_1=0.20	CUSUM k_T=0.40 h_T=1.24 T_0=-0.14 θ_1=0.20
1.00	500.00	500.00	500.00	500.00	500.00	500.00	500.00	500.00
0.95	451.27	430.08	412.98	399.28	297.73	320.72	358.53	379.62
0.90	405.04	366.99	337.87	315.55	181.26	204.84	255.24	284.49
0.85	361.31	310.39	273.51	246.54	113.22	130.90	180.37	210.38
0.80	320.08	259.94	218.83	190.23	72.80	84.08	126.64	153.28
0.70	245.10	176.04	134.47	108.47	32.97	36.12	61.32	77.63
0.60	180.12	112.47	77.27	57.75	16.74	16.98	29.16	36.84
0.50	**125.12**	**66.42**	**40.66**	**28.19**	**9.30**	**8.80**	13.75	16.45
0.20	**20.08**	**5.09**	**2.22**	**1.49**	1.70	1.48	**1.36**	**1.22**
0.10	5.05	0.85	0.43	0.42	0.72	0.62	0.49	0.42

A similar comparative study is also conducted with in-control ATS of 370.37. The in-control TBE mean is assumed to be 1 (θ_0=1.00), and the exponential EWMA chart and CUSUM chart are designed to detect the out-of-control TBE mean of 0.40 and 0.30, respectively. The results are shown in Table 3.4.

From the results in Table 3.3 and Table 3.4, similar conclusions can be drawn as in the comparison of upper-sided TBE charts. The superiority of exponential EWMA and CUSUM charts in ATS will be less significant when the in-control ATS decreases from 500 to 370.37. For larger process shifts, CQC-*4* chart shows similar performance as the exponential CUSUM and EWMA charts. The performance of the CQC chart in detecting process deterioration is worse than the rest. Therefore, exponential EWMA or CUSUM should be used when the shift is small, and CQC-*r* charts can be employed when the shift is large.

Table 3.4 ATS values of lower-sided CQC-*r* (*r* =1, 2, 3, 4) chart, exponential EWMA and exponential CUSUM charts (ATS_0 = 370.37)

θ	CQC α=0.0027 LCL=0.0027	CQC-2 α=0.0054 LCL=1077	CQC-3 α=0.0081 LCL=0.4032	CQC-4 α=0.0108 LCL=0.8424	EWMA λ_q=0.152 h_q=0.4662 q_0=2.00 θ_1=0.40	EWMA λ_q=0.228 h_q=0.3632 q_0=2.00 θ_1=0.30	CUSUM k_T=0.611 h_T=2.794 T_0=0 θ_1=0.40	CUSUM k_T=0.516 h_T=1.909 T_0=0 θ_1=0.30
1.00	370.37	370.37	370.37	370.37	370.73	370.17	370.65	370.56
0.95	334.31	318.75	306.41	296.61	243.94	256.22	259.22	271.88
0.90	300.06	272.15	251.12	235.14	162.35	177.39	179.75	197.24
0.85	267.67	230.33	203.69	184.36	109.62	123.05	123.78	141.48
0.80	237.13	193.04	163.33	142.81	75.29	85.69	84.85	100.40
0.70	181.60	130.97	100.90	82.20	37.68	42.37	39.83	49.13
0.60	133.46	83.88	58.39	44.31	20.47	21.77	19.18	23.45
0.50	92.72	49.70	31.02	22.00	11.91	11.71	9.73	11.19
0.40	**59.38**	**26.35**	**14.67**	**9.85**	**7.20**	6.54	**5.21**	5.47
0.30	**33.44**	**11.79**	**5.88**	**3.87**	4.34	**3.68**	2.85	**2.74**
0.20	14.90	3.92	1.83	1.32	1.72	1.96	1.47	1.32

3.3.3 Two-sided TBE Charts

Two-sided TBE charts are preferred when both process improvement and deterioration are of interest or the direction of the shift cannot be predicted. To assess the relative performance of the two-sided TBE charts, the ATS performance of the CQC-*r* chart (*r* =1, 2, 3, 4), exponential EWMA and exponential CUSUM charts are compared. The in-control ATS value is set to be 370.37, and the in-control TBE mean is assumed to be 1 (θ_0 = 1.00). The exponential CUSUM and EWMA charts are designed to be optimal in detecting the out-of-control TBE mean θ_1 of 0.3 and 3.0, respectively. Table 3.5 presents the ATS values of the two-sided TBE charts described above.

Table 3.5 ATS values of two-sided CQC-*r* (*r* =1, 2, 3, 4) chart, exponential EWMA and CUSUM charts (ATS_0 = 370.37)

θ	CQC α=0.0027 UCL=6.608 LCL=0.001	CQC2 α=0.0054 UCL=8.125 LCL=0.075	CQC3 α=0.0081 UCL=9.534 LCL=0.313	CQC4 α=0.0108 UCL=10.875 LCL=0.687	Two-sided CUSUM θ_s=0.3 θ_T=3.0 k_s=0.516 k_T=1.648 h_s=2.20 h_T=6.5	 θ_s=0.2 θ_T=5.0 k_s=0.402 k_T=2.012 h_s=1.33 h_T=5.366	Two-sided EWMA λ=0.202 h_q=0.36 h_Q=2.35 θ_1=0.3	 λ=0.152 h_q=0.43 h_Q=2.05 θ_1=3.0
0.30	66.76	22.45	10.17	6.04	**10.46**	11.33	**14.19**	15.72
0.50	185.15	97.29	58.21	39.29	13.79	19.56	14.99	14.89
0.60	264.80	164.95	111.76	82.06	31.32	45.52	30.07	27.94
0.70	348.62	254.13	193.92	155.29	72.32	99.55	64.47	57.51
0.80	411.04	347.84	298.98	262.51	160.26	197.33	142.98	128.26
0.90	419.00	398.38	379.59	363.51	300.81	321.92	288.07	275.27
1.00	**370.35**	**370.34**	**370.37**	**370.38**	**370.66**	**370.14**	**370.85**	**370.17**
1.10	298.19	295.85	293.70	291.35	285.70	301.74	269.21	247.09
1.20	231.40	222.25	214.39	207.31	185.21	211.74	162.46	135.40
1.50	114.38	100.96	91.58	84.63	65.24	80.70	50.60	36.98
1.80	68.70	58.78	52.66	48.59	37.28	44.60	26.75	19.04
2.00	53.45	45.57	41.02	38.22	29.80	34.52	20.58	14.72
3.00	27.03	24.25	23.40	23.53	**6.29**	6.53	4.06	**2.83**

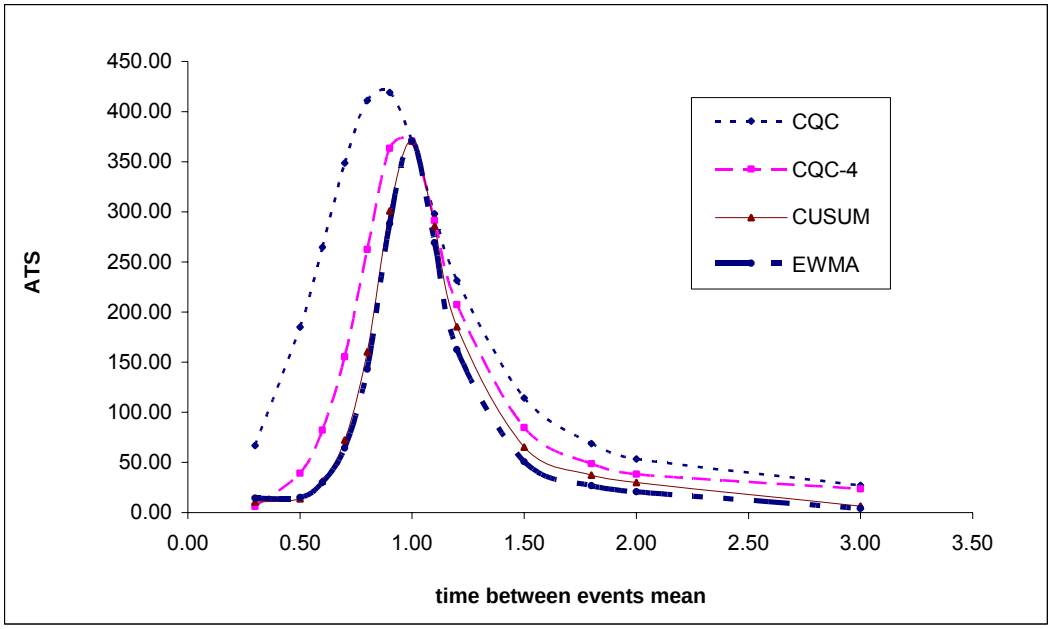

Figure 3.3 ATS curves for two-sided CQC, CQC-4, exponential CUSUM and exponential EWMA charts

Figure 3.3 displays the ATS curves for two-sided CQC, CQC-4, exponential CUSUM and exponential EWMA charts. It is obvious from Table 3.5 and Figure 3.3 that in general the exponential CUSUM and EWMA charts outperform the CQC-*r* charts. For the CQC-*r* charts, the larger the value of *r*, the better the chart performs. Moreover, when the process improves, the *r* value does not influence the ATS value a lot, while when the process deteriorates, the CQC-*r* chart with larger value of *r* (*r* = 2, 3 or 4) shows distinct superiority to the CQC chart, and the ATS performance of CQC-*4* chart is comparable to the corresponding exponential EWMA and exponential CUSUM charts. Moreover, the CQC-*4* chart overcomes the drawback of the CQC chart that the ATS value increases when the process has a small lower-sided shift.

A practical disadvantage of two-sided exponential CUSUM and exponential EWMA charts is that the design procedures are quite complicated. A two-sided EWMA chart with one smoothing factor and different upper and lower limits h_q and h_Q can only be designed to detect either an upper or lower shift quickly, while two charts with two sets of design parameters have to be employed if the users intend to detect certain upper and lower shifts quickly. For two-sided exponential CUSUM chart, two individual charts have to be used to detect shifts in different directions.

3.4 Results & Discussions

The following conclusions can be drawn by summarizing the analysis results above:

1. Among the upper-sided exponential TBE charts, the difference in ATS values is not very significant. When the process improvement is small, exponential EWMA charts are slightly better than exponential CUSUM chart, and both of them are better than the CQC and CQC-*r* charts. However, the CQC chart

shows better performance than the CQC-*r* charts, and its ATS is similar to the exponential EWMA and CUSUM charts when the shift becomes large.

2. Among the lower-sided exponential TBE charts, the ATS performance of exponential EWMA and CUSUM charts are much better than the CQC and the CQC-*r* chart. The exponential EWMA is more sensitive to small deterioration, while the exponential CUSUM is suitable for large deterioration. For the CQC-*r* charts, the larger the value of *r*, the better the performance of the chart, though at the expense of large false alarm probability.
3. Among the two-sided exponential TBE charts, the exponential CUSUM and exponential EWMA charts outperform the CQC-*r* charts. For CQC-*r* charts, when the process improves, the parameter *r* does not influence the ATS performance to a large extent, while when the process deteriorates, the CQC-*r* chart with large value of *r* shows distinct superiority to the CQC chart.
4. The in-control ATS value, as a design parameter of the TBE charts, has certain effect on the comparative performance of the charts. The superiority of exponential EWMA and exponential CUSUM charts in ATS will be less significant when the in-control ATS decreases, and thus making CQC and CQC-*r* charts better choices because of their simple design procedures and less requirement of process information.

Comparing the design procedures of CQC chart, CQC-*r* chart (Xie *et al.*, 2002b), exponential CUSUM chart (Gan,1994) and exponential EWMA chart (Gan, 1998), CQC and CQC-*r* chart are much easier to design because the upper and lower control limits can be easily calculated by formula (2.5) and (2.13) with predetermined False Alarm Rate α and value of *r*. On the other hand, to achieve the optimal design of

exponential CUSUM or exponential EWMA chart, the out-of-control level p_1 has to be known or well-estimated. The optimal design parameters are determined by following complicated design procedures with the formula and counterplots as shown in the corresponding papers. If the out-of-control shift level varies along the time, the optimal design parameters have to be adjusted also. The previous optimal design of exponential CUSUM or EWMA chart could not achieve its best performance if the design parameters are not adjusted in time.

Based on the analysis above, we recommend that if the purpose of employing a TBE chart is to monitor process improvement or when the users do not really know whether the process will improve or deteriorate, i.e. where it is difficult to predict the process shift, the CQC or the CQC-*r* chart is a better choice as they are easy to design and implement, and have relatively good ATS performance. On the other hand, if the focus is only on process deterioration, and the out-of-control shift can be accurately predicted according to past data or other information, the exponential CUSUM or EWMA charts will be more efficient tools especially when the shift is small. Alternatively, CQC-*r* charts can also be employed to detect relatively large deterioration.

3.5 On-line Process Monitoring Based on TBE Charts

For high-quality processes, products are generally manufactured automatically in a production line within a very short period. Thus early detection of change in the process parameters has become even more critical. Early detection of any malfunctions in a production line results in less defective items being produced and greater up time of critical process equipment, which in turn equates to higher profitability. As a result,

online process monitoring becomes a great need.

A typical on-line process monitoring system usually consists of several modules such as data acquisition and processing, SPC monitoring, Expert System diagnosing, and Engineering Process Control (EPC) adjustment. Firstly the data are collected from the processes by using sensors or other tools; then the most important process variables are prioritized in the initial implementation of SPC. This useful information is then sent into the on-line SPC module, which employs suitable control charts to monitor the process and provide useful information to diagnose the reasons of failures. For continuous flow process, data correlation also needs to be considered when designing a control chart. Some authors proposed using Artificial Neural Network (ANN) techniques, for control chart pattern (CCP) recognition, and expert system for cause diagnoses. The corrective actions are usually done by an EPC system which may make necessary feedback adjustment according to the information provided by SPC and failure diagnosis system. All those sub-systems in the process are important to fulfill on-line process monitoring. However, this study focuses on the SPC section, which is the most fundamental and effective part in the entire system.

From the analysis in the previous sections, it can be seen that the CQC and CQC-*r* charts have some advantages compared to exponential CUSUM and EWMA charts especially for on-line process monitoring. Firstly, they are more flexible and need less information about the process. This feature is very beneficial for implementing on-line process monitoring, because most of the time users are not sure about the out-of-control process defect rate that would be interested to be detected quickly, or even the direction of possible shifts.

Secondly, the flexibility of CQC and CQC-*r* charts make the on-line process monitoring system more stable without too many changes of the chart design parameters due to the change of user's requirements. Besides, the control limits and other important parameters such as the ARL and ATS are much easier to compute compared with exponential CUSUM and exponential EWMA. Therefore, the CQC and CQC-*r* charts are strongly suggested to be used for on-line process monitoring.

Besides, the CQC and CQC-*r* charts are also more suitable for on-line monitoring compared with Shewhart control charts. The CQC and CQC-*r* charts do not require a sampling interval to form a rational subgroup, and can directly show the time-between-event data along with time; therefore it allows continuous operation without stopping unless something has happened. On the other hand, for constructing Shewhart control charts, e.g. *c*-chart or *u*-chart, a rational subgroup is needed; thus the user has to wait for a sampling interval to form a rational subgroup and then plot the data point on the chart. This is not convenient for implementation in the sense of "on-line" monitoring.

The design parameter *r* of the CQC-*r* chart can be chosen based on the need and understanding of the processes. The advantage of CQC-*r* is that the decision is made on more than one data point and thus is more reliable than CQC chart. Meanwhile, the CQC-*r* chart compensates the drawback of the CQC chart that the ATS value increases when the process has a small lower-sided shift. However, the average time taken to plot a point increases with *r* and the average time to alarm increases as the process improves beyond a certain level. As shown in the above analysis results, the larger the value of *r*, the better the performance of the chart even with same probability of false

alarm.

Here a simple example is used to illustrate how the TBE charts work for on-line process monitoring. Suppose during the manufacturing process, the time between defects was recorded. Table 3.6 shows the time between two consecutive defects for the last 20 defects. Figures 3.4 and 3.5 show the CQC and CQC-2 charts plotted with the above data and the same false alarm probability of 0.0027. Figure 3.6 is the corresponding exponential CUSUM chart with in-control ARL equal to 370. The in-control time-between-events mean is estimated to be 10,000 minutes, and the shifted mean is estimated to be 5,000 minutes. The design parameters of exponential CUSUM chart are determined using the method provided by Gan (1994).

Table 3.6 Time between defects data

No.	TBD (minutes)	TBD_2 (minutes)	No.	TBD (minutes)	TBD_2 (minutes)
1	6395.4		11	97.2	
2	19390.8	25786.2	12	9384	9481.2
3	4948.6		13	10693.1	
4	9093.8	14042.4	14	1961.7	12654.8
5	19991.2		15	288.1	
6	5742.5	25733.7	16	3638.2	3926.3
7	8471.2		17	90.3	
8	2797.6	11268.8	18	49.3	139.6
9	4551.6		19	8509.2	
10	7081.4	11633	20	16110	24619.2

TBD: Time between two consecutive defects; TBD_2: Time interval for detecting two defects

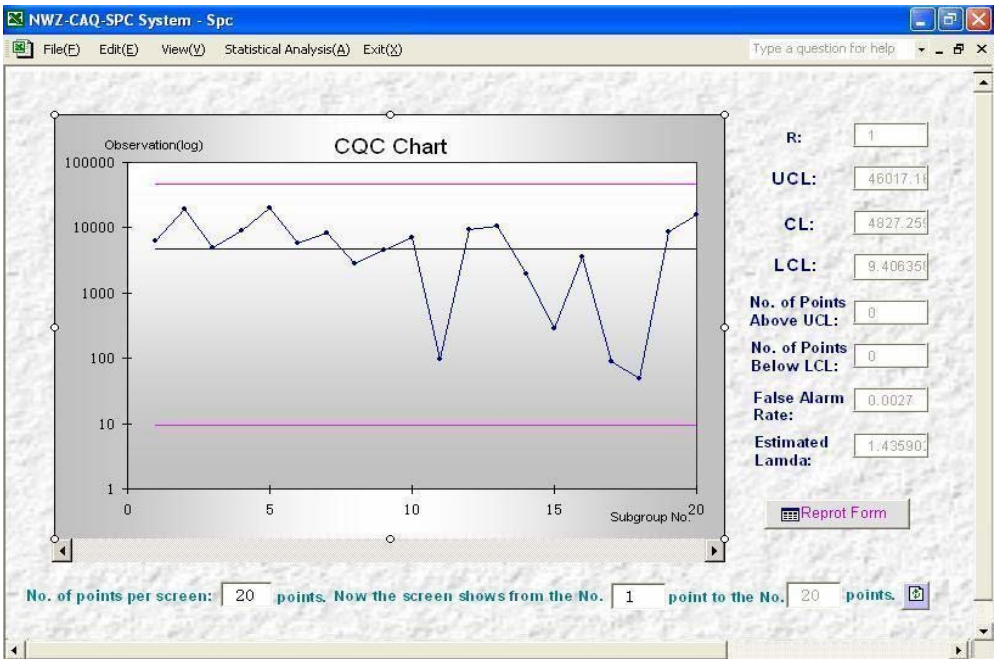

Figure 3.4 A CQC chart for on-line process monitoring

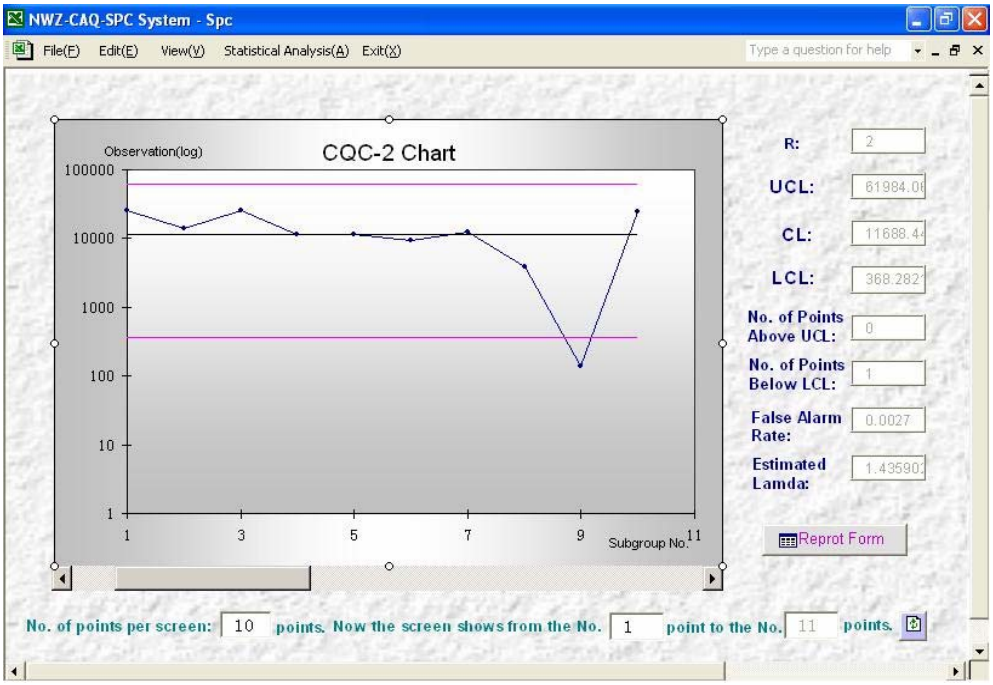

Figure 3.5 A CQC-2 chart for on-line process monitoring

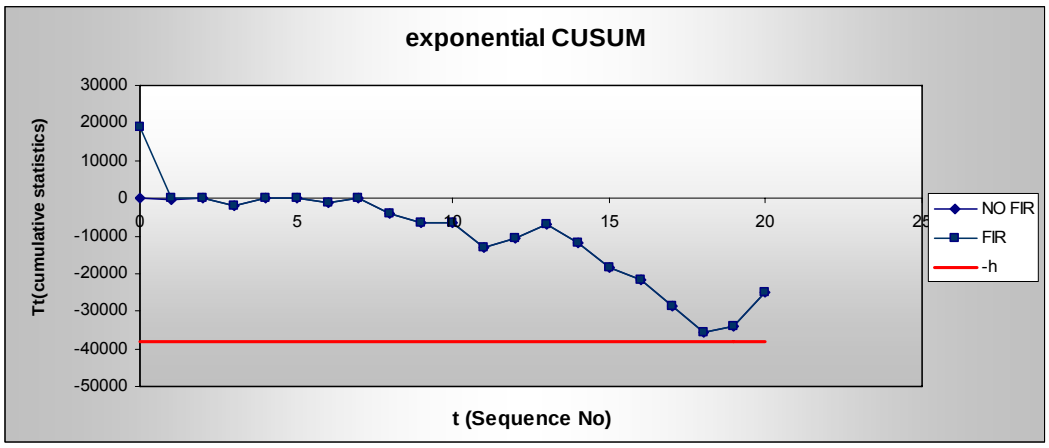

Figure 3.6 An Exponential CUSUM chart
(In-control ARL=370. k=6931.47, h=38000, θ_0=10,000, θ_1=5,000; FIR: Fast Initial Response = h/2)

It can be seen from Figures 3.4, 3.5 and 3.6 that the CQC-2 chart raised an alarm, while CQC chart and exponential CUSUM chart failed to do so. However, the pattern on both the CQC chart and exponential CUSUM chart revealed that there might be a process shift. This may provide straightforward evidence that CQC-2 chart is more sensitive to small changes compared with CQC chart, and may be even more sensitive than exponential CUSUM under certain conditions.

Besides SPC techniques, the effectiveness of on-line process monitoring system is also decided by many other factors such as the integration of EPC and SPC, the capacity of the expert system and its decision logic. Some scholars (see Smith and Boning,1997) have used artificial neural network (ANN) techniques for EPC compensation and achieved good effects. ANN methods can also be used for control chart pattern recognition. These methods can then be applied to check whether something really went wrong when there is an out of control situation or when there is some form of pattern present on the chart as in the case of the above example.

3.6 Conclusions

Today's industrial environment is data-rich and highly automated. Even a small delay in detecting process variability may cause large number of "bad" units being produced and thus reduce the efficiency and increase the cost of the product. Using TBE chart to monitor processes is a good solution to solve this problem and realize on-line process monitoring.

In this chapter the ATS performance of the CQC chart, CQC-*r* chart, exponential EWMA and exponential CUSUM chart are compared. The method of on-line process monitoring with TBE charts is described and an example is given to illustrate its application in practice. The findings in this study suggest that employing time-between-events charts, especially the CQC and CQC-*r* charts, is an effective way for implementing on-line process monitoring system.

Chapter 4 CUSUM Charts with Transformed Exponential Data

4.1 Introduction

Comparative study in Chapter 3 have shown that the exponential CUSUM and exponential EWMA charts are more sensitive to small shifts, while their design procedures are quite complicated. The CQC and CQC-*r* charts, on the other hand, are not so sensitive to small shifts, but are easy for design and implementation.

As reviewed in Chapter 2, an alternative to monitoring TBE is using of transformations. Previous study proposed several transformations that can be used for transforming exponentially distributed TBE data to normal and investigated their performance for setting up control charts with 3-sigma control limits, probability control limits, EWMA chart or CUSUM chart (Nelson, 1994; McCool and Joyner-Motley, 1998; Kittlitz, 1999). Montgomery (2005) again emphasized the idea of monitoring time between events data based on transformation method, and stated that "in many cases, the CUSUM and EWMA control charts would be better alternatives because these charts are more effective in detecting small shifts in mean." However, the former studies did not investigate the ARL properties and optimal design of the CUSUM chart with transformed exponential data.

In this chapter, a new CUSUM chart is proposed to monitor a set of exponentially distributed data after transformation. Different transformation methods such as Nelson's method, Double SQRT method, and log transformation are compared. The

calculation of ARL using Markov chain approach is investigated and the design procedures are developed. Comparative study on the ARL properties is also conducted between the transformed CUSUM and other control charts, such as the X-MR(Moving Average) chart, the CQC chart, and the exponential CUSUM chart. This study provided a proof of Montgomery's statement, and further proposed another alternative for monitoring TBE data.

4.2 Some Transformation Methods

Consider a set of time between events data $X_1, X_2,\ldots$,obtained from a process. Assume that the time between events X_i (i= 1, 2,…) can be modeled as independent and identically distributed (iid) exponential random variables with probability density function:

$$f(x)=\begin{cases}\theta^{-1}e^{-\frac{x}{\theta}}, if\ \ x\geq 0\\ 0, \quad otherwise\end{cases} \tag{4.1}$$

where θ is the mean of exponential data. Many normalizing transformation methods have been proposed by different authors (e.g. Box and Cox, 1964; Taneichi et al, 2002). However, to keep the control chart easy for implementation, only some simple transformations that can be applied to achieve approximate normal distributed data are discussed as follows.

- **Nelson's transformation**

Nelson (1994) suggested transforming the exponential random variable to a Weibull random variable W($\theta^{0.2777}$, 3.6) , which is an approximate normal distribution. The transformation formula is

$$y = x^{1/3.6} = x^{0.2777} \tag{4.2}$$

After this transformation, the user could construct a control chart on y, assuming that y follows a normal distribution.

- **The natural log transformation**

The natural log transformation may turn the right-skewed data to approximately symmetric or even normal. The formula for natural log transformation is

$$y = \ln(x), x > 0 \tag{4.3}$$

- **Double Square-root (SQRT) transformation**

Kittlitz (1999) has also investigated transforming the exponential for control charting purpose. He suggests using the transformation

$$y = x^{0.25}, x \geq 0 \tag{4.4}$$

Kittliz (1999) also explained that a log transformation will stabilize the variance of the exponential distribution, but produces a rather negatively skewed distribution. Independently, a similar method was proposed in Xie *et al.* (2000c).

To compare the performance of these transformation methods, 50,000 exponentially distributed random numbers were generated with mean θ equals to 1.0. The three transformation methods described above were applied separately, and the normality statistics skewness and kurtosis were calculated as shown in Table 4.1. As indicated with * in Table 4.1, Nelson's transformation is preferable in terms of skewness, while

the double SQRT transformation is better in kurtosis. The natural log is not a suitable choice since both of the two normality statistics are much worse than the other two methods. On the other hand, the difference between the normality statistics of data after the Nelson's transformation and double SQRT transformation is indistinctive. Since the double SQRT is much easier for implementation, it is chosen for setting up the CUSUM chart with transformed exponential data chart.

Table 4.1 Comparison results of Nelson's transformation, natural log transformation, and double SQRT transformation

	Nelson's	Natural log	Double SQRT
Skewness (=0 for normal distribution)	0.0111*	-1.1235	-0.0763
Kurtosis (=3 for normal distribution)	2.7133	5.3545	2.7413*

4.3 CUSUM Chart with Transformed Exponential Data

The idea of the proposed CUSUM chart is to use a simple transformation method to convert the exponential data to approximate normal data, and then apply conventional design methods of CUSUM chart for normal data to monitor the process. It can be set up by following the steps below.

***Step* 1**: Transform the exponential data to approximate normal, using double SQRT transformation (Formula 4.4);

***Step* 2**: Set up the tabular CUSUM designed for normal data, that is

$$\begin{aligned} C_t^+ &= \max\left\{0, y_t - (\mu_0 + K) + C_{t-1}^+\right\} \\ C_t^- &= \max\left\{0, (\mu_0 - K) - y_t + C_{t-1}^-\right\} \end{aligned} \tag{4.5}$$

where reference value $K = \frac{\delta}{2}\sigma = \frac{|\mu_1 - \mu_0|}{2}$. δ is the size of the shift in standard deviation units; μ_0 is the in-control mean of transformed data; μ_1 is the out-of-control mean after transformation that is specified to be detected quickly, and σ^2 is the variance of the data after transformation;

***Step* 3**: The process is considered to be out of control when either C_t^+ or C_t^- exceeds the decision interval H. The method of determining the optimal value of *H* will be introduced in section 4.5. The μ_0 and σ are estimated from the transformed exponential data with

$$\hat{\mu}_0 = \bar{y} = \sum_{i=1}^{n} y_i \,, \hat{\sigma} = \sqrt{\left(\sum_{i=1}^{n}(y_i - \bar{y})^2\right) \Big/ (n-1)} \tag{4.6}$$

X follows an exponential distribution with mean of θ, which is also a Weibull variable with parameters W(θ,1). It has been proved (Kittlitz, 1999) that after the double SQRT transformation $Y=X^{0.25}$, *Y* is also a Weibull variable with parameters W($\theta^{0.25}$,4). The mean and variance can be calculated as:

$$\begin{aligned} \hat{\mu} &= E(Y) = \theta^{0.25}\Gamma(1+0.25) = 0.9064\theta^{0.25} \\ \hat{\sigma} &= \sqrt{D(Y)} = \theta^{0.25}\sqrt{\Gamma(1+0.5) - \Gamma^2(1+0.25)} = 0.2543\theta^{0.25} \end{aligned} \tag{4.7}$$

Equation (4.7) can be used to estimate the mean and variance of the transformed data if the in-control exponential mean is known or can be well estimated.

4.4 Calculation of ARL with Markov Chain Approach

Hawkins (1992) studied the evaluation of ARL for CUSUM chart with an arbitrary data distribution. Basically, the ARL of CUSUM chart with transformed exponential data can be calculated using the Markov chain approach discussed by Brook and Evans (1972). The properties of the continuous-state Markov chain were approximately evaluated by discretizing the infinite-state transition probability matrix.

As shown in Figure 4.1, for either upper-sided or the lower-sided CUSUM chart with transformed exponential data chart, the interval between the upper and lower control limits $(0,H)$ can be divided into m sub-intervals of width w ($w=H/m$). The control statistics C_i is said to be in transient state (j) at time (i) if $jw \leq C_i < (j+1)w$ for $j=0,1,\ldots m-1$. The midpoint of the subinterval corresponding to state(j), can be written as $m_j=(j+0.5)w$, $j=0,1,\ldots m-1$. The control statistics C_i is in the absorbing state m if C_i falls beyond decision interval. i.e. $C_i \geq H$.

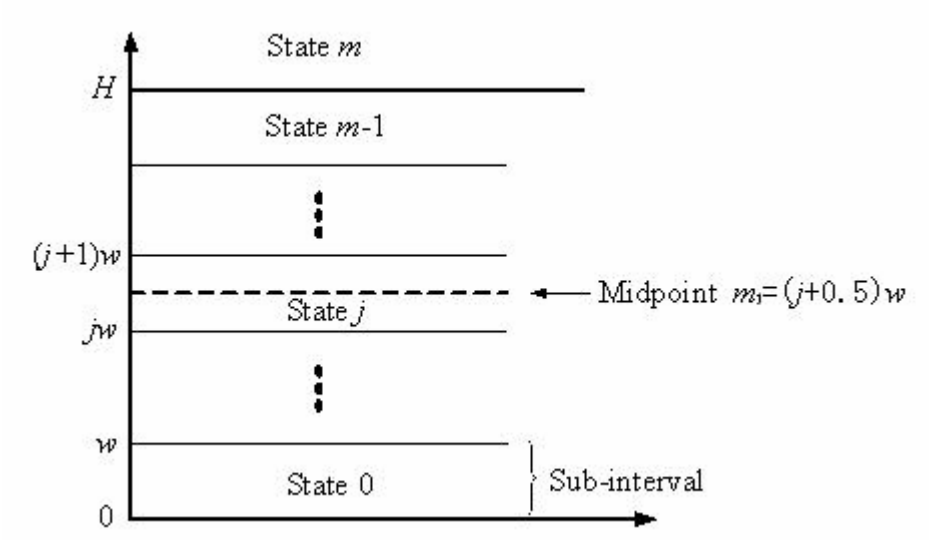

Figure 4.1 Subintervals division for CUSUM chart with transformed exponential data

Let P_{ij} represents the probability that the control statistics C_i goes from state (i) to state (j) in one step. To approximate the probability, it is assumed that the control statistics C_i is equal to m_i whenever it is in state (i).

For the upper-sided CUSUM chart with transformed exponential data, the elements of the transition probability matrix of the Markov chain $P = [\, p_{ij} \,]$ can be calculated with the following formulas:

$$p_{ij} = \begin{cases} \Pr\{Y - (\mu_0 + K) < -iw + 0.5w\}, i = 0,1,\ldots,m-1; j = 0 \\ \Pr\{(j-i)w - 0.5w \le Y - (\mu_0 + K) < (j-i)w + 0.5w\}, i = 0,1,\ldots,m-1, j = 1,2,\ldots m-1 \\ \Pr\{Y - (\mu_0 + K) \ge H - (i+0.5)w\}, i = 0,1,\ldots,m-1; j = m \\ 0, i = m; j = 0,1,\ldots m-1 \\ 1, i = m; j = m \end{cases} \quad (4.8)$$

Based on the Markov chain theory, the expected first passage times from state (i) to the absorbing state are

$$\mu_i = 1 + \sum_{j=0}^{m-1} p_{ij}\mu_j, i = 0,1,\ldots,m-1 \quad (4.9)$$

μ_i is the ARL given that the process started in state (i). Let R be the matrix of transition probabilities obtained by deleting the last row and column of P. The vector of ARLs μ can be calculated with

$$\mu = (I - R)^{-1}1 \quad (4.10)$$

where 1 is an $m \times 1$vector of 1s and I is a $m \times m$ identity matrix. The first element of the vector μ gives the average run length for the CUSUM chart starting from zero.

With the similar method, the ARL of lower-sided CUSUM chart with transformed exponential data, which is designed to detect the decrease of exponential mean θ, can also be calculated with Markov chain approach. The elements of the transition probability matrix of the Markov chain P=[p_{ij}] can be calculated with formulas (4.11):

$$p_{ij}=\begin{cases}\Pr\{Y-(\mu_0-K)>iw-0.5w\}, i=0,1,\ldots,m-1; j=0\\ \Pr\{(i-j)w-0.5w<Y-(\mu_0-K)<(i-j)w+0.5w\}, i=0,1,\ldots,m-1, j=1,2,\ldots m-1\\ \Pr\{Y-(\mu_0-K)\le(i+0.5)w-H\}, i=0,1,\ldots,m-1; j=m\\ 0, i=m; j=0,1,\ldots m-1\\ 1, i=m; j=m\end{cases} \quad (4.11)$$

The ARL of two-sided transformed CUSUM can be calculated by

$$\frac{1}{ARL}=\frac{1}{ARL_U}+\frac{1}{ARL_L} \quad (4.12)$$

Since Y follows Weibull distribution with W($\theta^{0.25}$,4), the p_{ij} can be calculated from the cumulative density function of Y, and then ARL values can be found. This can be easily done with computing software, e.g. Matlab.

4.5 Design of CUSUM Chart with Transformed Exponential Data

Previous studies have investigated the optimal design for CUSUM with normal data, exponential data, etc. see Hawkins and Olwell (1998). Basically, the reference value K is chosen for optimal response to specified shift, and the decision interval H is set to give an acceptable in-control ARL.

Define $H=h\sigma$ and $K=k\sigma$. For normal data, it has been proved that when $k=0.5\delta$, it comes very close to minimizing the ARL value for detecting a shift of size δ for fixed in-control ARL value. However, it is difficult to interpret the size of the shift of exponential mean in terms of δ. Therefore, an expression with exponential mean θ is needed for determining the value of k. The reference value K can be expressed as,

$$K = \frac{|\mu_1 - \mu_0|}{2} \approx \frac{|E(Y_1) - E(Y_0)|}{2} = 0.4532\left|\theta_1^{0.25} - \theta_0^{0.25}\right|$$
$$k = \frac{K}{\sigma} \approx \frac{0.4532\left|\theta_1^{0.25} - \theta_0^{0.25}\right|}{0.2543\theta_0^{0.25}} = 1.7821\frac{\left|\theta_1^{0.25} - \theta_0^{0.25}\right|}{\theta_0^{0.25}} \tag{4.13}$$

Let $\theta_1=q\theta_0$. k can be expressed by

$$k = 1.7821 \cdot \frac{\left|q^{0.25}\theta_0^{0.25} - \theta_0^{0.25}\right|}{\theta_0^{0.25}} = 1.7821 \cdot \left|q^{0.25} - 1\right| \tag{4.14}$$

It indicates that k is determined by the ratio of out-of-control mean θ_1 to the in-control mean θ_0. Meanwhile, it is worth noting that the in-control ARL of a CUSUM chart with transformed exponential data is not influenced by the value of θ_0. Therefore, the design of the CUSUM chart with transformed exponential data is conducted based on the parameters k and h.

According to the Markov chain method in the previous section, the in-control ARL can be calculated given k and h, based on which the contour plot of in-control ARL can be achieved. Figures 4.2, 4.3, 4.4, and 4.5 show the contour plots of in-control ARL from 100 to 2000, or 3000, with different range of h and k for two-sided CUSUM chart with transformed exponential data. The design procedures of a CUSUM chart with transformed exponential data is summarized in the following steps:

***Step* 1**: Choose the acceptable in-control ARL;

***Step* 2**: Decide the out-of-control mean θ_1 that is required to be detected quickly;

***Step* 3**: Use formula (4.13) to determine the value of k to minimize the out-of-control ARL value for detecting θ_1, the reference value $K=k\sigma$;

***Step* 4**: Find the value of h with in-control ARL and k value from Figures 4.2, 4.3, 4.4, or 4.5. Calculate the decision interval H with $H=h\sigma$.

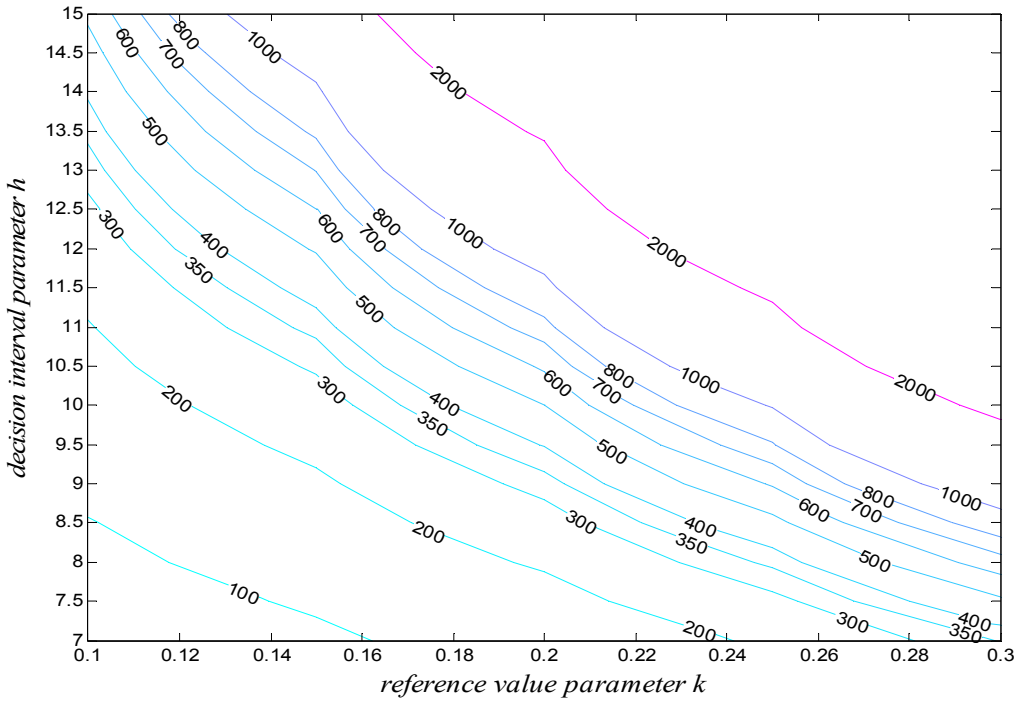

Figure 4.2 Values of h for two-sided CUSUM with transformed exponential data ($0.1 \leq k \leq 0.3$)

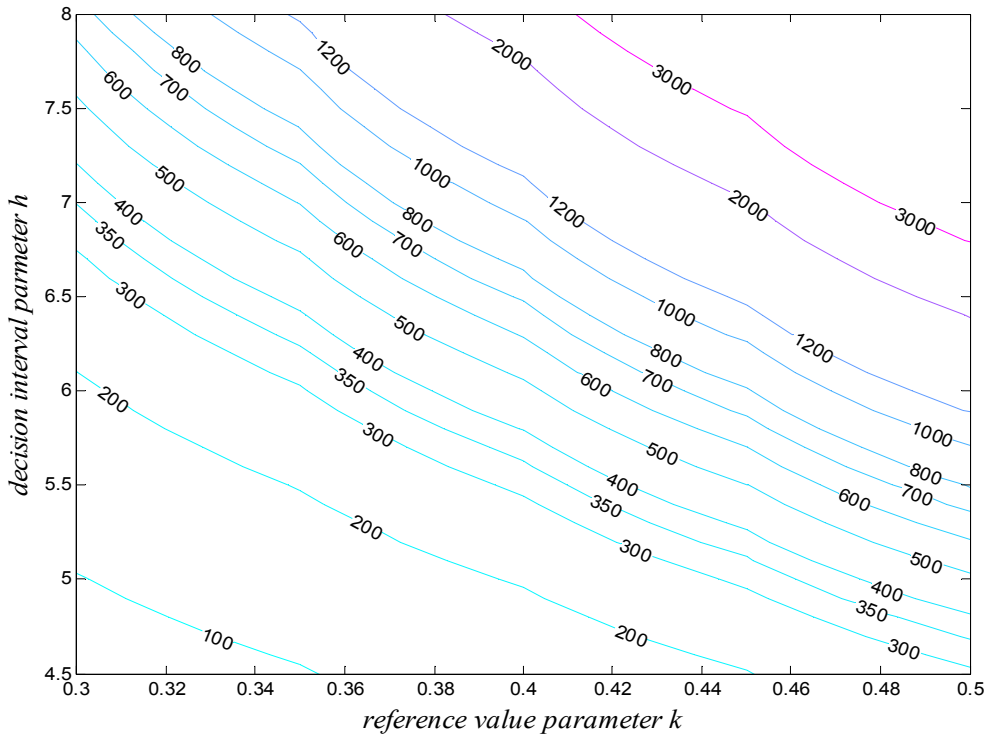

Figure 4.3 Values of h for two-sided CUSUM chart with transformed exponential data ($0.3 \leq k \leq 0.5$)

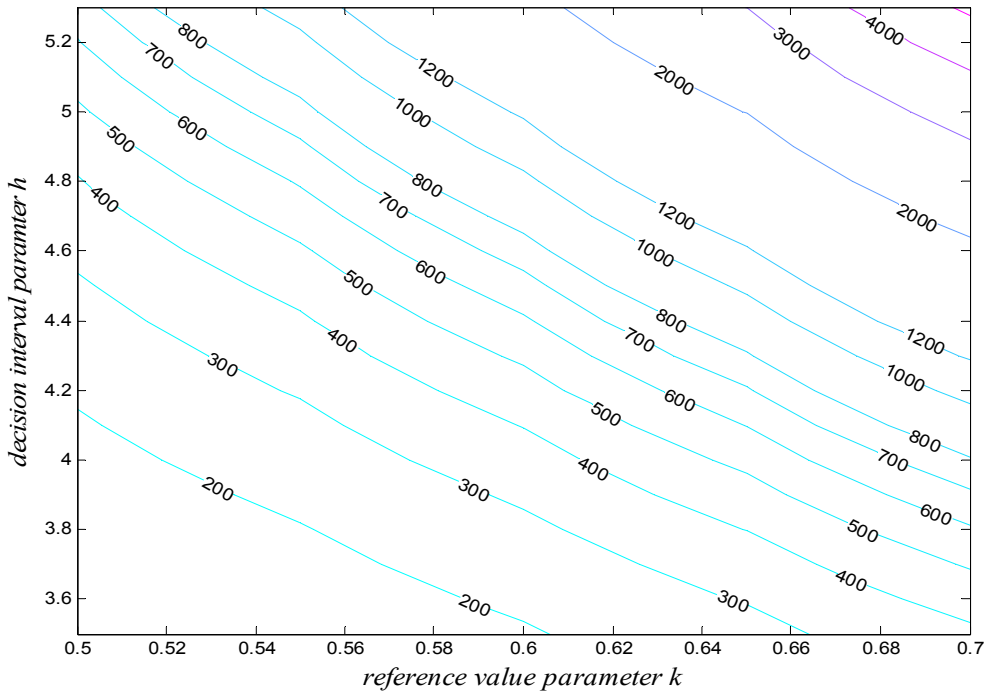

Figure 4.4 Values of h for two-sided CUSUM chart with transformed exponential data ($0.5 \leq k \leq 0.7$)

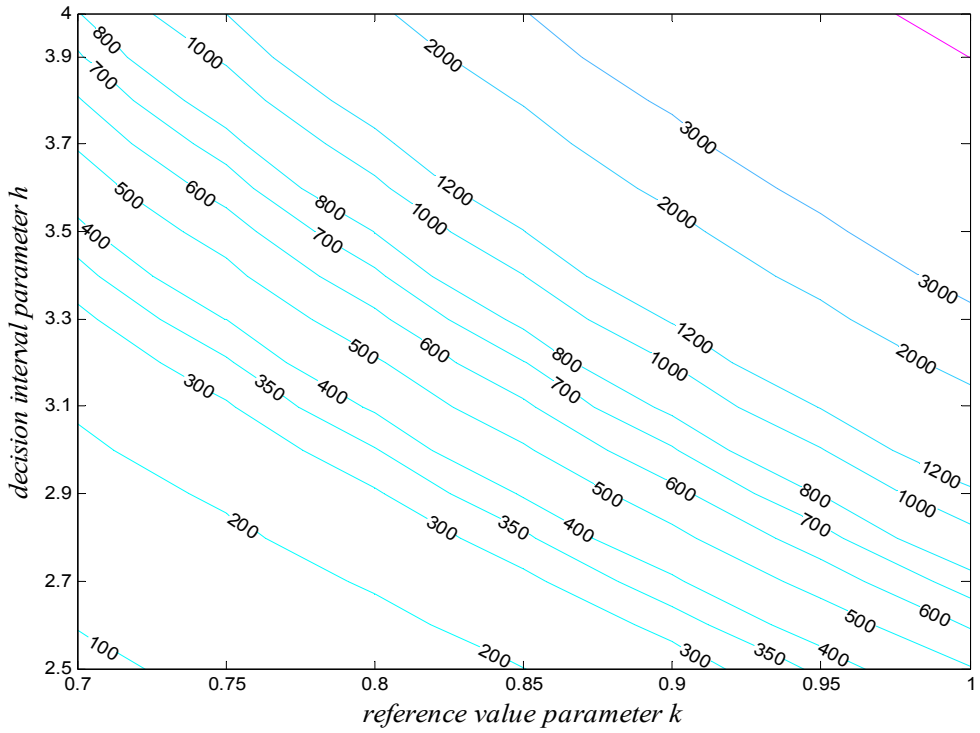

Figure 4.5 Values of h for two-sided CUSUM chart with transformed exponential data ($0.7 \leq k \leq 1$)

Here is an example to illustrate the procedures described above. Suppose now a CUSUM chart with transformed exponential data is required to quickly detect the out-of-control exponential mean θ_1=0.25, in-control θ_0=1.00, and in-control ARL =370 (FAR α= 0.0027). The design procedures are shown as follows,

1. Substitute the values of θ_0 and θ_1 to Formula (4.13), get k=0.52;
2. From Figure 4.4, find h=4.6;
3. Set up the CUSUM chart with transformed exponential data based on the steps explained in section 4.3.

To simplify the design procedures by avoiding checking Figures 4.2, 4.3, 4.4, and 4.5, some recommended values of h are listed in Table 4.2, which will give relative good

performance for commonly used control chart with in-control ARL approximately from 300 to 500. This is a rough way to decide the decision interval H, and more accurate h values can be found from the contour plots (Figure 4.2 ~ 4.5).

Table 4.2 Some recommended h values for the design of CUSUM chart with transformed exponential data

k	0.1~0.2	0.2~0.3	0.3~0.4	0.4~0.5	0.5~0.6	0.6~0.7	0.7~0.85	0.85~1
h	11	9	6.5	5.5	4.5	3.8	3.2	2.8

4.6 Comparative Study

4.6.1 CUSUM Chart with Transformed Exponential Data vs. X-MR Chart

To compare the performance of transformed CUSUM with that of the Shewhart chart (X-MR chart), a simulation is conducted by transforming the exponential data to normal using double SQRT transformation and then setting up the X-MR chart to monitor the data. Let the in-control exponential mean θ_0=1.0. When the actual exponential mean varies from 0.1 to 5.0, the ARL values of the X-MR chart with transformed data are calculated as shown in Table 4.3.

The corresponding transformed CUSUM is designed to have the same in-control ARL with the transformed X-MR chart (131.41). Assume the predicted θ_1=0.2. The reference value parameter k can be calculated from formula (4.13) (k=0.59); and h is approximated to 3.25 from Figure 4.4. After determining the design parameters, the

out-of-control ARL values can be calculated using the Markov chain method, and the results are shown in Table 4.3.

Table 4.3 ARL values of X-MR chart and CUSUM chart with transformed exponential data

θ_1	ARL		θ_1	ARL		θ_1	ARL	
	X-MR	transformed CUSUM		X-MR	transformed CUSUM		X-MR	transformed CUSUM
0.1	272.48	3.99	1.8	30.29	16.24	3.5	7.05	4.93
0.2	540.54	6.25	1.9	27.39	14.07	3.6	6.57	4.77
0.3	709.22	9.85	2	23.57	12.41	3.7	6.42	4.63
0.4	675.68	16.18	2.1	20.91	11.11	3.8	6.01	4.50
0.5	531.91	27.27	2.2	18.84	10.07	3.9	5.74	4.37
0.6	389.11	45.50	2.3	17.43	9.22	4	5.52	4.26
0.7	290.70	72.83	2.4	15.89	8.51	4.1	5.26	4.15
0.8	206.19	107.61	2.5	14.12	7.92	4.2	5.09	4.06
0.9	153.61	135.08	2.6	13.20	7.42	4.3	4.91	3.97
1	131.41	131.20	2.7	11.72	6.99	4.4	4.75	3.88
1.1	105.15	101.91	2.8	10.96	6.61	4.5	4.59	3.80
1.2	85.03	72.23	2.9	10.36	6.28	4.6	4.45	3.72
1.3	71.28	51.30	3	9.48	5.99	4.7	4.28	3.65
1.4	58.93	37.80	3.1	8.85	5.73	4.8	4.17	3.58
1.5	50.56	29.05	3.2	8.21	5.50	4.9	3.99	3.52
1.6	40.60	23.21	3.3	7.90	5.29	5	3.92	3.46
1.7	37.31	19.16	3.4	7.38	5.10			

Figure 4.6 displays the ARL curves of both X-MR chart and transformed CUSUM with double SQRT transformation. It can be seen from the results that when exponential mean θ increases from in-control level θ_0=1.0, which indicates process improvement, the CUSUM chart with transformed exponential data is more sensitive

than the transformed X-MR chart especially for small shifts. On the other hand, it is worth pointing out that the CUSUM chart with double SQRT transformation achieved the maximum ARL value at the in-control level θ_0=1.0. However, the maximum ARL value of transformed X-MR chart was achieved when exponential mean θ is about 0.3. The trend of ARL curve for the transformed X-MR chart implies that when the exponential mean drops from 1.0 to 0.3, the out-of-control ARL value will increase greatly, from 131.41 to 709.22. As a result, it will take longer time to raise an out-of-control signal even if the process has deteriorated a lot. Therefore, the CUSUM chart with transformed exponential data is more effective in detecting process deteriorations than the X-MR chart with double SQRT transformation.

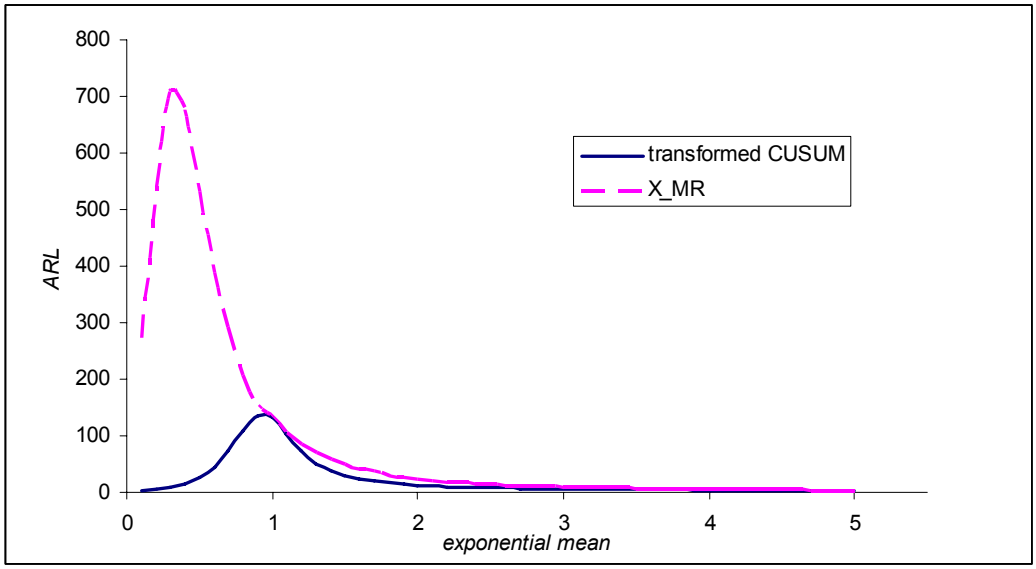

Figure 4.6 The ARL curves of X-MR chart and CUSUM chart with transformed exponential data

4.6.2 CUSUM Chart with Transformed Exponential Data vs. CQC Chart

In order to investigate the comparative performance of control charts with transformation and without transformation, another comparison of ARL properties was

conducted between CUSUM chart with transformed exponential data and CQC chart. The in-control ARL were set to be 370.37 for both of them, which is corresponding to the traditional three-sigma limits. Same as the former example, the transformed CUSUM is designed to detect out-of-control exponential mean shift at θ_1= 0.2, and the design parameters can be achieved by following the steps in section 5 (k=0.59, h= 4.093). The out-of-control ARL were calculated as shown in Table 4.4.

Table 4.4 ARL values of CQC chart and CUSUM chart with transformed exponential data

θ_1	ARL		θ_1	ARL		θ_1	ARL	
	CQC	transformed CUSUM		CQC	transformed CUSUM		CQC	transformed CUSUM
0.1	74.51	4.85	1.8	38.16	23.20	3.5	6.59	6.07
0.2	148.52	7.67	1.9	31.66	19.58	3.6	6.25	5.87
0.3	222.53	12.33	2	26.73	16.91	3.7	5.95	5.68
0.4	296.53	21.39	2.1	22.91	14.89	3.8	5.68	5.51
0.5	370.30	40.02	2.2	19.91	13.31	3.9	5.43	5.35
0.6	441.33	76.52	2.3	17.51	12.05	4	5.21	5.20
0.7	498.04	141.71	2.4	15.56	11.02	4.1	5.00	5.07
0.8	513.80	244.10	2.5	13.95	10.17	4.2	4.81	4.94
0.9	465.56	357.65	2.6	12.61	9.46	4.3	4.64	4.82
1	370.35	370.35	2.7	11.49	8.86	4.4	4.48	4.71
1.1	271.08	262.67	2.8	10.54	8.34	4.5	4.34	4.61
1.2	192.83	160.54	2.9	9.72	7.88	4.6	4.20	4.51
1.3	138.10	100.02	3	9.01	7.49	4.7	4.07	4.42
1.4	101.20	66.61	3.1	8.40	7.14	4.8	3.96	4.34
1.5	76.25	47.47	3.2	7.86	6.83	4.9	3.85	4.26
1.6	59.07	35.82	3.3	7.38	6.55	5	3.75	4.18
1.7	46.94	28.31	3.4	6.96	6.30			

The ARL curves in Figure 4.7 indicate that CUSUM chart with transformed exponential data can detect the process shifts faster than the CQC chart especially for the smaller process improvements or deteriorations. Only when the process improvements are very significant ($\theta_1 \approx 5$), the CQC chart is slightly better than the

CUSUM chart with transformed exponential data. In particular, when the in-control exponential mean decreases slightly from in-control level, the out-of-control ARL of transformed CUSUM will drop a lot, and thus the shift can be detected quickly. However, the out-of-control ARL values of CQC chart will increase for small process deterioration, and therefore they are not effective compared with the CUSUM chart with transformed exponential data. This can be attributed to the skewness of exponential distribution that makes the control limits not symmetrical without transformation.

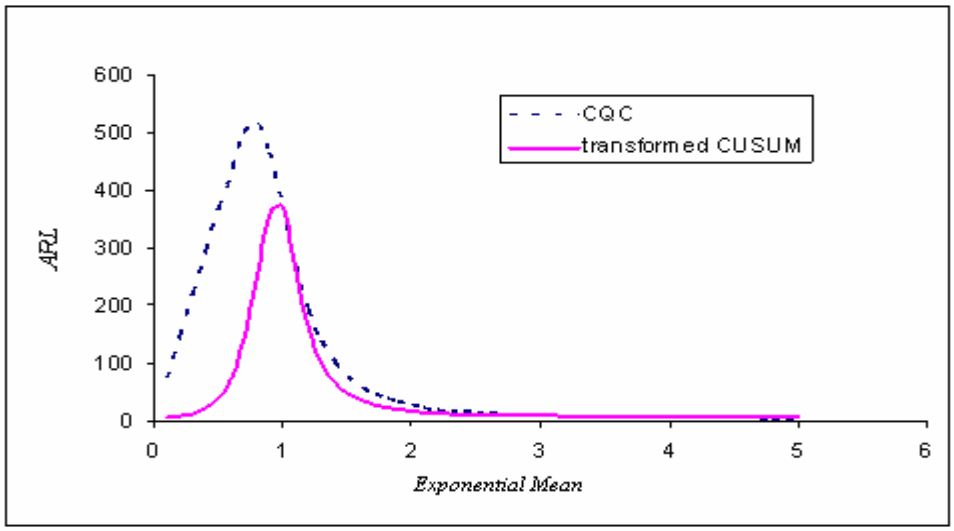

Figure 4.7 The ARL curves of CQC and CUSUM charts with transformed exponential data

4.6.3 CUSUM Chart with Transformed Exponential Data vs. Exponential CUSUM Chart

The performance of CUSUM chart with transformed exponential data and exponential CUSUM are also assessed. The upper-sided and lower-sided CUSUM are used separately, and the ARL profiles of these charts for detecting some intended out-of-

control means are compared. The statistics of upper-sided and lower-sided exponential CUSUM are given by:

$$\begin{aligned} S_i^+ &= \max\left\{0, (x_i - k) + S_{i-1}^+\right\} \\ S_i^- &= \min\left\{0, (x_i - k) + S_{i-1}^-\right\} \end{aligned} \tag{4.15}$$

An out-of-control signal occurs at the first i with $S_i^- \leq -h$ or $S_i^+ \geq h$.

Let the in-control exponential mean θ_0 equals to 1.0. The upper-sided CUSUM charts were designed for detecting out-of-control exponential mean of θ_1=2.0 and 5.0; and the lower-sided CUSUM charts are designed for detecting θ_1=0.5 and 0.2, respectively. The procedures of parameter determination are the same, except that the ARL contour plots for one-sided CUSUM chart with transformed exponential data obtained using Markov chain approach are used instead of that for two-sided CUSUM charts. All the CUSUM charts are designed with in-control ARL equal to or approximated to 500. The design parameters and ARL values of exponential CUSUM are quoted from Gan (1998). The results are shown in Table 4.5.

It can be seen from Table 4.5 that CUSUM charts with transformed exponential data and exponential CUSUM charts have similar performance in terms of ARL, and both of them can detect either upward or downward shifts in a shorter period. CUSUM chart with transformed exponential data tends to be slightly better than exponential CUSUM when the shift is large; while exponential CUSUM shows more superiority when the shift is small. One possible reason for this may be the transformation deflates the amount of mean shift in exponential mean, which in turn makes the CUSUM statistics

not very sensitive to the transformed data compared with monitoring exponential data directly.

Table 4.5 ARL values of exponential CUSUM and CUSUM charts with transformed exponential data

	Upper-sided CUSUM					Lower-sided CUSUM			
	Exp	Tran	Exp	Tran		Exp	Tran	Exp	Tran
	k=1.39	k=0.34	k=2.01	k=0.88		k=0.69	k=0.28	k=0.40	k=0.59
	h=7.42	h=5.804	h=4.86	h=2.426		h=4.16	h=6.859	h=1.24	h=3.877
θ	θ_1=2.0	θ_1=2.0	θ_1=5.0	θ_1=5.0	θ	θ_1=0.5	θ_1=0.5	θ_1=0.2	θ_1=0.2
1.00	500.0	500.2	500.0	500.1	1.00	500.0	500.1	500.0	499.8
1.02	411.7	411.2	431.5	428.0	0.95	337.6	354.4	399.6	397.1
1.04	342.4	341.9	374.6	368.8	0.90	227.6	249.6	316.1	307.6
1.10	208.0	209.2	253.1	245.1	0.85	154.0	175.4	247.5	240.3
1.20	106.1	109.6	144.5	138.0	0.80	105.1	123.8	191.6	184.1
1.30	63.5	67.4	90.7	86.4	0.70	51.6	64.1	110.9	100.3
1.50	30.8	34.8	44.1	42.4	0.60	28.3	36.4	61.4	57.3
2.00	**12.1**	**15.2**	15.1	15.1	0.50	**17.6**	**23.0**	32.9	26.5
5.00	3.1	4.8	**3.0**	**3.0**	0.20	7.4	8.3	**6.1**	**4.3**
10.00	1.9	3.1	1.8	2.0	0.10	6.2	5.9	4.2	4.0

* Exp stands for exponential CUSUM, and Tran stands for CUSUM chart with transformed exponential data.

Here is an example of using CUSUM chart with transformed exponential data and exponential CUSUM for detecting process shifts. The first 20 observations are generated following exponential distribution with mean equals to 1.0 (θ_0=1.0), and the next 10 points are generated using exponential mean θ = 0.2. The lower-sided CUSUM charts were employed to detect the deterioration of the process.

Table 4.6 Data for the CUSUM chart with transformed exponential data and exponential CUSUM

			Transformed CUSUM (K=0.59σ =0.126; H=3.877σ = 0.829)		exponential CUSUM (k=0.4; h=1.24)	
i	X_i	Y_i	μ_0-K-Y_i	C_i^-	X_i-k	S_i^-
0				0		-0.78
1	2.7804	1.2913	-0.4148	0.0000	2.3804	0.0000
2	2.1152	1.2060	-0.3294	0.0000	1.7152	0.0000
3	0.9873	0.9968	-0.1203	0.0000	0.5873	0.0000
4	0.5389	0.8568	0.0197	0.0197	0.1389	0.0000
5	1.2284	1.0528	-0.1762	0.0000	0.8284	0.0000
6	0.2314	0.6935	0.1830	0.1830	-0.1687	-0.1687
7	1.2952	1.0668	-0.1903	0.0000	0.8952	0.0000
8	0.7744	0.9381	-0.0615	0.0000	0.3744	0.0000
9	2.8236	1.2963	-0.4198	0.0000	2.4236	0.0000
10	0.0550	0.4843	0.3922	0.3922	-0.3450	-0.3450
11	1.2780	1.0632	-0.1867	0.2055	0.8780	0.0000
12	1.0056	1.0014	-0.1249	0.0806	0.6056	0.0000
13	2.1290	1.2079	-0.3314	0.0000	1.7290	0.0000
14	0.3715	0.7807	0.0958	0.0958	-0.0285	-0.0285
15	0.5484	0.8606	0.0160	0.1118	0.1484	0.0000
16	1.5206	1.1105	-0.2339	0.0000	1.1206	0.0000
17	2.1879	1.2162	-0.3397	0.0000	1.7879	0.0000
18	0.2967	0.7380	0.1385	0.1385	-0.1033	-0.1033
19	1.3015	1.0681	-0.1916	0.0000	0.9015	0.0000
20	1.5992	1.1245	-0.2480	0.0000	1.1992	0.0000
21	0.2178	0.6832	0.1934	0.1934	-0.1822	-0.1822
22	0.0220	0.3853	0.4913	0.6846	-0.3780	-0.5602
23	0.6398	0.8944	-0.0178	0.6668	0.2398	-0.3204
24	0.0202	0.3770	0.4996	**1.1664**	-0.3798	-0.7002
25	0.3751	0.7826	0.0940	1.2603	-0.0249	-0.7251
26	0.2046	0.6725	0.2040	1.4643	-0.1954	-0.9206
27	0.4263	0.8080	0.0685	1.5328	0.0263	-0.8943
28	0.0125	0.3344	0.5421	2.0750	-0.3875	**-1.2818**
29	0.0426	0.4542	0.4223	2.4973	-0.3574	-1.6392
30	0.0830	0.5367	0.3398	2.8370	-0.3170	-1.9562

With the design parameters shown in Table 4.5, two CUSUM charts are set up separately, and the calculation procedures are shown in Table 4.6. Figure 4.8 includes both the CUSUM chart with transformed exponential data and exponential CUSUM within one chart, from which we can see that the CUSUM chart with transformed exponential data becomes out-of-control at the 24th point while the exponential CUSUM chart raises the signal at the 28th point. Therefore, the CUSUM chart with transformed exponential data is superior to the exponential CUSUM chart in this case. This is consistent with the results in Table 4.5.

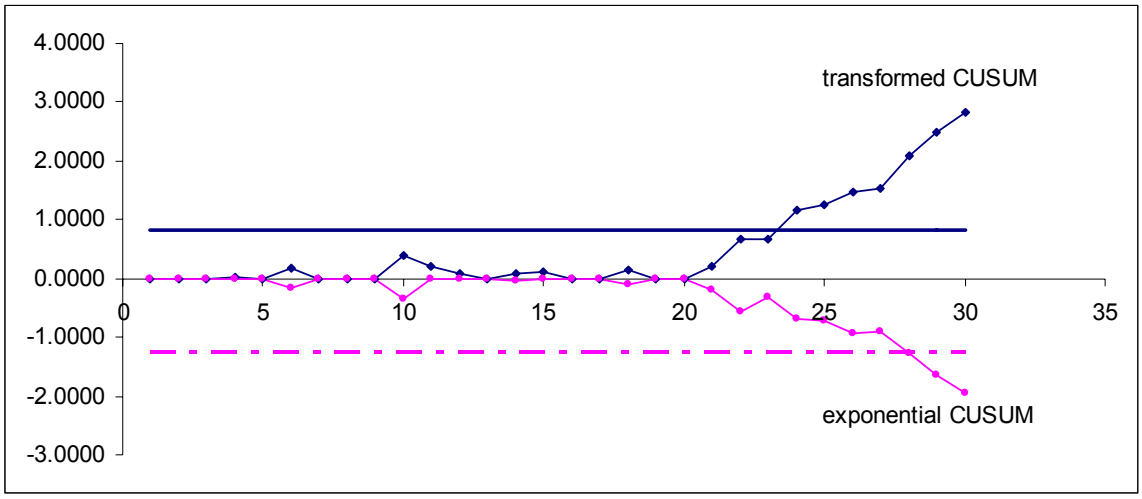

Figure 4.8 The CUSUM chart with transformed exponential data and exponential CUSUM chart

4.7 Conclusions

This chapter discusses an alternative way of monitoring exponential distributed time between events data by control chart. The exponential data can be transformed using double SQRT transformation, and then monitored by the CUSUM chart designed for normal data. The results indicate that the proposed CUSUM chart with transformed exponential data is more effective than the X-MR, CQC chart, and is comparable with exponential CUSUM in detecting either process improvement or deterioration. The

proposed method is easy for implementation especially when a company already has a system to monitor the normal mean with CUSUM charts.

Chapter 5 EWMA Charts with Transformed Exponential Data

5.1 Introduction

Similar to the idea of the previous chapter, using Exponentially Weighted Moving Average (EWMA) chart after transformation is another possible alternative to monitor the TBE data. The EWMA chart attracts great interests from engineers for its ability of detecting small process shifts and predicting the process level at the next time period. Refer to Chen & Guo (2001), Del Castillo & Rajagopal (2002), and Tseng & Hsu (2005).

Another favorable property of the EWMA chart is its robustness to nonnormality, which is beneficial for transformed scheme since the data after transformation will not strictly follow normal distribution even if a proper transformation method is applied. However, the previous studies did not investigate in detail on how to design the EWMA chart with transformed exponential data, and how the transformed EWMA performs compared to other control charts.

The purpose of this study is to investigate the performance of EWMA chart with transformed exponential data and develop the design method for it. The ARL properties are investigated and the design procedures are developed. Furthermore, the performance of EWMA chart with transformed exponential data is compared to that of the X-MR chart, CQC chart, and exponential EWMA, respectively. The robustness of

the proposed EWMA chart to Weibull TBE data is then investigated, followed by an illustrative example. This study provides an alternative for monitoring exponentially-distributed TBE data.

5.2 The Transformed EWMA Chart

5.2.1 Setting-up Procedures

Assume that TBE data follow exponential distribution with probability density function:

$$f(x) = \begin{cases} \theta^{-1} e^{-\frac{x}{\theta}}, if \;\; x \geq 0 \\ 0, \qquad otherwise \end{cases} \tag{5.1}$$

where θ is the mean of exponential time between events, which is also called Mean Time to Failure (MTTF) in reliability analysis. Kittlitz (1999) showed that double SQRT transformation produced similar properties as the power transformation suggested by Nelson (1994) with the added benefit of ease of use. Hence it is decided that the double SQRT transformation be used for this study. The main procedures of setting up an EWMA chart with transformed exponential data are as follows:

Step 1: Transform the exponential data X_t to approximate normal Y_t using the double SQRT transformation:

$$y = x^{0.25}, x \geq 0 \tag{5.2}$$

Step 2: Set up the two-sided EWMA chart with the recursion statistics:

$$z_t = \lambda \cdot y_t + (1-\lambda) z_{t-1} \tag{5.3}$$

where $0<\lambda\leq 1$ is the smoothing factor. The starting value is the target value μ_0, i.e. the mean of data after transformation.

Step 3: The center line and control limits can be calculated by

$$\begin{aligned} UCL &= \mu_0 + L\sigma_0\sqrt{\frac{\lambda}{(2-\lambda)}\left[1-(1-\lambda)^{2t}\right]} \\ CL &= \mu_0 \\ LCL &= \mu_0 - L\sigma_0\sqrt{\frac{\lambda}{(2-\lambda)}\left[1-(1-\lambda)^{2t}\right]} \end{aligned} \tag{5.4}$$

where L is a design parameter, which will be discussed later.

Step 4: The process is considered to be out-of-control when z_t exceeds either the UCL or LCL. The μ_0 and σ_0 can be estimated from the transformed data with

$$\hat{\mu}_0 = \bar{y} = \sum_{t=1}^{n} y_t, \text{ and } \hat{\sigma}_0 = \sqrt{\frac{1}{n-1}\left[\sum_{t=1}^{n}(y_t-\bar{y})^2\right]} \tag{5.5}$$

5.2.2 Calculation of Average Run Length (ARL)

There are mainly two approaches in the literature to the calculation of ARL for EWMA charts. One is the exact method based on the solution of a set of differential equations. Another is an approximate method using Markov chain method proposed by Brook and Evans (1972), where the properties of the continuous-state Markov chain can be approximately evaluated by discretizing the infinite-state transition probability matrix. Former studies on EWMA charts for normal data (Lucas and Saccucci, 1990) and Poisson data (Borror *et al.* 1998) have shown that Markov chain approach can

achieve an accurate approximation of ARL with enough number of states. Therefore, the Markov chain approach is employed to calculate the ARL for the EWMA chart with transformed exponential data.

Following the method in Lucas and Saccucci (1990), and Borror, Champ, and Rigdon (1998), the ARL of EWMA chart with transformed exponential data can be calculated with Markov chain approach. Consider a two-sided EWMA chart with transformed exponential data with design parameters λ and L. The interval between the lower control limit and upper control limit (LCL, UCL) is divided into m subintervals of width w. Since the control limits (LCL, UCL) will change with time t, and will be approximately constant when t is large, the asymptotic control limits are used to calculate the ARL instead of the exact control limits. Let h_{U} and h_{L} be the asymptotic control limits. Then

$$h_U = \mu_0 + L\sigma_0\sqrt{\frac{\lambda}{(2-\lambda)}},\ h_L = \mu_0 - L\sigma_0\sqrt{\frac{\lambda}{(2-\lambda)}} \tag{5.6}$$

Note that when calculating the in-control ARLs, the time t is usually large, and therefore this approximation of control limits will not influence the accuracy of the results a lot. On the other hand, when the process is going out-of-control at the very beginning before the real control limits reach the asymptotic value, the out-of-control ARLs that are obtained by this approximation method may under-estimate the performance of EWMA chart with transformed exponential data. This is especially the case when λ is very small, and the effect of starting value will last for a while before the upper and lower control limits converge to the asymptotic values. The Markov

chain approach with asymptotic control limits is not very accurate in that case and the real out-of-control ARLs may be even shorter.

Using the asymptotic control limits, w can be expressed as:

$$w = \frac{h_U - h_L}{m} = \frac{2L\sigma}{m}\sqrt{\frac{\lambda}{2-\lambda}} \tag{5.7}$$

The EWMA control statistics z_t is said to be in transient state (j) at time (t) if $h_L+jw \le z_t < h_L+(j+1)w$ for $j=0,1,\ldots,m-1$. The midpoint of subinterval corresponding to state (j) can be written as

$$m_j = h_L + (j+0.5)w, j = 0,1,\ldots m-1 \tag{5.8}$$

The control statistics z_t is regarded as in the absorbing state m if the point goes outside the control limits, i.e. $z_t \ge h_U$ or $z_t < h_L$.

Let p_{ij} represents the transition probability that the control statistics z_i goes from state (i) to state (j) in one step. To approximate the probability, we assume that the control statistics z_t is equal to m_i whenever it is in state (i). This approximation is accurate enough when the number of states m is large. Then p_{ij} is given by

$$\begin{aligned}
p_{ij} &= \Pr\{h_L + jw \le z_t < h_L + (j+1)w | z_{t-1} = m_i\} \\
&= \Pr\{h_L + jw \le \lambda y_t + (1-\lambda)z_{t-1} < h_L + (j+1)w | z_{t-1} = m_i\} \\
&= \Pr\left\{\frac{h_L + jw - (1-\lambda)m_i}{\lambda} \le y_t < \frac{h_L + (j+1)w - (1-\lambda)m_i}{\lambda}\right\}, i = 0,1,\ldots m-1; j = 0,1,\ldots m-1 \\
p_{im} &= \Pr\{z_t < h_L \text{ or } z_t \ge h_U | z_{t-1} = m_i\} \\
&= \Pr\{\lambda y_t + (1-\lambda)z_{t-1} < h_L \text{ or } \lambda y_t + (1-\lambda)z_{t-1} \ge h_U | z_{t-1} = m_i\} \\
&= \Pr\left\{y_t < \frac{h_L - (1-\lambda)m_i}{\lambda}\right\} + \Pr\left\{y_t \ge \frac{h_U - (1-\lambda)m_i}{\lambda}\right\}, i = 0,1,\ldots m-1
\end{aligned}$$

$$\begin{aligned} p_{mj} &= 0, j = 0,1,\ldots m-1 \\ p_{mm} &= 1 \end{aligned} \tag{5.9}$$

Based on the Markov chain theory, the expected first passage times from state (i) to the absorbing state are

$$\mu_i = 1 + \sum_{j=0}^{m-1} p_{ij}\mu_j, i = 0,1,\ldots,m-1 \tag{5.10}$$

μ_i is the ARL given that the process started in state (i). Let R be the matrix of transition probabilities obtained by deleting the last row and column of P. The vector of ARLs μ can be calculated with

$$\mu = (I - R)^{-1}1 \tag{5.11}$$

where 1 is an $m\times1$ vector of with all elements equal to 1, and I is an $m\times m$ identity matrix. The elements in the vector μ are the ARLs when the EWMA chart starts in various states. The first element in the vector μ gives the average run length for the EWMA chart starting from zero, and the ARL given that $z_0=\mu_0$ is just the middle entry, that is the ((m+1)/2)th element in the vector μ. In order to get a unique middle value, m is chosen to be an odd number.

Since X follows an exponential distribution with mean of θ, which is a special case of Weibull distribution with scale θ and shape 1.0, i.e. W(θ,1), it is easy to prove that after the double SQRT transformation, Y is also a Weibull variable which follows W($\theta^{0.25}$,4) (Murthy *et al.* 2004). The mean and variance can be estimated with:

$$\hat{\mu} = E(Y) = \theta^{0.25}\Gamma(1+0.25) = 0.9064\theta^{0.25}$$
$$\hat{\sigma} = \sqrt{D(Y)} = \theta^{0.25}\sqrt{\Gamma(1+0.5) - \Gamma^2(1+0.25)} = 0.2543\theta^{0.25} \quad (5.12)$$

Hence, the cumulative distribution function of Y can be expressed as

$$F(y) = 1 - \exp\left[-\left(\frac{y}{\theta^{0.25}}\right)^4\right] \quad (5.13)$$

Then the transition probability matrix can be computed and the ARLs can be easily obtained with the help of computing software like Matlab.

In order to find a suitable value of m, the in-control ARL of the EWMA chart given L and λ (L=3 and λ=0.2) is calculated following the above method. The results show that when m increases up to 301, the in-control ARL becomes stable. Therefore, the interval (h_L,h_U) is divided into m=301 subintervals for getting the ARLs with Markov chain approach.

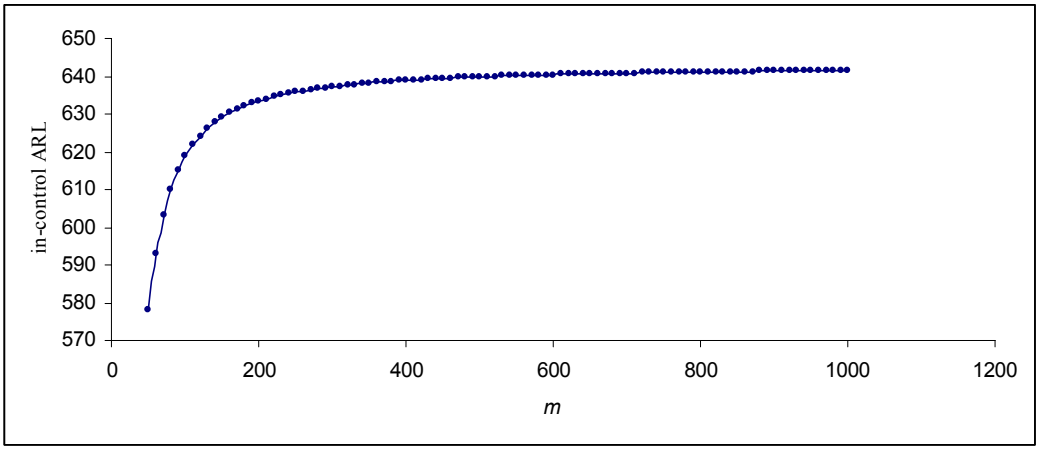

Figure 5.1 The in-control ARLs of an EWMA chart with transformed exponential data calculated with different m values (L=3 and λ=0.2)

5.3 Design of EWMA Chart with Transformed Exponential Data

Most of the previous studies on the design of EWMA chart or CUSUM are based on ARL consideration. That is, an acceptable in-control ARL is specified at the beginning to determine the probability of false alarm, and the optimal design is to find out the values of design parameters so as to provide the shortest ARL at certain specified out-of-control level.

5.3.1 In-control ARL

The in-control ARL values with different design parameters λ and L are calculated by the Markov chain approach. Figures 5.2 and 5.3 provide the contour plots for some commonly used in-control ARL levels. For other in-control ARL values, the relationship of λ and L can be achieved by interpolation. Appendix I also provide some in-control ARL values for different combinations of design parameters λ and L.

It is worth noting that the in-control ARL of an EWMA chart with transformed exponential data depends on the value of λ and L, and it is independent of the exponential mean θ. Therefore, Figures 5.2 and 5.3 can be used for any in-control exponential mean θ not only when $\theta_0=\theta_1=1$. The detailed proof is as follows:

Let $C = L\sqrt{\frac{\lambda}{2-\lambda}}, \mu_0 = 0.9064\theta_0^{0.25} = C_1\theta_0^{0.25}, \sigma_0 = 0.2543\theta_0^{0.25} = C_2\theta_0^{0.25}$ (based on formula 5.12). Then the p_{ij} (i =0, 1,…,m-1; j = 0,1,…,m-1) can be expressed as

$$p_{ij} = \Pr\left\{\frac{h_L + jw - (1-\lambda)m_i}{\lambda} \le y_t < \frac{h_L + (j+1)w - (1-\lambda)m_i}{\lambda}\right\}$$

$$= F\left(\frac{h_L + (j+1)w - (1-\lambda)m_i}{\lambda}\right) - F\left(\frac{h_L + jw - (1-\lambda)m_i}{\lambda}\right)$$

$$= 1 - \exp\left[-\left(\frac{h_L + (j+1)w - (1-\lambda)m_i}{\lambda \cdot \theta_1^{0.25}}\right)^4\right] - \left\{1 - \exp\left[-\left(\frac{h_L + jw - (1-\lambda)m_i}{\lambda \cdot \theta_1^{0.25}}\right)^4\right]\right\}$$

$$= \exp\left[-\left(\frac{\mu_0 - \sigma_0 C + j\cdot\left(\frac{2C\sigma_0}{m}\right) - (1-\lambda)\left[\mu_0 - C\sigma_0 + (i+0.5)\left(\frac{2C\sigma_0}{m}\right)\right]}{\lambda \cdot \theta_1^{0.25}}\right)^4\right]$$

$$- \exp\left[-\left(\frac{\mu_0 - \sigma_0 C + (j+1)\left(\frac{2C\sigma_0}{m}\right) - (1-\lambda)\left[\mu_0 - C\sigma_0 + (i+0.5)\left(\frac{2C\sigma_0}{m}\right)\right]}{\lambda \cdot \theta_1^{0.25}}\right)^4\right]$$

$$= \exp\left[-\left(\frac{\theta_0^{0.25}\left(C_1 - C_2 C + \frac{2C_2 C}{m}\cdot j - (1-\lambda)\left[C_1 - C_2 C + \frac{2CC_2(i+0.5)}{m}\right]\right)}{\lambda \cdot \theta_1^{0.25}}\right)^4\right]$$

$$- \exp\left[-\left(\frac{\theta_0^{0.25}\left(C_1 - C_2 C + \frac{2CC_2(j+1)}{m} - (1-\lambda)\left[C_1 - C_2 C + \frac{2CC_2(i+0.5)}{m}\right]\right)}{\lambda \cdot \theta_1^{0.25}}\right)^4\right] \quad (5.14)$$

It can be seen from the formula (5.14) that when the process is in-control, i.e. $\theta_0=\theta_1$, the value of p_{ij} only depends on the value of design parameters λ and L and calculation parameter m. Therefore, the in-control ARL value only depends on the value of λ and L, and is independent of the exponential mean θ. On the other hand, when the process becomes out-of-control, the proportion of θ_1 to θ_0 will influence the out-of-control ARL values.

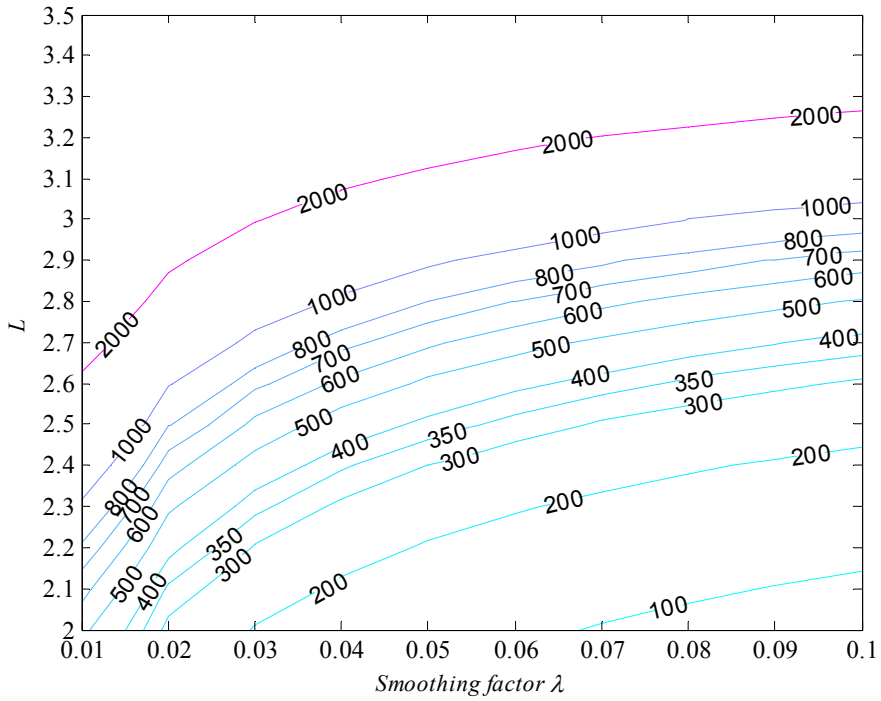

Figure 5.2 The in-control ARL contour plot of EWMA chart with transformed exponential data ($0< \lambda \leq 0.1$)

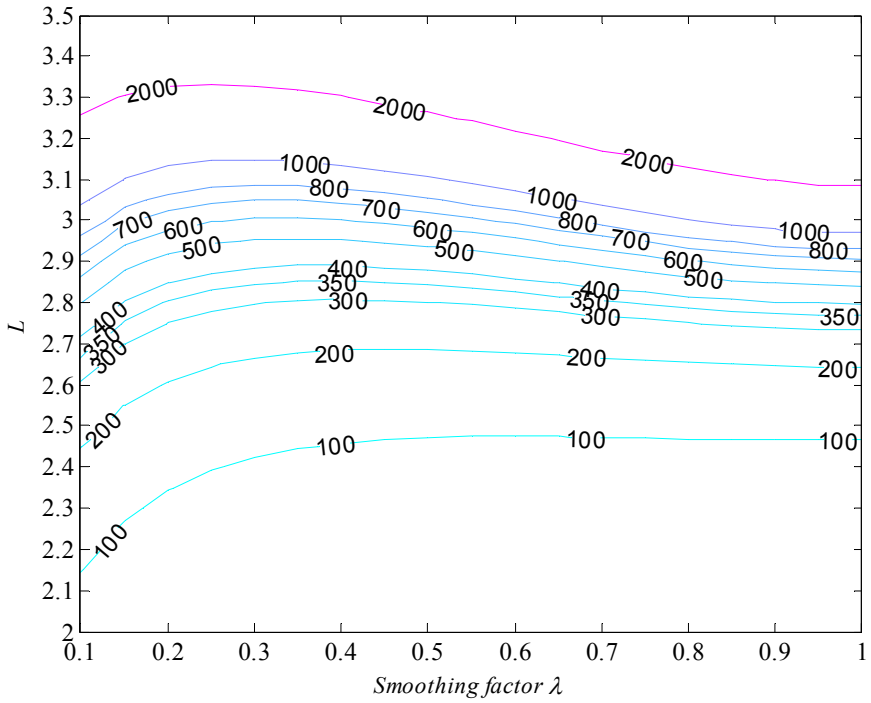

Figure 5.3 The in-control ARL contour plot of EWMA chart with transformed exponential data ($0.1< \lambda \leq 1$)

5.3.2 Out-of-control ARL

The out-of-control ARL is influenced by the shift level (θ_1/θ_0) as well as the design parameters λ and L. The optimal design scheme should have the shortest out-of-control ARL at certain shift level. The following Table 5.1 provides an illustration of this decision criterion with a fixed in-control ARL equals to 500.

Table 5.1 The ARLs of some selective EWMA charts with transformed exponential data (in-control ARL=500)

Shift	L	2.279	2.611	2.799	2.921	2.953	2.953	2.938	2.865	2.843
(θ_1/θ_0)	λ	0.02	0.05	0.1	0.2	0.3	0.4	0.5	0.8	1
0.1		8.44	6.67	5.65	***5.06***	5.13	5.71	6.98	22.84	88.84
0.2		11.35	9.23	8.18	***8.17***	9.55	12.40	17.32	59.31	177.18
0.3		14.85	12.48	***11.72***	13.38	17.82	25.29	36.52	109.71	265.52
0.4		19.53	***17.16***	17.38	22.95	33.36	48.43	68.54	174.05	353.86
0.5		26.39	***24.66***	27.50	41.17	61.61	87.30	118.03	252.60	442.06
0.6		***37.60***	38.26	47.42	76.11	110.92	149.01	190.26	345.28	528.33
0.7		***58.90***	66.82	89.90	142.28	193.35	242.06	290.21	448.08	603.08
0.8		***109.30***	136.85	184.80	262.26	321.17	369.80	413.93	540.18	639.74
0.9		***263.96***	319.67	376.61	436.24	470.10	494.49	515.82	570.45	604.59
1		500.00	500.00	500.00	500.00	500.00	500.00	500.00	500.00	499.95
1.2		***122.04***	137.01	160.76	194.59	216.72	231.59	241.84	256.63	266.27
1.5		42.28	***40.65***	43.44	51.58	59.46	66.49	72.71	88.06	101.42
1.8		26.25	23.27	***22.73***	24.54	27.11	29.78	32.41	40.36	48.65
2		21.36	18.39	***17.30***	17.77	19.05	20.54	22.11	27.33	33.29
2.5		15.17	12.54	11.19	***10.61***	10.75	11.12	11.61	13.72	16.64
3		12.17	9.87	8.57	7.78	***7.61***	7.65	7.80	8.78	10.44
3.5		10.38	8.33	7.13	6.30	6.03	***5.94***	5.95	6.43	7.47
4		9.19	7.32	6.20	5.39	5.08	4.93	***4.88***	5.10	5.81
5		7.67	6.06	5.08	4.33	4.00	3.81	***3.71***	***3.71***	4.09
10		4.96	3.88	3.21	2.66	2.38	2.21	2.10	***1.97***	2.02

It can be obviously seen in Table 5.1 that the EWMA charts with smaller λ are more sensitive to small shifts (θ_1/θ_0 close to 1), while those with larger λ are more effective in detecting larger shifts. For small downward shifts ($\theta_1/\theta_0<1$), the EWMA charts with

large λ between 0.5 and 1.0 may have longer out-of-control ARLs than their in-control ARLs. The reason behind this is that the data after double SQRT transformation is not exactly symmetric and is slightly skewed to the right; meanwhile, as λ approaches 1, an EWMA will approximate to a Shewhart chart, which is sensitive to non-normality. As indicated in bold and italic figures in Table 5.1, the optimal EWMA chart with transformed exponential data for a certain shift level (θ_1/θ_0) should have shortest out-of-control ARL among others. For example, when the proportion of θ_1 to θ_0 is equal to 0.5, the EWMA chart with λ=0.05 and L=2.611 is the optimal design with minimum out-of-control ARL=24.66. Consequently, optimal design schemes of EWMA chart with transformed exponential data can be found from the results in Table 5.1 when in-control ARL equals to 500.

Similarly, to facilitate the optimal design schemes of EWMA chart with transformed exponential data at other in-control ARL levels, the out-of-control ARL properties are investigated following the same procedures. Some commonly used in-control ARL levels are considered, i.e., in-control ARL=100, 300, 500, 800, 1000, and 2000. To simplify the calculation for achieving these optimal schemes, only some selective λ levels (0.02, 0.05, 0.08, 0.10, 0.20, 0.30, 0.40, 0.50, 0.60, 0.70, 0.80, 0.90, 1.00) are considered, and the L values are determined to achieve the specified in-control ARL with the help of Figures 5.2 and 5.3. Then the optimal design schemes are found to give the shortest out-of-control ARLs at certain shift levels (θ_1/θ_0). Table 5.2 lists the optimal design parameters as well as the optimal out-of-control ARL values achieved from the study.

Table 5.2 Optimal schemes of EWMA chart with transformed exponential data

Shift (θ_1/θ_0)		In-control ARL					
		100	300	500	800	1000	2000
0.2	λ	0.20	0.20	0.20	0.10	0.10	0.10
	L	2.344	2.752	2.921	2.963	3.037	3.256
	ARL_{min}	5.57	7.28	8.17	8.86	9.18	10.21
0.5	λ	0.05	0.05	0.05	0.05	0.05	0.05
	L	1.880	2.397	2.611	2.794	2.877	3.118
	ARL_{min}	15.23	21.48	24.66	27.74	29.27	34.29
0.8	λ	0.02	0.02	0.02	0.02	0.02	0.02
	L	1.469	2.033	2.279	2.490	2.585	2.862
	ARL_{min}	50.59	87.08	109.3	133.45	146.39	194.43
1.2	λ	0.05	0.02	0.02	0.02	0.02	0.02
	L	1.880	2.033	2.279	2.490	2.585	2.862
	ARL_{min}	52.44	95.94	122.04	150.22	165.26	220.94
1.5	λ	0.08	0.05	0.05	0.05	0.05	0.02
	L	2.065	2.397	2.611	2.794	2.877	2.862
	ARL_{min}	22.81	34.50	40.65	46.89	50.09	59.63
1.8	λ	0.20	0.10	0.10	0.08	0.08	0.05
	L	2.344	2.608	2.799	2.915	2.992	3.118
	ARL_{min}	13.92	19.72	22.73	25.53	26.94	31.37
2	λ	0.20	0.10	0.10	0.10	0.10	0.08
	L	2.344	2.608	2.799	2.963	3.037	3.218
	ARL_{min}	10.92	15.28	17.3	19.26	20.23	23.34
3	λ	0.50	0.40	0.30	0.30	0.30	0.20
	L	2.472	2.808	2.953	3.087	3.148	3.328
	ARL_{min}	5.26	6.84	7.61	8.34	8.70	9.82
4	λ	0.60	0.60	0.50	0.50	0.50	0.40
	L	2.476	2.787	2.938	3.055	3.108	3.303
	ARL_{min}	3.58	4.45	4.88	5.28	5.48	6.12
5	λ	0.70	0.70	0.50	0.60	0.60	0.60
	L	2.474	2.769	2.938	3.024	3.074	3.220
	ARL_{min}	2.82	3.38	3.71	3.91	4.04	4.44

The results in Table 5.2 indicate that the optimal λ for a certain amount of shift (θ_1/θ_0) decreases with the increase of in-control ARL level; however, it is rather stable for a

certain range of in-control ARLs. For example, when θ_1 is half of θ_0, the optimal λ is always 0.05 for the in-control ARL from 100 to 2000. The stableness of λ also justifies that in the above study, the selective values instead of the continuous range of λ can be accurate enough for application. Meanwhile, since the optimal value of λ is stable for a range of in-control ARLs, it is reasonable to choose a suitable λ value using Table 5.2 even if the desired in-control ARL is not included.

It is also worth noting that the design schemes with very small λ values less than 0.1 are optimal for small shifts of the process, and the corresponding ARL_{min} values are usually large. In that case, the inaccuracy of out-of-control ARL from the Markov chain approach is not very serious and will not affect the parameters chosen of EWMA chart with transformed exponential data. Moreover, the real out-of-control ARL is even better than that achieved from the Markov chain approach.

5.3.3 Optimal Design Procedures

Based on the analysis above, the recommended design procedures of an optimal EWMA chart with transformed exponential data are as follows:

***Step 1*:** Specify the desired in-control ARL and the out-of-control shift (θ_1/θ_0) to be detected quickly;

***Step 2*:** Find the λ value according to Table 5.2;

***Step 3*:** Obtain the corresponding L value using Figures 5.2 or 5.3;

***Step 4*:** The entire ARL profile for the EWMA chart can be achieved using the Markov chain approach. It can be used to evaluate the performance of the chart and ensure that the chart provides sufficient protection against other shifts.

5.4 A Comparative Study on Chart Performance

5.4.1 EWMA chart with transformed exponential data vs. X-MR chart

To compare the ARL property of EWMA chart with transformed exponential data and X-MR chart, a simulation is conducted by transforming the exponential data to normal using double SQRT transformation and then setting up the X-MR chart(with 3σ control limits) to monitor the data. On the other hand, two EWMA charts with transformed exponential data are designed so that the in-control ARL is almost equal to that of the X-MR chart. Two EWMA charts are designed to be optimal in detecting shift (θ_1/θ_0) equals to 0.5 and 2.0, respectively. Table 5.3 presents the ARL profiles of the charts, where $(\theta_1/\theta_0)_{opt}$ stands for the out-of-control shift (θ_1/θ_0) level at which the EWMA chart with transformed exponential data is optimal.

Figure 5.4 includes the ARL curves of X-MR chart and the EWMA charts with transformed exponential data described above. It can be seen from Table 5.3 that both EWMA charts achieve the maximum ARL value at the in-control level θ_1/θ_0=1.0. However, the maximum ARL value of transformed X-MR chart is achieved when the shift (θ_1/θ_0) is about 0.3. The trend of ARL curve for the transformed X-MR chart implies that when the downward shift occurs up to 0.3 of the in-control exponential mean, the out-of-control ARL value will increase greatly, from 131.41 to 709.22. As a result, it will take longer time to raise an out-of-control signal even if the process has

deteriorated a lot. Therefore, the X-MR chart is not effective in detecting process deteriorations. The ARL curves show that the EWMA chart with transformed exponential data is more sensitive in detecting process shifts than the X-MR chart for process improvement as well as process deterioration.

Table 5.3 The ARLs of X-MR chart and EWMA charts with transformed exponential data (TE EWMA)

Shift (θ_1/θ_0)	X-MR	TE EWMA1 λ=0.05 L=2.0151 $(\theta_1/\theta_0)_{opt}$=0.5	TE EWMA2 λ=0.20 L=2.4523 $(\theta_1/\theta_0)_{opt}$=2.0	Shift (θ_1/θ_0)	X-MR	TE EWMA1 λ=0.05 L=2.0151 $(\theta_1/\theta_0)_{opt}$=0.5	TE EWMA2 λ=0.20 L=2.4523 $(\theta_1/\theta_0)_{opt}$=2.0
0.1	272.48	5.10	3.97	1.4	58.928	32.31	35.27
0.2	540.54	6.92	5.98	1.5	50.556	25.71	27.09
0.3	709.22	9.14	8.90	1.6	40.601	21.38	21.73
0.4	675.68	12.19	13.51	1.7	37.313	18.36	18.04
0.5	**531.91**	**16.70**	**21.12**	1.8	30.294	16.14	15.40
0.6	389.11	24.06	33.89	1.9	27.39	14.46	13.43
0.7	290.7	37.31	55.20	**2**	**23.574**	**13.14**	**11.92**
0.8	206.19	63.33	88.38	2.5	14.118	9.31	7.81
0.9	153.61	108.50	125.15	3	9.4796	7.46	6.00
1	**131.41**	**131.42**	**131.42**	3.5	7.0507	6.37	4.99
1.1	105.15	96.40	101.45	4	5.5154	5.65	4.34
1.2	85.034	62.43	69.57	4.5	4.5884	5.12	3.89
1.3	71.276	43.17	48.31	5	3.9153	4.73	3.56

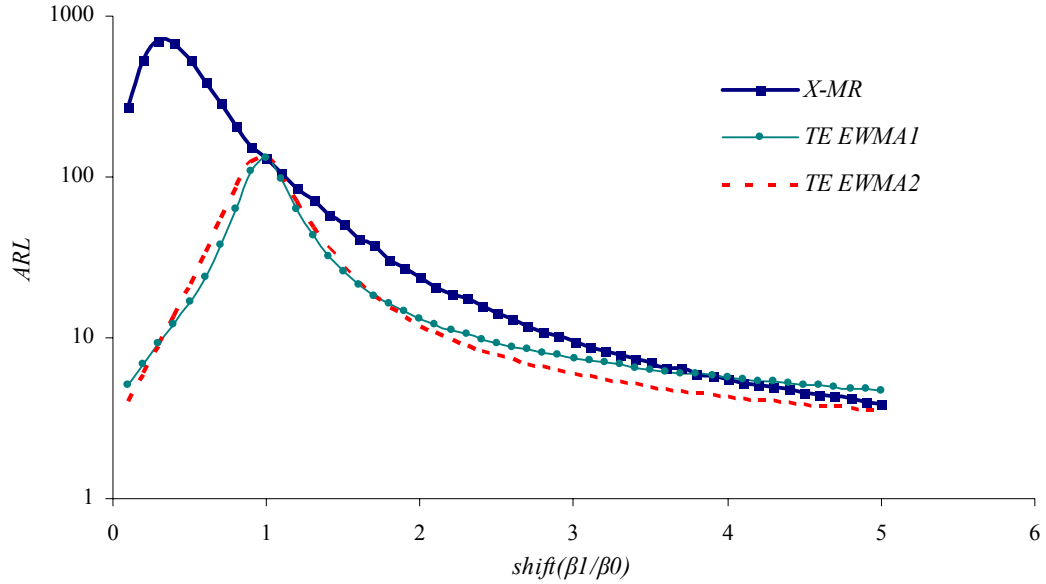

Figure 5.4 The ARL curves of the X-MR and EWMA charts with transformed exponential data

5.4.2 EWMA chart with transformed exponential data vs. CQC chart

Another comparison of ARL properties is conducted between EWMA chart with transformed exponential data and the CQC chart. Two EWMA charts with transformed exponential data and the CQC chart are designed to achieve equal in-control ARL (370.37). The EWMA charts with transformed exponential data are designed to be optimal in detecting shift (θ_1/θ_0) equal to 0.2 and 5.0, respectively. The control limits of the CQC chart are UCL=6.6226 and LCL=0.0013. The out-of-control ARLs are listed in Table 5.4.

The ARL curves in Figure 5.5 show that both of the EWMA charts can detect the process shifts faster than the CQC chart whenever the process improves or deteriorates. In particular, when the in-control exponential mean decreases slightly from in-control level, the out-of-control ARL of the EWMA charts with small λ will drop greatly, and thus the shift can be detected quickly. However, the out-of-control ARLs of the CQC

chart will increase for small process deterioration, and therefore it is not effective in this case. This can be attributed to the skewness of exponential distribution that makes the control limits not symmetrical without transformation. Note that when the smoothing factor λ is relatively large, EWMA chart with transformed exponential data may also have longer out-of-control ARL for downward shifts, but this is not so serious compared with the CQC chart. Furthermore, for EWMA chart with transformed exponential data, large smoothing factor λ will be employed only for detecting large upward mean shift. Thus it will not affect the performance of the chart.

Table 5.4 The ARLs of CQC chart and EWMA charts with transformed exponential data (TE EWMA)

Shift (θ_1/θ_0)	CQC chart	TE EWMA1 λ=0.20 L=2.8235 $(\theta_1/\theta_0)_{opt}$=0.2	TE EWMA2 λ=0.70 L=2.8193 $(\theta_1/\theta_0)_{opt}$=5.0	Shift (θ_1/θ_0)	CQC chart	TE EWMA1 λ=0.20 L=2.8235 $(\theta_1/\theta_0)_{opt}$=0.2	TE EWMA2 λ=0.70 L=2.8193 $(\theta_1/\theta_0)_{opt}$=5.0
0.1	74.51	4.81	11.69	1.4	101.20	62.62	94.92
0.2	**148.52**	**7.64**	**30.52**	1.5	76.25	44.68	69.02
0.3	222.53	12.22	59.16	1.6	59.07	33.86	52.01
0.4	296.53	20.34	98.73	1.7	46.94	26.89	40.50
0.5	370.30	35.30	150.41	1.8	38.16	22.15	32.45
0.6	441.33	63.14	215.13	1.9	31.66	18.78	26.65
0.7	498.04	114.48	291.64	2	26.73	16.29	22.36
0.8	513.80	204.95	367.71	2.5	13.95	9.94	11.68
0.9	465.56	329.89	406.57	3	9.01	7.37	7.71
1	370.35	370.40	370.36	3.5	6.59	6.00	5.78
1.1	271.08	261.15	282.49	4	5.21	5.16	4.68
1.2	192.83	154.54	196.81	4.5	4.34	4.58	3.98
1.3	138.10	94.53	135.14	**5**	**3.75**	**4.16**	**3.49**

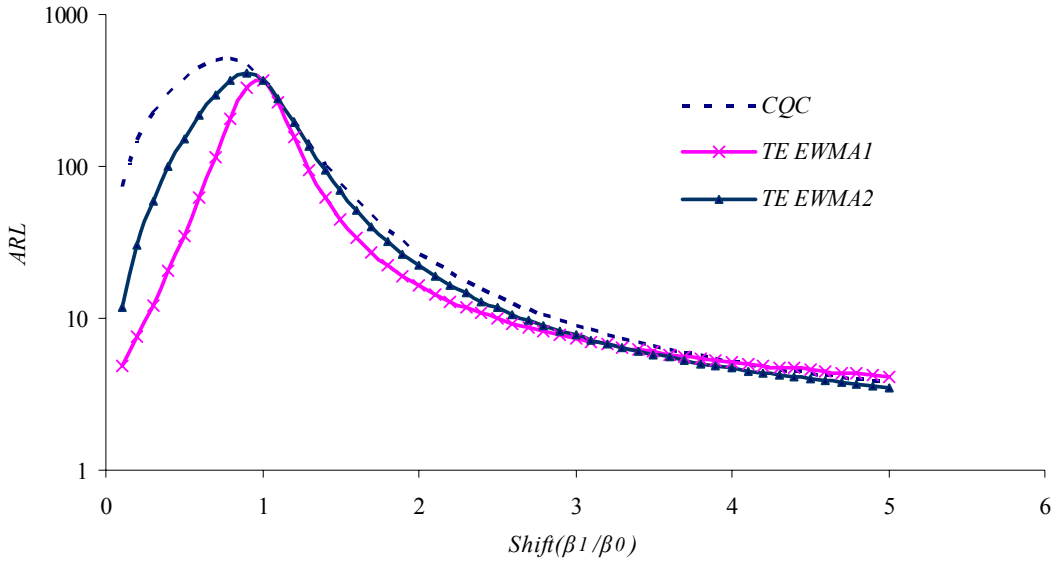

Figure 5.5 The ARL curves of the CQC chart and EWMA charts with transformed exponential data

5.4.3 EWMA chart with transformed exponential data vs. Exponential EWMA

It is worth comparing the performance of EWMA chart with transformed exponential data with the exponential EWMA (Gan, 1998), which has been shown to be effective in monitoring the exponentially-distributed TBE data. Four pairs of two-sided EWMA charts are designed to achieve in-control ARL=500, while optimal in detecting downward or upward shifts at different levels (θ_1/θ_0 = 0.3, 0.5, 2.0, and 3.0 respectively). The out-of-control ARLs are calculated accordingly and the results are shown in Table 5.5. The relative difference in Table 5.5 is calculated by

$$\text{Relative difference} = (ARL_{TE} - ARL_{Exp})/ARL_{Exp} \quad (5.15)$$

Table 5.5 The ARLs of EWMA charts with transformed exponential data and exponential EWMA chart

Shift (θ_1/θ_0)	$(\theta_1/\theta_0)_{opt}$=0.3 TE 1 λ=0.1 L=2.799	Exp 1 λ=0.190 h_L=0.361 h_U=2.359	Relative difference	$(\theta_1/\theta_0)_{opt}$=0.5 TE 2 λ=0.05 L=2.611	Exp 2 λ=0.100 h_L=0.502 h_U=1.801	Relative difference
0.2	8.18	8.11	0.01	9.23	9.80	-0.06
0.3	11.72	10.96	0.07	12.48	12.25	0.02
0.4	17.38	16.08	0.08	17.16	16.24	0.06
0.5	27.50	26.05	0.06	24.66	23.38	0.05
0.6	47.42	46.84	0.01	38.26	37.83	0.01
0.7	89.90	92.23	-0.03	66.82	71.12	-0.06
0.8	184.80	192.21	-0.04	136.85	156.80	-0.13
0.9	376.61	379.86	-0.01	319.67	365.51	-0.13
1	500.00	500.00	0.00	500.00	500.00	0.00
1.2	160.76	194.02	-0.17	137.01	140.19	-0.02
1.5	43.44	49.59	-0.12	40.65	36.87	0.10
1.8	22.73	22.85	-0.01	23.27	18.77	0.24
2	17.30	16.21	0.07	18.39	14.01	0.31
2.5	11.19	9.27	0.21	12.54	8.67	0.45
3	8.57	6.57	0.30	9.87	6.40	0.54
Shift (θ_1/θ_0)	$(\theta_1/\theta_0)_{opt}$=2.0 TE 3 λ=0.1 L=2.799	Exp 3 λ=0.100 h_L=0.504 h_U=1.806	Relative difference	$(\theta_1/\theta_0)_{opt}$=3.0 TE 4 λ=0.3 L=2.953	Exp 4 λ=0.144 h_L=0.429 h_U=2.100	Relative difference
0.2	8.18	9.73	-0.16	9.55	8.59	0.11
0.3	11.72	12.16	-0.04	17.82	11.10	0.61
0.4	17.38	16.09	0.08	33.36	15.37	1.17
0.5	27.50	23.11	0.19	61.61	23.33	1.64
0.6	47.42	37.25	0.27	110.92	39.67	1.80
0.7	89.90	69.62	0.29	193.35	76.12	1.54
0.8	184.80	152.45	0.21	321.17	161.77	0.99
0.9	376.61	355.09	0.06	470.10	345.91	0.36
1	500.00	500.00	0.00	500.00	500.00	0.00
1.2	160.76	143.23	0.12	216.72	181.59	0.19
1.5	43.44	37.37	0.16	59.46	45.20	0.32
1.8	22.73	18.95	0.20	27.11	21.40	0.27
2	17.30	14.13	0.22	19.05	15.45	0.23
2.5	11.19	8.73	0.28	10.75	9.11	0.18
3	8.57	6.44	0.33	7.61	6.57	0.16

* TE represents the EWMA chart with transformed data, Exp stands for exponential EWMA chart.

Figure 5.6 presents the ARL curves for the four pairs of EWMA charts, from which we can see the two charts have similar performance in terms of ARL. The EWMA charts with transformed exponential data are slightly worse in detecting designed shifts, and the relative difference is very small. Especially, when the chart is designed for detecting process deterioration, i.e., the optimal shift $(\theta_1/\theta_0)_{opt}$ is less than 1.0, the EWMA charts with transformed exponential data have shorter out-of-control ARL for small process shifts. Only when the chart is designed for detecting large process improvement (e.g. $(\theta_1/\theta_0)_{opt}$=3.0), the overall performance of exponential EWMA is better than the EWMA chart with transformed exponential data.

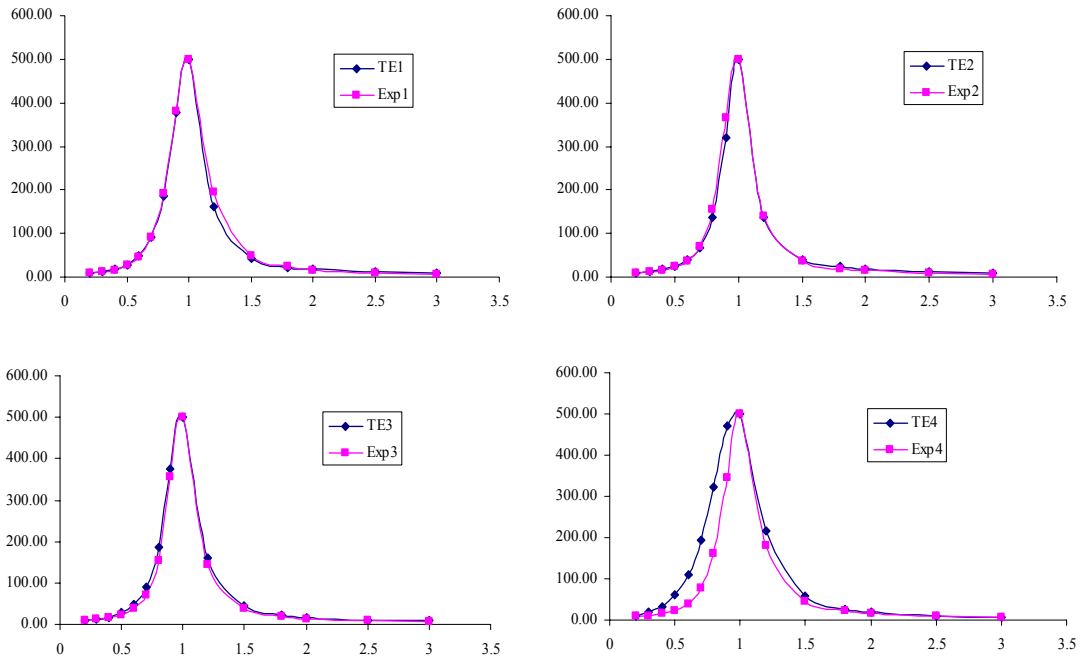

Figure 5.6 The ARL curves of EWMA charts with transformed exponential data and exponential EWMA charts

5.5 Robustness of EWMA Chart with Transformed Exponential Data to Weibull Data

The above study is carried out based on the assumption that the TBE data can fit into an exponential distribution with a constant event occurrence rate. However, this is not always true in many cases, and Weibull distribution can be a better alternative to model the time between events data when the event occurrence rate varies with time. A former study (Borror *et al.*, 1999) on the EWMA chart for normal data proved that the EWMA chart can be designed so that it is robust to the normality assumption. Borror *et al.* (2003) investigated the robustness of the TBE CUSUM and demonstrated that the TBE CUSUM is robust for a wide variety of parameter values for the Weibull distribution. Since in this study the TBE data are transformed to close normal, we suspect it may also have the robust property to other distributions besides exponential. The following study is to test this supposition.

As Weibull distribution is a more widely used distribution to model the time between events data, the robustness of the EWMA chart with transformed exponential data to Weibull data is investigated in this study. The probability density function (pdf) of the two-parameter Weibull distribution can be written as:

$$f(x) = \frac{\eta}{\theta}\left(\frac{x}{\theta}\right)^{\eta-1} e^{-\left(\frac{x}{\theta}\right)^{\eta}}, x > 0, \theta > 0, \delta > 0 \qquad (5.16)$$

where θ is the scale parameter and η is the shape parameter. When η is equal to 1, the Weibull distribution will reduce to the exponential distribution.

Note that a Weibull distribution with scale parameter θ and shape parameter η, i.e. W(θ, η) is still a Weibull distribution W($\theta^{0.25}$, 4η) after the double SQRT transformation. Therefore, the Markov chain approach for calculating ARL is still applicable while the mean and variance can be estimated with

$$\begin{aligned} \hat{\mu} &= E(Y) = \theta^{0.25}\Gamma\left(1+\frac{1}{4\eta}\right) \\ \hat{\sigma} &= \sqrt{D(Y)} = \theta^{0.25}\sqrt{\Gamma\left(1+\frac{1}{2\eta}\right)-\Gamma^2\left(1+\frac{1}{4\eta}\right)} \end{aligned} \tag{5.17}$$

The cumulative distribution function changes to

$$F(y) = 1 - \exp\left[-\left(\frac{y}{\theta^{0.25}}\right)^{4\eta}\right] \tag{5.18}$$

It has been proved that the in-control ARL value of EWMA chart with transformed exponential data depends on the design parameters λ and L, and is independent of the scale parameter θ for exponentially-distributed TBE data. A study on the in-control ARL of EWMA chart with transformed Weibull data shows that this conclusion is true for Weibull TBE data as well. When keeping the shape parameter η as a constant, the in-control ARL of EWMA chart with transformed Weibull data is also constant even if the scale parameter θ varies. However, different shape parameters η lead to different in-control ARLs. Therefore, without loss of generality, we fix the scale parameter θ to 1.0, and change the shape parameter η to investigate the in-control ARL properties.

Table 5.6 presents some in-control ARLs of eight selective EWMA charts with double SQRT transformation while the actual TBE data follow Weibull distributions. The first four charts are designed to obtain approximately the same in-control ARL of 500, and

the last four charts with in-control ARL close to 370.4. It can be observed from Table 5.6 that the smaller the smoothing factor λ, the better the robustness of the EWMA chart. Figure 5.7 presents the trend of in-control ARLs with different shape parameters η (with data from the first four columns in Table 5.6). When the smoothing factor λ is equal to 0.05, the in-control ARL is very stable. In fact, when the shape parameter η is larger than 0.5, the in-control ARL is always within 3% of 500 which is designed for the exponential data. The trend is the same for EWMA charts with transformed Weibull data when in-control ARL equals to 370.4. According to the optimal design schemes (Table 5.2), small smoothing factor λ (=0.05) is also favorable since it is optimal in detecting small process shifts.

Table 5.6 In-control ARLs of EWMA charts with transformed Weibull data

		EWMA charts with transformed Weibull data							
	$(\theta_1/\theta_0)_{opt}$	0.2	**0.5**	**2**	5	0.2	**0.5**	**2**	5
	λ	0.20	**0.05**	**0.10**	0.50	0.20	**0.05**	**0.10**	0.70
η	L	2.921	**2.611**	**2.799**	2.938	2.824	**2.487**	**2.689**	2.819
0.2		144.22	428.67	261.78	63.91	130.30	355.32	229.48	46.43
0.5		400.73	499.22	476.13	217.32	316.93	371.82	361.47	138.01
0.8		510.44	501.04	503.30	523.14	377.51	370.76	372.75	392.22
1		499.54	500.16	499.61	499.88	370.23	370.30	370.48	370.11
1.5		435.49	497.20	481.17	296.53	333.04	369.46	361.09	189.33
2		389.93	494.61	465.44	219.36	305.64	368.83	353.13	138.58
2.5		361.18	492.57	453.86	185.97	287.75	368.35	347.20	118.29
3		342.12	490.97	445.26	168.06	275.59	367.96	342.75	107.71
3.5		328.75	489.69	438.71	157.06	266.92	367.66	339.32	101.29
4		318.92	488.65	433.58	149.66	260.47	367.41	336.63	97.00
4.5		311.42	487.80	429.48	144.35	255.50	367.20	334.45	93.94
5		305.53	487.08	426.13	140.38	251.56	367.03	332.67	91.66

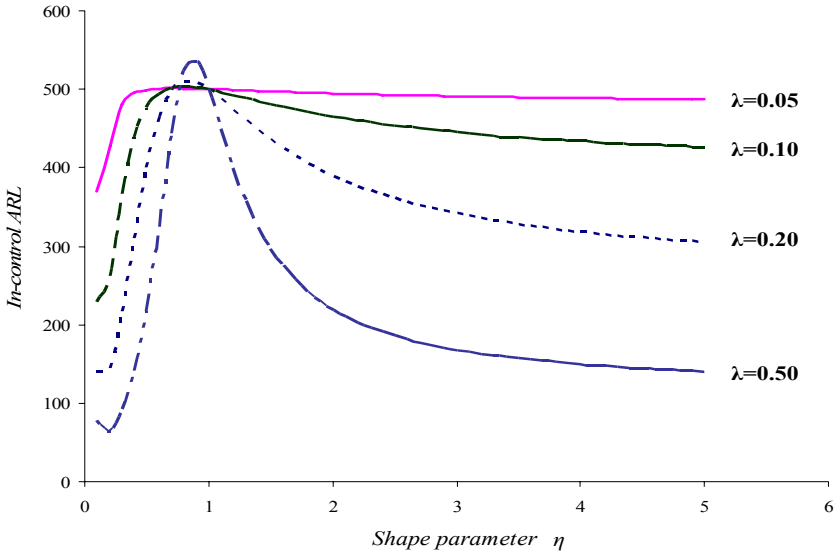

Figure 5.7 In-control ARL curves of EWMA chart with transformed Weibull distribution with different shape parameters η

For the out-of-control situations, four EWMA charts (as indicated in bold) with good robustness of in-control ARL are chosen from the Table 5.6. The TBE data following Weibull distribution with some specified shape parameters η=0.5, 1.0, 2.0, 3.0, and 4.0 are investigated. The out-of-control ARLs are calculated in different mean shift levels. For a certain shape parameter η value, mean shifts occur due to a change in scale parameter θ. The out-of-control ARLs are listed in Table 5.7.

The ARLs in the same row of Table 5.7 provide the out-of-control ARLs when the Weibull distributions have same shape parameter η and different scale parameters so that the shift in the mean ($\mu_1/\mu_0= \theta_1/\theta_0$) will be at the different levels. This is reasonable since in practical applications the scale parameter is more likely to change due to assignable causes, while the shape parameter is more related to the natural properties of the system and is rather stable.

Table 5.7 Out-of-control ARLs of EWMA charts with transformed Weibull data

EWMA		shift in mean (θ_1/θ_0)							
	η	0.5	1.0	1.5	2.0	2.5	3.0	3.5	4.0
	0.5	73.48	499.22	92.70	42.00	27.62	21.14	17.48	15.13
λ=0.05	1	24.66	500.16	40.65	18.39	12.54	9.87	8.33	7.32
L=2.611	2	10.48	494.61	16.94	8.50	6.09	4.93	4.25	3.79
$(\theta_1/\theta_0)_{opt}$ =0.5	3	6.72	490.97	10.56	5.61	4.12	3.40	2.95	2.64
	4	5.00	488.65	7.70	4.24	3.18	2.61	2.30	2.14
	0.5	132.52	476.13	93.32	41.37	26.25	19.56	15.86	13.53
λ=0.10	1	27.49	499.61	43.43	17.30	11.19	8.57	7.12	6.20
L=2.799	2	9.47	465.44	16.03	7.31	5.10	4.08	3.50	3.11
$(\theta_1/\theta_0)_{opt}$ =2	3	5.72	445.26	9.31	4.67	3.38	2.77	2.43	2.23
	4	4.15	433.58	6.56	3.49	2.58	2.21	2.00	1.79
	0.5	63.59	371.82	81.27	38.32	25.60	19.75	16.41	14.24
λ=0.05	1	22.77	370.30	36.96	17.19	11.83	9.35	7.91	6.96
L=2.487	2	9.89	368.83	15.85	8.06	5.80	4.71	4.06	3.63
$(\theta_1/\theta_0)_{opt}$ =0.5	3	6.39	367.96	9.97	5.34	3.94	3.25	2.82	2.53
	4	4.77	367.41	7.31	4.06	3.04	2.50	2.23	2.10
	0.5	104.86	361.47	81.00	37.42	24.21	18.23	14.88	12.75
λ=0.10	1	24.84	370.48	38.75	16.10	10.56	8.14	6.79	5.93
L=2.689	2	8.95	353.13	14.92	6.95	4.88	3.92	3.36	3.00
$(\theta_1/\theta_0)_{opt}$ =2	3	5.46	342.75	8.81	4.48	3.25	2.68	2.36	2.17
	4	3.98	336.63	6.26	3.35	2.50	2.16	1.93	1.71

The data in Table 5.7 reveal that the EWMA chart is more sensitive for Weibull distribution with shape parameter η>1 than for exponential distribution (η =1.0), for both upward and downward shifts. The larger the shape parameter, the better the performance of the EWMA chart. One possible reason for this property could be the different shift levels are caused by the change of scale parameters. The increase of scale parameter θ while holding shape parameter η constant has the effect of stretching out the pdf curve, which in turn leads to a shorter out-of-control ARL. However, the performance of the EWMA chart is not good for transformed Weibull data with η<1.0, and this maybe because the double SQRT transformation is not suitable in that case. It

is worth noting that in order to transform Weibull distribution to approximate normal, power transformation can still be applied; however instead of using the power of 0.25, the following transformation can be employed.

$$U = \left(\frac{X}{\theta} \right)^{0.25\eta} \tag{5.19}$$

In this case, the optimal design procedures will be similar to the described in Section 5.3, while optimal parameters may be somewhat different. Basically, small smoothing factor λ (=0.05, 0.10, or 0.20) is also suggested when the EWMA chart is designed to detect small process shifts.

5.6 An Illustrative Example

A simulated example is shown below to demonstrate the use of EWMA chart with transformed exponential data for detecting process shifts. The first 20 observations are generated following exponential distribution with mean equals to 1.0, and the next 10 points are generated using exponential mean θ =0.2. The in-control ARL is set to be 500. The design parameters of the EWMA chart are determined following the procedures discussed above (λ=0.20, L=2.921), and the starting value Z_0 is the mean of the first 20 observations. Figure 5.8 presents the EWMA charts with transformed exponential data, which becomes out-of-control at the 24th point.

Table 5.8 The data for the EWMA chart with transformed exponential data

Failure No	Time between failures(X_t)	Transformed data(Y_t)	TE EWMA (Z_t)	UCL	LCL
0			1.0027		
1	2.7804	1.2913	1.0604	1.1276	0.8778
2	2.1152	1.2060	1.0895	1.1627	0.8427
3	0.9873	0.9968	1.0710	1.1815	0.8238
4	0.5389	0.8568	1.0281	1.1926	0.8127
5	1.2284	1.0528	1.0331	1.1994	0.8060
6	0.2314	0.6935	0.9652	1.2036	0.8018
7	1.2952	1.0668	0.9855	1.2063	0.7991
8	0.7744	0.9381	0.9760	1.2080	0.7974
9	2.8236	1.2963	1.0401	1.2090	0.7964
10	0.0550	0.4843	0.9289	1.2097	0.7957
11	1.2780	1.0632	0.9558	1.2101	0.7953
12	1.0056	1.0014	0.9649	1.2104	0.7950
13	2.1290	1.2079	1.0135	1.2106	0.7948
14	0.3715	0.7807	0.9670	1.2107	0.7947
15	0.5484	0.8606	0.9457	1.2108	0.7946
16	1.5206	1.1105	0.9786	1.2108	0.7946
17	2.1879	1.2162	1.0261	1.2109	0.7945
18	0.2967	0.7380	0.9685	1.2109	0.7945
19	1.3015	1.0681	0.9884	1.2109	0.7945
20	1.5992	1.1245	1.0157	1.2109	0.7945
21	0.2178	0.6832	0.9492	1.2109	0.7945
22	0.0220	0.3853	0.8364	1.2109	0.7945
23	0.6398	0.8944	0.8480	1.2109	0.7945
24	0.0202	0.3770	0.7538	1.2109	0.7945
25	0.3751	0.7826	0.7595	1.2109	0.7945
26	0.2046	0.6725	0.7421	1.2109	0.7945
27	0.4263	0.8080	0.7553	1.2109	0.7945
28	0.0125	0.3344	0.6711	1.2109	0.7945
29	0.0426	0.4542	0.6277	1.2109	0.7945
30	0.0830	0.5367	0.6095	1.2109	0.7945

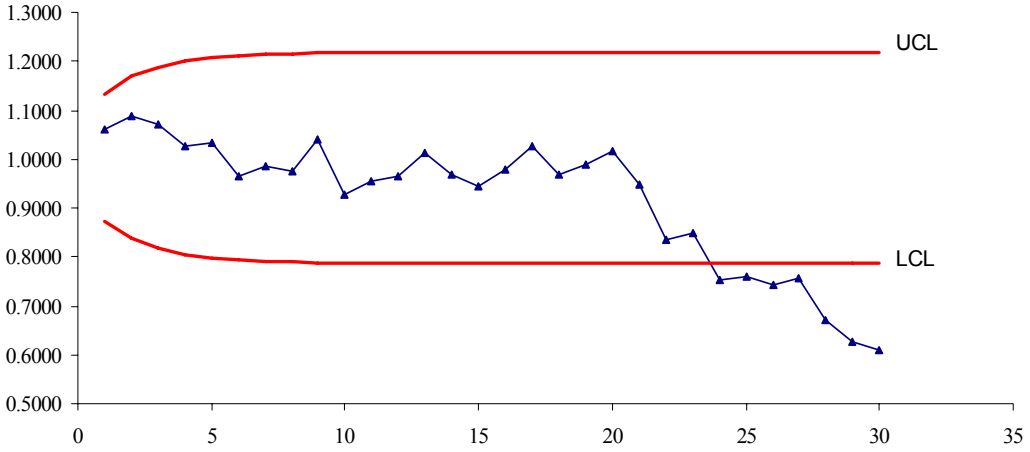

Figure 5.8 The EWMA chart with transformed exponential data

5.7 Conclusions

This chapter discusses an alternative way of monitoring exponentially distributed TBE data, which can help to monitor the processes with very low fraction nonconforming levels. The exponential data can be transformed using double SQRT transformation and then monitored by the EWMA chart. Comparisons showed that the proposed EWMA chart with transformed exponential data is more effective than the X-MR and CQC charts especially in detecting process deteriorations. It has similar ARL performance to the exponential EWMA chart. Besides, the proposed EWMA chart with small smoothing factor λ (=0.05) is very robust to Weibull distribution for the in-control ARL. It can be even more sensitive for Weibull data with shape parameter η>1 than it is for the exponential data.

The results also show that the performance of EWMA chart with transformed exponential data is not very sensitive to the design parameters λ and L, thus leading to rather easy design procedures without too much rigorous parameter-chosen procedures

as the exponential EWMA. This may encourage the engineers to use it more frequently in practical applications, and in turn help to enhance process quality.

Chapter 6 CCC Charts with Variable Sampling Intervals

6.1 Introduction

As introduced in chapter 2, CCC chart monitors the cumulative number of conforming items between two consecutive nonconforming items based on geometric distribution, and it is particularly suitable for high-quality processes with very low FNC. A summary of research and application of this useful technique can be found in Xie *et al.* (2002).

Bourke (1991) suggested using 100% inspection for generating the CCC chart. However, when taking into consideration practical factors such as inspection time and cost, this may lead to a relatively high inspection cost and thus limit the application of the CCC chart. Because of the memoryless property of geometric distribution, one possible approach to solve this problem is to use the CCC chart with Variable Sampling Intervals (VSI). Instead of inspecting the items one by one, we take samples from them. Note that we regard every individual item inspected as a sample (i.e., the sample size is equal to one), and the sampling interval is the time between taking two successive samples.

The motivation of employing variable sampling scheme is to reduce the inspection cost while maintaining the detection speed of control charts for process changes. For a VSI chart, the length of sampling interval varies with the process status. A shorter sampling

interval is used if there is some indication that the process may have changed, and a longer sampling interval is used if there is no such indication. This means that a shorter sampling interval should be used next if the current value of the control statistic is close to but not actually outside the control limits, and a longer sampling interval should be used if the current value is close to the target. If the current value is actually outside the control limits, then the chart signals in the same way as the standard Fixed Sampling Interval (FSI) chart, in which the sampling interval length is fixed without any change through the sampling process.

A significant amount of research has been carried out on VSI control charts to improve their sensitivity of detecting process disturbances without increasing the rate of inspected items and false alarm occurrences. Reynolds *et al.* (1988) investigated the normally distributed processes monitored by the $\overline{X}$ chart using sample means. They evaluated the Average Time to Signal (ATS) and the Average Number of Samples to Signal (ANSS) properties for the FSI and VSI $\overline{X}$ charts, and showed that the VSI chart is substantially more efficient.

Prabhu *et al*. (1993) and Costa (1994) proposed Variable Sample Size (VSS) schemes for $\overline{X}$ chart. They used a smaller sample size for the next sample when the current $\overline{X}$ value is close to the center line, and a larger sample size otherwise. Subsequent studies, see Prabhu *et al*. (1994) and Costa (1997), considered both the VSI and VSS schemes. Carot *et al.* (2002) further combined the double sampling method with the VSI $\overline{X}$ chart. Lin & Chou (2005) studied the design of VSS and VSI $\overline{X}$ charts under non-normality based on Burr distribution. Besides, Lee & Bai (2000) further extended the idea and developed two VSI schemes in $\overline{X}$ control charts with run rules. Bai & Lee

(2002) then proposed the VSI $\overline{X}$ control charts with an improved switching rule and proved that the proposed charts can reduce the average number of switches between short and long sampling intervals with comparable ATS.

Moreover, the variable sampling methods can also be used to improve the efficiency of control charts for attributes, see Epprecht & Costa (2001), and Vaughan (1993). Recently, Epprecht *et al*. (2003) developed a general model for adaptive *c, np, u* and *p* control charts in which one, two or three design parameters, i.e., sample size, sampling interval and control limit width, switch between two values. They also provided general guidance on choosing effective design schemes. Wu & Luo (2004) investigated the optimal design of the VSI, VSS and VSIVSS *np* charts, and found that the adaptive *np* charts do improve effectiveness significantly, especially for detecting small or moderate process shifts.

Saccucci *et al.* (1992) extended the VSI method to EWMA chart, and Reynolds & Arnold (2001) investigated the EWMA charts with both VSI and VSS schemes. The VSS CUSUM chart was studied by Annadi *et al.* (1995), and the VSSVSI CUSUM chart was developed by Arnold & Reynolds (2001). Subsequently, Villalobos *et al*. (2005) studied the FSI and VSI multivariate SPC charts for on line SMD (surface mounted devices) monitoring.

On the other hand, studies on economic design of control charts also revealed that VSI control charts show better performance than FSI charts with respect to cost. Bai & Lee (1998) constructed a cost model which involves the cost of false alarms, the cost of detecting and eliminating an assignable cause, and the cost of sampling and testing, etc.

It is proved that with proper design parameters, the VSI $\overline{X}$ chart provides lower expected cost per unit time compared with the corresponding FSI $\overline{X}$ chart. Furthermore, Chen (2004) extended this study to the VSI $\overline{X}$ chart with non-normal data.

In this study the variable sampling scheme was extended to the CCC chart. Note that individual observations are used when implementing the CCC chart; therefore only the CCC chart with variable sampling intervals, namely, CCC_{VSI} chart, will be discussed. The description and properties of the CCC_{VSI} chart are discussed, followed by comparisons of performance between the CCC_{VSI} and the CCC_{FSI} chart. Finally, the design procedures and decision rules of the CCC_{VSI} chart are described together with an example.

6.2 Description of the CCC_{VSI} Chart

Notations:

p_0 the in-control process nonconforming rate.

p' the out-of-control process nonconforming rate.

α the acceptable probability of false alarm.

α' the true probability of false alarm.

X_i the cumulative count of items inspected after the (i-1)th nonconforming item until the ith nonconforming item is observed (including the last nonconforming item).

n the number of different interval lengths of the CCC_{VSI} chart.

d_j j=1,2,…, n. sampling interval lengths of the CCC_{VSI} chart, , i.e., the time between two items inspected consecutively ($d_n<d_{n-1}<...<d_2<d_1$).

d the sampling interval length of the CCC_{FSI} chart.

IL_j the interval limits in the CCC_{VSI} chart which divide the region between UCL and LCL into n sub-regions $I_1, I_2, \ldots, I_n$ ($IL_{n-1} < IL_{n-2} < \ldots < IL_2 < IL_1$).

R the number of points in the CCC chart until an alarm arises.

S the total number of items inspected before a signal occurs, $S = \sum_{i=1}^{R} X_i$.

L_i the sampling interval length which is used to get X_i.

ARL the average run length.

ATS_V the in-control average time to signal of the CCC_{VSI} chart.

ATS_F the in-control average time to signal of the CCC_{FSI} chart.

ATS_V' the out-of-control average time to signal of the CCC_{VSI} chart.

ATS_F' the out-of-control average time to signal of the CCC_{FSI} chart.

I improvement factor, defined as $I = \frac{ATS_V^{'}}{ATS_F^{'}}$,

q_j the probability that point X_i falls in region I_j when the process nonconforming rate is p_0, i.e. $q_j = P\{X_i \in I_j \mid p = p_0\}, j = 1,2,\cdots,n; i = 1,2,...R$

q_j' the probability that point X_i falls in region I_j when the process nonconforming rate shifted to p', i.e., $q_j^{'} = P\{X_i \in I_j \mid p = p' > p_0\}, j = 1,2,\cdots,n; i = 1,2,...R$.

Let X denote the cumulative counts of items inspected until a nonconforming item is observed. X can be modeled using the geometric distribution with parameter p_0, and the mass probability function of X is:

$$P\{X = x\} = (1 - p_0)^{x-1} p_0, \quad x = 1, 2, \cdots \tag{6.1}$$

Since the geometric distribution is highly skewed, instead of using the traditional $k\sigma$ as control limits, probability control limits are used, see Xie & Goh (1997). On the other

hand, because the geometric distribution is discrete, the control limits are rounded to integers and the points that fall on the UCL and LCL are regarded as out-of-control signals, i.e., $P\{X \geq UCL\} = P\{X \leq LCL\} = \alpha / 2$. The UCL and LCL of the CCC chart can be calculated as follows:

$$UCL = \left[\frac{\ln(\frac{\alpha}{2})}{\ln(1-p_0)} + 1 \right], \quad LCL = \left[\frac{\ln(1-\frac{\alpha}{2})}{\ln(1-p_0)} \right] \tag{6.2}$$

where [Y] stands for the largest integer not greater than Y.

Note that because the control limits are rounded to integers, the true false alarm rate α' may not be exactly equal to the given value of α. Rather, it can be expressed as

$$\alpha' = (1-p_0)^{UCL-1} + 1 - (1-p_0)^{LCL} \tag{6.3}$$

However, since CCC charts are used in high-quality environment where p_0 is very small, α' should be very close to α, and the difference between α and α' can be neglected.

Generally speaking, the VSI schemes are used for the CCC chart in order to detect the increase of nonconforming rate quickly. The CCC_{VSI} chart refers to CCC chart designed based on variable sampling intervals, that is, the sampling interval varies with the accumulative count of conforming items. The sampling interval length L_i used for inspection between the (i-1)th nonconforming item and the ith nonconforming item depends on the value of X_{i-1}.

When implementing the CCC_{VSI} chart, a finite number of sampling interval lengths d_1, d_2, ..., d_n ($d_n<d_{n-1}<...<d_2<d_1$) are used. These sampling interval lengths should be chosen under practical considerations of manufacturing processes. For example, the minimum sampling interval length could not be less than the time lag between two continuous items. In that case, we use 100% inspection. The maximum sampling interval length can be chosen according to the maximum amount of time that is allowed for the process to run without inspection.

On the other hand, interval limits IL_1, IL_2,..., IL_{n-1} ($IL_{n-1} < IL_{n-2} < ... < IL_2 < IL_1$) are added in the CCC_{VSI} chart, and thus divide the region between UCL and LCL into n sub-regions I_1, I_2,..., I_n, corresponding to the n different sampling interval lengths. It follows that

$$L_i = \begin{cases} d_1,\ X_{i-1} \in I_1 = (IL_1, UCL) \\ d_2, X_{i-1} \in I_2 = (IL_2, IL_1] \\ ..... \\ d_n, X_{i-1} \in I_n = (LCL, IL_{n-1}] \end{cases} \tag{6.4}$$

The IL_1, IL_2,…, IL_{n-1} can be calculated by the following formulas

$$\begin{cases} IL_1 = \left\lceil \dfrac{\ln(\frac{\alpha}{2} + q_1)}{\ln(1-p_0)} \right\rceil, \\ IL_2 = \left\lceil \dfrac{\ln(\frac{\alpha}{2} + q_1 + q_2)}{\ln(1-p_0)} \right\rceil, \\ \cdots \\ IL_{n-1} = \left\lceil \dfrac{\ln(\frac{\alpha}{2} + q_1 + q_2 + \cdots + q_{n-1})}{\ln(1-p_0)} \right\rceil \end{cases} \tag{6.5}$$

For example, when n =3, three different sampling interval lengths are employed. To implement the CCC_{VSI} scheme, control limits IL_1 and IL_2 are added between UCL and LCL, and the region (LCL, UCL) is thus divided into three sub-regions as shown in Figure 6.1.

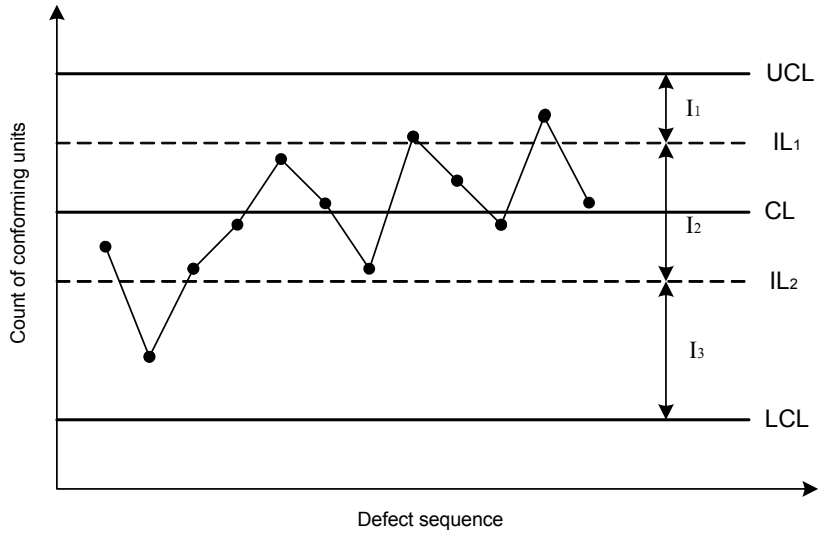

Figure 6.1 The CCC_{VSI} chart with three sampling interval lengths

When $X_i \in I_1$, the process is running very well, and its quality even has a large possibility to have improved. In this case, a longer sampling interval length d_1 (d_1>d) is used in the following inspection of items in order to reduce cost. When $X_i \in I_2$, the nonconforming rate of the process most probably remains unchanged, so the equal sampling interval length d_2 as the corresponding CCC_{FSI} chart (d_2=d) is chosen. When $X_i \in I_3$, the process nonconforming rate may have increased, and the next point X_{i+1} has a large probability to fall below LCL, which means the process will be out of control. Then a relatively shorter sampling interval length d_3 (d_3<d) is employed in order to judge whether the next point will fall below LCL in a shorter period and therefore reduce the amount of time the out-of-control condition remains undetected.

Note that a larger sampling interval is used when the nonconforming rate decreases to a certain level and a smaller sampling interval is employed when it increases; therefore this CCC_{VSI} chart scheme is only suitable for monitoring the increase of nonconforming rate. In practice, we suggest using the shortest interval length as the initial sampling interval length in order to protect against problems that may occur during start-up.

6.3 Properties of the CCC_{VSI} Chart

The Average Run Length (ARL), i.e., the average number of points that must be plotted before a point indicates an out-of-control condition, is a useful performance measure of control charts. However, because the sampling intervals of a VSI chart are not constant, it is necessary to record both the time and the number of samples inspected until a signal occurs. Average Time to Signal (ATS) and Average Number of Items inspected (ANI) are two parameters to evaluate those properties. ATS is defined as the average length of time it takes the chart to produce a signal. When the process is in control, larger ATS may reduce the false alarm rate; whereas when process is out of control, smaller ATS may help detect the increase of nonconforming rate p more quickly. ANI is defined as the expected value of the number of items inspected until a nonconforming signal occurs.

For common control charts, such as Shewhart, CUSUM and EWMA charts applied to the statistics X-bar, R, S, np, p, c, u, etc., the ATS is the average length of time the chart takes to produce a signal only under the condition that the state of the process does not change between two samples. When the process shifts from the in-control to

the out-of-control state between two samples, the average time from the moment of the shift to the moment the chart signals can be obtained by subtracting from the ATS the amount of time between the last sample before the shift and the moment of shift. However, due to the memoryless property of the geometric distribution, ATS of the CCC chart is a good approximation to the average time from the moment of the shift to the moment of the signal when p' is small.

As defined before, R is the number of points in the CCC chart until an alarm arises, i.e., the accumulative count of nonconforming items until an alarm arises. The expected value of R is the average number of points in the chart before an alarm arises including the point that gives the alarm, i.e., the ARL for the CCC chart. Using Wald's identity, the ANI for both the CCC_{FSI} and the CCC_{VSI} chart can be calculated as:

$$ANI = E(S) = E(\sum_{i=1}^{R} X_i) = E(R)E(X_i) = \frac{ARL}{p} \tag{6.6}$$

The ARL for the CCC chart can be expressed as

$$ARL = \frac{1}{1-(1-p)^{LCL}+(1-p)^{UCL-1}} \tag{6.7}$$

Therefore, ATS_F can be calculated using following equation

$$ATS_F = ANI \times d = \frac{ARL}{p} \times d \tag{6.8}$$

On the other hand, for the CCC_{VSI} chart, the total time used before an alarm arises can be calculated as $T = \sum_{i=1}^{R} X_i L_i$, and the ATS_V can be expressed as

$$ATS_V = E(\sum_{i=1}^{R} X_i L_i) = E(R)E(XL) \tag{6.9}$$

If the process is in-control, it satisfies

$$P(L_i = d_j) = P\{X_{i-1} \in I_j \mid X_{i-1} \in (LCL, UCL)\} = \frac{q_j}{1-\alpha} = \frac{q_j}{q_1 + q_2 + \cdots + q_n},\ i = 2,3,\cdots R. \tag{6.10}$$

Then the ATS_v can be calculated as

$$\begin{aligned} ATS_V = ARL \cdot \{&E(X_i L_i \mid L_i = d_1)P(L_i = d_1) + E(X_i L_i \mid L_i = d_2)P(L_i = d_2) + \cdots + \\ &+ E(X_i L_i \mid L_i = d_n)P(L_i = d_n)\} = \frac{ARL}{p} \cdot \frac{d_1 q_1 + d_2 q_2 + \cdots + d_n q_n}{q_1 + q_2 + \cdots + q_n} \end{aligned} \tag{6.11}$$

Note that equation (6.11) is derived under the assumption that $P(L_1 = d_j) = q_j/(1-\alpha)$, i.e., the sampling interval length used before observing the first nonconforming item is chosen at random with these probabilities. As mentioned before, it is recommended to use the shortest sampling interval during process start-up in practice. In such a case, equation (6.11) is not exactly accurate; however, it is a good approximation to the ATS_V because the effect of the initial sampling interval length can be neglected provided that nonconforming rate p_0 is very small and the ARL is large.

6.4 Performance Comparisons between the CCC_{VSI} and the CCC_{FSI} Chart

To evaluate the efficiency of the CCC_{VSI} chart, we compared its performance with that of the CCC_{FSI} chart. Note that with same nonconforming rate p_0 and acceptable false alarm rate α, both the CCC_{FSI} and the CCC_{VSI} chart have the same *ANI* function. In

order to compare their ATS property under a constant standard, proper design parameters of the CCC_{VSI} and the CCC_{FSI} chart are chosen so that the equation $ATS_F = ATS_V$ is satisfied. Therefore the CCC_{VSI} chart will be matched to the corresponding CCC_{FSI} chart in the sense that when $p=p_0$ both of them have the same in-control *ATS*. On the other hand, when the process nonconforming rate shifts to p' ($>p_0$), we compare the value of ATS_F' and ATS_V'. The control chart with smaller out-of-control ATS' is considered to be able to detect the increase of nonconforming rate more quickly.

Let $ATS_F = ATS_V$, the following equation should be satisfied according to equations (6.8) and (6.11).

$$d = \frac{d_1 q_1 + d_2 q_2 + \cdots + d_n q_n}{q_1 + q_2 + \cdots + q_n} = \frac{d_1 q_1 + d_2 q_2 + \cdots + d_n q_n}{1-\alpha} \tag{6.12}$$

Without loss of generality, the sampling interval length of the CCC_{FSI} chart is set to 1, i.e. d=1. By choosing suitable values of $(d_1, d_2, \cdots, d_n)$ and $(q_1, q_2, \cdots, q_n)$ that satisfy equation (6.12), the matched CCC_{VSI} and CCC_{FSI} charts that have same in-control ATS can be obtained. Then, when the process nonconforming rate shifts to p', the performance of the CCC_{VSI} chart can be evaluated by calculating the value of I, which is the ratio of out-of-control ATS of the CCC_{VSI} and the CCC_{FSI} chart.

$$I = \frac{ATS_V'}{ATS_F'} = \frac{d_1 q_1' + d_2 q_2' + \cdots + d_n q_n'}{q_1' + q_2' + \cdots + q_n'} \tag{6.13}$$

When I is less than 1.00, the ATS_V' is less than ATS_F', which means that the CCC_{VSI} chart outperforms the CCC_{FSI} chart. Here we name I as improvement factor. The smaller the improvement factor, the better the performance of the CCC_{VSI} chart.

The values of q_j' can be calculated using the following equations,

$$\begin{cases} q_1^{'} = (1-p^{'})^{IL1} - (1-p')^{UCL-1} \\ q_2^{'} = (1-p^{'})^{IL2} - (1-p')^{IL1} \\ \cdots \\ q_{n-1}^{'} = (1-p^{'})^{ILn-1} - (1-p')^{ILn-2} \\ q_n^{'} = (1-p^{'})^{LCL} - (1-p')^{ILn-1} \end{cases} \tag{6.14}$$

6.4.1 Improvement Factors for Different Numbers of Sampling Intervals

Following the above calculation method, we now investigate the behavior of CCC_{VSI} chart for different numbers of sampling interval lengths n. Here the equal probability intervals are used, i.e.

$$q_1 = q_2 = \cdots = q_n = \frac{1-\alpha}{n} \tag{6.15}$$

Using equation (6.12) and d =1, the following equation can be obtained,

$$1-\alpha = d_1 q_1 + d_2 q_2 + \cdots d_n q_n = \frac{1-\alpha}{n}(d_1 + d_2 + \cdots + d_n)$$

which is equal to the following equation,

$$d_1 + d_2 + \cdots + d_n = n \tag{6.16}$$

Given α and p_0, for example, α =0.0027 and p_0=0.0005, some representative values of nonconforming rate p' are chosen for this analysis. The sampling interval lengths ($d_1, d_2, \ldots, d_n$) can be chosen as follows: Fixed d=1; n=2, d_1=1.9,d_2=0.1; n=3, d_1=1.9, d_2=1, d_3=0.1; n=5, d_1=1.9, d_2=1.5, d_3=1, d_4=0.5, d_5=0.1; n=7, d_1=1.9, d_2=1.7, d_3=1.5,

d_4=1, d_5=0.5, d_6=0.3, d_7=0.1. Using formulas (6.5), (6.13) and (6.14), the values of corresponding improvement factors I are calculated, and the results are shown in Table 6.1.

Table 6.1 Improvement factors I for representative number of intervals

p'/p_0	Improvement Factor I			
	n=2	n=3	n=5	n=7
1	1.000	1.000	1.000	1.000
1.1	0.940	0.945	0.949	0.948
1.2	0.884	0.895	0.902	0.901
1.3	0.832	0.848	0.859	0.857
1.4	0.783	0.804	0.819	0.816
1.5	0.738	0.764	0.782	0.778
1.6	0.695	0.726	0.747	0.743
1.7	0.655	0.692	0.716	0.710
1.8	0.618	0.659	0.686	0.680
1.9	0.584	0.629	0.658	0.652
2	0.551	0.601	0.633	0.625

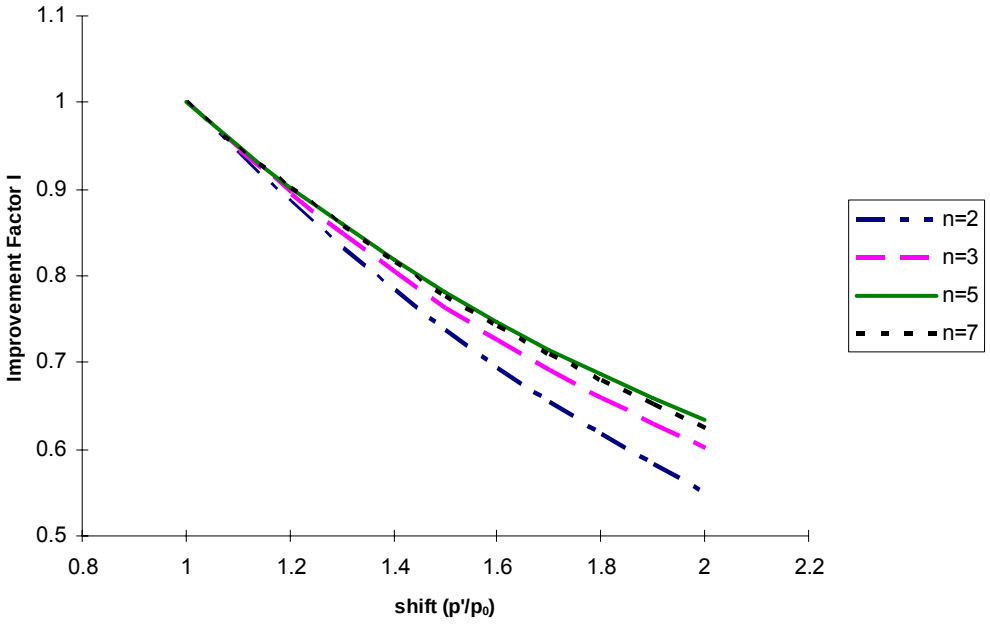

Figure 6.2 Improvement factors with different number of sampling intervals

Figure 6.2 shows how improvement factor I changes with different process shifts using different numbers of sampling intervals, from which it can be seen that the greater the increase in the nonconforming rate(p'/p_0), the smaller the improvement factor I, and the greater improvement in the CCC_{VSI} chart compared with the matched CCC_{FSI} chart.

As shown in Table 6.1, when the nonconforming rate p becomes twice as much as the original level, I =0.55106 provided that n=2. That means the average time for the CCC_{VSI} chart to detect the process shift is about half of that of the CCC_{FSI} chart. Meanwhile, the results also reveal that among the four different numbers of sampling intervals n=2, 3, 5, and 7, the CCC_{VSI} chart gets the best performance when n=2. This is also convenient for practical applications since there are only two different sampling interval lengths, and consequently it may be easier to control the inspection sampling rate without frequent changes.

6.4.2 Improvement Factors for Different Sampling Interval Lengths

Based on the analysis above, we fix the number of sampling intervals n=2 here, and change the length of sampling intervals to investigate how the performance of CCC_{VSI} charts vary. Four different sets of (d_1, d_2) are used and their corresponding improvement factors I are calculated. Other parameters remain unchanged as in the last example. The results are shown in Table 6.2. The summarized results indicating the trends of improvement factors are also shown in Figure 6.3.

It can be seen from Figure 6.3 that when the shift of nonconforming rate from original level (p'/p_0) becomes larger, improvement factor I decreases and the performance of

CCC_{VSI} charts becomes better compared with the matched CCC_{FSI} charts. Moreover, it also shows that the larger the difference of interval lengths (d_1 - d_2), the smaller the improvement factor I , and the better the performance of CCC_{VSI} charts.

Table 6.2 Improvement factors I with different sampling interval lengths

p'/p_0	FSI	VSI			
	(1,1)	(1.9, 0.1)	(1.7, 0.3)	(1.5, 0.5)	(1.2, 0.8)
1	1	1.000	1.000	1.000	1.000
1.1	1	0.940	0.954	0.967	0.987
1.2	1	0.884	0.910	0.936	0.974
1.3	1	0.832	0.869	0.907	0.963
1.4	1	0.783	0.831	0.880	0.952
1.5	1	0.738	0.796	0.854	0.942
1.6	1	0.695	0.763	0.831	0.932
1.7	1	0.655	0.732	0.808	0.923
1.8	1	0.618	0.703	0.788	0.915
1.9	1	0.584	0.676	0.769	0.907
2	1	0.551	0.651	0.751	0.900

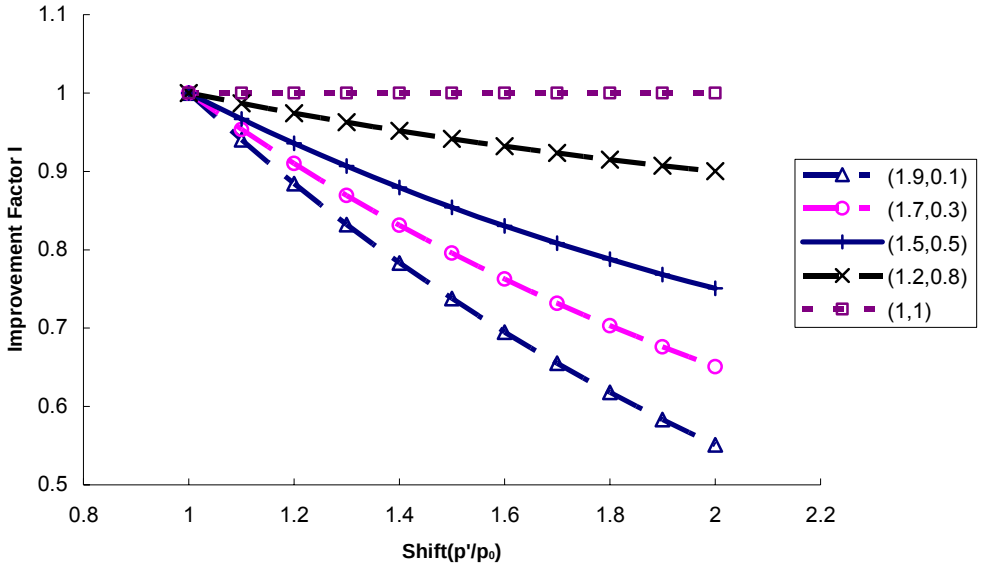

Figure 6.3 Improvement factors with different sampling interval lengths

6.4.3 Improvement Factors for Different Probability Allocations

The above analysis on the number of sampling intervals and the length of sampling interval is based on the equal probability allocation, i.e., the region between UCL and LCL is divided into n parts so that the points have equal probability of falling into the n regions ($q_1=q_2=\ldots=q_n$). The results indicate that when the number of sampling intervals n=2, a larger difference between d_1 and d_2, i.e. (d_1 - d_2), may produce better performance for the CCC_{VSI} chart.

In order to investigate the performance of CCC_{VSI} charts when the equation $q_1=q_2=\ldots=q_n$ is not satisfied, we fix n=2 and d_1= 1.9, and only change the value of q_1. The corresponding value of p_2 and d_2 can be achieved using equation (6.12), and the corresponding improvement factors I are then calculated. The results are shown in Table 6.3 as follows.

Note that

$$d_2 = \frac{1-\alpha-d_1 q_1}{q_2} > 0 \tag{6.17}$$

So for fixed d_1, q_1 should satisfy the inequality $q_1 < (1-\alpha)/d_1$. Table 6.3 and Figure 6.4 indicate that when (q_2-q_1) decreases, the improvement factor I also decreases, and the performance of CCC_{VSI} charts becomes better. So it is reasonable to use equal probabilities $q_1=q_2=\ldots=q_n$ when designing a CCC_{VSI} chart.

Table 6.3 Improvement factors *I* with different probability allocation

	(q_1,q_2)	(0,10, 0.8973)	(0.2,0.7973)	(0.3,0.6973)	(0.4, 0.5973)	(0.49865, 0.49865)
	(d_1,d_2)	(1.9,0.8997)	(1.9,0.7742)	(1.9,0.6128)	(1.9,0.3973)	(1.9, 0.1)
p'/p_0	1	1.000	1.000	1.000	1.000	1.000
	1.1	0.980	0.967	0.957	0.948	0.940
	1.2	0.964	0.939	0.918	0.900	0.884
	1.3	0.951	0.914	0.884	0.856	0.832
	1.4	0.940	0.894	0.853	0.816	0.783
	1.5	0.932	0.876	0.826	0.780	0.738
	1.6	0.925	0.861	0.802	0.747	0.695
	1.7	0.920	0.848	0.781	0.716	0.655
	1.8	0.916	0.837	0.762	0.688	0.618
	1.9	0.913	0.828	0.745	0.663	0.584
	2	0.910	0.820	0.730	0.640	0.551

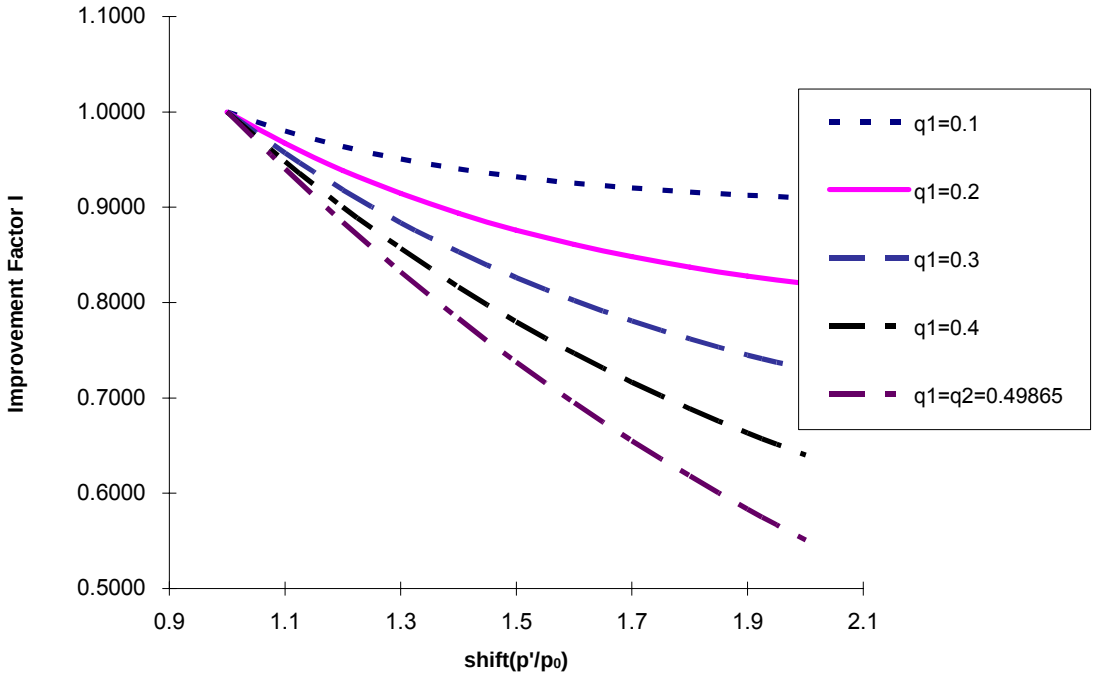

Figure 6.4 Improvement factors with different probability allocation

6.5 Design of a CCC_{VSI} Chart

Based on the above analysis results, the design procedures of a CCC_{VSI} chart are suggested to be the following:

***Step* 1: Determine the control limits for fixed false alarm rate α**

The control limits UCL and LCL of a CCC_{VSI} chart can be calculated using equation (6.2). In order to get a meaningful LCL ($LCL = \left\lceil \frac{\ln(1-\alpha/2)}{\ln(1-p)} \right\rceil > 1$), the inequality $p<\alpha/2$ should be satisfied, i.e. $\alpha>2p$. Notice that the CCC chart is particularly suitable for high-quality processes, which have very low nonconforming rate p, so this is not a serious problem. Here it is assumed that the nonconforming rate p is known, or it can be estimated from historical data.

***Step* 2: Choose the number of sampling intervals *n*=2.**

***Step* 3: Use equal probability allocation $q_1 = q_2 = \frac{1-\alpha}{2}$, so the interval limit is $IL_1 = \frac{\ln(0.5)}{\ln(1-p_0)}$.**

Step* 4: Calculate the sampling interval lengths *(d_1, d_2)

Given n=2 and $q_1 = q_2 = \frac{1-\alpha}{2}$, from equation (6.12) we may get $d_1 + d_2 = 2$.

It can be seen from Table 6.2 and Figure 6.3 that larger difference of interval lengths (d_1 - d_2) may produce better performance for CCC_{VSI} charts. However, the difference of interval lengths (d_1 - d_2) cannot be too large. Suppose that the matched CCC_{FSI} takes one sample for every m items, when using n=2 and equal probability allocation q_1=q_2, d_2 must not be less than 1/m, and d_1 should not be larger than (2- 1/m). In the case when d_2=1/m and d_1= (2-1/m), we take every item as a sample if the process becomes worse. Table 6.4 shows the recommended values of d_1 and d_2 for CCC_{VSI} charts with respect to the sampling frequency of the matched CCC_{FSI} chart. With increasing m, (d_1 - d_2) also increases. Hence, the efficiency of the matched CCC_{VSI} chart becomes more significant. However, since the CCC chart is particularly suitable for high-quality processes with very low nonconforming rate p, m cannot be too large. Meanwhile, when determining the value of m, as well as d_1, other factors, e.g. the maximum amount of time that is allowed for the process to run without sampling, should be taken into consideration.

Table 6.4 Sampling Interval Lengths (d_1, d_2) for the CCC_{VSI} Charts with Different Matched Sampling Interval Lengths m for the CCC_{FSI} Charts

m	1	2	3	4	5	6	7	8	9	10
d_1	1	1.5	1.67	1.75	1.8	1.83	1.86	1.88	1.89	1.90
d_2	1	0.5	0.33	0.25	0.2	0.17	0.14	0.13	0.11	0.10

***Step* 5: Evaluate the efficiency of CCC_{VSI} charts**

All the design parameters of the CCC_{VSI} chart can be determined following the four steps mentioned above. Given the shifted nonconforming rate p', the probability (q_1', q_2') that a point falls into each region can be calculated using equation (6.14), and

then the improvement factor I can be calculated using equation (6.13), which can be used to evaluate the efficiency of the CCC_{VSI} chart.

Note that because the geometric distribution is discrete, the equation $q_1=q_2=...= q_n$ may not be rigorously satisfied. However, given that p_0 is very small, the formulas above are accurate enough for a good design.

6.5.1 Charting Procedures of a CCC_{VSI} Chart

After determining all the design parameters following the five steps mentioned above, the CCC_{VSI} chart is ready for process monitoring. Figure 6.5 presents the charting and decision making procedures for the CCC_{VSI} chart. To protect against problems that may arise when the process starts up, the initial sampling interval length is set to be the shortest interval d_n. The charting procedure is same as for the traditional CCC chart except that the sampling interval length varies with the position of preceding point plotted. Therefore, the users have to determine the sampling interval length for plotting X_i, according to the region in which X_{i-1} has fallen in.

6.5.2 An Example

To illustrate the design method of a CCC_{VSI} chart, an example with simulated data is discussed in this section. Table 6.5 shows a set of randomly generated data that follow the geometric distribution with nonconforming rate p_0=0.0005.

Let false alarm rate α=0.0027. Using formula (6.2), we get UCL= 13212, LCL= 2. Let $q_1= q_2 = (1-\alpha)/2 = 0.49865$, we obtain the interval limit IL_1= 1385 using equation (6.5).

Given that the sampling frequency for the CCC_{FSI} chart is one sample every five items, we set d_2=0.2, and the corresponding d_1=1.8. The CCC_{VSI} chart is shown in Figure 6.6.

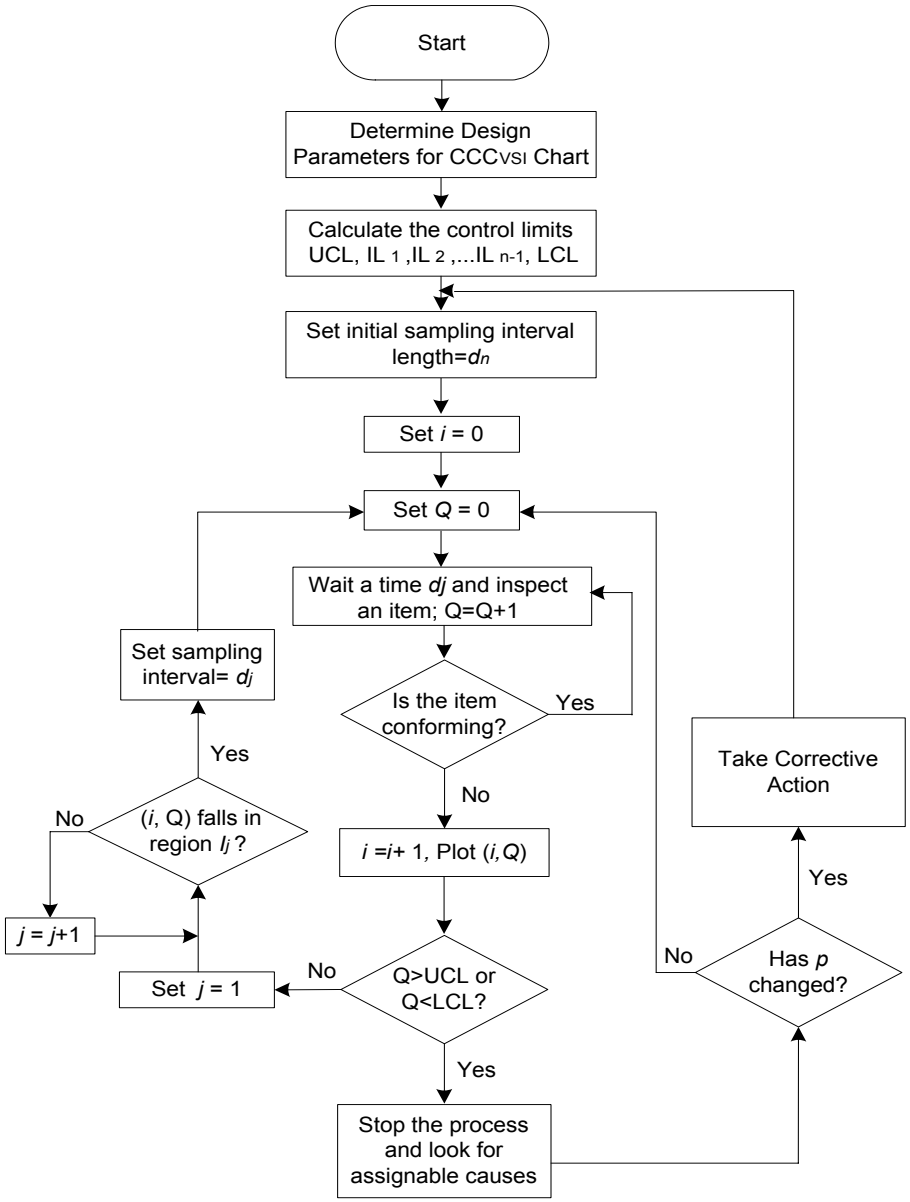

Figure 6.5 Charting procedures and decision rules for the CCC_{VSI} chart.

Table 6.6 shows the improvement factors I when different amount of shifts in the nonconforming rate p' occurs. The results shows that when p' increases to 0.001, the ATS of the CCC_{VSI} chart is only 60.09% of that of the matched CCC_{FSI} chart.

Table 6.5 A set of data from geometric distribution with nonconforming rate p_0=0.0005

Defect Sequence	CCC	Defect Sequence	CCC	Defect Sequence	CCC	Defect Sequence	CCC	Defect Sequence	CCC
1	102	11	970	21	5696	31	8361	41	353
2	2928	12	466	22	2082	32	583	42	7858
3	998	13	162	23	413	33	1618	43	767
4	1442	14	606	24	9235	34	141	44	1937
5	230	15	3470	25	3947	35	1526	45	368
6	543	16	1803	26	3190	36	1741	46	1374
7	1568	17	133	27	3230	37	333	47	686
8	7977	18	173	28	1008	38	1287	48	1692
9	393	19	1781	29	2601	39	3191	49	2376
10	1620	20	224	30	3229	40	794	50	3324

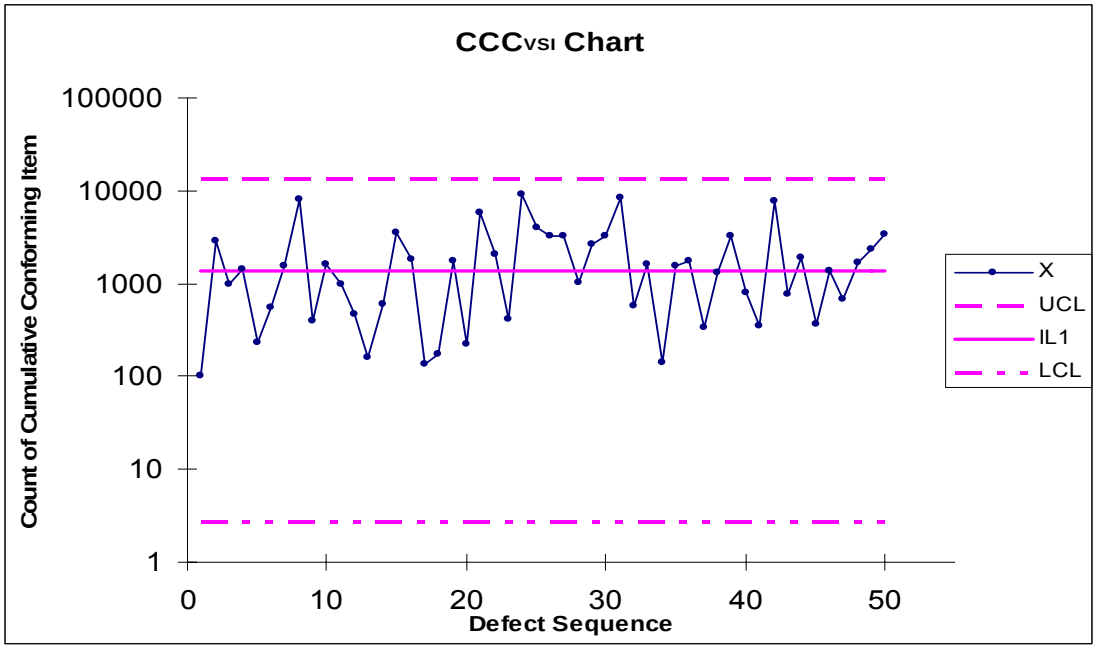

Figure 6.6 An example of the CCC_{VSI} chart

Table 6.6 Improvement factors I with different p' values

p'	0.0005	0.00055	0.0006	0.00065	0.0007	0.00075
I	1	0.9469	0.8972	0.8507	0.8073	0.7667
p'	0.00075	0.0008	0.00085	0.0009	0.00095	0.001
I	0.7667	0.7288	0.6935	0.6605	0.6297	0.6009

6.6 Conclusions

From the analysis above, it can be seen that compared with the CCC_{FSI} chart, the CCC_{VSI} chart can detect increase in the nonconforming rate more quickly, and thus reduce the average count of nonconforming items of the process. The greater the increase in the nonconforming rate, the greater the improvement in the CCC_{VSI} chart performance relative to the performance of the matched CCC_{FSI} chart with equal in-control ATS. On the other hand, when the amount of nonconforming rate shift p' remains constant, the efficiency of CCC_{VSI} charts can be enhanced by increasing the difference of interval lengths (d_1 - d_2). When designing a CCC_{VSI} chart, the number of sampling intervals n is suggested to be two, and the discrete uniform probability distribution $q_1=q_2=...=q_n$ is recommended to be used.

Since in practical applications, people are more concerned about the process deterioration rather than improvement, this CCC_{VSI} chart is designed to detect the increase of process nonconforming rate. In the case that process improvement is the major concern, the design method of a CCC_{VSI} chart is similar to the scheme presented above, except that a shorter sampling interval should be chosen when the nonconforming rate decreases and a longer sampling interval is to be used when it increases.

Chapter 7 Sampling CCC Chart with Random Shift Model and Implementation Issues

7.1 Introduction

CCC chart is originally designed under full inspection plan in order to detect the process shifts as fast as possible (Bourke,1991). It is convenient for implementation when the inspection is done by machines and the inspection results can be automatically saved in computers or database. However, even in highly-automated manufacturing industry, manual inspections are still in use for some processes due to the limitation of technology or facility. In this case, sampling methods can help to minimize the inspector's work as well as inspection cost. Therefore, it is necessary to investigate the design and performance of CCC chart with sampling inspection so as to provide some guidance for engineers when the full inspection cannot be applied.

The adaptive sampling plan, i.e., the CCC chart with variable sampling intervals, has been studied in Chapter 6. In this chapter, sampling CCC chart with random-shift model will be discussed. The commonly used method for evaluating the performance of a TBE control chart has implicitly assumed that the process shift occurs exactly when the events happen, say, a nonconforming item was found. This is called the "fixed-shift" model in Wu & Spedding (1999). However, in practical situations, the process shift may occur anytime during the process, not only when an event happens, and this phenomenon can be modeled with a more realistic model, namely, the "random-shifted" model (see Wu & Spedding, 1999).

The rest of this chapter is organized as follows. Section 7.2 discusses the minimum sample size required for the estimation of fraction nonconforming *p*. The calculation method of Average Number of items Inspected (ANI) with sampling plan based on random-shift model is presented in Section 7.3, together with the selection of sampling frequency based on the specified Average Time to Signal (ATS) value. In Section 7.4 a case study on the implementation of CCC chart is presented, some practical issues are discussed and a prototype experiment was carried out to verify the effectiveness of proposed methods in practical applications. The case study was done with a semiconductor manufacturing company in Singapore to improve the effectiveness of CCC chart for the monitoring of automatic testing process.

7.2 Estimation of Fraction of Nonconforming (FNC)

Assume that the inspection of each item can be modeled as a sequence of Bernoulli trials, and thus the number of nonconforming items *x* in each sample (sample size=*n*) follows binomial distribution with probability mass function:

$$f(x) = P\{X = x\} = \binom{n}{x} p_0{}^x (1 - p_0)^{n-x} \tag{7.1}$$

Here the value of fraction of nonconforming p_0 is usually estimated from observed process data. A traditional approach is to simply divide the total number of nonconforming items by the total number of items inspected i.e.

$$\overline{p}_0 = \sum_{i=1}^{k} r_i \Big/ \sum_{i=1}^{k} n_i \tag{7.2}$$

where k is the total number of samples taken, n_i is the sample size of the i_{th} sample, and r_i is the number of nonconforming items in the ith sample.

However, this formula may become meaningless when the number of nonconforming items in samples is always zero. This may frequently occur when the fraction nonconforming p_0 is very low at ppm or even ppb levels and the sample size is not large enough.

A possible alternative is to estimate the fraction nonconforming based on binomial distribution. Assume that a sample of size n was taken and r nonconforming items were found. If additional sampling with same sample size is taken, the process would produce no more than r nonconforming items with 50% chance; and more than r nonconforming items with 50% probability as well. The reason why the probability 0.5 is chosen is that n could be a good estimation of minimum sample size required in the sense that it creates at least 50% opportunity for observing r nonconforming items in the additional sample rather than less than r or even zero nonconforming items..

Based on this assumption, the estimation of p_0 can be achieved by solving the following equation:

$$\sum_{i=0}^{r}\binom{n}{i}{p_0}^{i}(1-p_0)^{n-i}=0.5 \tag{7.3}$$

The relationship between sample size, and the probability that zero-defect may be found within a sample can be derived from formula (7.1), i.e.

$$f(0) = \binom{n}{0} p_0{}^0 (1-p_0)^n = (1-p_0)^n \Rightarrow n = \frac{\ln(0.5)}{\ln(1-p_0)} \tag{7.4}$$

Figure 7.1 provides a curve of the minimum sample size that is required to get zero-defect and non-zero-defects in a sample with same probability (=0.5). Some detailed values of sample size *n* can be found in Table 7.1, where Categories A, B, C, and D were grouped according to four ranges of the process fraction nonconforming average normally used in practice.

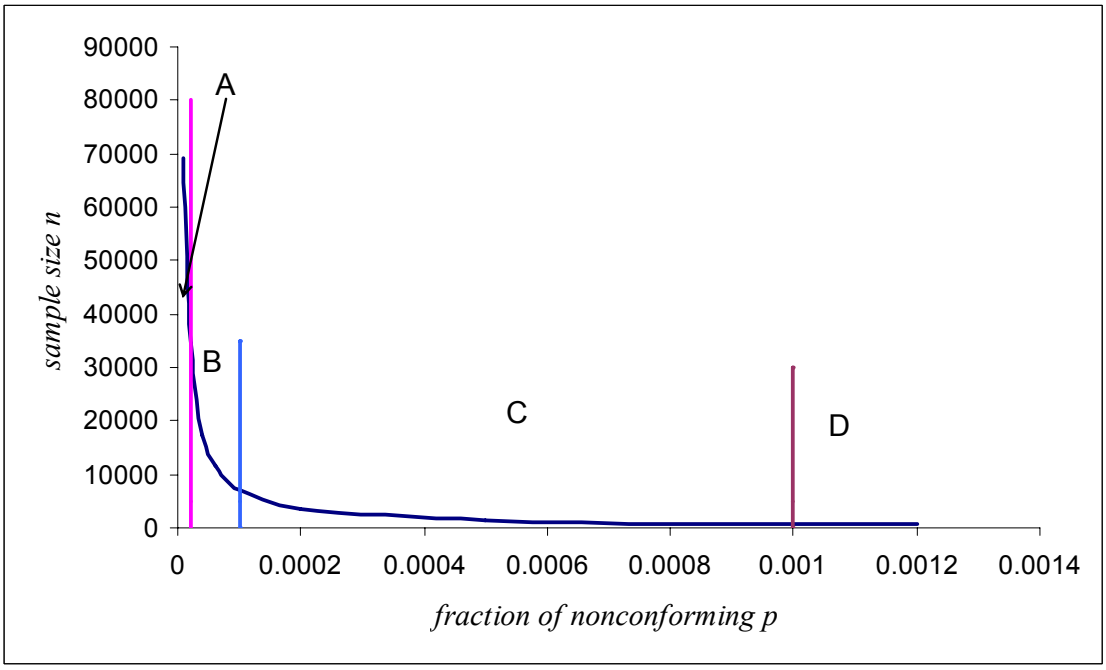

Figure 7.1 Sample size *n* with different fraction nonconforming levels p_0

Table 7.1 Some sample size *n* values with different fraction nonconforming levels p_0

	Category A (<20ppm)	Category B (20-100ppm)			Category C (100-1000ppm)			Category D (>1000ppm)
p(ppm)	20	40	60	100	200	500	1000	1200
n	34657.01	17328.33	11552.11	6931.13	3465.39	1385.95	692.80	577.28

Based on the analysis above, the following procedures are suggested for setting up a CCC chart:

Step 1: Estimate the process fraction nonconforming according to historical data or experience;

Step 2: Find a proper sample size n that is corresponding to the estimated p_0, based on values suggested in Figure 7.1 or Table 7.1;

Step 3: Do the sampling inspection, and get the number of nonconforming items r within the sample;

Step 4: Determine the estimation of process fraction nonconforming p_0 using formula (7.3)

Step 5: Set up the CCC chart using the estimated value p_0. The control limits can be calculated by formula (2.3). If they are not integer values, the UCL can be rounded down and LCL rounded up to an integer as shown in formula (2.4). An out-of-control signal will be raised when CCC is above UCL or below LCL.

7.3 Sampling CCC with Random-shift Model

ARL is the most frequently used criterion to measure the performance of a control chart. However, since the number of items inspected to plot every point is different for CCC chart, ANI, which is defined as the expected value of the number of items inspected until an out-of-control signal occurs, would be a better measurement to evaluate the performance of a CCC chart. An effective CCC chart should have a large

in-control ANI value to keep the false alarm rate to an acceptable level, and a small out-of-control ANI so that shifts in process fraction nonconforming can be detected in a short time.

The ANI of a CCC chart based on fixed-shift model may be calculated with equation (7.5) and the in-control ARL and out-of-control ARL' can be expressed as formula (7.6).

$$ANI_{fix} = E(S) = E\left(\sum_{i=1}^{R} X_i\right) = E(R)E(X_i) = \frac{ARL_{fix}}{p} \tag{7.5}$$

$$ARL_{fix} = \frac{1}{\alpha}; \tag{7.6}$$
$$ARL'_{fix} = \frac{1}{1-\beta} = \frac{1}{1+q^{UCL}-q^{LCL-1}}$$

where q =1- p.

It is worth noting that formulas (7.5) and (7.6) are derived based on the fixed-shift model assumption, i.e., that the fraction nonconforming shifts immediately after a nonconforming item and will not occur in the middle of a run length while conforming items are accumulated. That is to say the shift will directly cause a nonconforming immediately without any delay of the cumulative effect. From a practical point of view, especially when p_0 is very small and the CCC is always large, this assumption will be too restrictive and cannot represent the real process accurately. Wu & Spedding (1999) discussed this issue and derived a set of accurate formulas for the random-shift model of CCC chart with full (100%) inspection, where a shift may occur at any time

between two nonconforming units. The random-shift model ANI can be calculated with formulas (7.7) and (7.8).

$$ANI_{full} = \frac{p}{q}\left[\frac{q}{p^2} + ANI_{fix}\left(\frac{q}{p} - G\right)\right] \tag{7.7}$$

$$G = G1 + G2 + G3$$

$$G1 = \frac{q\left(1 - q^{LCL-1}\right)}{p} + \left(q_0^{UCL+1} - q_0^{LCL}\right) \times \frac{\left(\frac{q}{q_0}\right) \cdot \left[1 - \left(\frac{q}{q_0}\right)^{LCL-1}\right]}{1 - \left(\frac{q}{q_0}\right)}$$

$$G2 = \frac{q_0^{UCL+1}\left(\frac{q}{q_0}\right)^{LCL}\left[1 - \left(\frac{q}{q_0}\right)^{UCL-LCL+1}\right]}{1 - \left(\frac{q}{q_0}\right)} \tag{7.8}$$

$$G3 = \frac{q^{UCL+1}}{p}$$

For the random-shift model with 100% inspection, the shift may occur at a nonconforming item with probability p_0, and occur at a conforming item with probability q_0=1-p_0, where a cross-over CCC including two geometric random variables with fraction of nonconforming p_0 and p_1, respectively, will be observed. Correspondingly, the observed CCC data before and after a shift can be either of the following two cases:(i) A series of conforming counts produced by a process with fraction of nonconforming p=p_0, followed by a series of conforming counts from a process with p=p_1; (ii) A series of conforming counts produced by a process with fraction of nonconforming p=p_0, followed immediately by a cross-over count of conforming, and then a series of conforming counts from a process with p=p_1. For easy

referring, the CCC data generated in case (i) is named as CCC-single, and for case(ii), namely CCC-crossover.

In most sampling plans, the inspection process may have periods of inspection of n contiguous items, alternating with periods of non-inspection, with an overall sampling fraction at certain stable level, say f. f indicates the percentage of number of items sampled within the total number of items produced throughout the process. Under sampling inspection, there will be four situations for generating CCC data. Table 7.2 lists the types of CCC data and the probability of each situation corresponding to the four situations.

Table 7.2 Four situations for generating CCC data under sampling plans

	Shift occur at a nonconforming item	Shift occur at a conforming item
The shift item is sampled	CCC-single $f \cdot p_0$	CCC-crossover $f \cdot (1-p_0)$
The shift item is not sampled	CCC-crossover $(1-f) \cdot p_0$	CCC-crossover $(1-f) \cdot (1-p_0)$

As can be seen from Table 7.2, under sampling plans, since the shift of p may occur during the non-inspection period, the probability of CCC-crossover will increase compared with that of the 100% inspection (1-p_0). Therefore, formulas (7.7) and (7.8) have to be modified when calculating the ANI with sampling plans.

The ANI with 100% inspection can be expressed as:

$$ANI_{full} = p \cdot ANI_{fix} + (1-p) \cdot ANI_{ran} \tag{7.9}$$

Therefore, the ANI_{ran} which stands for the ANI based on random-shift model can be derived from equations (7.7) and (7.9):

$$ANI_{ran} = \frac{1}{q}\left[\frac{1}{p} + ANI_{fix}\left(q - \frac{p}{q} \cdot G\right)\right] \tag{7.10}$$

Based on the probability provided in Table 7.2, the overall ANI under sampling plan can be calculated with:

$$ANI_{sampling} = fp_0 ANI_{fix} + (1-fp_0)ANI_{ran} = \left[1 - \frac{Gp(1-fp_0)}{q^2}\right]ANI_{fix} + \frac{1-fp_0}{pq} \tag{7.11}$$

The ATS can then be estimated with

$$ATS = \frac{ANI}{m \cdot f}, \quad f = \frac{ANI}{ATS \cdot m} \tag{7.12}$$

where m is the average number of items produced per day. A proper sampling fraction f can be chosen based on the required ANI and ATS values according to formula (7.12).

In order to provide a more straightforward understanding on how the factors influence ANI property, the ANI for fixed-shift model and random-shift model with sampling plans are calculated with some representative process fraction nonconforming levels and sampling frequency (Table 7.3). Figure 7.2 provides ANI curves of CCC chart with full inspection and 50% inspection, respectively. The in-control fraction nonconforming p_0=0.0002 (200ppm), and the out-of-control p varies from 0.0001 to

0.05. The ANI achieved the maximum value when the process was in-control and dropped sharply when p increased or decreased from p_0.

Table 7.3 The ANI values with some representative parameters (with α=0.0027)

p_0	f	p_1	ANI_{fix}	$ANI_{sampling}$
0.0002	0.1	0.0001	267725	258409
		0.0004	1041918	1041604
		0.001	167084	167802
		0.002	41875	42313
	0.5	0.0001	267725	258409
		0.0004	1041918	1041604
		0.001	167084	167802
		0.002	41875	42313
	1	0.0001	267725	258410
		0.0004	1041918	1041605
		0.001	167084	167802
		0.002	41875	42313
0.0005	0.1	0.00025	107335	103588
		0.001	499796	499446
		0.0025	80100	80365
		0.005	20050	20221
	0.5	0.00025	107335	103589
		0.001	499796	499446
		0.0025	80100	80365
		0.005	20050	20221
	1	0.00025	107335	103590
		0.001	499796	499446
		0.0025	80100	80365
		0.005	20050	20221
0.001	0.1	0.0005	53649	51777
		0.002	249774	249599
		0.005	40000	40133
		0.01	10000	10086
	0.5	0.0005	53649	51777
		0.002	249774	249599
		0.005	40000	40133
		0.01	10000	10086
	1	0.0005	53649	51778
		0.002	249774	249600
		0.005	40000	40133
		0.01	10000	10086

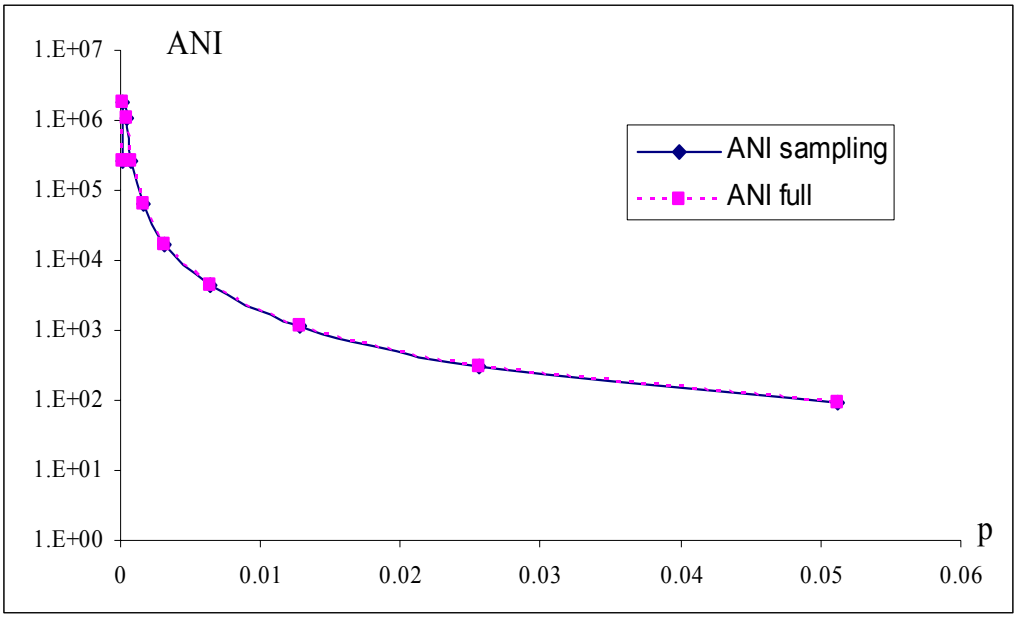

Figure 7.2 The ANI curves with full and sampling inspection

From Table 7.3 and Figure 7.2, it can be found that the sampling frequency *f* has slight influence on the ANI value. This can be attributed to the memoryless property of geometric distribution and the very small value of *p*, which reduce the effect of *f* on $ANI_{sampling}$ value as can be seen from formula (7.11). However, it is worth noting that although the sampling frequency *f* does not influence the average number of items inspected (ANI) until a signal arises much, when the production frequency is stable, smaller sampling fraction *f* will lead to a longer data collection time, which may in turn increase the ATS of the CCC chart. Therefore, it may also cause a delay of signaling a shift if the sampling frequency is very low.

It can also be observed from Table 7.3 that the use of random-shift model does affect the ANI value compared with the fixed-shift model. The reason for this could also be due to the low fraction nonconforming level, which leads to a long run length between two successive nonconforming items, and a larger possibility of process shifts in between.

7.4 Implementation of the CCC Chart: A Case Study

A case study was done by looking at the Automatic Test Equipment (ATE) process, where the Cumulative Count of Conforming (CCC) chart is used with visual inspection data. The operation procedures and data collection process were reviewed. Some implementation problems were analyzed and possible improvements methods were proposed. A prototype experiment was done on one ATE handler (SUM31/NPT03) for three consecutive weeks, and results show that the proposed inspection scheme can improve the effectiveness of the CCC chart currently in use.

7.4.1 Review of the processes

The ATE is employed for the initial class test. Two types of test are conducted in this step: electronic test and mechanical test. The electronic test is to test the performance of the chips, and the mechanical test is to check whether there is any reject (e.g. bending, chipping, appearance, etc.) caused during the process of moving due to the handler setting. Before doing the electronic test, the chips are moved by a handler from outside to the test equipment. After testing, there will be a mechanical test by visual inspection to check whether the chips have any problem caused by the handler. Figure 7.3 shows the detailed testing procedures.

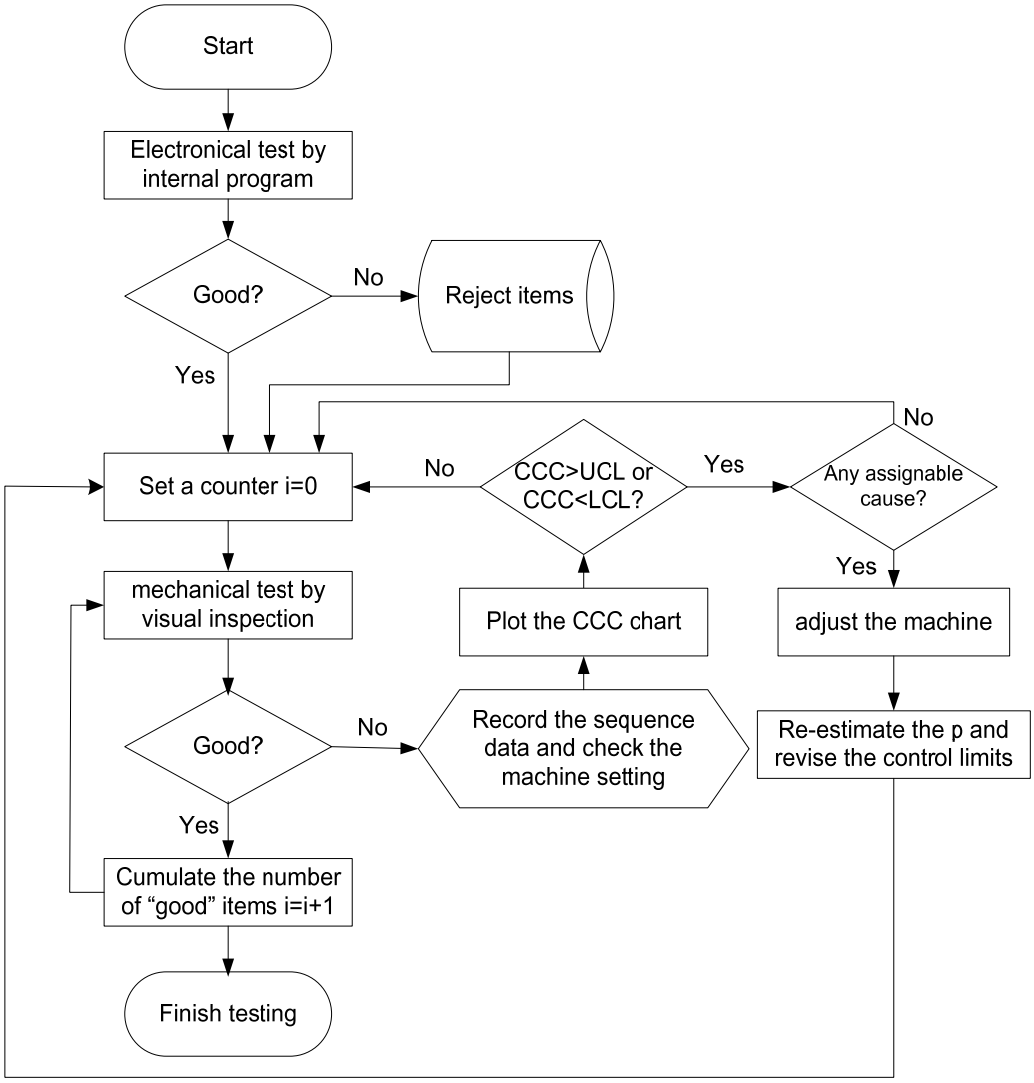

Figure 7.3 Flowchart for the testing procedures

As for the mechanical testing, the visual inspection is done 100% or by sampling, depending on the product. For those types of products with high requirement on quality, full inspection (100%) will be done. For the sampling process, the visual inspection is done for every new lot or when the operator shifts. The current sample size is 2 trays with 24 chips. It is worth noting that before the new lot is tested; a trial model instead of the real products will be put in the machine and run, to make sure the setting of the handler is fine. If everything is fine, the real products will be put into the

machines and run. If any rejection occurs, the machine will be re-set by the technicians. The sampling procedures are shown in Figure 7.4.

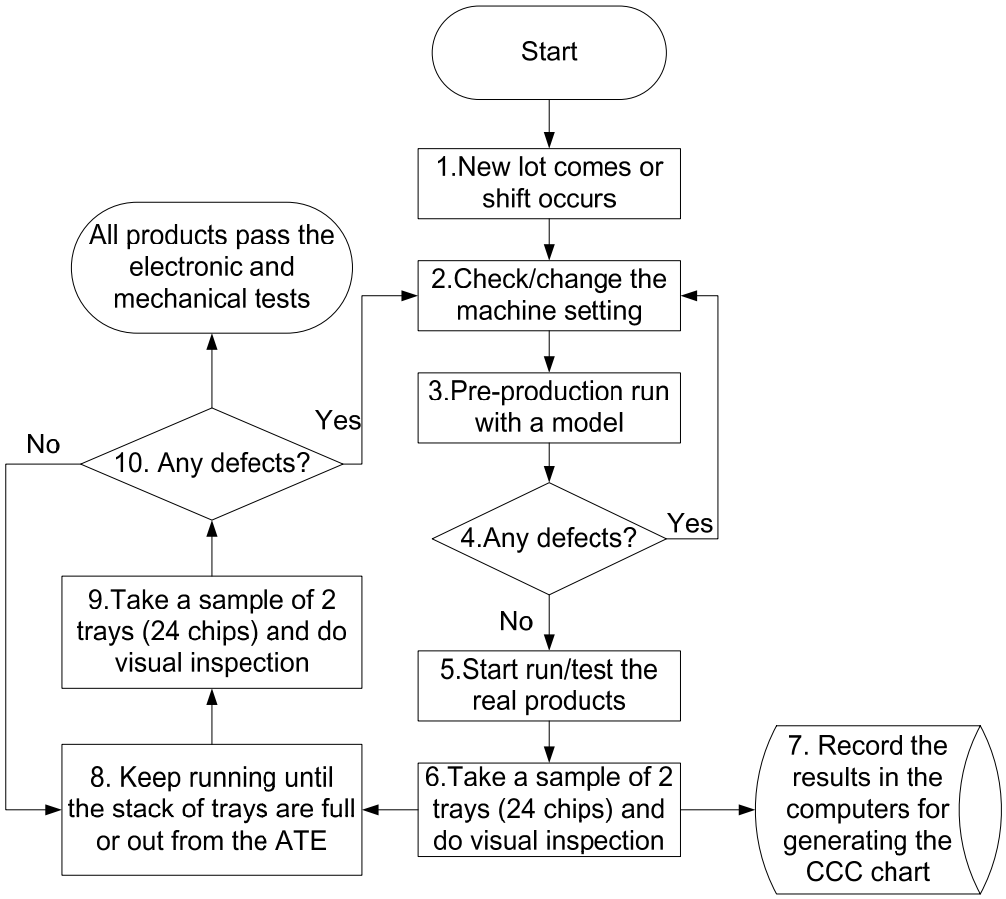

Figure 7.4 Flowchart for sampling procedures

The CCC chart is used to monitor the number of conforming chips between successive nonconforming chips, which in turn indicates the setting of the handler. The CCC chart is supposed to detect any setting problem of the handler within a short period of time to avoid more nonconforming from arising. There are around 50 ATE machines, and a separate CCC chart for each individual machine/handler.

The control limits (UCL and LCL) of the CCC chart are calculated based on the estimated process fraction of nonconforming (FNC) *p* according to the formula

$$EstPbar.(ppm) = \frac{(r + 0.7)}{n} \cdot 1{,}000{,}000 \tag{7.13}$$

where *n* is the sample size, and *r* is the number of nonconforming in the sample (Calvin,1983).

The control limits of CCC chart are calculated by the formulas

$$CL = 0.7\bar{n}; LCL = \left(\frac{\alpha}{2}\right)\bar{n}; UCL = -\bar{n}\ln\left(\frac{\alpha}{2}\right) \tag{7.14}$$

where $\bar{n} = 1/\bar{p}$ is the expected average number of units that have to be inspected before finding a nonconforming unit, and α is the false alarm rate. When the actual CCC from sampling data goes beyond the UCL, the *p* will be estimated again with the recent data, and the UCL and LCL will be updated to a new value.

7.4.2 Existing problems of implementation

Some problems are observed from current implementation of CCC chart for the ATE processes:

- The cumulative count of conforming may keep on hitting the UCL of CCC chart, and the control limits were revised again and again, without an end;

- No nonconforming was found throughout the whole process for quite a long time;

- Should the user combine all data from different ATE machines, or use individual CCC chart for each machine?

- Different handlers may have different nonconforming rate *p*. How to balance the ppm level among all handlers?

7.4.3 Cause-and-effect analysis

A cause-and-effect analysis is conducted to isolate the potential causes that affect the effectiveness of CCC chart. Figure 7.5 is the cause-and-effect (fishbone) diagram.

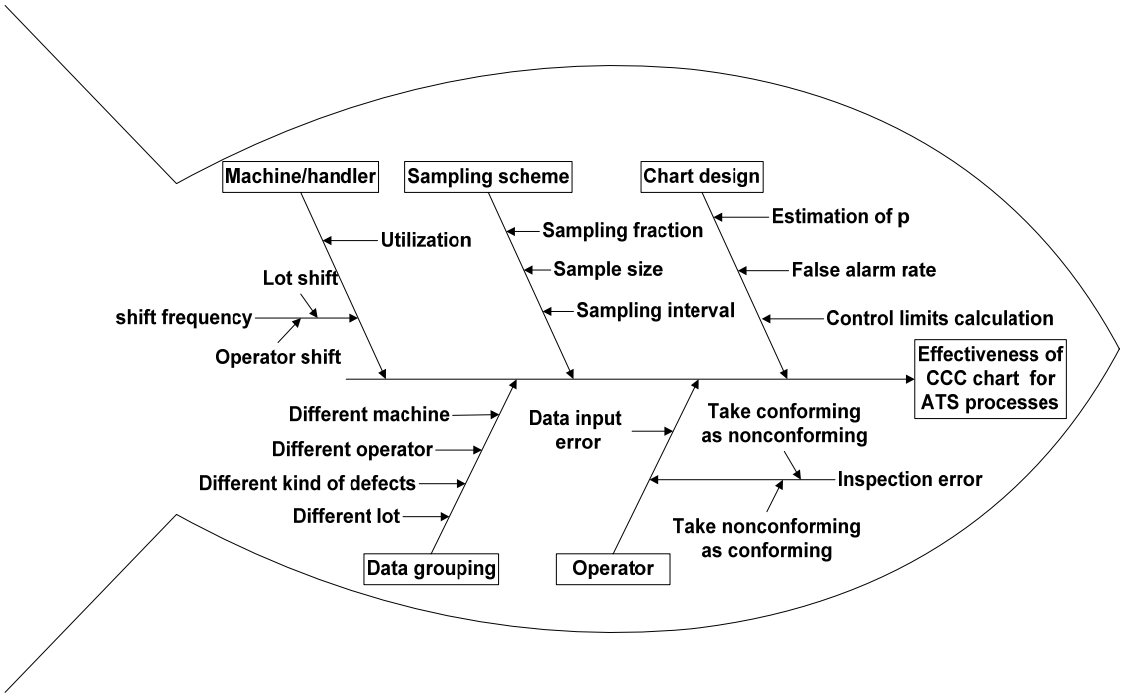

Figure 7.5 The cause-and-effect diagram for the effectiveness of CCC chart

From the cause-and-effect diagram, some influence factors and possible improvements can be found as elaborated in the following. The bold and italic characters indicate the factors shown in the cause-and-effect diagram.

7.4.3.1 Chart design

The ***estimation of p*** is made based on historical data; it is important to collect more data under the same or at least similar conditions, e.g. the type of machine, kind of chips, etc.

The acceptable ***false alarm*** α is chosen so that it will not cause too many false alarms (if it is too large); while the CCC chart can maintain its sensitivity on small process shifts (detect the p-bar change in a short period of time). Usually, 0.0027 is used to keep consistent to traditional Shewhart charts, or a little larger value can be chosen to be strict with the monitoring since the process quality is quite high, and any delay on signal of undesired shift may lead to great cost.

Control limits can be calculated with formulas (2.3) or (2.4) for a more accurate result.

7.4.3.2 Sampling scheme

Study shows that ***sampling fraction*** has slight effect on the Average Number of Items Inspected (ANI) until a signal occurs for a certain shift. However, when the production rate is rather constant/stable, it will take a longer time to detect the shift if sampling fraction is small. Therefore, we encourage enlarging the sampling fraction to a certain acceptable level while taking into consideration of the inspection cost, manpower, etc.

Sample size may influence the accuracy of the estimation of p for initial set-up of the CCC chart. Also larger sample size is preferred to a smaller one.

Sampling interval can be adjusted based on the status of the process. A general guideline is to have a larger sampling interval when the process is running well, and take a smaller sampling interval when any indication of process deterioration appears.

7.4.3.3 Operator

Operator plays a very important role in the implementation of any control chart. For CCC chart, two possible kinds of ***inspection error*** may occur: to take a nonconforming one as conforming, or take a conforming one as nonconforming. ***Data input error*** may also happen occasionally or even purposely. Training may be helpful to reduce such kind of error by operators. On the other hand, if the error can be well-estimated with certain probability, the design of control chart may also be changed by a certain adjustment factor to compensate the error following the method reviewed in Chapter 2.

7.4.3.4 Data grouping

If the purpose of employing a CCC chart for the ATE handler is to detect any problem caused by the handler, then a separate CCC chart would be recommended as it may focus on detecting the system variation of certain handler instead of all handlers at the same time, with one single control chart. Therefore, data from ***different ATE machines*** are suggested to be separated.

Data from the same ATE handler with ***different lots, operator, and type of defects*** can be put together if these factors will not cause big variance on the level of p.

7.4.3.5 Machine/handler

Machine utilization need to be balanced and optimized to reduce the variation of the process caused by ***different lots, operator, and type of defects***, etc. Also, the less frequent s***hift of product or the operator***, the more stable the process will be.

From the investigation of the process, we also notice that one important factor that leads to the poor effectiveness of the CCC chart is the data collection. In many cases, the data of the CCC chart is not fully captured. Some improvement ways are suggested as follows:

- During the inspection, no matter full inspection or sampling inspection, all the nonconforming data need to be recorded. This can be done by design of certain paper-based forms if it cannot be implemented with computer at this stage.

- For the sampling process, if a pre-production model is used to check the setting of the handler, the sampling inspection can be done some time later after the real product starts running, instead of taking samples just after the trial. The time interval that the operator has to wait to take the first sample can be decided based on past data and experience.

- Not every nonconforming/rejects from visual inspection means the process is out-of-control and the machine setting has to be adjusted. Too many adjustment of machine setting may cause more problems. Control chart is a way to help engineers to check whether and when the machines really need adjustment.

7.4.4 Prototype experiment

A prototype experiment was done on the handler SUM31/NPT03 for three consecutive weeks in November 2005 following the improvement suggestions. The cumulative number of conforming items were recorded when the next non-conforming item was found or the machine restarts due to undock or device failure. The sampling fraction is 2 out of 5 trays, i.e. 40%. The raw data from production engineers are shown in Table 7.4.

From Table 7.4, the total number of rejections is 6, and total number of sampling items is 6756 (total number of insertions × sampling fraction). The process FNC level can be estimated using formula (7.13)

$$EstPbar.(ppm) = \frac{(r+0.7)}{n} \cdot 1{,}000{,}000 = \frac{6+0.7}{6756} \times 10^6 = 992 \ \ ppm$$

Therefore, the control limits can be calculated by formula (2.3). Figure 7.6 presents the CCC chart with data listed in Table 7.4. In the CCC chart, the dotted lines represent the UCL and LCL calculated based on 3-sigma control limits (false alarm α=0.0027), the dashed lines show the UCL and LCL with 2-sigma limits (false alarm α=0.0455) , and the solid lines denote the 1 sigma limits with false alarm α=0.3173. From the CCC chart, it can be seen that no out-of-control signal appears during this period, and the process is stable. On the other hand, following the old data collection methods, none rejects can be shown in the CCC chart and the cumulative number of conforming items keeps on increasing, which may give a wrong indication that the process is improving all the way.

Table 7.4 The raw data from handler SUM31/NPT03

No	No of insertions	No of VM rejects	Remark	Badge no/Shift
1	0	0	Start	311829/E
2	3509	0	Undock; failed device	324819/B
3	3048	0	Undock; failed device	324713/A
4	3747	0	Undock; failed device	324713/A
5	1406	1	Bent lead due to device drop	427884/C
6	1143	2	Bent lead	427884/C
7	223	3	Bent lead due to input gantry	427884/C
8	54	0	Undock	427884/C
9	3516	0	Undock	427884/C
10	243	0	Undock	323956/C

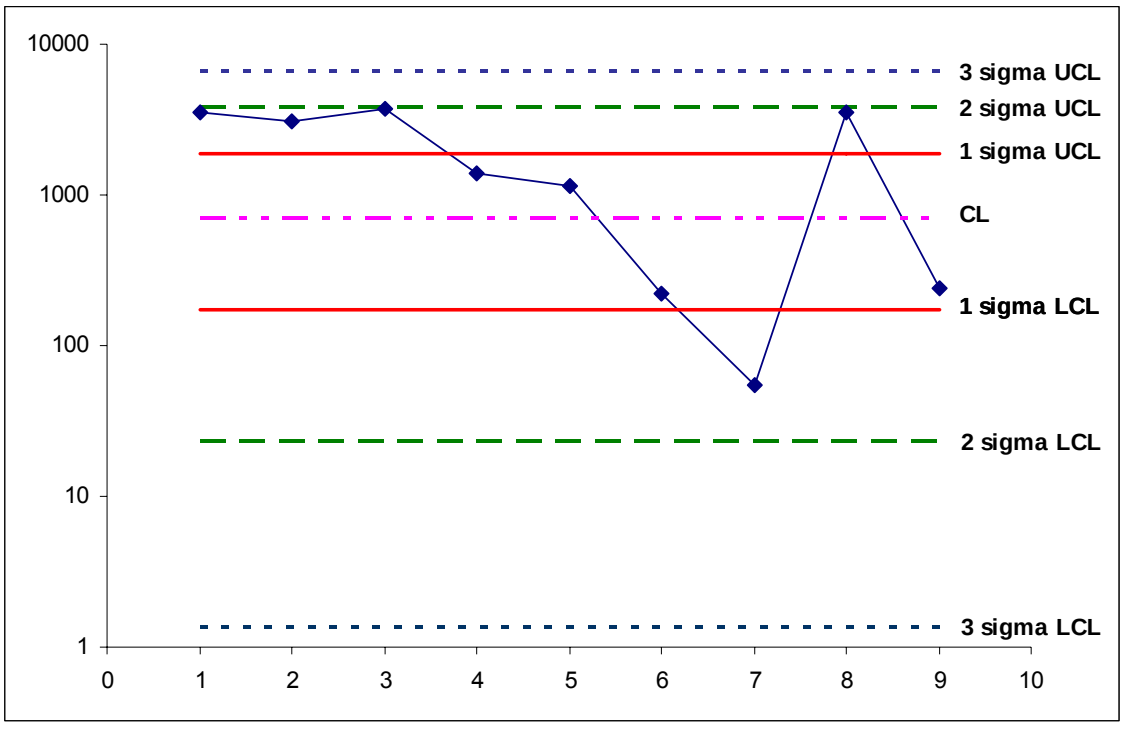

Figure 7.6 The CCC chart for handler SUM31/NPT03

7.5 Conclusions

In this chapter, the CCC chart with sampling plan based on random-shift model is discussed. The results indicate that the sampling frequency *f* does not influence ANI much, especially when the process FNC is low. However, smaller sampling fractions *f* will increase the ATS of the CCC chart, and thus may cause a delay in signaling a shift if the sampling frequency is very low.

The case study on the implementation of CCC chart does reveal some problems which may not be serious issues from the research point of view, but does affect the effectiveness of the TBE chart for practical applications. On the other hand, it also revealed that the TBE chart can be very useful for the monitoring of high-quality processes, and the CQC and CCC charts attract engineers' interests because of their simplicity for application.

Chapter 8 EWMA Chart for Weibull-distributed Time Between Events

8.1 Introduction

It has been pointed out in Chapter 2 that most of the current studies on TBE charts are based on the assumption that the occurrence of events can be modeled by a homogeneous Poisson process, and thus the time between two successive events follows exponential distribution. However, the assumption is true only when the events occurrence rate is constant, and thus may limit the application scope of TBE charts. A possible extension is to use Weibull distribution to simulate various TBE situations (including exponential) with non-constant events occurrence rate by varying its scale and shape parameters. This is especially useful in reliability monitoring, where events occurrence rate is rarely constant due to the aging property.

A detailed literature survey on the monitoring of Weibull-distributed TBE data can be found in Section 2.2.5. Earlier studies focus on Shewhart control charts (e.g. Nelson, 1979; Ramalhoto and Morais, 1999), and then control charts based on probability, namely, t-chart was proposed by Xie *et al.*(2002b). The performance of t-chart shows that when the shape parameter shifts from the original value, the chart can only detect the decrease of shape parameter, and the increasing shift cannot be detected effectively. The optimal design of CUSUM for Weibull data is limited to fixed shape parameter and can only detect the shifts in scale parameter (Hawkins and Olwell, 1998). However, there are few studies on EWMA for Weibull TBE data, especially on the method of

detecting shifts in shape parameter. Zhang and Chen (2004) developed lower-sided and upper-sided EWMA charts for detecting mean changes of censored Weibull lifetimes with fixed censoring rate and shape parameter.

In this study the EWMA for complete Weibull data with known parameters is investigated. A summary of parameter estimation methods for Weibull distribution can be found in Murthy et al (2004).

8.2 The Weibull EWMA Chart

Let X_1, X_2, …denote a sequence of time between events data, which are independent Weibull random variables with probability density function:

$$f(x) = \frac{\eta}{\theta}\left(\frac{x}{\theta}\right)^{\eta-1} e^{-\left(\frac{x}{\theta}\right)^{\eta}}, x > 0, \theta > 0, \eta > 0 \tag{8.1}$$

where θ is the scale parameter and η is the shape parameter. The mean and variance can be expressed as:

$$\mu = \theta \cdot \Gamma\left(1+\frac{1}{\eta}\right), \ \sigma^2 = \theta^2\left[\Gamma\left(1+\frac{2}{\eta}\right) - \Gamma^2\left(1+\frac{1}{\eta}\right)\right] \tag{8.2}$$

Define

$$Y = X^{\eta} \tag{8.3}$$

Then Y is also Weibull-distributed with scale parameter θ^{η} and shape parameter 1 as an exponential variable. Therefore, if the shape parameter η can be assumed to be a constant, the monitoring of Weibull random variable can be easily done by

transforming to exponential first using formula (8.3), and then following the design method of exponential EWMA proposed in Gan (1998) or the method proposed in Chapter 5. Otherwise, if the shape parameter η may also vary during the process, a Weibull EWMA is needed to monitor the changes.

The statistic for two-sided Weibull EWMA is

$$Z_t = \lambda X_t + (1 - \lambda) Z_{t-1} \tag{8.4}$$

where λ is the smoothing constant that satisfies $0 < \lambda \leq 1$. Usually the starting value is set to be the process target, i.e. the mean of Weibull data,

$$Z_0 = \mu_0 \tag{8.5}$$

With this definition, it can be obtained that

$$E(Z_t) = \mu_0,\ Var(Z_t) = \sigma_0^2 \frac{\lambda}{(2-\lambda)}\left[1-(1-\lambda)^{2t}\right] \tag{8.6}$$

Therefore, the UCL, CL and LCL for two-sided Weibull EWMA can be calculated by

$$\begin{aligned} UCL &= \mu_0 + L_U\sqrt{Var(Z_t)} \\ CL &= \mu_0 \\ LCL &= \mu_0 - L_L\sqrt{Var(Z_t)} \end{aligned} \tag{8.7}$$

where the L_U and L_L are the design parameters which influence the width of the control limits, and by convention, they are set to be equal, i.e. $L_U = L_L$. An out-of-control signal will arise when X exceeds either UCL or LCL. Since the time between events is always positive, the LCL will be set to be zero if the calculated LCL is less than zero.

For large values of t, the variance of Z_t will be approximately constant, and the upper and lower asymptotic control limits h_U and h_L are given by

$$\begin{aligned} h_U &= \mu_0 + L_U \sigma_0 \sqrt{\frac{\lambda}{2-\lambda}} \\ h_L &= \mu_0 - L_L \sigma_0 \sqrt{\frac{\lambda}{2-\lambda}} \end{aligned} \tag{8.8}$$

An out-of-control signal will arise when $Z_t \leq h_L$ or $Z_t \geq h_U$.

On the other hand, if the direction of the shift can be well predicted, the upper-sided or lower-sided Weibull EWMA chart is recommended for use to detect an increase or decrease in mean, respectively. The successive values of one-sided Weibull EWMA can be described by

$$\begin{aligned} Z_t^U &= \max\left\{A, (1-\lambda_U) Z_{t-1}^U + \lambda_U X_t\right\} \\ Z_t^L &= \min\left\{B, (1-\lambda_L) Z_{t-1}^L + \lambda_L X_t\right\} \end{aligned} \tag{8.9}$$

against t (t =1,2,3…), where λ_U and λ_L are smoothing constants such that $0<\lambda_U\leq 1$, $0<\lambda_L\leq 1$. Reflecting boundaries A and B are included to prevent the EWMA statistics from drifting to one side indefinitely. The starting values are Z_0^U and Z_0^L that satisfy $A\leq Z_0^U < h_U$ and $h_L < Z_0^L \leq B$.

8.3 Calculation of ARL and ATS

The ARL properties of an EWMA scheme can be approximated using Markov Chain approach similar to that described by Brook and Evans (1972). The continuous state Markov chain is evaluated by discretizing the infinite-state transition probability matrix.

8.3.1 Two-sided Weibull EWMA

Consider a two-sided Weibull EWMA chart with design parameters λ, h_U and h_L, and the interval between the lower and upper control limits (h_L, h_U) is divided into m subintervals of width w. w can be expressed as:

$$w = \frac{h_U - h_L}{m} \tag{8.10}$$

The EWMA control statistics Z_t is said to be in transient state (j) at time (t) if $h_L+jw \le Z_t < h_L+(j+1)w$ for j=0,1,…,m-1. The midpoint of the subinterval corresponding to state (j) can be written as

$$m_j = h_L + (j+0.5)w, j = 0,1,\ldots m-1 \tag{8.11}$$

The control statistics Z_t is regarded as in the absorbing state m if the point goes outside the control limits, i.e. $Z_t \ge h_U$ or $Z_t < h_L$.

Let p_{ij} represents the transition probability that the control statistics Z_t goes from state (i) to state (j) in one step. To approximate the probability, it is assumed that the control statistics Z_t is equal to m_i whenever it is in state (i). This approximation is accurate enough when the number of states m is large. Then p_{ij} is given by

$$\begin{aligned} p_{ij} &= P\{h_L + jw \le Z_t < h_L + (j+1)w \,|\, Z_{t-1} = m_i\} \\ &= P\{h_L + jw \le \lambda X_t + (1-\lambda)Z_{t-1} < h_L + (j+1)w \,|\, Z_{t-1} = m_i\} \\ &= P\left\{\frac{h_L + jw - (1-\lambda)m_i}{\lambda} \le X_t < \frac{h_L + (j+1)w - (1-\lambda)m_i}{\lambda}\right\}, i = 0,1,\ldots m-1; j = 0,1,\ldots,m-1 \end{aligned}$$

$$
\begin{aligned}
&p_{im} = P\{Z_t < h_L \text{ or } Z_t > h_U \mid Z_{t-1} = m_i\} \\
&= P\{\lambda X_t + (1-\lambda)Z_{t-1} < h_L \mid Z_{t-1} = m_i\} + P\{\lambda X_t + (1-\lambda)Z_{t-1} > h_U \mid Z_{t-1} = m_i\} \\
&= P\left\{X_t < \frac{h_L - (1-\lambda)m_i}{\lambda}\right\} + P\left\{X_t > \frac{h_U - (1-\lambda)m_i}{\lambda}\right\}, i = 0,1,\ldots m-1 \\
&p_{mj} = 0, j = 0,1,\ldots m-1 \\
&p_{mm} = 1
\end{aligned}
\tag{8.12}
$$

Based on the Markov chain theory, the expected first passage times from state (i) to the absorbing state are

$$\varphi_i = 1 + \sum_{j=0}^{m-1} p_{ij}\varphi_j, i = 0,1,\ldots,m-1 \tag{8.13}$$

φ_i is the ARL given that the process started in state (i). Let Q be the matrix of transition probabilities obtained by deleting the last row and column of P. The vector of ARLs φ can be calculated with

$$\varphi = (I - Q)^{-1}1 \tag{8.14}$$

where 1 is an $m\times1$ vector of 1s and I is a $m\times m$ identity matrix. The elements in the vector φ are the ARLs when the EWMA chart starts in various states. The first element in the vector φ gives the average run length for the Weibull EWMA chart starting from zero. Let the kth element be the ARL that the EWMA chart starts from k, it can be achieved by

$$k = \left[\frac{Z_0 - h_L}{w}\right] \tag{8.15}$$

where [C] stands for the largest integer not greater than C.

The ATS, defined as the expected value of total length of time to observe an out-of-control point, can be calculated with Wald's identity. Let S be the total amount of time before an out-of-control signal occurs. It satisfies

$$S = \sum_{i=1}^{R} X_i \tag{8.16}$$

where R is the number of points plotted on the chart until an out-of-control signal occurs. Then the ATS of Weibull EWMA can be obtained as

$$ATS = E(S) = E\left(\sum_{i=1}^{R} X_i\right) = E(R)E(X) = ARL \cdot \beta \cdot \Gamma\left(1+\frac{1}{\eta}\right) \tag{8.17}$$

8.3.2 One-sided Weibull EWMA

The calculation method of ARL for one-sided Weibull EWMA chart is similar except that the in-control interval and transition probability matrix will be somewhat different.

For upper-sided Weibull EWMA chart, the interval (A, h_U) is divided into m subintervals and the width w_U can be expressed as:

$$w_U = \frac{h_U - A}{m} \tag{8.18}$$

The EWMA control statistics Z_t^U is said to be in transient state (j) at time (t) if $A+jw_U \le Z_t^U < A+(j+1)w_U$ for j=0, 1,…,m-1. The midpoint of the subinterval corresponding to state (j) can be written as

$$m_j^U = A+(j+0.5)w_U, j=0,1,\ldots m-1 \tag{8.19}$$

The control statistics Z_t^U is regarded as in the absorbing state m if $Z_t^U \geq h_U$.

Let $p^U{}_{ij}$ represents the transition probability that the control statistics Z_t^U goes from state (i) to state (j) in one step. The $p^U{}_{ij}$ can be derived as

$$
\begin{aligned}
&p_{ij}^U = P\left\{A \leq Z_t^U < A + w_U \middle| Z_{t-1}^U = m_i^U\right\} = P\left\{\lambda_U X_t + (1-\lambda_U) Z_{t-1}^U < A + w_U \middle| Z_{t-1}^U = m_i^U\right\} \\
&= P\left\{X_t < \frac{A + w_U - (1-\lambda_U) m_i^U}{\lambda_U}\right\}, i = 0,1,...m-1; j = 0 \\
&p_{ij}^U = P\left\{A + jw_U \leq Z_t^U < A + (j+1) w_U \middle| Z_{t-1}^U = m_i^U\right\} \\
&= P\left\{A + jw_U \leq \lambda_U X_t + (1-\lambda_U) Z_{t-1}^U < A + (j+1) w_U \middle| Z_{t-1}^U = m_i^U\right\} \\
&= P\left\{\frac{A + jw_U - (1-\lambda_U) m_i^U}{\lambda_U} \leq X_t < \frac{A + (j+1) w_U - (1-\lambda_U) m_i^U}{\lambda_U}\right\}, i = 0,1,...,m-1; j = 1,...,m-1
\end{aligned}
$$

$$
\begin{aligned}
&p_{im}^U = P\left\{Z_t^U \geq h_U \middle| Z_{t-1}^U = m_i^U\right\} = P\left\{\lambda_U X_t + (1-\lambda_U) Z_{t-1}^U \geq h_U \middle| Z_{t-1}^U = m_i^U\right\} \\
&= P\left\{X_t \geq \frac{h_U - (1-\lambda_U) m_i^U}{\lambda_U}\right\}, i = 0,1,...m-1
\end{aligned}
$$

$$
\begin{aligned}
&p_{mj}^U = 0, j = 0,1,\ldots m-1 \\
&p_{mm}^U = 1
\end{aligned}
\tag{8.20}
$$

For lower-sided Weibull EWMA chart, the interval (h_L, B) is divided into m subintervals with width w_L.

$$
w_L = \frac{B - h_L}{m} \tag{8.21}
$$

Similarly, the Weibull EWMA control statistics Z_t^L is said to be in transient state (j) at time (t) if $B - (j+1) w_L < Z_t^L \leq B - jw_L$ for j=0,1,…,m-1. The midpoint of the subinterval corresponding to state (j) can be written as

$$
m_j^L = B - (j+0.5) w_L, j = 0,1,\ldots m-1 \tag{8.22}
$$

The control statistics Z_t^L is regarded as in the absorbing state m if $Z_t^L \le h_L$.

The elements $p^L{}_{ij}$ of transition probability matrix of Markov chain can be derived as

$$
\begin{aligned}
&p_{ij}^L = P\left\{B - w_L < Z_t^L \le B \middle| Z_{t-1}^L = m_i^L\right\} = P\left\{\lambda_L X_t + (1-\lambda_L) Z_{t-1}^L > B - w_L \middle| Z_{t-1}^L = m_i^L\right\} \\
&= P\left\{X_t > \frac{B - w_L - (1-\lambda_L) m_i^L}{\lambda_L}\right\}, i = 0,1,...m-1; j = 0 \\
&p_{ij}^L = P\left\{B - (j+1) w_L < Z_t^L \le B - j w_L \middle| Z_{t-1}^L = m_i^L\right\} \\
&= P\left\{B - (j+1) w_L < \lambda_L X_t + (1-\lambda_L) Z_{t-1}^L \le B - j w_L \middle| Z_{t-1}^L = m_i^L\right\} \\
&= P\left\{\frac{B - (j+1) w_L - (1-\lambda_L) m_i^L}{\lambda_L} < X_t \le \frac{B - j w_L - (1-\lambda_L) m_i^L}{\lambda_L}\right\}, i = 0,1,..., m-1; j = 1,..., m-1 \\
&p_{im}^L = P\left\{Z_t^L \le h_L \middle| Z_{t-1}^L = m_i^L\right\} = P\left\{\lambda_L X_t + (1-\lambda_L) Z_{t-1}^L \le h_L \middle| Z_{t-1}^L = m_i^L\right\} \\
&= P\left\{X_t \le \frac{h_L - (1-\lambda_L) m_i^L}{\lambda_L}\right\}, i = 0,1,...m-1
\end{aligned}
$$

$$
\begin{aligned}
&p_{mj}^L = 0, j = 0,1,\ldots m-1 \\
&p_{mm}^L = 1
\end{aligned}
\qquad (8.23)
$$

The ARL vector can then be calculated with formulae (8.13) and (8.14) after achieving the transition probability matrix. The ATS can also be obtained by formula (8.17).

8.4 Design of Two-sided Weibull EWMA

Based on the calculation methods described above, the in-control ARL can be achieved with known chart parameters λ, L_U, and L_L, and Weibull distribution parameters θ, and η. Compared to the design of exponential EWMA chart, Weibull EWMA is more complicated since the in-control ARL not only varies with chart parameters λ, L_U, and L_L, but is also affected by the Weibull distribution parameters.

As known from previous research on EWMA chart, the optimal design scheme would have the particular combination of design parameters λ, L_U, and L_L so that the chart will achieve the desired in-control ARL and have the shortest out-of-control ARL at the specified shift level. The smoothing factor λ is determined to be optimal at certain out-of-control shift level and the control limits parameters L_U and L_L are selected to achieve the specified in-control ARL.

Note that given the design parameters of Weibull EWMA, the in-control ARL is affected only by the shape parameter η, and the scale parameter has no influence. This can be proved using the calculation method shown in Section 8.3. Assuming control chart design parameters λ, L_U, and L_L are fixed, and the in-control ARLs of Weibull EWMA with various Weibull distributions are can be calculated. Therefore, to achieve a certain in-control ARL, the chart design parameters λ, L_U, and L_L are determined by the shape parameter η.

To make the design procedures simpler, the smoothing factor λ is suggested to be 0.05, 0.10 or 0.20. This is reasonable as from former study on EWMA chart for normal data (Lucas and Saccucci, 1990), EWMA for exponential (Gan, 1998), EWMA for Poisson (Borror *et al.* 1998), Weibull EWMA for censored data (Zhang and Chen, 2004), or the EWMA chart proposed in Chapter 5 of this thesis, there is a common result that values of smoothing factor λ in the interval [0.05, 0.25] works well in practice for small to median shifts, and a smaller value of λ is preferred to detect smaller shifts.

Therefore, for each value of smoothing factor λ (0.05, 0.10 and 0.20), the in-control ARLs are calculated given different combinations of control limits parameter L (Set

L_U=L_L=L) and shape parameter η. The detailed ARL values are listed in Appendix II. Based on the results, the in-control ARL contour plots are drawn to facilitate the design procedures (Figures 8.1, 8.2, 8.3, 8.4, 8.5, and 8.6). From the in-control ARL study (Appendix II), it can be found that when shape parameter η is greater than 2, the in-control ARL is very stable with only slight changes; in this case, the value of control limits parameter L can be chosen according to the L value when η=2.

Hence, the design procedures of Weibull EWMA chart can be described as follows:

***Step 1*:** Specify the desired in-control ARL, and estimate the out-of-control mean shift (μ_1/μ_0) to be detected quickly;

***Step 2*:** Choose a λ value from 0.05, 0.10, or 0.20 according to the out-of-control mean shift (μ_1/μ_0). A smaller value of λ is suggested for smaller process shifts;

***Step 3*:** Obtain the corresponding L value according to the value of shape parameter η and the in-control ARL (using Figure 8.1~8.6);

***Step 4*:** The entire ARL profile for the Weibull EWMA chart can be achieved using the Markov chain approach described in Section 8.3. This can be used to evaluate the performance of the chart and ensure that the chart provides sufficient protection against other shifts.

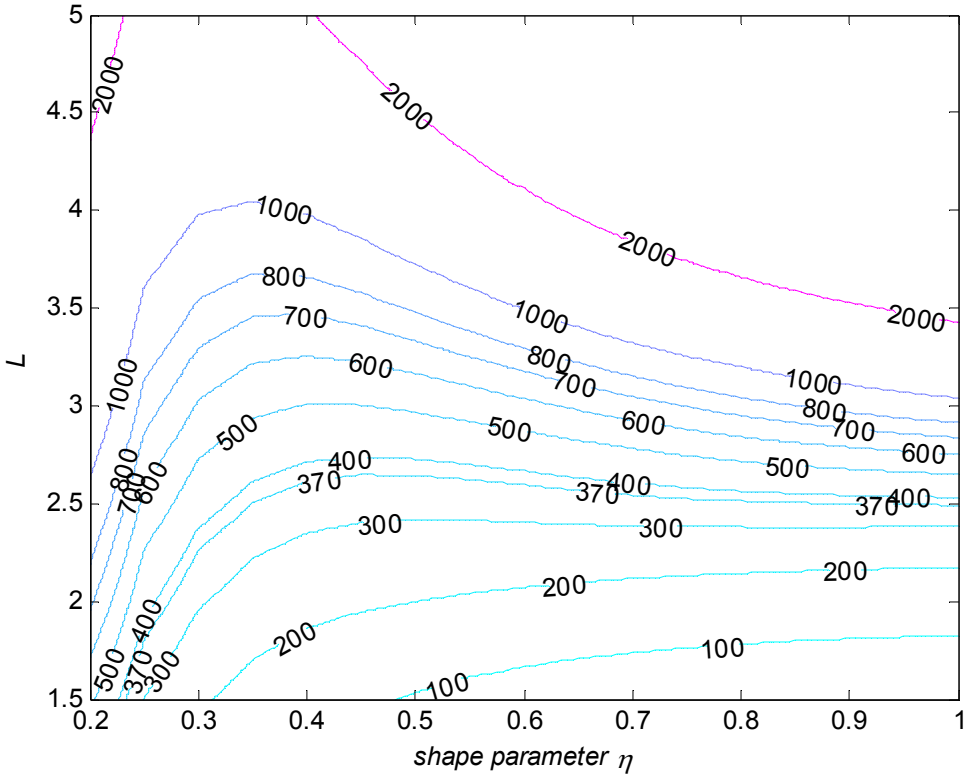

Figure 8.1 The in-control ARL contour plot of Weibull EWMA chart (λ=0.05, shape parameter $0.2 \leq \eta \leq 1$. $L_U=L_L=L$)

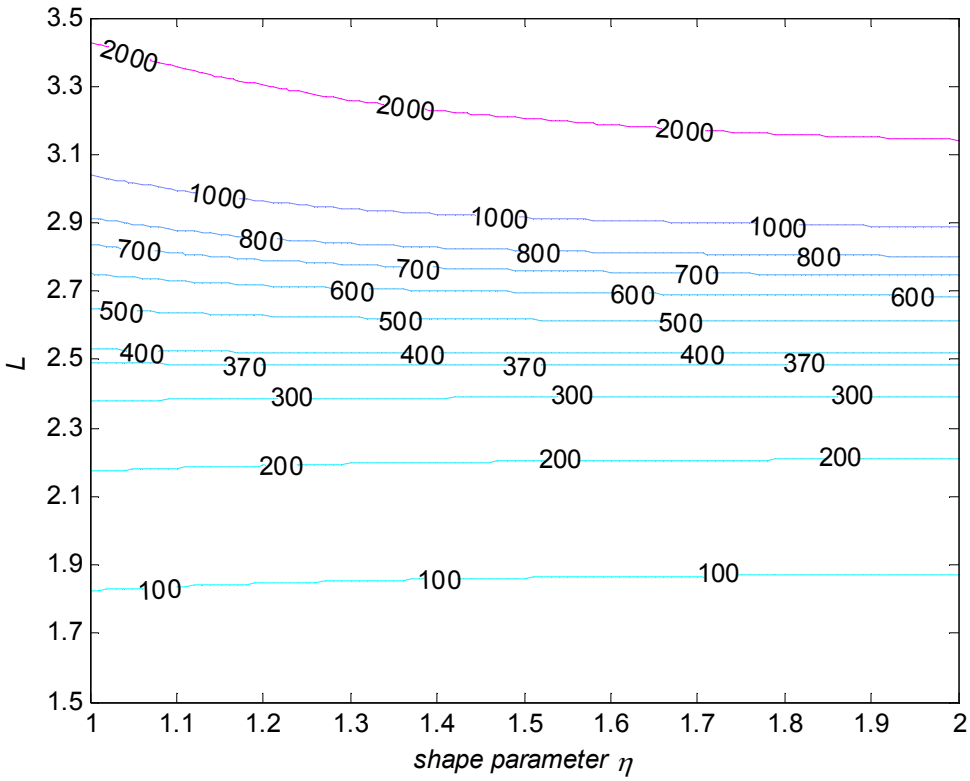

Figure 8.2 The in-control ARL contour plot of Weibull EWMA chart (λ=0.05, shape parameter $1 \leq \eta \leq 2$. $L_U=L_L=L$)

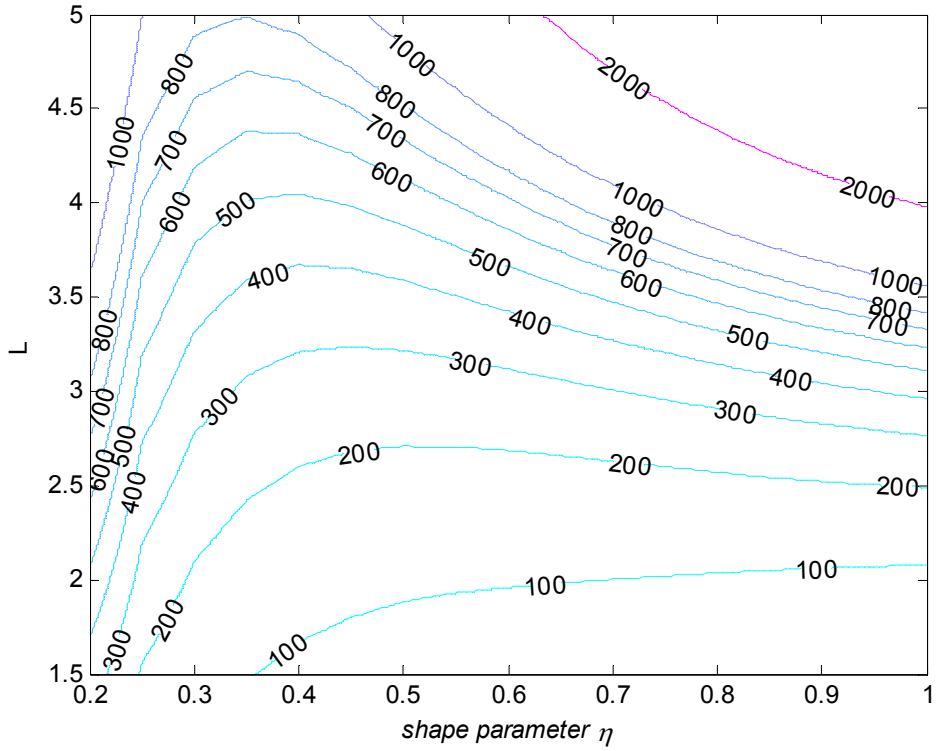

Figure 8.3 The in-control ARL contour plot of Weibull EWMA chart (λ=0.1, shape parameter $0.2 \leq \eta \leq 1$. $L_U=L_L=L$)

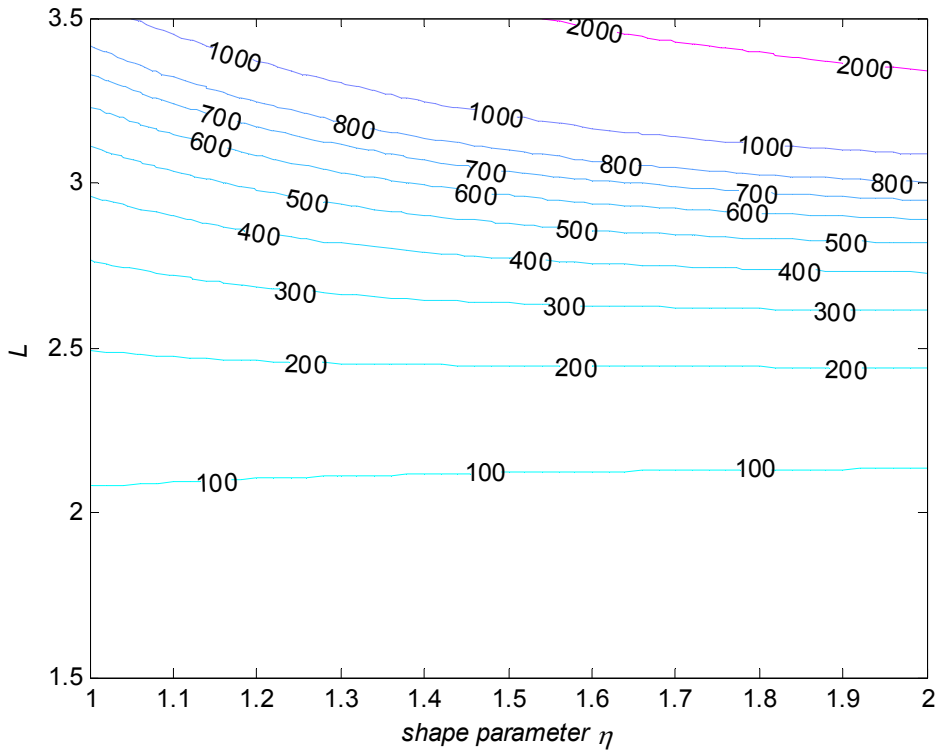

Figure 8.4 The in-control ARL contour plot of Weibull EWMA chart (λ=0.1, shape parameter $1 \leq \eta \leq 2$. $L_U=L_L=L$)

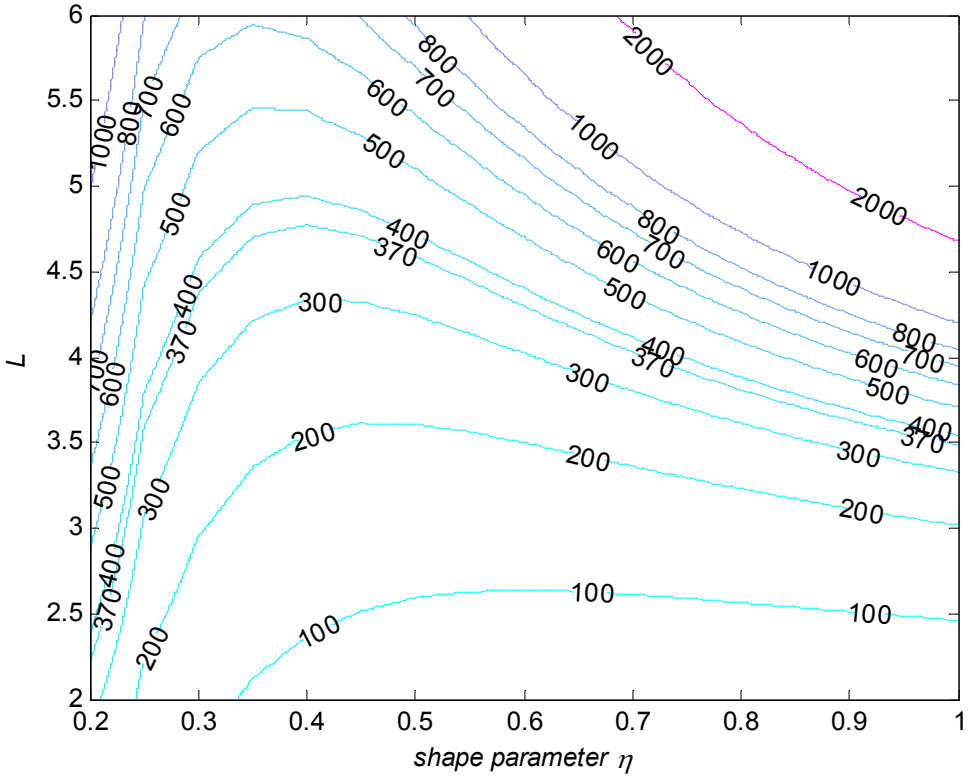

Figure 8.5 The in-control ARL contour plot of Weibull EWMA chart (λ=0.2, shape parameter $0.2 \leq \eta \leq 1$. $L_U=L_L=L$)

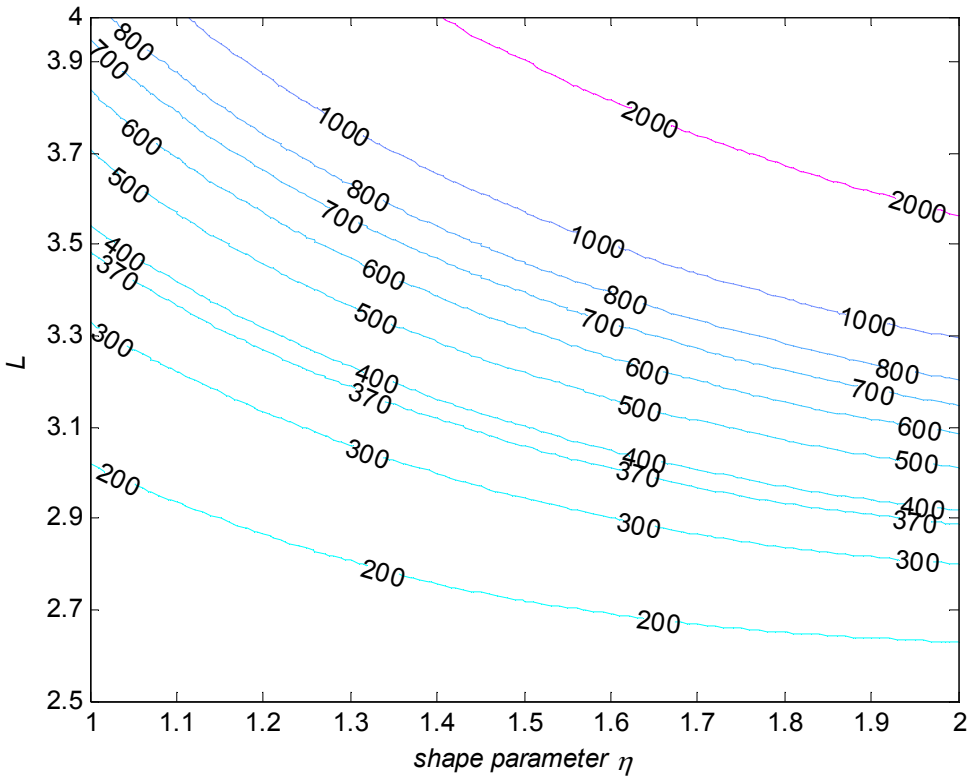

Figure 8.6 The in-control ARL contour plot of Weibull EWMA chart (λ=0.2, shape parameter $1 \leq \eta \leq 2$. $L_U=L_L=L$)

A major difficulty in the design of the Weibull EWMA chart is that Weibull distribution contains two parameters and a shift in any of them may cause an out-of-control signal. Former studies on Weibull CUSUM and Weibull EWMA with censored data are all based on the assumption that the shape parameter is fixed at certain level. It is somewhat reasonable since the scale parameter is usually related to operating condition and is likely to change because of assignable causes. However, sometimes the shape parameter may also change due to assignable causes. Since the fixed shape parameter Weibull variable can be easily transformed to an exponential variable using formula (8.3), the existing exponential EWMA and exponential CUSUM can be applied.

On the other hand, if only the shape parameter varies, most probably, the shape parameter tends to increase along with time. This could be attributed to the nature aging property from a practical point of view. In reliability engineering studies, most time between failure data will have three main phases: the infant mortality phase, when the sample is newly introduced and has a high failure rate; the constant failure rate phase, when the product is stable and with low failures; followed by the wear-out phase, when the failure rate is significantly increased. This kind of time between events data can be modeled with a combined or extended Weibull distribution referred to as bathtub shaped failure rate (BFR) distribution. During this process, the shape parameter of the Weibull distributions is increasing from less than 1, equal to 1, to finally greater than 1. According to the bathtub curve, the shape parameter of Weibull TBE data is more likely to increase with time.

As can be deduced from the formula (8.2), when the scale parameter is fixed, the shift in mean (μ_1/μ_0) is determined by

$$\frac{\mu_1}{\mu_0} = \frac{\theta_1 \Gamma\left(1+\frac{1}{\eta_1}\right)}{\theta_0 \Gamma\left(1+\frac{1}{\eta_0}\right)} = \frac{\Gamma\left(1+\frac{1}{\eta_1}\right)}{\Gamma\left(1+\frac{1}{\eta_0}\right)} \tag{8.24}$$

As shown in Figure 8.7 and Table 8.1, a study on the relationship between shift in mean and shift in shape parameter shows that when the shape parameter first increases from a very small in-control value, say, 0.2 or 0.5, the mean of the Weibull variable will decrease fast at the beginning. However, it tends to be stable when the out-of-control shape parameter reaches 1.0 or 1.5. That is to say, when the out-of-control shape parameter is greater than 1.0 or 1.5, the shift in shape parameter will have little influence on the shift in mean, and therefore, the Weibull EWMA which monitors the mean shift may not be able to detect the shift at that time. On the other hand, it can detect the increase in shape parameter when it varies within the range (0, 2) in a short time since the shift in mean is significant. However, when both shape and scale parameter varies at the same time, the trend in mean may have various situations, and it has to be studied case by case.

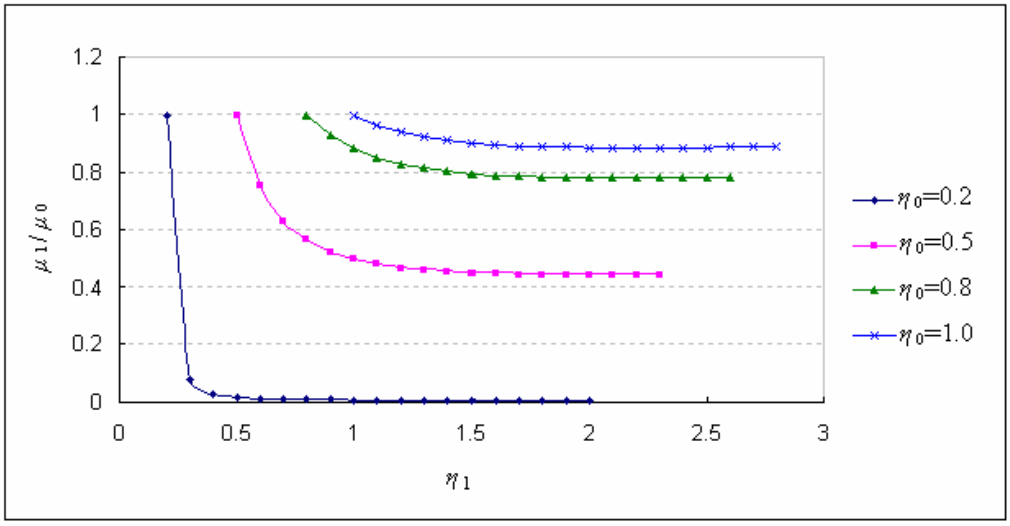

Figure 8.7 The trend of mean shift when the shape parameter η varies

Table 8.1 The mean shift (μ_1/μ_0) values when the shape parameter η varies

(η_0=0.2)		(η_0=0.5)		(η_0=0.8)		(η_0=1)	
η_1	μ_1/μ_0	η_1	μ_1/μ_0	η_1	μ_1/μ_0	η_1	μ_1/μ_0
0.2	1.0000	0.5	1.0000	0.8	1.0000	1	1.0000
0.3	0.0772	0.6	0.7523	0.9	0.9287	1.1	0.9649
0.4	0.0277	0.7	0.6329	1	0.8826	1.2	0.9407
0.5	0.0167	0.8	0.5665	1.1	0.8516	1.3	0.9236
0.6	0.0125	0.9	0.5261	1.2	0.8302	1.4	0.9114
0.7	0.0105	1	0.5000	1.3	0.8152	1.5	0.9027
0.8	0.0094	1.1	0.4825	1.4	0.8044	1.6	0.8966
0.9	0.0088	1.2	0.4703	1.5	0.7968	1.7	0.8922
1	0.0083	1.3	0.4618	1.6	0.7913	1.8	0.8893
1.1	0.0080	1.4	0.4557	1.7	0.7875	1.9	0.8874
1.2	0.0078	1.5	0.4514	1.8	0.7849	2	0.8862
1.3	0.0077	1.6	0.4483	1.9	0.7832	2.1	0.8857
1.4	0.0076	1.7	0.4461	2	0.7822	2.2	0.8856
1.5	0.0075	1.8	0.4446	2.1	0.7817	2.3	0.8859
1.6	0.0075	1.9	0.4437	2.2	0.7817	2.4	0.8865
1.7	0.0074	2	0.4431	2.3	0.7819	2.5	0.8873
1.8	0.0074	2.1	0.4428	2.4	0.7824	2.6	0.8882
1.9	0.0074	2.2	0.4428	2.5	0.7831	2.7	0.8893
2	0.0074	2.3	0.4430	2.6	0.7839	2.8	0.8905

8.5 An Illustrative Example

Here is an illustrative example of the Weibull EWMA chart. Table 8.2 shows a set of time between failures data for monitoring the reliability of a process. The first 20 observations are simulated following Weibull distribution with shape parameter η=2 and scale parameter θ=10 hours. The next 20 observations were generated following Weibull distribution with η=2 and θ=5 hours. A two-sided Weibull EWMA chart is designed so that the in-control ARL=370 (λ=0.10, L_U=L_L=2.70). Figure 8.8 shows the Weibull EWMA chart for the data in Table 8.2. An out-of-control alarm is raised from the 33rd point, which indicates that the mean time to failure may have decreased. Therefore, engineers need to check the process and try to find out the reasons for it so as to further improve the reliability of the process.

Table 8.2 Time between failures (TBF) data for Weibull EWMA chart

Failure No.	TBF (hours)	EWMA	UCL	LCL	Failure No.	TBF (hours)	EWMA	UCL	LCL
1	8.37	6.31	6.85	5.33	21	1.13	6.69	7.82	4.35
2	3.25	6.01	7.11	5.06	22	6.05	6.63	7.82	4.35
3	4.43	5.85	7.28	4.89	23	3.53	6.32	7.82	4.35
4	6.62	5.93	7.40	4.77	24	4.25	6.11	7.83	4.35
5	4.48	5.78	7.49	4.68	25	1.70	5.67	7.83	4.35
6	6.44	5.85	7.56	4.61	26	2.61	5.36	7.83	4.35
7	10.36	6.30	7.62	4.55	27	4.43	5.27	7.83	4.34
8	11.13	6.78	7.66	4.51	28	5.99	5.34	7.83	4.34
9	10.37	7.14	7.69	4.48	29	2.22	5.03	7.83	4.34
10	7.92	7.22	7.72	4.45	30	3.50	4.88	7.83	4.34
11	5.65	7.06	7.74	4.43	31	3.48	4.74	7.83	4.34
12	10.83	7.44	7.76	4.41	32	2.41	4.50	7.83	4.34
13	4.20	7.11	7.77	4.40	33	1.43	4.20	7.83	4.34
14	7.52	7.16	7.78	4.39	34	2.75	4.05	7.83	4.34
15	9.97	7.44	7.79	4.38	35	4.59	4.11	7.83	4.34
16	5.94	7.29	7.80	4.37	36	4.75	4.17	7.83	4.34
17	7.77	7.34	7.81	4.37	37	1.29	3.88	7.83	4.34
18	9.00	7.50	7.81	4.36	38	1.47	3.64	7.83	4.34
19	6.04	7.36	7.81	4.36	39	4.72	3.75	7.83	4.34
20	6.90	7.31	7.82	4.35	40	1.68	3.54	7.83	4.34

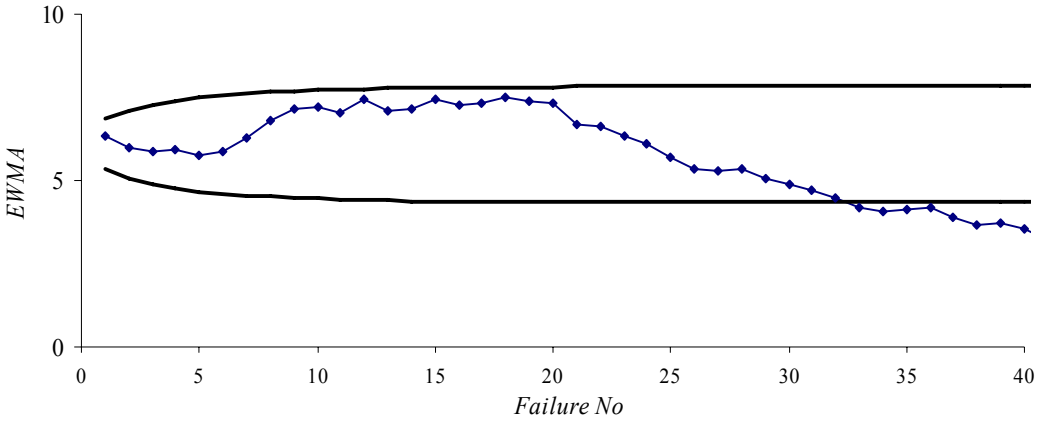

Figure 8.8 The two-sided EWMA chart for monitoring Weibull distributed time between failures

Table 8.3 lists some ARL and ATS values for the Weibull EWMA chart in the illustrative example (λ=0.10, L_U=L_L=2.70). The shape parameter is fixed at 2.0, and scale parameter varies from 2 to 10. The in-control scale θ=10 hours, and in-control ARL=370. Fig. 8.9 presents the ARL curve for the Weibull EWMA chart, from which we can see that the Weibull EWMA chart is very sensitive to the scale parameter shifts. The ATS value implies that the average time to an out-of-control alarm will be around 46 hours for detecting the scale parameter's change from 10 hours to 5 hours.

Table 8.3 Some ARL and ATS values for the Weibull EWMA chart

Scale θ	2	5	6	8	8.5	9	10
ARL	5.34	10.38	15.16	64.94	120.67	249.19	370.84
ATS	9.47	**45.99**	80.63	460.40	908.99	1987.51	3286.48
Scale θ	11	12	13	14	15	18	20
ARL	89.19	35.14	19.89	13.55	10.24	5.98	4.74
ATS	869.48	373.76	229.12	168.14	136.14	95.40	84.07

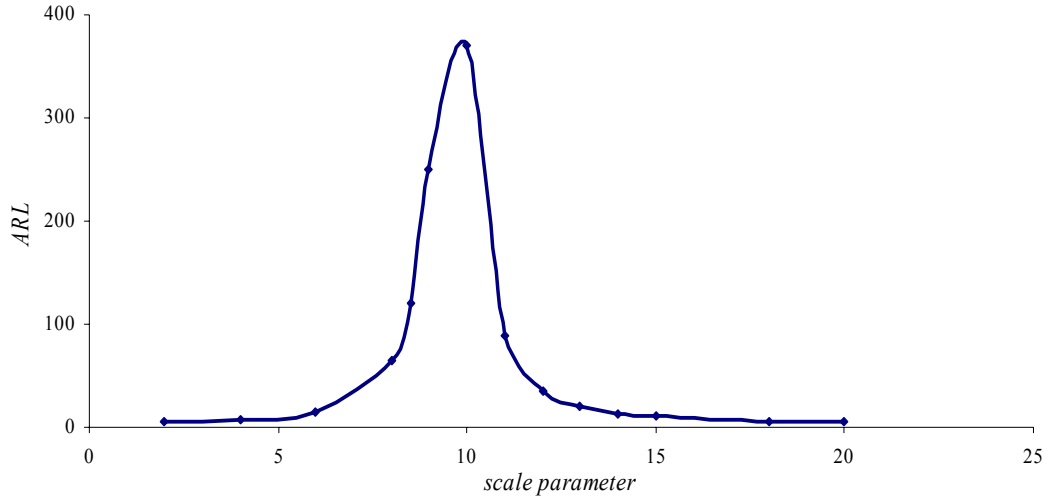

Figure 8.9 The ARL curve of the Weibull EWMA chart

8.6 Conclusions

In this chapter, an EWMA scheme for the monitoring of Weibull-distributed TBE data is proposed, the calculation of ARL and ATS is discussed and the design procedures of the chart are investigated. Weibull EWMA chart can be very effective for TBE monitoring when the events occurrence rate is not constant.

Chapter 9 Conclusions and Future Research

This study was motivated by the problems and deficiencies that existing control charts encountered when monitoring high-quality processes. The aim of the study is to explore the causes and effects of those problems and develop new control schemes that make the monitoring of high-quality processes more efficient and economical. With a focus on modeling and monitoring of time between events, this study investigated some issues of existing control charting methods, and developed several new schemes that enhanced the performance of existing methods. The results and methodologies proposed in this study can be applied to not only manufacturing processes, but also other areas such as reliability monitoring, maintenance or service industries. Served as the end of the thesis, this chapter summarizes major contributions and significances of this study; besides, some recommendations for future research are also presented.

9.1 Major Contributions

This study has investigated several topics on modeling and monitoring of TBE data. There are especially six major contributions.

Firstly, a comparative study of some existing TBE charts was conducted, and the performance of CQC chart, CQC-*r* chart, exponential EWMA and exponential CUSUM charts were compared based on Average Time to Signal (ATS). These control charts, although have been proposed by different researchers and shown to be effective under their particular situations, may make the users more confused when several

approaches are available. Using an unsuitable TBE chart may lead to lower efficiency if not useless. The results of the comparative study in Chapter 3 provide useful guidelines of how to choose an appropriate TBE chart in different situations. Based on the comparison results, the method of on-line process monitoring with TBE charts has been described and an example was given to illustrate its application in practice. The findings in this study suggest that employing time-between-events charts, especially the CQC and CQC-*r* charts, is an effective way for implementing on-line process monitoring system.

Secondly, a new CUSUM chart with transformed exponential data is proposed. CUSUM chart has been known to be very effective in detecting small and persistent shifts because of its inherent ability of accumulating deviations for successive observations. Using transformations before setting up control charts is not a new idea, and it is strongly suggested by many researchers because of its ease of use property and applicability to a wide range of data which are unnecessarily normally-distributed as most of the control charts require. On the other hand, an undesirable feature of control charts with transformed data is that points plotted on the chart may lose their original meaning thus leading to difficulties for interpreting the results. However, transformation will not induce such problems for the proposed CUSUM chart because the CUSUM statistic is a recursive function and does not have as apparent meaning as Shewhart control charts do. Results in Chapter 4 have shown that CUSUM charts with transformed exponential data are effective in detecting shifts in mean of TBE. The design and performance of CUSUM chart with transformed exponential data were investigated. Different transformation methods such as Nelson's method, Double SQRT transformation, and log transformation were examined in order to find the most

appropriate transformation method. The calculation method of ARL was derived and the performance of the CUSUM chart was assessed. A comparative study on the performance between the CUSUM chart with transformed exponential data and the X-MR chart, the CQC chart and the exponential CUSUM chart was conducted, respectively. Furthermore, the optimal design procedures of CUSUM chart with transformed exponential data were proposed. This study provides another possible alternative for monitoring TBE data with easy design procedures and relatively good performance.

Thirdl, with similar motivation of CUSUM chart with transformed exponential data, a new EWMA chart was proposed to monitor exponentially-distributed TBE data with the help of transformation. Previous studies have shown that EWMA charts have similar efficiency in detecting process shifts as CUSUM charts do. Moreover, additional advantages of EWMA charts include the ability of predicting the process level at the next time period, and the robustness to nonnormality. In Chapter 5, a new EWMA scheme was proposed in which the TBE data are transformed to approximate normal using the double square root (SQRT) transformation before applying EWMA method. The ARL properties of EWMA chart with transformed exponential data were investigated, based on which the control chart optimal design procedures were developed. Subsequently, the performance of the EWMA chart with transformed exponential data was compared to that of the X-MR chart, the CQC chart and the exponential EWMA chart respectively. Moreover, the robustness of proposed EWMA chart to Weibull-distributed TBE data was examined, followed by an example to illustrate the design and application procedures. Results of this study show that the

EWMA chart with transformed exponential data performs well in monitoring exponentially-distributed TBE data.

Fourthly, a variable sampling interval CCC chart was proposed. The CCC chart was shown to be useful for process monitoring in automated and discrete manufacturing. Current design of CCC chart is based on fixed sampling interval scheme which prevents the application of CCC chart to those processes where fixed sampling plan is not convenient if not impossible. Moreover, fixed sampling schemes may lead to longer detection time of assignable causes, more inspection effort or higher inspection cost, which in turn lose interests from customers. In this study, the CCC chart with variable sampling intervals was investigated. The ATS was calculated, and the efficiency of variable sampling interval CCC chart was compared with that of fixed sampling interval CCC chart. Based on the results from the comparative study, the design procedures of variable sampling interval CCC chart were developed. It has been proved in this study that the use of variable sampling interval scheme can further enhance the cost effectiveness of CCC chart implementation from a practical point of view.

Fifthly, the sampling CCC chart with random-shift model was studied which considers a more realistic case where the shift may occur any time during the process. Previous study on CCC chart relies on an implicit assumption that the process shifts occur just at the moment when events happen, e.g. a nonconforming item was found. However, in reality, the process shifts always randomly arise at any time between successive events, rather than only happen together with an event in the meanwhile. In chapter 7, sampling CCC chart with random-shift model was studied. The minimum sample size

required for estimation of fraction nonconforming was derived; performance of sampling CCC chart was evaluated; and the methods of selecting appropriate sampling frequency were also presented. A case study was done in a semiconductor manufacturing company in order to verify the proposed methods and to further improve this research with consideration of practical implementation issues. Although the research in this chapter looked at monitoring fraction of nonconforming in manufacturing processes, the methods can be applied to monitoring events occurrence rate for other processes as well.

Last but not the least, the TBE charts were extended to Weibull-distributed TBE data, and thus can serve for more general situations where events occurrence rate varies along with time. Existing TBE charts for exponentially-distributed data assume that events occurrence rate is constant throughout the whole 'life' of monitoring. This is only true when the process is stable with constant events occurrences rate, or lifetime is relatively short and variability in events occurrence rate can be ignored. Actually, processes with variable events occurrence rate are not rare in practice, and the monitoring of those processes is of great interest for both researchers and users. The Weibull distribution is recommended to model the time-between-events because of its versatility in modelling a variety of events occurrence behaviors. In this study, a Weibull EWMA chart was proposed to monitor TBE with increasing, decreasing, or constant events occurrence rate. The performance of Weibull EWMA chart is evaluated in terms of ARL and ATS, based on which the design procedures are recommended. At the end, a simulated example is given to illustrate the design and implementation of the chart.

In this study, although motivated by some modelling and monitoring problems from high-quality manufacturing processes, the results can also be used in more broad areas such as service processes, traffic systems or even management processes to improve their performance as long as it could fit in the model proposed. For example, the study of time between customers arrival may help the hospital to optimize the service system and shorten the waiting time. The time-between-events monitoring may also help to detect some changes in a chemical reaction process. As the fourth coordinate other than the traditional three-dimensional space, time becomes a very important measure for many kinds of processes, and the time-between-events monitoring can be helpful in the monitoring and control of those kinds of processes and helps to detect the process shifts as fast as possible.

These control charting methods can be applied to most of the TBE data the users may have from the practical processes. This study is conducted based on the exponential and Weibull distributions. The real data may not be able to fit those distributions quite well. In that case the performance of the control chartings schemes may not be so good as the designed scheme with the assumed mathematical model. The robustness study in chapter 5 proved that the EWMA chart with transformed TBE data still shows good ability to monitor the process if the distribution of data is not quite far from the model.

Another limitation found during the process of case studies is that this study focused on the design of control charts and starts from the stage where the data have been collected already, and ends with the in-time alarms for any process shifts or changes. In some cases, the real data may need to be processed before employing the control charting procedures as proposed in the thesis to filter out the noise or useless

information. Also, since the high-quality processes are often highly automated, after the signal is found from the control charts, timely failure diagnosis and feedback adjustment are also important to improve the overall performance of the monitoring and control system.

9.2 Future Research

Although this thesis attempts to provide more comprehensive, efficient and effective control charting methods for modeling and monitoring TBE data, there are still some aspects that were not addressed yet, and deserve further explorations.

Firstly, it is interesting to investigate how the control charts perform when the data actually departs from the original assumed distribution. The influence factors may include the estimation error of process parameters, inspection error, etc. The proposed control charts may need some modification or adjustment to compensate for the deviations. On the other hand, the users may also consider using transformation methods to help fit the data to a certain model developed.

Secondly, the performances of proposed control chart schemes in this study are evaluated using the Average Run Length or Average Time to Signal. Further study on confidence interval of the ARL and ATS values could be carried out by deriving run length distribution of the control charts or running Monte Carlo simulation.

Thirdly, since the delay of feedback to the process may also lead to a big loss, timely diagnosis and feedback adjustment are also quite important for the overall performance of the system. Some studies have devoted to these issues with the help of Artificial

Intelligence, Artificial Neural Network, Expert System techniques etc., and have shown good effect to solve these problems. How to connect and integrate the control charts monitoring system with the failure diagnosis and feedback adjustment is a useful topic and deserves attention.

Finally, the TBE charts can be extended to multivariate variables, since in reality there are always several events happening at the same time during the process, and the events occurrence rate may be different or may also be correlated among all the events. Therefore, a multivariate TBE chart can be used to analyze several TBE variables at the same time, identify the relationships of different TBE variables, and thus control the multivariable processes more effectively.

References

Annadi, H.P., Keats, J.B., Runger, G.C. and Montgomery, D.C. (1995). "An Adaptive Sample Size CUSUM Control Chart," *International Journal of Production Research,* **33**, 1605-1616.

Arnold, J.C. and Reynolds, M. R. JR. (2001). "CUSUM Control Charts with Variable Sample Sizes and Sampling Intervals," *Journal of Quality Technology,* **33**(1), 66-81.

Bai, D.S. and Choi, I. S.(1995). "$\overline{X}$ and R Chart for Skewed Populations," *Journal of Quality Technology*, **27**(2), 120-131.

Bai, D.S., and Lee, K.T. (1998). "An Economic Design of Variable Sampling Interval $\overline{X}$ Control Charts," *International Journal of Production Economics*, **54**, 57-64.

Bai, D.S., and Lee, K.T. (2002). "Variable Sampling Interval $\overline{X}$ Control Charts with an Improved Switching Rule," *International Journal of Production Economics*, **76**, 189-199.

Benneyan, J.C., Lloyd, R.C. and Plsek, P.E. (2003). "Statistical Process Control as a Tool for Research and Healthcare Improvement," *Quality & Safety in Health Care*, **12** (6): 458-464.

Bischak, D.P. and Silver,E.A.(2001). "Estimating the Rate at Which a Process Goes Out of Control in a Statistical Process Control Context, " *International Journal of Production Research*, **39** (13), 2957-2971.

Borror, C. M., Keats, J.B. and Montgomery, D.C. (2003). "Robustness of the Time Between Events CUSUM," *International Journal of Production Research*, **41**(5), 3435-3444.

Borror, C.M., Champ, C.W. and Rigdon, S.E. (1998). "Poisson EWMA Control Charts," *Journal of Quality Technology*, **30** (4), 352-361.

Borror,C.M., Montgomery,D.C., and Runger, G.C. (1999). "Robustness of the EWMA control chart to non-normality," *Journal of Quality Technology*, **31**(3), 309-316.

Bourke, P.D. (1991). "Detecting Shift in Fraction Nonconforming Using Run-length Control Charts with 100% Inspection," *Journal of Quality Technology*, **23**, 225-238.

Bourke, P.D. (2001). "The Geometric CUSUM Chart with Sampling Inspection for Monitoring Fraction Defective," *Journal of Applied Statistics*, **28**(8), 951-972.

Box, G.E.P. and Cox, D.R. (1964). "An Analysis of Transformations," *Journal of the Royal Statistical Society- Series B*, **26**, 211-252.

Box, G.E.P. and Kramer, T. (1992). "Statistical Process Monitoring and Feedback Adjustment - A Discussion," *Technometrics*, **34** (3), 251-267.

Braun, W.J. (1999). "Run Length Distributions for Estimated Attribute Charts," *Metrika*, **50**, 121-129.

Brook, D. and Evans,D.A.(1972). "An Approach to the Probability Distribution of CUSUM Run Length," *Biometrika*, **59**(3), 539-549.

Cai, D.Q., Xie, M., and Goh, T.N. (2001). "SPC in Automated Manufacturing Environment." *International Journal of Computer Integrated Manufacturing*, **14**(2), 206-211.

Calvin, T.W. (1983). "Quality Control Techniques for 'Zero-defects'," *IEEE Transactions on Components, Hybrid and Manufacturing Technology*, **6**, 323-328.

Carot, V., Jabaloyes, J. M., and Carot,T. (2002). "Combined Double Sampling and Variable Sampling Interval $\overline{X}$ Chart," *International Journal of Production Research*, **40**(9), 2175-2186.

Champ, C. W. (1992). "Steady-state Run Length Analysis of a Shewhart Quality Control Chart with Supplementary Runs Rules, " *Communications in Statistics-Theory and Methods*, **21**(3), 765–777.

Chan, L.Y., Xie, M. and Goh,T.N. (1997). "Two-stage Control Charts for High Yield Processes," *International Journal of Reliability, Quality and Safety Engineering*, **4**(2), 149-165.

Chan, L. Y.; Xie, M., and Goh, T. N. (2000). "Cumulative Quantity Control Charts for Monitoring Production Processes," *International Journal of Production Research*, **38**, 397-408.

Chan, L.Y., Lin, D.K.J., Xie, M. and Goh, T.N. (2002). "Cumulative Probability Control Charts for Geometric and Exponential Process Characteristics," *International Journal of Production Research*, **40**(1),133-150.

Chan, L.Y., Lai, C.D., Xie, M. and Goh.T.N. (2003). "A Two-stage Decision Procedure For Monitoring Processes with Low Fraction Nonconforming," *European Journal of Operational Research*, **150**(2), 420-436.

Chang, Y.S. and Bai, D.S. (2001). "Control Charts for Positively-skewed Populations With Weighted Standard Devistions," *Quality and Reliability Engineering International*, **17**, 397-406.

Chen, G. (1997). "The Mean and Standard Deviation of the Run Length Distribution of $\overline{X}$ charts When Control Limits are Estimated," *Statsitica Sinica*, **7**, 789-798.

Chen, G. (1998). "The Run Length Distribution of R, s, and s^2 Control Charts When σ is Estimated," *Canadian Journal of Statistics*, **26**, 311-322.

Chen, Y.K. (2004). "Economic Design of $\overline{X}$ Control Charts for Non-normal Data Using Variable Sampling Policy," *International Journal of Production Economics*, **92**(1), 61-74.

Chen, H.F. and Cheng, Y.Y. (2006). "Non-normality Effects on the Economic-statistical Design of $\overline{X}$ Charts with Weibull In-control Time," *European Journal of Operational Research*, in press.

Chen, Y.K. (2004). "Economic Design of X-bar Control Charts for Non-normal Data Using Variable Sampling Policy," *International Journal of Production Economics*, **92** (1), 61-74.

Chen, Y.K. (2006). "Economic Design of an Adaptive T^2 Control Chart," *Journal of the Operational Research Society,* in press.

Cheng, C.S., and Cheng, S. S. (2001). "A Neural Network-based Procedure for the Monitoring of Exponential Mean," *Computers & Industrial Engineering*, **40**, 309-321.

Chou, C.Y., Chen, C.H. and Liu, H.R. (2001). "Economic Design of X-bar Charts for Non-normally Correlated Data," *International Journal of Production Research*, **39**, 1931-1941.

Chou, Y. M.; Polansky, A. M.; and Mason, R. L. (1998). "Transforming Non-normal data to Normality in Statistical Process Control," *Journal of Quality Technology*, **30**,133-141.

Collins, R. and Case, K. (1978). "The p Control Chart Under Inspection Error," *Transactions, 32nd American Society for Quality Control Annual Technical Conference*, Chicago, Illinois, 516-525.

Costa, A.F.B. (1994). "$\overline{X}$ Charts with Variable Sample Size," *Journal of Quality Technology*, **26**,155-163.

Costa, A.F.B. (1997). "$\overline{X}$ Charts with Variable Sample Size and Sampling Intervals," *Journal of Quality Technology*, **29**,197-204.

Crowder, S.V. (1989). "Design of Exponentially Weighted Moving Average Schemes," *Journal of Quality Technology*, **21** (3),155-162.

Crowder, S.V., and Hamilton, M.D. (1992). "An EWMA for Monitoring a Process Standard Deviation," *Journal of Quality Technology*, **24** (1),12-21.

Davis, R. B., and Woodall, W. H. (2002). "Evaluating and Improving the Synthetic Control Chart," *Journal of Quality Technology*, **34**(2), 200–208.

Duncan, A.J. (1956). "The Economic Design of $\overline{X}$ Charts Used to Maintain Current Control of a Process," *Journal of the American Statistical Association* **51**, 228 – 242.

Epprecht, E.K. and Costa, A.F.B. (2001). "Adaptive Sample Size Control Charts for Attributes," *Quality Engineering*, **13**(3), 465-473.

Epprecht, E.K., Costa, A.F.B. and Mendes, F.C.T. (2003). "Adaptive Control Charts for Attributes," *IIE Transactions*, **35**, 567-582.

Fraser, R.E., (2001) *Process Measurement and Control: Introduction to Sensors, Communication, Adjustment, and Control* (Prentice-Hall Inc.).

Gan, F. F. (1992). "Exact Run Length Distributions for One-sided Exponential CUSUM schemes," *Statistica Sinica* , **2**, 297-312.

Gan, F.F. (1993). "Exponentially Weighted Moving Average Control Charts with Reflecting Boundaries," *Journal of Statistical Computation and Simulation*, **46** (1-2), 45-67.

Gan, F.F. (1994). "Design of Optimal Exponential CUSUM Control Charts," *Journal of Quality Technology*, **26**,109-124.

Gan, F.F. and Choi, K.P. (1994). "Computing Average Run Lengths for Exponential CUSUM schemes," *Journal of Quality Technology*, **26**, 134-143.

Gan, F.F. (1998). "Designs of One- and Two-sided Exponential EWMA Charts," *Journal of Quality Technology*, **30**(1), 55-69.

Gan, F.F. and Chang, T.C. (2000). "Computing Average Run Lengths of Exponential EWMA Chart," *Journal of Quality Technology*, **32**(2),183-187.

Goh, T.N. (1987). "A Control Chart for Very High Yield Processes," *Quality Assurance*, **13**, 18-22.

Goh, T.N, and Xie, M. (2003). "Statistical Control of a Six Sigma Process," *Quality Engineering*, **15**, 587-592.

Guh, R.S. (2003). "Integrating Artificial Intelligence into On-line Statistical Process Control," *Quality and Reliability Engineering International*, **19**(1), 1-20.

Guh, R.S. (2005). "Real-time Pattern Recognition in Statistical Process Control: a Hybrid Neural Network/Decision Tree-based Approach," *Proceedings of the Institution of Mechanical Engineers Part B-Journal of Engineering Manufacture*, **219** (3), 283-298.

Guh, R.S., Shiue, Y.R. (2005). "On-line Identification of Control Chart Patterns Using Self-organizing Approaches," *International Journal of Production Research*, **43** (6),1225-1254.

Guthrie, B., Love, T., Fahey, T., Morris, A. and Sullivan, F. (2005). "Control, Compare and Communicate: Designing Control Charts to Summarise Efficiently Data from Multiple Quality Indicators," *Quality & Safety in Health Care*, **14** (6): 450-454.

Hawkins, D.M. (1993). "Cumulative Sum Control Charting: An Underutilized SPC Tool," *Quality Engineering*, **5**(3): 463-477.

Hawkins,D.M., and Olwell, D.H. (1998). *Cumulative Sum Charts and Charting for Quality Improvement,* New York: Springer.

Herbert, D., Curry, A. and Angel, L. (2003). "Use of Quality Tools and Techniques in Services," *Service Industries Journal*, **23** (4), 61-80.

Hoerl, R.W. and Palm, A.C. (1992). "Discussion of Statistical Process Monitoring and Feedback Adjustment—a Discussion," *Technometrics*, **34**, 268-272.

Huang, H.W. (1996). *Adaptive and Predictive Modeling for Real-time Statistical Process Control*. Berkeley: University of California.

Johnson, N. L. (1966). "Cumulative Sum Control Charts and the Weibull Distribution," *Technometrics*, **8**(3), 481-491.

Jones L.A., Champ C. W. (2001). "The Performance of Exponentially Weighted Moving Average Charts With Estimated Parameters," *Technometrics*, **43**(2), 156-167.

Jones, L.A. (2002). "The Statistical Design of EWMA Control Charts with Estimated Parameters," *Journal of Quality Technology*, **34**(3), 277-288.

Jones, L. A. and Champ, C. W. (2002). "Phase I Control Charts for Times Between Events," *Quality and Reliability Engineering International*, **18**, 479-488.

Kanji,G.K. and Arif, O.H. (2001). "Median Rankit Control Chart for Weibull Distribution," *Total Quality Management*, **12**(5), 629-642.

Kittlitz, R.G. Jr. (1999). "Transforming the Exponential for SPC Applications," *Journal of Quality Technology*, **31**(3), 301-308.

Knoth, S. (2005). "Accurate ARL Computation for EWMA-S^2 Control Charts," *Statistics and Computing*, **15** (4), 341-352.

Kuralmani, V., Xie, M., Goh,T.N. and Gan, F.F. (2002). "A Conditional Decision Procedure For High Yield Processes," *IIE Transactions*, **34**, 1021-1030.

Lawless, J. F. (2003). *Statistical Models and Methods for Lifetime Data* (Second Edition) John Wiley & Sons, Inc. Hoboken, New Jersey, USA.

Lai,C.D., Chan,L.Y. Xie, M. (2001). "Distribution of Runs in a Two-stage Process Monitoring Model," *Communications in Statistics: Simulation and Computation*, **30**(3), 547-557.

Lee, K.T. and Bai, D.S. (2000). "Variable Sampling Interval $\overline{X}$ Control Charts with Runs Rules," *International Journal of Industrial Engineering—Theory, Application, and Practice*, **7**(2), 147-158.

Lin, Y.C. and Chou, C. Y. (2005). "On the Design of Variable Sample Size and Sampling Intervals $\overline{X}$ Charts Under Non-normality," *International Journal of Production Economics*, **26**(2), 249-261.

Lorenzen, T.J. and Vance,L.C. (1986). "The Economic Design of Control Charts: A Unified Approach," *Technometrics*, **28,** 3-10.

Lucas, J.M. (1985). "Counted Data CUSUM's," *Technometrics*, **27**, 129-144.

Lucas, J.M., and Saccucci, M.S.(1990). "Exponentially Weighted Moving Average Control Schemes: Properties and Enhancements. *Technometrics*, **32**(1), 1-12.

MacGregor, J.F., and Harris,T.J. (1993). "The Exponentially Weighted Moving Variance," *Journal of Quality Technology*, **25** (2)**,** 106-117.

McCool, J.I., and Joyner-Motley,T. (1998). "Control Charts Applicable When the Fraction Nonconforming is Small," *Journal of Quality Technology*, **30,** 240-247.

Montgomery, D.C. (2005). *Introduction to Statistical Quality Control* (fifth edition), John Wiley& Sons, Inc., 390-395.

Murthy, D.N.P., Xie, M. and Jiang, R.Y. (2004). *Weibull Models*, John Wiley & Sons, Inc., Hoboken, New Jersey. pp58-82 (Weibull parameter estimation).

Nelson, L. S. (1984). "The Shewhart Control Chart—Tests for Special Causes," *Journal of Quality Technology*, **16**(4), 237–239.

Nelson, L. S. (1985). "Interpreting Shewhart Control Charts," *Journal of Quality Technology*, **17**(2), 114–116.

Nelson, L. S. (1988). "Control Charts: Rational Subgroups and Effective Applications," *Journal of Quality Technology*, **20** (1), 73-75.

Nelson, L.S. (1994). "A Control Chart for Parts per Million Nonconforming Items," *Journal of Quality Technology*, **26**, 239-240.

Nelson, P.R. (1979). "Control Charts for Weibull Processes with Standards Given," *IEEE Transactions on Reliability*, **28**, 283-287.

Ohta,H., Kusukawa,E.,Rahim,A. (2001). "A CCC-r Chart for High-yield Processes," *Quality and Reliability Engineering International*, **17**, 439-446.

Pacella, M., and Semeraro, Q. (2005). "Understanding ART-based Neural Algorithms as Statistical Tools for Manufacturing Process Quality Control," *Engineering Applications of Artificial Intelligence*, **18**(6): 645-662.

Page, E.S. (1961). "Cumulative Sum Chart," *Technometrics*, **3**,1-9.

Perry, M.B., Spoerre, J.K. and Velasco, T. (2001). "Control Chart Pattern Recognition Using Back Propagation Artificial Neural Networks", *International Journal of Production Research*, **39**(15): 3399-3418.

Pettersson, M. (2004). "SPC with Applications to Churn Management**,**" *Quality and Reliability Engineering International*, **20**(5), 397-406.

Prabhu, S.S., Montgomery, D.C. and Runger, G.C. (1994). "A Combined Adaptive Sample Size and Sampling Interval $\overline{X}$ Control Scheme," *Journal of Quality Technology*, **26**, 164-176.

Prabhu, S.S., Runger, G.C. and Keats, J.B. (1993). "An Adaptive Sample Size $\overline{X}$ Chart," *International Journal of Production Research*, **31**, 2895-2909.

Radaelli, G. (1998). "Planning Time-between-events Shewhart Control Charts," *Total Quality Management*, **9**, 33-140.

Ramalhoto, M. F. and Morais, M. (1999). "Shewhart Control Charts for the Scale Parameter of a Weibull Control Variable with Fixed and Variable Sampling Intervals," *Journal of Applied Statistics*, **26** (1),129-160.

Ranjan, P., Xie, M., and Goh, T.N. (2003). "Optimal Control Limits for CCC Charts in Presence of Inspection Errors," *Quality and Reliability Engineering International*, **19**(2),149-160.

Ranjan, P., Xie, M., and Goh, T.N. (2003). "On Some Control Chart Procedures for Monitoring the Inter-arrival Times," *Proceedings of Ninth ISSAT conference on Reliability and Quality in design*, 60-64.

Reynolds Jr., M.R., Amin, R.W., Arnold, J.C., and Nachlas, J.A. (1988). "X-bar Charts with Variable Sampling Intervals," *Technometrics*, **30**(2), 181-192.

Reynolds, M.R.Jr, and Arnold, J.C. (2001). "EWMA Control Charts with Variable Sampling Sizes and Variable Sampling Intervals," *IIE Transactions*, **33**, 511-530.

Reynolds, M. R., Jr. and Stoumbos, Z. G. (2001). "Individuals Control Schemes for Monitoring the Mean and Variance of Processes Subject to Drifts," *Stochastic Analysis and Applications*, **19**, 863-892.

Reynolds, M. R., Jr. and Stoumbos, Z. G. (2001). "Monitoring the Process Mean and Variance Using Individual Observations and Variable Sampling Intervals," *Journal of Quality Technology*, **33**, 181-205.

Roberts, S.W. (1959). "Control Chart Tests Based on Geometric Moving Average" *Technometrics*, **1**(3), 239-250.

Saccucci, M.S., Amin, R.W. and Lucas, J.M. (1992). "Exponentially Weighted Moving Average Control Schemes with Variable Sampling Intervals," *Communications in Statistics—Simulation and Computation*, **21**, 627-657.

Schipper, S. and Schmid, W. (2001). "Control Charts for GARCH Processes," *Nonlinear Analysis-Theory Methods & Applications*, **47**(3), 2049-2060.

Schwertman, N.C. (2005). "Designing Accurate Control Charts Based on the Geometric and Negative Binomial Distributions," *Quality and Reliability Engineering International*, **21**,743-756.

Shewhart, W.A. (1926). "Quality Control Charts," *The Bell System Technical Journal*, Oct, 593-603.

Shewhart,W.A. (1931) *Economic Control of Quality of Manufactured Product*. Van Nostrand, New York.

Stoumbos, Z. G. and Reynolds, M. R. Jr. (2000). "Robustness to Non-normality and Autocorrelation of Individuals Control Charts for Monitoring the Process Mean and Variance," *Journal of Statistical Computation and Simulation*, **66**, 145-187.

Stoumbos, Z. G. and Reynolds, M. R. (2005). "Economic Statistical Design of Adaptive Control Schemes for Monitoring the Mean and Variance: An Application to Analyzers," *Nonlinear Analysis-Real World Applications*, **6**(5), 817-844.

Suich, R. (1988). "The c Control Chart Under Inspection Error," *Journal of Quality Technology*, **20**, 263-266.

Sun, J. and Zhang, G.X. (2000). "Control Charts Based on the Number of Consecutive Conforming Items for the Near Zero-nonconformity Processes," *Total Quality Management*, **11**(2), 235-250.

Tang, X.Y., Xie, M. and Goh, T.N. (2000). "A Note on Economic-statistical Design of Cumulative Count of Conforming Chart," *Economic Quality Control*, **15**, 3-14.

Tang, L.C., and Cheong, W.T. (2006). "A Control Scheme for High-yield Correlated Production Under Group Inspection," *Journal of Quality Technology*, **38**(1), 45-55.

Testik, M.C., and Borror, C.M. (2004). "Design Strategies for the Multivariate Exponentially Weighted Moving Average Control Chart," *Quality and Reliability Engineering International*, **20**(6), 571-577.

Tsacle, E.G. and Aly, N.A. (1996). "An Expert System Model for Implementing Statistical Process Control in the Health Care Industry," *Computers & Industrial Engineering*, **31**(1-2), 447-450.

Vardeman, S. and Ray, D. (1985). "Average Run Length for CUSUM Schemes When Observations are Exponentially Distributed," *Technometrics*, **27**,145-150.

Vaughan, T.S. (1993). "Variable Sampling Interval np Process Control Chart," *Communications in Statistics—Theory and Method*, **22**,147-167.

Villalobos, J.R., Muñoz, L., and Gutierrez, M.A. (2005). "Using Fixed and Adaptive Multivariate SPC Charts for Online SMD Assembly Monitoring," *International Journal of Production Economics*, **95**(1), 109-121.

Western Electric (1956). *Statistical Quality Control Handbook*, Western Electric Corporation, Indianapolis, IN.

Wong, H.B., Gan, F.F. and Chang, T.C. (2004). "Designs of Moving Average Control Chart," *Journal of Statistical Computation and Simulation*, **74** (1), 47-62.

Woodall,W.H. (1997). "Control Charts Based on Attribute Data: Bibliography and Review," *Journal of Quality Technology*, **31**(4), 376-386.

Woodall,W.H. and Montgomery, D.C. (1999). "Research Issues and Ideas in Statistical Process Control," *Journal of Quality Technology*, **29**(2), 172-183.

Woodall, W.H. (2006). "The Use of Control Charts in Health-Care and Public-Health Surveillance," *Journal of Quality Technology*, **38**(2), 89-104.

Wu, Z. and Luo, H. (2004). "Optimal Design of the Adaptive Sample Size and Sampling Interval np Control Chart," *Quality and Reliability Engineering International*, **20**(6), 553-570.

Wu, Z., Yeo, S.H. and Fan, H. (2000). "A Comparative Study of the CRL-Type Control Charts," *Quality and Reliability Engineering International*, **16**: 269-279.

Wu, Z. and Spedding, T.A. (1999). "Evaluation of ATS for CRL Control Chart," *Process Control and Quality*, **11**(3), 183-191.

Wu, Z. and Spedding, T.A. (2000). "A Synthetic Control Chart for Detecting Small Shifts in the Process Mean," *Journal of Quality Technology*, **32**(1), 32-38.

Wu, Z., Zhang, X. and Yeo, S.H. (2001). "Design of the Sum-of-conforming-run-length Control Charts," *European Journal of Operational Research*, **131**(1), 187-196.

Xie, M, Goh, T.N. and Xie, W. (1997). "A Study of Economic Design of Control Charts for Cumulative Count of Conforming Chart," *Communications in Statistics: Simulation and Computation*, **26** (3), 1009-1027.

Xie, M. and Goh, T.N. (1997b). "The Use of Probability Limits for Process Control Based on Geometric Distribution," *International Journal of Quality and Reliability Management*, **14** (1), 64-73.

Xie, M.; Goh,T.N. and Lu, X. S.(1998). "A Comparative Study of CCC and CUSUM Charts," *Quality and Reliability Engineering International*, **14**, 339-345.

Xie, M.; Lu, X.S.; Goh,T.N. and Chan,L.Y. (1999). "A Quality Monitoring and Decision-making Scheme for Automated Production Processes," *International Journal of Quality and Reliability Management*, **16**, 148-157.

Xie, M. , Goh, T.N., Kuralmani, V. (2000). "On Optimal Setting of Control Limits for Geometric Chart," *International Journal of Reliability, Quality and Safety Engineering*, **7**(1), 17-25.

Xie, M., Yang, Z.L., and Gaudoin, O. (2000b). "More on the Mis-specification of the Shape Parameter with Weibull-to-exponential Transformation," *Quality and Reliability Engineering International*, **16**, 281-290.

Xie, M., Goh, T.N., and Tang, X.Y. (2000c). "Data Transformation for Geometrically Distributed Quality Characteristics," *Quality and Reliability Engineering International*, **16**, 9-15.

Xie, M., Tang, X.Y. and Goh,T.N. (2001). "On Economic Design of Cumulative Count of Conforming Chart," *International Journal of Production Economics*, **72**(1), 89-97.

Xie, M., Goh,T. N., and Kuralmani, V. (2002). *Statistical Models and Control Charts for High-quality Processes*, Boston, Kluwer Academic Publisher.

Xie, M., Goh, T. N. and Ranjan, P. (2002b). "Some Effective Control Chart Procedures for Reliability Monitoring," *Reliability Engineering and Systems Safety*, **77**,143-150.

Yang, Z.H., Xie, M., Kuralmani, V., and Tsui,K.L. (2002). "On the Performance of Geometric Charts with Estimated Control Limits," *Journal of Quality Technology*, **34**(4), 448-458.

Yang, J.H., and Yang, M.S. (2005). "A Control Chart Pattern Recognition System Using a Statistical Correlation Coefficient Method," *Computers & Industrial Engineering*, **48**(2), 205-221.

Yang, S.F. and Rahim M.A.(2005). "Economic Statistical Process Control for Multivariate Quality Characteristics under Weibull Shock Model, " *International Journal of Production Economics,* **98**(2), 215-226.

Yu, F.J., and Chen, Y.S. (2005). "An Economic Design for a Variable-sampling-interval X-bar Control Chart for a Continuous-flow Process," *International Journal of Advanced Manufacturing Technology,* **25**(3-4), 370-376.

Zhang, C.W., Xie, M., and Goh, T.N. (2005). "Economic Design of Exponential Charts for Time Between Events Monitoring," *International Journal of Production Research,* **43**(23), 5019-5032.

Zhang, L.Y., and Chen, G.M. (2004). "EWMA Charts for Monitoring the Mean of Censored Weibull Lifetimes," *Journal of Quality Technology*, 36(3), 321-328.

Zhang, L.Y. Govindaraju, K., Bebbington, M., and Lai, C.D. (2004). "On the Statistical Design of Geometric Control Charts," *Quality Technology and Quantitative Management*, **1**(2), 233-243.

Zhang, S., and Wu, Z. (2005). "Design of Control Charts with Supplementary Runs Rules, " *Computers and Industrial Engineering*, **49**(1),76-97.

Zorriassatine, F., Tannock, J.D.T. (1998). "A Review of Neural Networks for Statistical Process Control," *Journal of Intelligent Manufacturing*, **9**(3): 209-224.

Publications

Liu, J.Y., Xie, M., Goh, T. N., Liu, Q.H. and Yang, Z.H.(2006). Cumulative Count of Conforming Chart with Variable Sampling Intervals. *International Journal of Production Economics*, 101(2), 286-297.

Liu, J.Y., Xie, M., Goh, T. N. and Sharma, P.R. (2006). A Comparative Study of Exponential Time Between Events Charts. *Quality Technology and Quantitative Management*, 3(3), 347-359.

Liu, J.Y., Xie, M., Goh, T. N., and Chan, L.Y. (2007). A study of EWMA Chart with Transformed Exponential Data. *International Journal of Production Research*, 45(3), 743-763.

Liu, J.Y., Xie, M., and Goh, T. N. (2007), CUSUM Chart with Transformed Exponential Data. *Communications in Statistics: Simulation and Computation*, in press.

Liu, J.Y., Xie, M., and Goh, T. N. (2006). Some Advanced Control Charts For Monitoring Weibull-distributed Time Between Events. *2006 Asian International Workshop on Advanced Reliability Modeling*, Aug 24-26, Korea.

Seow, C., **Liu, J.Y.** (2006). Innovation in Maintenance Strategy Through Six Sigma: Insights of a Malaysian SME. *The 3rd IEEE International Conference on Management of Innovation and Technology*, June 21-23, Singapore, 793-797.

Zhang, C.W., **Liu, J.Y.**, and Goh, T. N. (2005). On Statistical Monitoring of Exponentially Distributed Time Between Events. *International Conference on Modeling and Analysis of Semiconductor Manufacturing*, Oct 6-7, Singapore. 304-311.

Liu, J.Y., Xie, M., Goh, T. N., and Ranjan, P.(2004). Time Between Events Charts for On-line Process Monitoring. *International Engineering Management Conference 2004,* 1061-1065.

Appendix

Appendix I: In-control ARLs of EWMA Chart with Transformed Exponential Data

Table A.1 the in-control ARLs of EWMA chart with transformed exponential data ($0< \lambda \leq 0.07$)

L	λ						
	0.01	0.02	0.03	0.04	0.05	0.06	0.07
2	526.02	280.61	196.51	153.60	127.43	109.73	96.94
2.05	581.33	310.38	217.50	170.11	141.21	121.66	107.53
2.1	643.13	343.69	241.03	188.64	156.68	135.08	119.46
2.15	712.31	381.05	267.45	209.47	174.10	150.19	132.90
2.2	789.93	423.05	297.19	232.95	193.75	167.26	148.11
2.25	877.19	470.34	330.73	259.46	215.97	186.58	165.33
2.3	975.51	523.73	368.65	289.47	241.16	208.50	184.89
2.35	1086.53	584.14	411.62	323.52	269.76	233.42	207.16
2.4	1212.17	652.63	460.41	362.24	302.33	261.84	232.57
2.45	1354.68	730.48	515.96	406.38	339.51	294.31	261.65
2.5	1516.70	819.17	579.34	456.81	382.04	331.50	294.98
2.55	1701.31	920.43	651.84	514.58	430.82	374.20	333.31
2.6	1912.16	1036.34	734.95	580.90	486.90	423.37	377.48
2.65	2153.54	1169.33	830.47	657.24	551.53	480.10	428.52
2.7	2430.52	1322.27	940.51	745.33	626.21	545.74	487.64
2.75	2749.12	1498.58	1067.60	847.21	712.72	621.87	556.30
2.8	3116.46	1702.34	1214.73	965.35	813.18	710.39	636.24
2.85	3541.02	1938.40	1385.50	1102.69	930.13	813.60	729.56
2.9	4032.89	2212.54	1584.19	1262.75	1066.63	934.23	838.78
2.95	4604.15	2531.70	1815.95	1449.75	1226.36	1075.59	966.96
3	5269.20	2904.19	2086.96	1668.80	1413.75	1241.68	1117.76
3.05	6045.35	3340.00	2404.66	1926.04	1634.16	1437.33	1295.66
3.1	6953.38	3851.17	2778.04	2228.89	1894.08	1668.40	1506.08
3.15	8018.30	4452.24	3217.98	2586.36	2201.39	1942.03	1755.64
3.2	9270.32	5160.78	3737.66	3009.41	2565.67	2266.92	2052.39
3.25	10745.93	5998.11	4353.09	3511.33	2998.64	2653.69	2406.22
3.3	12489.36	6990.15	5083.79	4108.39	3514.57	3115.34	2829.24
3.35	14554.34	8168.43	5953.56	4820.46	4130.98	3667.84	3336.35
3.4	17006.22	9571.46	6991.53	5671.90	4869.40	4330.85	3945.90
3.45	19924.73	11246.35	8233.42	6692.65	5756.30	5128.60	4680.59
3.5	23407.33	13250.83	9723.10	7919.57	6824.36	6091.04	5568.52

Table A.2 the in-control ARLs of EWMA chart with transformed exponential data ($0.07< \lambda \leq 0.30$)

	λ						
L	0.08	0.09	0.10	0.15	0.20	0.25	0.30
2	87.23	79.62	73.47	54.67	45.04	39.18	35.26
2.05	96.82	88.41	81.62	60.88	50.27	43.83	39.53
2.1	107.62	98.32	90.82	67.91	56.20	49.12	44.41
2.15	119.80	109.52	101.22	75.90	62.97	55.18	50.01
2.2	133.59	122.20	113.01	84.98	70.71	62.12	56.45
2.25	149.23	136.59	126.40	95.35	79.56	70.10	63.88
2.3	167.01	152.97	141.66	107.21	89.74	79.30	72.49
2.35	187.27	171.66	159.08	120.81	101.45	89.94	82.47
2.4	210.41	193.02	179.01	136.44	114.98	102.27	94.10
2.45	236.91	217.51	201.89	154.47	130.65	116.62	107.67
2.5	267.34	245.66	228.21	175.31	148.84	133.35	123.58
2.55	302.35	278.09	258.56	199.46	170.02	152.93	142.27
2.6	342.76	315.55	293.66	227.53	194.75	175.89	164.30
2.65	389.49	358.93	334.36	260.24	223.73	202.92	190.36
2.7	443.70	409.30	381.66	298.47	257.75	234.83	221.28
2.75	506.73	467.94	436.79	343.27	297.84	272.62	258.10
2.8	580.20	536.38	501.21	395.92	345.21	317.51	302.07
2.85	666.09	616.48	576.70	457.97	401.35	371.02	354.78
2.9	766.74	710.47	665.39	531.30	468.08	434.99	418.19
2.95	885.00	821.06	769.87	618.23	547.65	511.72	494.71
3	1024.34	951.52	893.30	721.55	642.82	604.08	587.41
3.05	1188.95	1105.86	1039.49	844.73	757.00	715.60	700.11
3.1	1383.93	1288.92	1213.14	992.02	894.42	850.73	837.63
3.15	1615.51	1506.65	1419.97	1168.66	1060.35	1015.03	1006.06
3.2	1891.30	1766.33	1667.00	1381.11	1261.32	1215.49	1213.13
3.25	2220.63	2076.90	1962.88	1637.41	1505.55	1460.92	1468.70
3.3	2614.98	2449.34	2318.24	1947.54	1803.29	1762.48	1785.34
3.35	3088.48	2897.25	2746.27	2323.95	2167.48	2134.37	2179.22
3.4	3658.57	3437.39	3263.27	2782.20	2614.43	2594.64	2671.17
3.45	4346.86	4090.60	3889.50	3341.80	3164.80	3166.42	3288.13
3.5	5180.13	4882.75	4650.22	4027.28	3844.81	3879.40	4065.09

Table A.3 the in-control ARLs of EWMA chart with transformed exponential data ($0.30< \lambda \leq 0.65$)

	λ						
L	0.35	0.40	0.45	0.50	0.55	0.60	0.65
2	32.46	30.38	28.78	27.53	26.54	25.75	25.11
2.05	36.47	34.21	32.48	31.14	30.09	29.25	28.57
2.1	41.07	38.62	36.76	35.33	34.21	33.33	32.63
2.15	46.37	43.72	41.72	40.20	39.02	38.11	37.39
2.2	52.49	49.62	47.49	45.88	44.66	43.73	43.01
2.25	59.57	56.48	54.21	52.53	51.28	50.35	49.66
2.3	67.80	64.48	62.08	60.35	59.10	58.20	57.57
2.35	77.39	73.84	71.33	69.57	68.35	67.54	67.03
2.4	88.60	84.82	82.22	80.48	79.36	78.70	78.37
2.45	101.74	97.75	95.11	93.45	92.50	92.08	92.05
2.5	117.20	113.04	110.42	108.92	108.26	108.22	108.63
2.55	135.46	131.17	128.66	127.45	127.24	127.76	128.83
2.6	157.08	152.76	150.49	149.75	150.20	151.55	153.58
2.65	182.78	178.54	176.70	176.69	178.10	180.65	184.05
2.7	213.44	209.47	208.32	209.37	212.18	216.42	221.79
2.75	250.14	246.70	246.61	249.19	253.99	260.64	268.80
2.8	294.24	291.69	293.18	297.96	305.55	315.60	327.74
2.85	347.40	346.29	350.06	357.94	369.47	384.30	402.08
2.9	411.75	412.80	419.84	432.08	449.11	470.67	496.46
2.95	489.92	494.16	505.83	524.18	548.90	579.91	617.07
3	585.27	594.11	612.29	639.16	674.63	718.93	772.27
3.05	702.01	717.43	744.72	783.46	833.96	896.97	973.38
3.1	845.53	870.25	910.25	965.52	1037.05	1126.50	1235.87
3.15	1022.68	1060.47	1118.18	1196.50	1297.51	1424.38	1581.00
3.2	1242.26	1298.34	1380.70	1491.18	1633.62	1813.63	2038.22
3.25	1515.60	1597.20	1713.86	1869.31	2070.16	2325.88	2648.57
3.3	1857.31	1974.47	2138.94	2357.40	2640.85	3004.86	3469.64
3.35	2286.39	2453.08	2684.27	2991.28	3391.94	3911.45	4582.83
3.4	2827.60	3063.30	3387.79	3819.62	4387.29	5131.00	6103.81
3.45	3513.38	3845.30	4300.58	4909.02	5715.63	6783.94	8197.99
3.5	4386.42	4852.71	5491.89	6351.14	7501.06	9041.31	11103.14

Table A.4 the in-control ARLs of EWMA chart with transformed exponential data ($0.65< \lambda \leq 1$)

	λ						
L	0.70	0.75	0.80	0.85	0.90	0.95	1.00
2	24.59	24.18	23.86	23.62	23.46	23.35	23.32
2.05	28.03	27.61	27.28	27.03	26.85	26.75	26.71
2.1	32.07	31.64	31.30	31.05	30.87	30.77	30.73
2.15	36.83	36.39	36.06	35.82	35.64	35.54	35.50
2.2	42.46	42.04	41.73	41.50	41.34	41.25	41.21
2.25	49.15	48.78	48.50	48.31	48.18	48.11	48.07
2.3	57.14	56.84	56.65	56.52	56.44	56.39	56.37
2.35	66.72	66.56	66.49	66.47	66.47	66.47	66.46
2.4	78.27	78.32	78.45	78.59	78.72	78.80	78.82
2.45	92.28	92.65	93.07	93.48	93.81	94.01	94.07
2.5	109.34	110.20	111.08	111.88	112.50	112.90	113.02
2.55	130.25	131.83	133.40	134.79	135.87	136.55	136.77
2.6	156.03	158.68	161.25	163.53	165.31	166.44	166.81
2.65	188.01	192.21	196.29	199.91	202.75	204.55	205.15
2.7	227.92	234.39	240.72	246.36	250.81	253.65	254.61
2.75	278.06	287.86	297.51	306.20	313.13	317.59	319.11
2.8	341.49	356.16	370.76	384.09	394.84	401.82	404.22
2.85	422.29	444.07	466.08	486.50	503.20	514.17	517.98
2.9	525.97	558.18	591.29	622.59	648.64	666.00	672.08
2.95	659.98	707.52	757.34	805.45	846.32	873.98	883.77
3	834.54	904.65	979.68	1053.88	1118.42	1162.90	1178.81
3.05	1063.68	1167.12	1280.28	1395.11	1497.63	1569.84	1595.98
3.1	1366.85	1519.61	1690.54	1868.70	2032.35	2150.44	2193.77
3.15	1771.21	1997.10	2255.57	2532.24	2793.96	2987.83	3060.06
3.2	2314.91	2649.38	3040.28	3469.26	3886.57	4203.98	4324.12
3.25	3051.86	3547.68	4138.24	4799.99	5458.72	5971.42	6168.35
3.3	4058.77	4794.29	5683.97	6695.15	7714.90	8519.20	8831.09
3.35	5445.31	6536.37	7869.97	9392.68	10923.66	12124.10	12588.47
3.4	7369.00	8985.71	10969.58	13216.99	15421.32	17087.49	17715.84
3.45	10056.81	12446.63	15366.93	18601.10	21619.74	23734.07	24481.10
3.5	13836.62	17354.80	21595.47	26115.45	30040.19	32504.01	33277.92

Appendix II: In-control ARLs of Two-sided Weibull EWMA Chart

Table A.5 The in-control ARLs of Weibull EWMA chart (λ=0.10, shape parameter $0.2 \leq \eta \leq 0.55$. $L_U=L_L=L$)

L	Shape parameter η							
	0.20	0.25	0.30	0.35	0.40	0.45	0.50	0.55
1.5	352.31	191.24	131.20	102.67	86.88	77.26	68.27	58.41
1.6	377.23	205.56	141.61	111.03	94.47	84.27	77.50	69.69
1.7	402.60	220.28	152.33	120.04	102.33	91.76	85.13	79.42
1.8	428.67	235.51	163.50	129.36	110.96	99.96	93.06	88.58
1.9	455.30	251.22	175.19	139.39	119.91	108.50	101.56	97.26
2	482.40	267.45	187.38	149.70	129.43	117.87	110.91	106.54
2.1	510.18	284.04	200.05	160.62	139.54	127.71	120.75	116.77
2.2	538.43	301.26	213.28	172.10	150.26	138.24	131.38	127.67
2.3	567.34	319.02	227.03	184.16	161.64	149.51	142.86	139.77
2.4	596.73	337.15	241.27	196.80	173.70	161.58	155.24	152.77
2.5	626.69	355.91	256.15	210.08	186.46	174.47	168.63	166.91
2.6	657.31	375.23	271.58	223.99	199.93	188.23	183.08	182.30
2.7	688.42	394.94	287.40	238.35	214.24	202.93	198.64	199.04
2.8	720.10	415.26	304.00	253.57	229.35	218.61	215.41	217.28
2.9	752.41	436.04	321.18	269.51	245.31	235.32	233.46	237.10
3	785.24	457.36	338.78	285.96	262.13	252.86	252.88	258.66
3.1	818.63	479.41	357.19	303.37	279.64	271.80	273.78	281.71
3.2	852.65	501.83	376.05	321.48	298.34	292.01	295.92	307.13
3.3	887.19	524.98	395.70	340.22	318.03	313.50	320.05	334.74
3.4	922.31	548.52	415.84	360.01	338.52	336.05	345.96	364.69
3.5	957.99	572.62	436.83	380.39	360.30	360.32	373.45	396.81
3.6	994.26	597.45	458.30	401.86	382.98	385.78	403.28	432.05
3.7	1031.13	622.70	480.46	423.97	407.07	413.12	435.30	470.25
3.8	1068.55	648.52	503.47	447.23	432.11	442.11	469.27	511.25
3.9	1106.54	675.07	527.03	471.17	458.66	472.55	506.03	556.06
4.0	1145.10	702.06	551.49	496.29	486.26	505.11	545.03	604.19

Table A.6 The in-control ARLs of Weibull EWMA chart (λ=0.10, shape parameter $0.60 \leq \eta \leq 0.95$. $L_U=L_L=L$)

L	Shape parameter η							
	0.60	0.65	0.70	0.75	0.80	0.85	0.90	0.95
1.5	50.69	45.26	41.43	38.64	36.52	34.90	33.66	32.67
1.6	61.78	55.46	50.78	47.33	44.79	42.75	41.16	39.91
1.7	72.98	66.96	61.79	57.75	54.63	52.25	50.32	48.76
1.8	83.99	78.74	73.84	69.82	66.32	63.53	61.34	59.51
1.9	94.03	90.68	86.79	82.92	79.64	76.80	74.36	72.40
2	104.19	102.15	99.68	97.14	94.34	91.76	89.58	87.54
2.1	114.72	113.68	112.91	111.63	110.07	108.43	106.67	105.17
2.2	126.11	125.95	126.36	126.65	126.74	126.30	125.79	124.95
2.3	138.75	139.22	140.70	142.56	144.18	145.62	146.48	147.20
2.4	152.55	153.95	156.46	159.64	163.08	166.28	169.19	171.58
2.5	167.60	170.17	173.97	178.56	183.71	188.93	194.00	198.64
2.6	184.20	188.13	193.41	199.80	206.78	214.20	221.58	228.88
2.7	202.42	208.06	215.20	223.65	232.85	242.65	252.83	262.97
2.8	222.43	230.30	239.57	250.47	262.47	275.18	288.48	302.03
2.9	244.40	254.34	266.74	280.75	296.10	312.40	329.49	347.14
3	268.50	281.46	297.24	315.01	334.40	355.11	376.87	399.60
3.1	294.99	311.52	331.40	353.70	378.07	404.22	431.89	460.80
3.2	323.63	344.84	369.65	397.27	427.90	460.80	495.73	532.43
3.3	355.51	381.77	412.48	447.02	484.69	525.99	569.90	616.46
3.4	390.47	422.26	459.95	502.53	549.90	601.13	656.37	715.15
3.5	428.81	467.66	513.69	565.98	624.10	688.09	757.19	831.20
3.6	470.40	517.98	573.91	637.85	709.43	788.50	874.66	967.88
3.7	516.46	573.74	640.88	718.72	807.14	904.78	1012.42	1129.43
3.8	566.91	635.05	716.53	811.00	918.51	1039.66	1173.10	1319.93
3.9	621.74	703.51	801.33	915.64	1046.89	1195.35	1361.79	1545.99
4.0	682.26	779.35	895.82	1033.72	1194.15	1376.71	1583.35	1813.44

Table A.7 The in-control ARLs of Weibull EWMA chart (λ=0.10, shape parameter $1.00 \leq \eta \leq 2.40$. $L_U=L_L=L$)

L	Shape parameter η							
	1.0	1.2	1.4	1.6	1.8	2.0	2.2	2.4
1.5	31.88	29.86	28.81	28.21	27.84	27.61	27.46	27.36
1.6	38.92	36.37	35.05	34.28	33.81	33.51	33.32	33.19
1.7	47.53	44.36	42.70	41.74	41.15	40.76	40.51	40.34
1.8	58.01	54.18	52.13	50.95	50.21	49.72	49.40	49.18
1.9	70.71	66.25	63.82	62.39	61.47	60.88	60.47	60.20
2	85.87	81.05	78.32	76.65	75.58	74.86	74.37	74.04
2.1	103.61	99.13	96.33	94.52	93.33	92.52	91.96	91.56
2.2	124.23	121.01	118.63	116.96	115.79	114.96	114.36	113.93
2.3	147.42	147.19	146.17	145.16	144.32	143.65	143.13	142.73
2.4	173.63	178.38	180.12	180.63	180.69	180.55	180.34	180.11
2.5	202.85	214.96	221.62	225.23	227.17	228.24	228.79	229.03
2.6	235.67	257.89	272.22	281.13	286.70	290.15	292.28	293.55
2.7	272.98	307.99	333.61	351.22	362.98	370.84	375.98	379.29
2.8	315.65	366.70	408.05	438.78	460.88	476.32	486.95	494.06
2.9	365.08	435.97	498.19	548.33	586.49	614.65	634.79	648.77
3	422.90	518.06	607.87	685.21	747.98	796.51	832.70	858.70
3.1	490.69	616.28	741.74	856.88	955.71	1036.24	1098.83	1145.34
3.2	570.65	734.62	906.18	1072.64	1223.79	1353.10	1458.09	1539.08
3.3	665.13	877.94	1109.49	1345.20	1570.51	1773.24	1945.22	2083.00
3.4	777.04	1052.41	1362.23	1691.34	2021.03	2332.09	2608.20	2838.51
3.5	909.81	1265.68	1678.32	2133.19	2609.01	3078.73	3514.64	3893.51
3.6	1067.67	1527.27	2075.76	2700.68	3380.17	4080.32	4759.21	5374.58
3.7	1255.74	1849.06	2577.74	3433.68	4397.64	5431.06	6476.21	7464.48
3.8	1479.82	2246.06	3214.46	4385.49	5747.61	7262.47	8857.49	10430.00
3.9	1747.95	2737.19	4025.39	5627.89	7548.91	9759.39	12177.29	14660.44
4.0	2068.36	3346.28	5062.01	7257.72	9966.71	13184.53	16832.93	20730.72

Table A.8 The in-control ARLs of Weibull EWMA chart (λ=0.10, shape parameter $2.60 \leq \eta \leq 4.00$. $L_U=L_L=L$)

L	Shape parameter η							
	2.6	2.8	3.0	3.2	3.4	3.6	3.8	4.0
1.5	27.29	27.25	27.22	27.21	27.21	27.22	27.23	27.24
1.6	33.10	33.04	33.01	32.99	32.98	32.99	33.00	33.01
1.7	40.23	40.15	40.10	40.08	40.07	40.07	40.07	40.09
1.8	49.03	48.94	48.87	48.84	48.82	48.81	48.82	48.83
1.9	60.01	59.88	59.80	59.75	59.72	59.70	59.70	59.71
2	73.80	73.64	73.53	73.45	73.41	73.38	73.38	73.38
2.1	91.27	91.07	90.93	90.83	90.77	90.73	90.70	90.69
2.2	113.61	113.37	113.20	113.07	112.98	112.91	112.86	112.83
2.3	142.41	142.16	141.96	141.80	141.67	141.56	141.47	141.40
2.4	179.89	179.67	179.47	179.28	179.11	178.94	178.78	178.64
2.5	229.09	229.02	228.87	228.68	228.45	228.19	227.93	227.66
2.6	294.25	294.55	294.59	294.44	294.15	293.77	293.33	292.84
2.7	381.31	382.42	382.89	382.90	382.57	382.01	381.28	380.43
2.8	498.63	501.36	502.74	503.15	502.84	502.02	500.82	499.35
2.9	658.08	663.89	667.10	668.37	668.21	667.01	665.05	662.54
3	876.55	888.08	894.77	897.80	898.09	896.37	893.16	888.90

Table A.9 The in-control ARLs of Weibull EWMA chart (λ=0.05, shape parameter $0.2 \leq \eta \leq 0.55$. $L_U=L_L=L$)

L	Shape parameter η							
	0.20	0.25	0.30	0.35	0.40	0.45	0.50	0.55
1.5	518.91	296.96	210.50	167.99	142.01	111.01	92.87	79.54
1.6	556.90	320.12	228.02	183.05	158.24	136.22	113.02	96.69
1.7	595.52	344.50	246.93	199.36	174.34	156.28	133.78	118.97
1.8	635.33	369.77	266.45	216.20	189.95	173.94	157.27	141.93
1.9	676.15	396.01	286.99	234.68	206.72	191.39	180.05	165.17
2	717.96	423.23	308.98	253.78	225.07	209.94	200.36	189.53
2.1	760.78	451.44	331.68	274.10	244.56	229.60	221.27	215.57
2.2	804.49	480.65	355.50	295.67	266.14	250.46	243.58	240.25
2.3	849.33	510.85	380.49	318.57	288.62	273.79	267.95	266.40
2.4	895.07	541.69	406.63	343.35	312.72	298.66	294.19	294.82
2.5	941.92	573.92	434.05	369.07	338.53	325.72	323.50	326.53
2.6	989.71	607.18	462.33	395.80	366.17	355.04	355.21	361.07
2.7	1038.57	641.47	492.19	424.59	395.73	386.77	389.81	399.75
2.8	1088.40	676.48	523.60	455.01	427.33	421.10	427.46	442.43
2.9	1139.24	712.87	556.36	487.14	460.46	458.20	469.16	489.54
3	1191.16	750.02	589.96	521.03	496.49	498.29	514.79	541.52
3.1	1244.05	788.56	625.51	556.79	534.94	540.79	564.69	598.58
3.2	1297.98	827.90	662.50	593.99	575.92	587.50	618.30	662.72
3.3	1352.95	868.63	700.40	633.64	619.57	637.88	677.90	733.78
3.4	1408.93	910.20	740.35	675.40	665.45	692.17	742.98	812.46
3.5	1465.95	953.15	781.28	718.83	714.92	749.88	814.03	898.43

Table A.10 The in-control ARLs of Weibull EWMA chart (λ=0.05, shape parameter $0.60 \leq \eta \leq 0.95$. $L_U=L_L=L$)

L	Shape parameter η							
	0.60	0.65	0.70	0.75	0.80	0.85	0.90	0.95
1.5	71.02	66.08	62.05	59.35	57.27	55.62	54.42	53.38
1.6	87.76	80.48	75.94	72.36	69.73	67.77	66.16	64.95
1.7	106.45	98.47	92.54	88.14	85.01	82.46	80.57	79.00
1.8	128.02	119.72	112.15	107.51	103.33	100.53	98.06	96.22
1.9	154.25	143.32	136.53	130.03	126.03	122.12	119.58	117.20
2	180.75	170.58	163.62	157.57	152.39	148.84	145.32	143.03
2.1	207.82	201.74	193.83	189.20	183.71	180.11	177.05	173.98
2.2	236.27	233.35	228.72	224.26	221.12	216.87	214.47	212.03
2.3	266.94	266.49	266.53	263.67	262.64	260.88	258.37	257.19
2.4	298.93	302.35	306.30	308.61	309.22	310.78	310.56	310.29
2.5	333.31	341.58	349.53	357.30	362.06	366.98	371.27	373.22
2.6	371.21	384.48	397.16	410.41	422.13	431.02	440.10	447.61
2.7	414.27	432.09	450.75	469.86	488.53	504.63	519.18	533.08
2.8	461.77	485.42	511.14	537.26	563.54	588.76	610.90	632.23
2.9	515.00	545.93	579.69	614.41	649.57	684.58	717.92	748.44
3	574.95	613.97	657.31	703.06	749.21	795.74	842.06	885.55
3.1	642.00	691.80	746.88	805.26	865.11	926.03	987.56	1047.93
3.2	717.47	779.89	849.45	923.27	1000.73	1079.56	1159.80	1240.39
3.3	802.34	879.62	967.21	1060.69	1159.27	1260.73	1364.80	1470.63
3.4	896.10	994.27	1102.66	1220.37	1345.69	1476.25	1610.35	1747.85
3.5	1002.81	1123.76	1258.38	1406.17	1564.82	1731.81	1904.46	2083.47

Table A.11 The in-control ARLs of Weibull EWMA chart (λ=0.05, shape parameter $1.00 \leq \eta \leq 1.50$. $L_U=L_L=L$)

L	Shape parameter η					
	1	1.1	1.2	1.3	1.4	1.5
1.5	52.61	51.39	50.53	49.90	49.43	49.08
1.6	63.91	62.40	61.34	60.56	59.99	59.54
1.7	77.75	75.86	74.53	73.57	72.85	72.30
1.8	94.70	92.40	90.74	89.53	88.63	87.94
1.9	115.41	112.59	110.63	109.21	108.11	107.25
2	140.78	137.66	135.29	133.53	132.24	131.25
2.1	172.00	168.31	165.72	163.87	162.34	161.16
2.2	209.52	206.19	203.66	201.54	199.97	198.76
2.3	255.46	252.82	250.40	248.72	247.29	246.06
2.4	310.57	309.33	308.59	307.67	306.71	306.07
2.5	375.52	378.52	380.42	381.12	381.90	382.02
2.6	452.67	462.58	468.43	473.29	476.39	478.78
2.7	544.68	562.98	576.95	587.86	595.70	602.17
2.8	652.07	683.68	710.35	730.11	746.75	759.21
2.9	778.05	829.46	872.57	907.54	936.66	960.09
3	927.30	1005.19	1070.92	1128.77	1176.11	1217.27
3.1	1105.52	1216.24	1314.73	1403.07	1479.21	1545.58
3.2	1319.50	1472.01	1615.43	1745.05	1863.36	1966.56
3.3	1576.81	1784.31	1986.06	2173.76	2349.46	2508.48
3.4	1887.98	2168.03	2445.51	2713.60	2967.96	3207.76
3.5	2266.72	2641.59	3019.16	3395.36	3759.32	4111.20

Table A.12 The in-control ARLs of Weibull EWMA chart (λ=0.05, shape parameter $1.60 \leq \eta \leq 2.00$. $L_U=L_L=L$)

L	Shape parameter η				
	1.6	1.7	1.8	1.9	2
1.5	48.80	48.59	48.42	48.28	48.17
1.6	59.20	58.92	58.71	58.53	58.39
1.7	71.87	71.52	71.25	71.03	70.86
1.8	87.41	86.98	86.64	86.37	86.15
1.9	106.59	106.07	105.65	105.31	105.04
2	130.44	129.80	129.30	128.88	128.55
2.1	160.25	159.51	158.91	158.43	158.03
2.2	197.72	196.92	196.27	195.71	195.27
2.3	245.15	244.33	243.68	243.14	242.67
2.4	305.32	304.77	304.27	303.84	303.48
2.5	382.18	382.19	382.15	382.10	381.99
2.6	480.56	481.83	482.86	483.56	484.15
2.7	606.82	610.75	613.62	616.05	617.86
2.8	769.69	777.74	784.49	789.75	794.16
2.9	979.52	995.31	1008.31	1019.02	1027.76
3	1250.66	1279.46	1302.90	1322.87	1339.28
3.1	1602.45	1650.84	1692.43	1727.18	1757.02
3.2	2059.11	2138.57	2208.36	2268.17	2319.43
3.3	2652.40	2781.27	2894.30	2994.65	3081.06
3.4	3426.96	3629.26	3810.54	3973.08	4117.47
3.5	4442.38	4751.87	5038.50	5297.67	5532.90

Table A.13 The in-control ARLs of Weibull EWMA chart (λ=0.20, shape parameter $0.20 \leq \eta \leq 0.55$. $L_U=L_L=L$)

	Shape parameter η							
L	0.20	0.25	0.30	0.35	0.40	0.45	0.50	0.55
1.5	244.69	127.76	85.24	65.20	54.10	47.38	42.96	39.95
1.6	261.26	136.73	91.49	70.16	58.44	51.26	46.62	43.52
1.7	278.11	146.01	98.04	75.35	62.95	55.48	50.64	47.43
1.8	295.34	155.51	104.73	80.84	67.69	59.86	54.82	51.53
1.9	312.82	165.23	111.67	86.47	72.75	64.50	59.40	56.06
2.0	330.64	175.26	118.89	92.39	78.02	69.53	64.19	60.80
2.1	348.75	185.57	126.27	98.56	83.56	74.76	69.30	65.91
2.2	367.17	196.07	133.97	104.99	89.37	80.29	74.73	71.40
2.3	385.97	206.87	141.94	111.69	95.47	86.13	80.55	77.30
2.4	405.02	217.89	150.13	118.58	101.85	92.32	86.74	83.63
2.5	424.38	229.24	158.55	125.81	108.56	98.87	93.33	90.41
2.6	444.11	240.80	167.31	133.33	115.50	105.78	100.34	97.70
2.7	464.10	252.71	176.26	141.08	122.87	112.97	107.78	105.51
2.8	484.40	264.81	185.55	149.22	130.58	120.65	115.72	113.87
2.9	505.01	277.19	195.05	157.66	138.55	128.73	124.15	122.82
3.0	525.97	289.88	204.91	166.33	146.97	137.16	132.97	132.28
3.1	547.21	302.80	214.99	175.40	155.74	146.14	142.46	142.51
3.2	568.76	316.00	225.43	184.72	164.83	155.60	152.52	153.48
3.3	590.62	329.55	236.09	194.42	174.41	165.43	163.07	165.20
3.4	612.79	343.31	247.04	204.42	184.31	175.88	174.36	177.58
3.5	635.27	357.35	258.33	214.86	194.74	186.86	186.33	190.94
3.6	658.07	371.68	269.89	225.56	205.50	198.28	198.88	205.07
3.7	681.20	386.32	281.76	236.62	216.81	210.35	212.29	220.28
3.8	704.62	401.22	294.01	248.14	228.49	222.93	226.34	236.49
3.9	728.35	416.40	306.51	259.96	240.74	236.13	241.33	253.64
4.0	752.39	431.88	319.33	272.16	253.39	250.07	257.04	272.08
4.1	776.75	447.65	332.48	284.86	266.54	264.57	273.77	291.56
4.2	801.42	463.79	346.05	297.87	280.28	279.88	291.29	312.46
4.3	826.40	480.15	359.86	311.29	294.49	295.79	309.80	334.56
4.4	851.69	496.81	374.01	325.23	309.25	312.56	329.43	358.07
4.5	877.30	513.77	388.50	339.50	324.69	329.98	350.02	383.23
4.6	903.23	531.03	403.40	354.21	340.60	348.20	371.86	409.82
4.7	929.47	548.60	418.59	369.43	357.11	367.37	394.73	438.23
4.8	956.01	566.47	434.13	385.04	374.33	387.28	418.83	468.26
4.9	982.87	584.71	450.04	401.12	392.08	408.07	444.36	500.28
5.0	1010.05	603.20	466.31	417.67	410.49	429.88	471.07	534.13
5.1	1037.54	621.99	483.04	434.71	429.67	452.56	499.18	570.06
5.2	1065.35	641.10	500.05	452.33	449.43	476.22	528.89	608.33
5.3	1093.47	660.53	517.44	470.36	469.90	500.90	559.99	648.75
5.4	1121.90	680.27	535.21	488.90	491.08	526.78	592.67	691.59
5.5	1150.66	700.33	553.38	507.96	513.12	553.62	627.15	737.17
5.6	1179.73	720.72	571.93	527.55	535.81	581.59	663.22	785.26
5.7	1209.11	741.42	590.92	547.78	559.28	610.85	701.10	836.19
5.8	1238.82	762.50	610.27	568.46	583.55	641.21	740.98	890.11
5.9	1268.84	783.86	630.03	589.71	608.64	672.81	782.71	947.34
6	1299.18	805.54	650.19	611.52	634.65	705.71	826.48	1007.70

Table A.14 The in-control ARLs of Weibull EWMA chart (λ=0.20, shape parameter $0.60 \leq \eta \leq 0.95$. $L_U=L_L=L$)

	Shape parameter η							
L	0.60	0.65	0.70	0.75	0.80	0.85	0.90	0.95
1.5	37.67	34.88	31.70	28.88	26.64	24.83	23.43	22.32
1.6	41.38	39.58	37.35	34.80	32.47	30.48	28.81	27.45
1.7	45.21	43.66	42.28	40.56	38.62	36.73	35.02	33.53
1.8	49.28	47.83	46.79	45.84	44.64	43.23	41.77	40.36
1.9	53.81	52.31	51.44	50.88	50.36	49.66	48.76	47.74
2.0	58.61	57.32	56.51	56.15	56.06	55.99	55.79	55.39
2.1	63.80	62.64	62.09	61.90	62.09	62.49	62.92	63.25
2.2	69.41	68.45	68.13	68.26	68.75	69.52	70.46	71.43
2.3	75.48	74.78	74.76	75.24	76.13	77.32	78.74	80.30
2.4	82.18	81.66	82.03	82.94	84.27	86.02	88.00	90.19
2.5	89.29	89.16	90.00	91.45	93.37	95.77	98.42	101.33
2.6	96.83	97.33	98.75	100.85	103.48	106.74	110.17	113.97
2.7	105.12	106.22	108.33	111.23	114.75	118.96	123.40	128.32
2.8	114.06	115.89	118.85	122.71	127.28	132.46	138.36	144.63
2.9	123.72	126.42	130.38	135.38	141.25	147.84	155.28	163.08
3.0	134.15	137.85	142.86	149.40	156.80	165.09	174.41	184.25
3.1	145.39	150.14	156.72	164.70	174.12	184.47	196.07	208.40
3.2	157.37	163.68	171.91	181.82	193.23	206.25	220.37	235.97
3.3	170.42	178.38	188.55	200.73	214.75	230.72	248.16	267.46
3.4	184.48	194.35	206.62	221.64	238.74	258.01	279.67	303.21
3.5	199.48	211.54	226.61	244.56	265.48	288.96	315.41	344.40
3.6	215.79	230.37	248.51	270.09	295.10	323.78	355.75	391.56
3.7	233.34	250.65	272.31	298.32	328.37	362.73	401.83	445.60
3.8	252.06	272.83	298.58	329.32	365.46	406.85	454.18	507.30
3.9	272.36	296.91	327.33	363.79	406.63	456.51	513.44	578.39
4.0	294.01	322.85	358.61	401.68	452.81	512.22	581.10	659.73
4.1	317.45	351.16	393.05	443.77	504.09	575.24	657.82	753.47
4.2	342.46	381.67	430.55	490.26	561.56	646.00	745.41	861.21
4.3	369.47	414.92	471.78	541.41	625.67	726.03	845.12	984.81
4.4	398.31	450.76	516.68	598.14	696.97	816.23	958.40	1127.33
4.5	429.44	489.76	565.99	660.57	776.77	917.64	1087.73	1291.08
4.6	462.65	531.80	619.69	729.76	865.57	1032.26	1234.81	1479.97
4.7	498.44	577.48	678.60	805.92	964.88	1161.24	1402.74	1697.27
4.8	536.62	626.74	742.76	890.24	1075.44	1306.96	1593.88	1948.03
4.9	577.54	680.02	813.07	983.07	1198.78	1471.01	1812.12	2236.82
5.0	621.55	737.85	889.65	1085.52	1336.64	1656.05	2060.71	2570.22
5.1	668.48	800.15	973.47	1198.82	1490.14	1865.02	2344.57	2954.54
5.2	718.91	867.69	1064.77	1323.56	1661.61	2100.42	2668.09	3398.40
5.3	772.68	940.45	1164.41	1461.40	1852.55	2366.23	3037.22	3910.46
5.4	830.19	1019.03	1273.37	1613.14	2065.73	2665.71	3458.76	4502.07
5.5	891.86	1104.08	1391.97	1780.46	2303.13	3003.79	3939.52	5185.05
5.6	957.62	1195.67	1521.31	1965.13	2567.79	3384.77	4488.57	5974.12
5.7	1027.88	1294.49	1662.55	2168.41	2863.06	3814.44	5114.95	6886.28
5.8	1103.13	1401.30	1816.24	2392.65	3191.85	4299.31	5830.01	7940.20
5.9	1183.28	1516.26	1983.70	2639.39	3558.23	4845.77	6646.67	9158.94
6	1268.86	1640.19	2166.35	2911.15	3966.71	5461.98	7578.70	10567.75

Table A.15 The in-control ARLs of Weibull EWMA chart (λ=0.20, shape parameter $1.0 \leq \eta \leq 1.5$. $L_U=L_L=L$)

L	Shape parameter η					
	1.0	1.1	1.2	1.3	1.4	1.5
2.0	54.85	53.54	52.22	51.05	50.06	49.22
2.1	63.39	63.20	62.65	61.95	61.23	60.57
2.2	72.33	73.64	74.33	74.57	74.52	74.33
2.3	81.92	84.91	87.26	88.96	90.10	90.85
2.4	92.51	97.24	101.58	105.24	108.16	110.45
2.5	104.44	111.02	117.59	123.67	129.01	133.55
2.6	118.03	126.71	135.78	144.71	153.11	160.70
2.7	133.55	144.78	156.76	169.05	181.16	192.69
2.8	151.31	165.69	181.21	197.51	214.15	230.64
2.9	171.66	189.98	209.91	231.16	253.36	276.06
3.0	195.00	218.23	243.72	271.19	300.37	330.89
3.1	221.86	251.16	283.65	319.05	357.13	397.63
3.2	252.77	289.61	330.92	376.44	425.99	479.42
3.3	288.09	334.53	387.01	445.46	509.85	580.16
3.4	329.11	387.22	453.66	528.67	612.32	704.79
3.5	376.43	449.01	533.03	629.23	737.90	859.54
3.6	431.08	521.28	627.70	751.05	892.23	1052.36
3.7	493.98	606.59	741.02	898.95	1082.42	1293.39
3.8	567.06	707.05	876.39	1078.94	1317.46	1595.65
3.9	651.68	825.17	1039.15	1298.37	1608.66	1975.91
4.0	749.47	964.97	1234.72	1566.83	1970.45	2455.73

Table A.16 The in-control ARLs of Weibull EWMA chart (λ=0.20, shape parameter $1.6 \leq \eta \leq 2.0$. $L_U=L_L=L$)

L	Shape parameter η				
	1.6	1.7	1.8	1.9	2.0
2.0	48.54	47.97	47.49	47.10	46.77
2.1	59.98	59.45	59.00	58.61	58.27
2.2	74.07	73.78	73.49	73.21	72.94
2.3	91.30	91.56	91.69	91.72	91.70
2.4	112.18	113.49	114.47	115.18	115.71
2.5	137.30	140.37	142.85	144.83	146.40
2.6	167.38	173.16	178.07	182.19	185.61
2.7	203.37	213.05	221.65	229.16	235.65
2.8	246.58	261.62	275.52	288.15	299.44
2.9	298.75	320.94	342.23	362.25	380.77
3.0	362.23	393.85	425.16	455.58	484.62
3.1	440.15	484.11	528.86	573.63	617.65
3.2	536.46	596.66	659.37	723.75	788.80
3.3	656.30	738.03	824.85	915.97	1010.28
3.4	806.24	916.74	1036.09	1163.76	1298.74
3.5	994.71	1143.91	1307.47	1485.34	1676.93
3.6	1232.61	1434.18	1658.19	1905.44	2176.20
3.7	1534.06	1806.75	2113.85	2457.55	2839.65
3.8	1917.45	2287.04	2708.84	3187.36	3726.87
3.9	2406.84	2908.76	3489.46	4157.24	4920.57
4.0	3033.77	3716.82	4518.36	5452.91	6535.99